The parageneses of sulphide minerals in transgressive carbonatite of the Palabora Carbonatite Complex, South Africa.

Dissertation submitted by

Pieter George Du Plessis

In fulfilment of the requirements in respect of the Master's Degree in Geology in the Department of Geology in the Faculty of Natural and Agricultural Sciences at the University of the Free State.

Supervisor: Prof. Frederick Roelofse

Co-supervisors: Prof. Christoph D.K. Gauert, R. Johannes Giebel, and Raimund Rentel

Submission date: 2019-03-21

“Use a picture. It’s worth a thousand words.”

Arthur Brisbane (1864-1936)

DECLARATION

I, Pieter George du Plessis, declare that the Master's Degree research dissertation that I herewith submit for the Master's Degree qualification in Geology at the University of the Free State is my independent work, and that I have not previously submitted it for a qualification at another institution of higher education.

Signature: 

ABSTRACT

The Palabora Complex, also known as the Palabora Carbonatite Complex, is situated in the Limpopo Province, next to the town of Phalaborwa. The complex intruded the Kaapvaal Craton in early Proterozoic times. The centre of the complex is known as the Loolekop pipe and hosts the youngest rock types of the complex. These rock types are phoscorite (older), banded carbonatite (younger), and transgressive carbonatite (youngest). Transgressive carbonatite hosts one of the world's largest copper deposits in the form of sulphide group minerals. The paragenesis of the various sulphide minerals is not well known, and a back and forth dispute exists of the formational processes (e.g. magmatic, hydrothermal, autometasomatic, etc.) which led to sulphide mineral crystallisation. This study shows that these sulphide minerals form part of different repetitive assemblages. These assemblages have distinguishable mineralogical, petrographical, geochemical, and paragenetic characteristics. Some assemblages that contain more than one generation of a certain sulphide mineral show differences in mineral chemistry (e.g. pentlandite group minerals, pyrrhotite, chalcopyrite, and sphalerite). The same assemblages that form part of transgressive carbonatite are also found in banded carbonatite. However, the sulphide mineral assemblage of phoscorite is completely different. This is indicative of different sulphide mineralisation events within the Loolekop pipe. The majority of transgressive carbonatite minerals show evidence of a magmatic origin, and most of them have been modified due to hydrothermal activity. Both processes are also responsible for sulphide mineral formation. This study also shows the discovery of sulphide minerals (e.g. heazlewoodite and shandite) and Cu-rich veinlets that have not been observed from this area in the past.

Keywords: Paragenesis; Sulphide Minerals; Palabora Carbonatite Complex; Loolekop Pipe; Phoscorite; Transgressive Carbonatite; Banded Carbonatite; Magmatic; Hydrothermal; Sulphide Mineral Assemblages.

ACKNOWLEDGMENTS

First and foremost, I would like to thank Prof. Frederick Roelofse and Prof. Christoph Gauert for their guidance and pioneering ideas. I give thanks to Johannes Giebel for sharing crucial insight and knowledge of the studied area. I would also like to thank Raimund Rentel for sharing his productive insight about sulphide mineral textures with me and for always being available when I needed assistance.

I would like to thank the Department of Geology at the University of the Free State for providing me with an ideal working environment and for the fruitful access to their preparation laboratories and research instruments. Great thanks go out to the Palabora Mining Company. In particular to Thabitha Moyana, Paulien Lourens, Bongani Mabunda, Tshepang Molloane, and Nyiko Makhubele for providing core material, for assistance during different sampling campaigns, and for productive discussions. Both Thabitha Moyana and Paulien Lourens also shared helpful 3D models with me, which I am very grateful for. I am also grateful for receiving the National Research Foundation Free-standing Block Grant for 2017 (SFH160603167608).

TABLE OF CONTENTS

APPENDICES

LIST OF FIGURES

ABBREVIATIONS

Sulphides/Sulfides:		
Bornite	bn	Cu_5FeS_4
Chalcocite	cct	Cu_2S
Chalcopyrite	ccp	$CuFeS_2$
Cobalt pentlandite	Co-pn	$(Co,Ni,Fe)_9S_8$
Covelline/covellite	cv	CuS
Cubanite	cub	$CuFe_2S_3$
Galena	gn	PbS
Heazlewoodite	hzl	Ni_3S_2
Pentlandite	pn	$(Fe,Ni)_9S_8$
Pyrrhotite	po	$Fe_{1-x}S$; (x = 0 to 0.17)
Mackinawite	mk	$(FeNi)_{1+x}S$; (x = 0 to 0.11)
Millerite	mlr	NiS
Shandite	sh	$Pb_2Ni_3S_2$
Sphalerite	sp	(Zn,Fe)S
Valleriite	val	$4(Fe,Cu)S•3[(Mg,Al)(OH)_2]$
X-bornite	x-bn	between Cu_3FeS_3 and Cu_9FeS_6
Sulfates		
Baryte/Barite	brt	$BaSO_4$
Other terms	**Abbreviations**	
Palabora Mining Company	PMC	
Reflected Light	RL	

Scanning Electron Microscopy	SEM
Transmitted Light	TL

CHAPTER 1. INTRODUCTION

Carbonatites are known by petrologists as rare igneous rocks formed predominantly of carbonate (Jones *et al*., 2013). They occur mainly as intrusive bodies of generally modest dimensions (as much as few tens of square kilometres) and to a lesser extent as volcanic rocks (flows and derived deposits), which are associated with a wide range of alkali silicate rocks (nephelinites, urtites, syenites, nepheline syenites, ijolites, etc.) (Richardson and Birkett, 1996). They can also occur as hydrothermal or replacement bodies depending on formational processes (Jones *et al.,* 2013).

The Loolekop pipe, which is developed by the PMC open pit and underground mining (Sharygin *et al.,* 2011), is composed of two types of carbonatites (banded and transgressive) and phoscorite (Fontana, 2006). This pipe crops out near the centre of the Palabora Carbonatite Complex and constitutes the copper ore deposit that was injected as copper sulphides (Kuschke and Tonking, 1971; Yuhara *et al.,* 2005). The complex is situated in the Limpopo Provinve (Figure 1.1), next to the town of Phalaborwa (Eriksson, 1984).

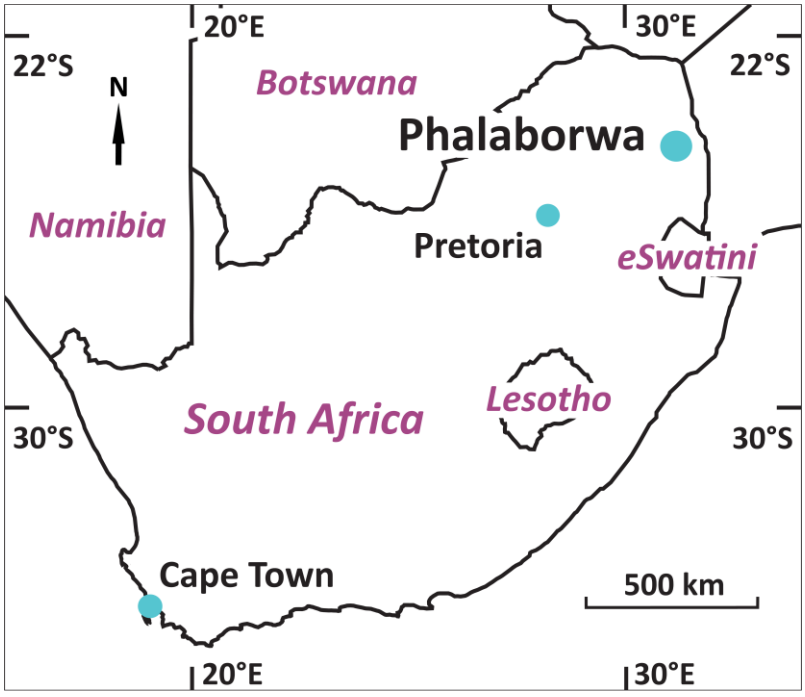

Figure 1.1: Location of Phalaborwa, with coordinates of 23°56'34.76"S and 31°8'27.85"E. eSwatini was formerly known as Swaziland (modified after Google Earth, 2018; Wu *et al.,* 2011).

The PMC pit has a diameter of approximately 2 km (Yuhara *et al.,* 2005) and a depth of over 800 m (Sharygin *et al.,* 2011). Open pit mining methods stopped after 37 years of sustained copper production when the limit of economic mining had been reached. This was followed by underground mining via a block-caving technique that still continues to this day (Verwoerd and Du Toit, 2006).

For this particular research project, work done by Forster (1958), Hanekom *et al.* (1965), Aldous (1980), and Giebel *et al.* (2017) is of greater interest than any other sources. Not only do these authors describe a large list of minerals found in transgressive carbonatites, but they also explain their paragenesis to a certain extent.

The earliest work on the paragenetic sequence of sulphide minerals present within these carbonatites is presented by Forster (1958). The author indicates that primary minerals (uranoan thorianite/uranothorianite, baddeleyite, magnetite, and ilmenite) represents a hydrothermal phase formed at temperatures well above 400°C, before *in situ* cataclasis, followed by the formation of primary "ascendant" sulphides (chalcopyrite, pentlandite, pentlandite-like minerals, zincblende, precious metals, bornite, galena, and magnetite) at temperatures close to 400°C, and lastly, the formation of secondary "descendant" ore (bravoite, millerite, chalcocite, covellite/covelline, pyrite, bornite, and valleriite) at lower temperatures. Both the primary and secondary "descendant" ores are described as forming after *in situ* cataclasis.

The described study does contain textural information of certain sulphide minerals within the Palabora Carbonatite Complex. However, the paragenetic sequence is not very detailed, seeing that the minerals are categorised in a table form with just three categories, and question marks are used at certain sulphide minerals categorised within the last group. The order of appearance of the minerals within each group is also uncertain. Also, no back-scattered electron images are available, which is crucial for an in-depth paragenetic study. Not even applicable reflected light microscopy images are available, which can be used as evidence to show the different sulphide mineral associations in greater detail.

More recent work done by Giebel *et al.* (2017) shows the paragenesis of rare earth element (REE) mineralisation of the Palabora Carbonatite Complex in great detail. The positions of these REE minerals and that of the main minerals (e.g. forsterite, baddeleyite, apatite,

phlogopite, dolomite, calcite, and magnetite) present within banded and transgressive carbonatites are presented within a paragenetic scheme. Unfortunetaly the scheme does not elaborate on the paragenetic sequence of the various sulphide minerals. However, the author does explain that the formation of the main minerals is followed by the injection of a sulphide-rich liquid, and that the interaction of a sulphide magma with a carbonatite magma is suspected during this stage.

Giebel *et al.* (2017) does not give reasons for a magmatic origin, seeing that it is not the topic of the study. Gupta and Krishnamurthy (2005) also illustrate the deposit type for the principal sulphide minerals to be of the magmatic kind, while previous work done by Hanekom *et al.* (1965) suggests a hydrothermal origin for sulphide mineralisation.

Taking a possible hydrothermal origin into account, Aldous (1980) proposed that mineralisation occurred autometasomatically in a continuum between carbonatite melt and residual fluids at temperatures between 600°C and 200°C, and low fO_2. In the described study, the different sulphide minerals were primarily identified via reflected light microscopy. Also, the study does contain textural information on the different sulphide minerals that formed in banded and transgressive carbonatites, but lacks sufficient paragenetic-associated information and visual evidence (only showing reflected light microscopy images of certain sulphide minerals) on which the paregenetic scheme is based upon. Not all the described sulphide minerals are included in the paragenetic scheme. Uncertainty also remains on how all of the identified sulphide minerals of the same and different kind differ in major and/or minor elemental amounts.

1.1. Research objectives.

It is clear that differences in opinions exist for the formational processes that led to sulphide mineralisation in transgressive carbonatites. Also, the paragenetic models created by the previous authors regarding sulphide mineral formation are outdated, lacking information, and in a sense, summarised. Visual evidence for these paragenetic schemes in relation to the description of sulphide minerals is also completely unsatisfactory. Thus, the main objective of this project is to study the parageneses of sulphide mineralisation in transgressive carbonatite by using optimal analytical methods. Additional objectives include:

a) The study of the paragenesis of other (non-sulphide) minerals that form part of transgressive carbonatite.
b) The mineralogical and petrographical characterisation of certain banded carbonatite and phoscorite samples in order to make appropriate comparisons.
c) Obtain elemental weight percentages from the different sulphide minerals, primarily of transgressive carbonatite, and secondarily of banded carbonatite and phoscorite.
d) The integration of petrographical and geochemical data, and the translation of findings into paragenetic schemes, focusing on sulphide mineralisation of the three rock types.
e) The discovery of sulphide minerals that have not previously been reported from this area.
f) The elaboration of the connection between various transgressive carbonatite minerals and the different formational processes.

Notice: The research project will make use of the term “non-sulphide” instead of the term “gangue” where applicable to refer to minerals that are not categorised into the sulphide group. This is due to the fact that certain types of minerals in transgressive carbonatite are also economically recoverable. Thus the term “gangue” cannot be used to describe these minerals.

Terms with alternative spelling (in parentheses), as observed from multiple sources, include: sulphides (sulfides); covelline (covellite); cobalt pentlandite (cobaltpentlandite); back-scattered electron image (backscattered electron image); cross-polarised light (cross polarised light); subpoikilitic (sub-poikilitic).

CHAPTER 2. CARBONATITES

2.1. Carbonatites in general.

2.1.1. What is a carbonatite?

As previously mentioned, carbonatites are known by petrologists as rare igneous rocks composed predominantly of carbonate (Jones *et al.,* 2013). Dawson and Hinton (2003) argue that carbonatites are the crystalline products of low-volume, high temperature carbonate melts that evolved from the upper mantle for at least the past 2.6 Ga, and that this rock type can provide potentially important information on the rare-metal budget of the upper mantle.

The geochemistry of carbonatites are typified by high abundances of Sr, Ba, P, and the light rare-earth elements (LREE) (Jones *et al.,* 2013). To qualify as a carbonatite a rock must be composed of more than 50% carbonate minerals (Le Bas, 1981; Woolley and Kempe, 1989). However, Mitchell (2005) defined carbonatites as a rock that contains greater than 30 vol.% primary igneous carbonate, regardless of silica content.

It is common for carbonatites to be surrounded by metasomatically altered rocks called fenites. The fenites are produced by the reaction of country rock with peralkaline fluids released from the carbonatite complex (Richardson and Birkett, 1996). According to Le Bas (2008), fenitisation is defined as the process of alkali metasomatism associated with igneous activity, usually alkaline igneous activity. Most carbonatites do not contain negligible alkalis, thus they are not usually recognised as alkaline (Le Bas, 2008). Le Bas (2008) entertains the argument that many carbonatitic magmas were originally alkaline and that the alkalinity was lost during the process of fenitisation. The conclusion is made that “alkaline igneous activity” may thus be understood to be “alkali silicate and associated carbonatite igneous activity” (Le Bas, 2008).

Carbonatite associated deposits can be primarily subdivided into metasomatic and magmatic types. Metasomatic deposits are formed by the reaction of fluids released during crystallisation with pre-existing carbonatite or country rocks, whereas magmatic deposits are formed only through processes associated with the crystallisation of carbonatites (Richardson and Birkett, 1996).

Jones *et al.* (2013) describes a similar classification for carbonatites by suggesting a process-related classification that would divide carbonatites into two main groups: primary carbonatites and carbothermal residua. Carbothermal residua carbonatites form as low-temperature fluids rich in CO_2, H_2O, and F, whereas primary carbonatites form by partial melting. The primary carbonatites can further be divided into groups of magmatic carbonatites associated with kimberlite, nephelinite, melilitite, and specific mantle-derived silicate magmas (Jones *et al.,* 2013).

Although there is a strong association of carbonatites with alkali rocks, the inverse relationship does not reflect the same association (Richardson and Birkett, 1996). Thus Woolley and Kjarsgaard (2008) argues that the physical relationship between silicate rocks and carbonatites may be fortuitous in some cases, and that the juxtaposition of the two rock types does not necessarily imply consanguinity. Therefore, Woolley and Kjarsgaard (2008) believe that the widely used word "associated" is not completely appropriate. It is suggested that it would be better to refer to carbonatites and their "accompanying" instead of "associated" silicate rocks (Woolley and Kjarsgaard, 2008). However, Le Bas (2008) argues that there is usually no liquid line of decent relationship between carbonatite and silicate magma, but there are certainly silicate rocks that are more loosely related insofar as they are probably a product of the same, or closely related thermal event(s). Also, the fact that 80% of carbonatites occur together with alkali silicate rocks in time and space is a strong argument that they are associated in the genetic sense, hence the word "associated" may be appropriate (Le Bas 2008).

2.1.2. Tectonic setting of carbonatites.

Guilbert and Park (1986) & Sawkins (1990) explain that carbonatites are situated in cratons that are so deeply rifted that upper mantle partial melting is tapped or generated. Sawkins (1990) continues to explain that carbonatites, as well as kimberlites and alkali rocks, are uncommon in orogenic belts, seeing that they only occur along lineaments within stable continental interiors. Unconventional tectonic associations for carbonatites (i.e. not continental rifts) include oceanic islands, shear zones, ophiolites, deep subduction zones, and even connections to ultra-high pressure (UHP) metamorphic terranes (Jones *et al.,* 2013).

Over 527 carbonatite occurrences are known (Woolley and Kjarsgaard, 2008). Approximately a third of the known carbonatites occur in Africa (Woolley and Kjarsgaard, 2008). The majority of these carbonatites are concentrated in or close to the East African Rift (Figure 2.1), occurring in a large area that stretches from Kenya into South Africa (Woolley, 1989).

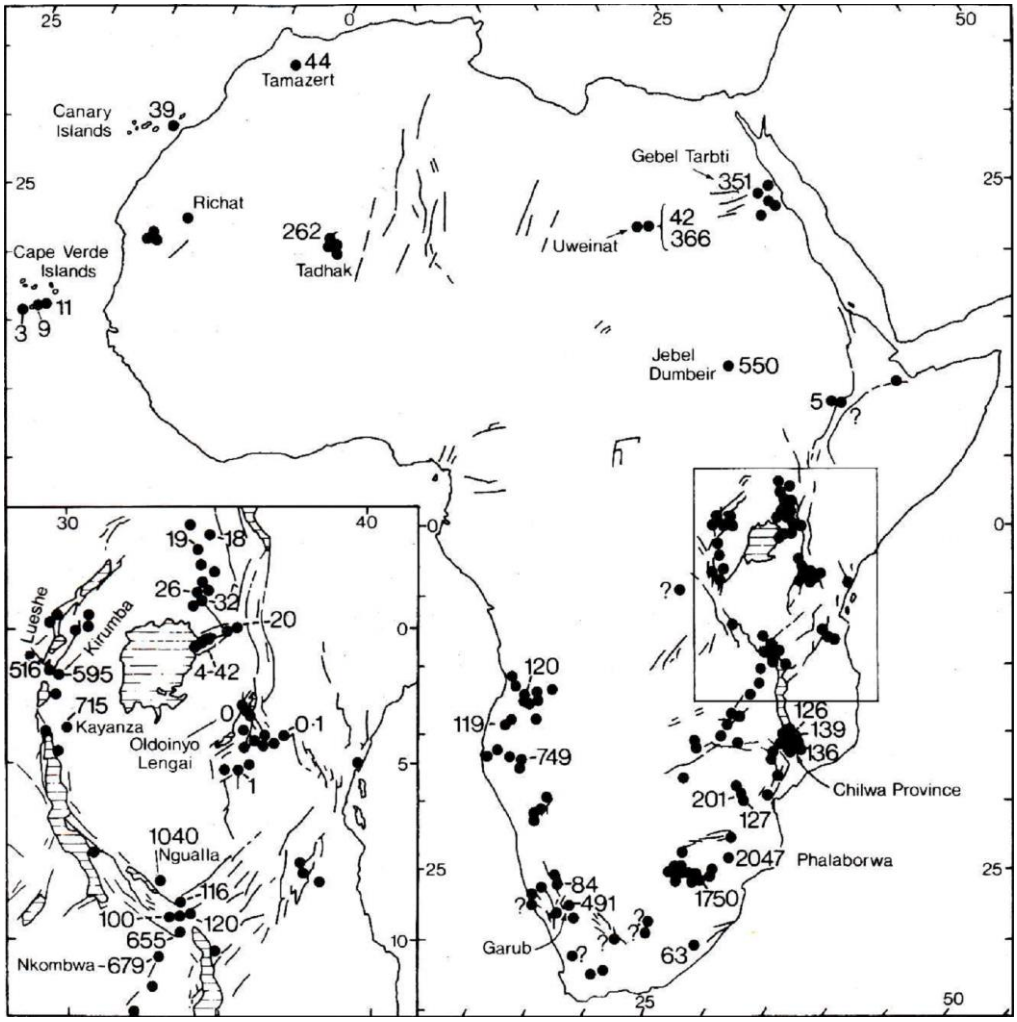

Figure 2.1: Locations and ages (in Ma) of carbonatites in Africa. The region where carbonatites are distributed along the East African Rift is magnified. Illustration from Woolley (1989).

2.1.3. Classification of carbonatites based on main carbonate components and chemical analyses.

Le Bas (1981) divided carbonatites into 4 main classes with respect to their main carbonate components. The first main class is known as calcite-carbonatites (named calciocarbonatite

by Jones *et al.,* 2013). This class can be sub-divided into sövites if coarse-grained and alvikites if medium- to fine-grained. Calcite forms the bulk of the carbonate minerals in this group (Le Bas, 1981). With the use of weight proportions obtained from whole rock chemical analysis, this class has a chemical characteristic (boundary) of CaO/ (CaO + FeO+ MgO) > 0, 80 (Jones *et al.,* 2013).

The second main class is known as dolomite-carbonatites (named magnesiocarbonatite by Jones *et al.,* 2013) and includes beforsites. Dolomite forms the bulk carbonate mineral in this class (Le Bas, 1981). Lee *et al.* (2000) suggests that rauhaugite also forms part of this class. This group is less common compared to sövites and alvikites (Le Bas, 1981). The chemical characteristic of this class shows a (Ca, Mg)-rich nature (Jones *et al.,* 2013). Some carbonatites contain both calcite and dolomite. The dolomite may show extensive solid solution toward ankerite (Lee *et al.,* 2000). By far, the most abundant carbonatites are those composed largely of calcite or dolomite-ankerite (Harmer and Gittins, 1997). Lee *et al.* (2000) claims that the average composition (wt.%) for calciocarbonatite is CaO = 49,12%, MgO = 1,80%, SiO_2 = 2,72% and H_2O = 0,76%, while the average composition for magnesiocarbonatite is CaO = 30,12%, MgO = 15,06%, SiO_2 = 3,63% and H_2O = 1,20%. Magnesiocarbonatite has variable ankerite in solid solution (Lee *et al.,* 2000) and shows a chemical characteristic of MgO > (FeO + MnO) (Jones *et al.,* 2013).

The third main class is known as ferrocarbonatites (Jones *et al.,* 2013), and it is quite uncommon (Le Bas, 1981). These carbonatites carry essential iron-rich carbonate minerals (e.g. ankerite and siderite). This class shows a chemical characteristic of (FeO_T (total iron) + MnO) > MgO (Jones *et al.,* 2013).

The last main class is known as natrocarbonatites and is composed of Na-Ca-K carbonates (Le Bas, 1981). It contains up to ± 40 wt.% (Na_2O + K_2O) with very high amounts of CaO and CO_2, very low amounts of SiO_2, TiO_2, and Al_2O_3, and considerable SrO, BaO, P_2O_5, SO_3, Cl, F, and MnO in comparison to silicate igneous rocks (Jones *et al.,* 2013). The natrocarbonatite lava of the active volcano Oldoinyo Lengai in Tanzania is the only known example of alkali carbonatite (Harmer and Gittins, 1997). This class shows a chemical characteristic of (Na_2O + K_2O) > (CaO + MgO + FeO) (Jones *et al*., 2013).

A large number of exotic or rare minerals also occur in carbonatites (Richardson and Birkett, 1996). Jones *et al.* (2013) extends carbonatite nomenclature by including the rare earth (RE)-carbonatite class. (RE)-carbonatites have variable grain sizes and modal REE minerals, with RE_2O_3 (total REE oxides) > 1 wt.% (Jones *et al.,* 2013).

Gittins and Harmer (1997) propose a revised classification for ferrocarbonatites, seeing that the IUGS system treats FeO, Fe_2O_3, and MnO as a single component, thus making it unable to distinguish between carbonatites that are composed largely of Fe-rich calcite (or of siderite and ankerite) and carbonatites that contain hematite and magnetite. The modified chemical classification is as follows: ferrocarbonatite: CCMF < 0.5; MgO/FeO < 1.0; ferruginous calciocarbonatite: 0.5 < CCMF < 0.75; MgO/FeO < 1.0; calciocarbonatite: CCMF > 0.75; magnesiocarbonatite: CCMF < 0.75; MgO/FeO > 0.1, where CCMF is the molar ratio CaO/ (CaO + MgO + FeO + MnO), and FeO refers to molar FeO if Fe_2O_3 and FeO are both ascertained and total Fe as FeO if not. This classification divides the ferrocarbonatite field of the IUGS system into two parts and uses molar rather than weight proportions in order to restrict the term 'ferrocarbonatites' to much more Fe-rich rocks and to recognise a group of rocks to be known as ferruginous calciocarbonatites (Gittins and Harmer, 1997).

2.1.4. Classification of carbonatites based on processes of emplacement.

As previously mentioned, carbonatites can be classified into two major groups: primary carbonatites and carbothermal residua (Jones *et al.,* 2013). The latter major group can also be described as carbo(hydro)thermal residua (Mitchell, 2005; Woolley and Kjarsgaard, 2008). The function of these two groups are to define/classify carbonatites in a mineralogical-genetic point of view. Very detailed explanations, with regard to these two major groups, are presented by Mitchell (2005).

The first major group describes mainly four varieties of carbonatite (as well as their associations) that could be considered as primary magmatic "carbonatite" *sensu stricto*: The nephelinite-clan carbonatites, the melilitite-clan carbonatites, the aillikite-carbonatite association, and the peralkaline nephelinite-natrocarbonatite association. Carbonatites linked to the above mentioned associations can have a multiplicity of origins. They may be formed via fractional crystallisation, partial melting or liquid immiscibility. A kimberlite-clan-

calcite kimberlites group is also discussed. However Mitchell (2005) argues strongly against the terminology of calcite kimberlites being considered as *bona fide* carbonatites (given they are ultimately formed from mantle-derived magma) as it leads to unwarranted genetic speculation as to the relationships between kimberlite and other unrelated magma-types.

The other major group explains carbonate-rich rocks associated with diverse potassic or sodic peralkaline saturated to undersaturated magmas derived predominantly from metasomatised lithospheric mantle, together with REE-carbonate-rich rocks of undetermined genesis as being carbothermal residua, rather than carbonatite. Two groups are explained here, namely the potassic-suite "carbonatites" and the sodic-suite "carbonatites" (Mitchell, 2005).

"Carbonatites" from the first mentioned group are associated with potassic plutonic rocks. Examples include occurrences at Rocky Boy (Montana), Mountain Pass (California), and Little Murun (Yakutia). The characteristics of most of these occurrences are their association with diverse saturated to undersaturated potassic syenitic rocks, the total absence of members of the ijolite and melilitolite suites, and high abundances of REE-bearing carbonates and baryte (Mitchell, 2005).

A stockwork of veins of carbonatite and silicate-bearing carbonatite occur within a "sericitised" potassic syenite, at the Rock Boy (Montana) occurrence. These "carbonatites" are interpreted to be fractional crystallisation residua derived from the potassic syenitic parental magma (Mitchell, 2005).

Carbonatites or carbo(hydro)thermal residual fluids associated with sodic peralkaline syenite (e.g. Khibina complex and Russia) form part of the sodic-suite "carbonatites" group. These carbonatites form through the differentiation of sodic peralkaline magmas to residual fluids, which then crystallise REE-, Na-, and Ca-carbonates (Mitchell, 2005). Carbo(hydro)thermal carbonatites appear to be related to fluids from two distinct sources: carbonatite magmas and alkaline silicate magmas (Woolley and Kjarsgaard, 2008). Woolley and Kjarsgaard (2008) define carbo(hydro)thermal carbonatites as those precipitated at subsolidus temperatures from a mixed CO_2 – H_2O fluid that can be either CO_2-rich (i.e. carbothermal) or H_2O-rich (i.e. hydrothermal).

According to Jones *et al.* (2013), carbothermal or hydrothermal fluids enriched in F and CO_2 can cause the remobilisation of Nb and REEs. The remobilisation process can result in secondary enrichment. It is believed that the REE-enriched nature of carbonatites is due to its tendency to favour transport via molecular CO_3^{2-} complexes in the melt during immiscible separation between coexisting silicate and carbonate melts. This results in an increased La/Lu ratio in the carbonatite relative to silicate melt (Jones *et al.,* 2013).

Fluorine also plays a role in the evolution of carbonatite magma. Jago and Gittins (1991) studied the effect of fluorine on carbonate liquidi and compared it with that of water. Experimental results show that in several carbonatite systems, ±8 wt.% fluorine lowers the minimum melting temperatures and liquidus temperatures to a similar extent as very large amounts of water (±95 wt.%). They continue to explain that the alkali carbonatite lava flows at Oldoinyo Lengai provide strong evidence for the importance of fluorine in the evolution of carbonatite magma. These lava flows contain up to 15 wt.% F + Cl in approximately equal amounts, but very little water (<0.5 wt.% H_2O). Thus water is neither the only nor necessarily the main agent by which carbonatite magmas can remain liquid, despite the fact that it may very well be present in most carbonatite magmas (Jago and Gittins, 1991).

2.1.5. Crystallisation differentiation and fractionation sequence in carbonatites.

According to Lee *et al.* (2000), it is very common to find the successive emplacement of calcitic then ankeritic sövite, followed by sideritic carbonatites (ferrocarbonatites). Le Bas' (1981) research concurs with this statement and argues that carbonatites show an almost constant sequence of emplacement. The author continues to explain that sövite (C_1) is usually the earliest carbonatite emplaced within a complex, and that alvikites and any beforsites (C_2) invariably cuts the sövite as swarms of dykes and cone-sheets (Le Bas, 1981). Transgressing the C_1 and C_2 carbonatites are the ferrocarbonatite (C_3) dykes and veins (Lee *et al.,* 2000). In some instances thin veins and stringers (C_4) of late-stage residual calcite-carbonatite can be present and can be entirely composed of a mosaic of small crystals, or in some cases, the vein can look sövitic and can have large calcite crystals (Le Bas, 1981).

Studies of the temperature of homogenisation conducted on primary fluid inclusions within apatites of both carbonatites and their associated ijolites indicate normal magmatic

temperatures in the region of 1000-1100°C for the ijolites. However, a much lower set of temperatures were determined for the carbonatites, as sövites indicate temperatures of about 400-600°C, with beforsites, alvikites, and ferrocarbonatites falling in the region of 200-400°C (Le Bas, 1981).

2.2. Palabora carbonatites.

2.2.1. General geology.

The Palabora Complex (Figure 2.2), also known as the Palabora Carbonatite Complex, is approximately 2060 Ma in age (Bernard-Griffiths *et al.,* 1988; Reischmann *et al.,* 1995; Shankar *et al.,* 2014). The 8 x 3 km main complex (Groves *et al.,* 2010) is an elongate, irregularly-shaped, tripartite pipe-like body with a vertical extent of approximately 5 km (Eriksson, 1984). The complex occupies an area of approximately 16 km^2 and can be subdivided into the Northern Pyroxenite, the central Loolekop pipe, and the Southern Pyroxenite (Verwoerd, 1993). Only the Loolekop pipe hosts a carbonatite-phoscorite association (Verwoerd, 1993).

The concentrically zoned multistage intrusions that form the Palabora Complex intruded the Archaean basement at the edge of the Kaapvaal Craton in Early Proterozoic times (Dawson *et al.,* 1996; Fontana, 2006; Mücke, 2017). The initial stage (ultramafic stage) is represented by clinopyroxenites (mica pyroxenites to glimmerites) and forms the host of the complex (Sharygin *et al.,* 2011). The clinopyroxenites also occur in the form of pipes, together with syenite pipes, which surround the main complex (Eriksson *et al.,* 1985). The intruded Archaean terrain consists mainly of granites, quartzites, gneisses, amphibolite, granulites, talc, and serpentine schists (Yuhara *et al.,* 2003).

Subsequent fenite formation was followed by extended metasomatic activity during which pegmatitic pyroxenites were emplaced at three centres in the main pyroxenite body (Vail, 1989; Wu *et al.,* 2011). This was followed by modification of the central part of the complex (Figure 2.3) due to the intrusion of phoscorite and banded carbonatite, and lastly by the intrusion of transgressive carbonatite (Reischmann, 1995; Wilson, 1998; Wu *et al.,* 2006). The entire complex was transected by a suite of dolerite dykes afterwards (Verwoerd, 1986).

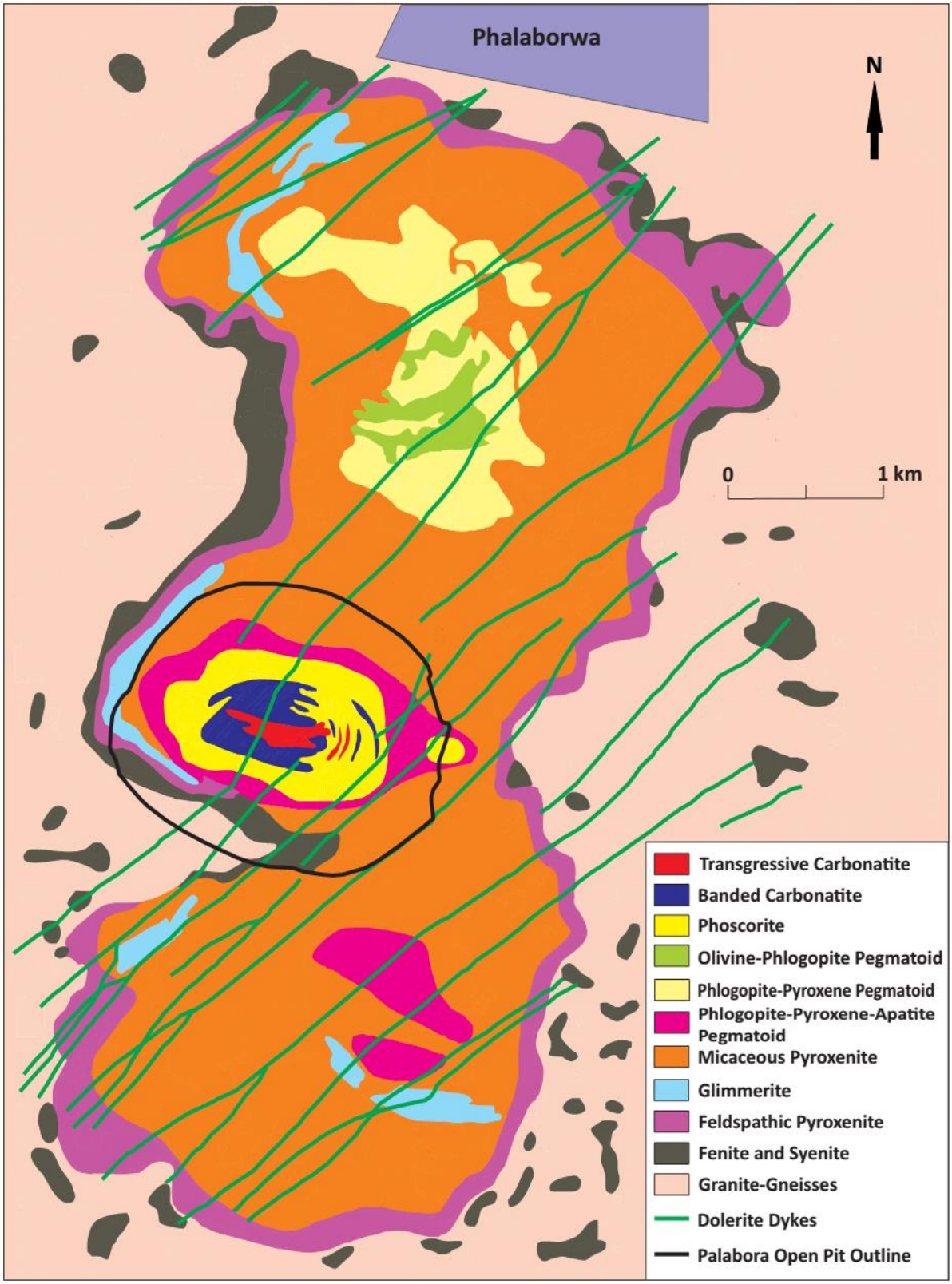

Figure 2.2: Generalised geological map of the Palabora Complex (modified after Wilson, 1998; Verwoerd and Du Toit, 2006).

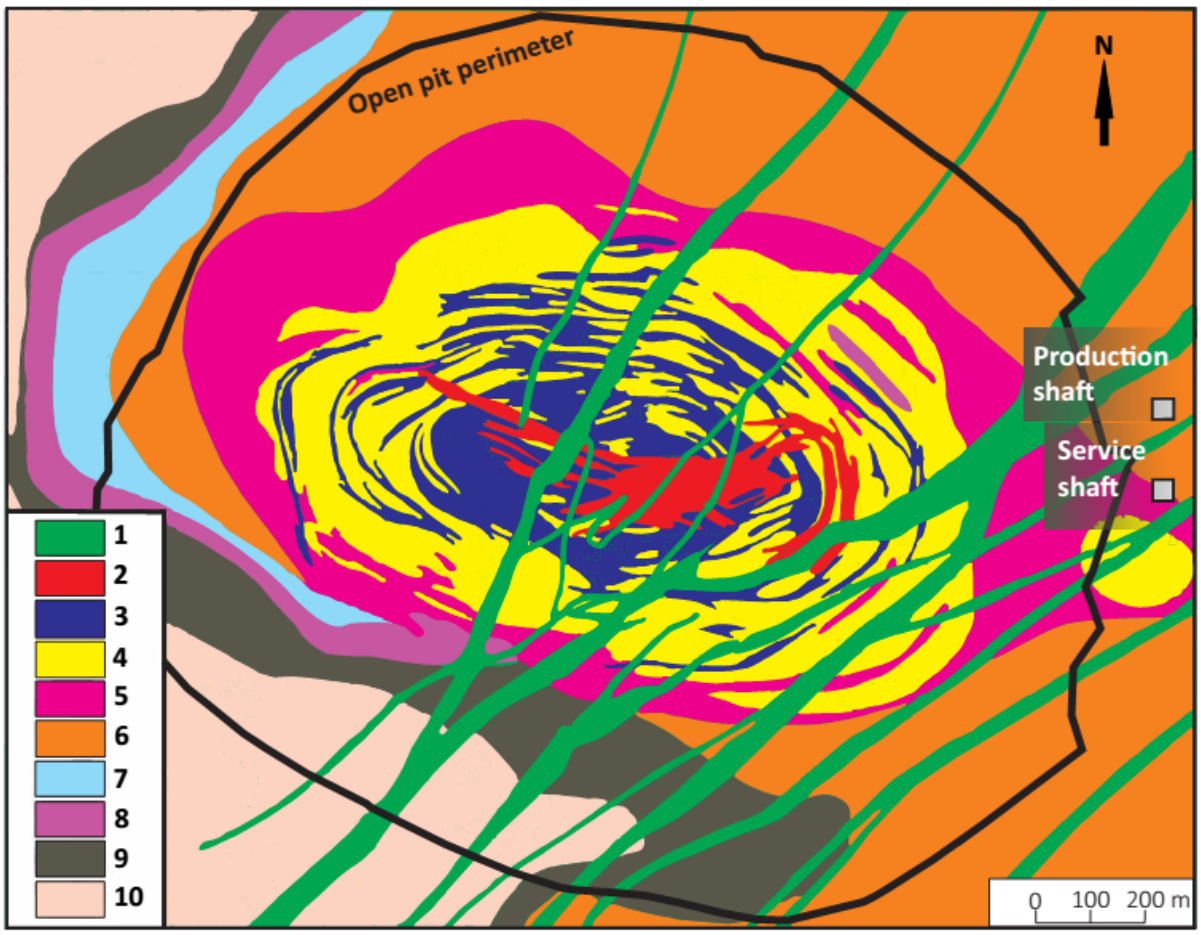

Figure 2.3: Generalised geological map of the Loolekop pipe, at the centre of the Palabora Complex. 1 = Dolerite Dykes; 2 = Transgressive Carbonatite; 3 = Banded Carbonatite; 4 = Phoscorite; 5 = Pegmatiod (Clinopyroxenite); 6 = Micaceous Clinopyroxenite; 7 = Glimmerite; 8 = Feldspathic Clinopyroxenites; 9 = Fenites; 10 = Granite-Gneisses (modified after Sharygin *et al.,* 2011).

Both the banded carbonatite and transgressive carbonatite are classified as sövitic carbonatites (Hornig-Kjarsgaardh, 1998). The banded carbonatite is a white, coarse- to medium-grained rock which forms an elliptical vertical plug central to the phoscorite mass, while the transgressive carbonatite is generally more finer-grained than the banded carbonatite and is distinguished from older carbonatite through the lack of banding and foliation (Lombaard *et al.,* 1964; Vielreicher *et al.,* 2000). There is also no clean-cut (intermeshed) division between the banded carbonatite and phoscorite, while the main transgressive carbonatite body forms a well-defined but irregularly shaped intrusion, as well as a series of narrow dykes or offshoots (Suwa *et al.,* 1975). Transgressive carbonatites

situated in the central area are generaly more coarse-grained, while those forming narrow veins are fine-grained to sugary (Vielreicher *et al.,* 2000).

Two intersecting sents of fractures, N. 70° E. and N. 70° W., controlled the emplacement of the vertical subparallel dykes of transgressive carbonatite. The thickness of the dykes ranges from hundered or more feet to just a few inches. The main juncture (just east of the centre of the banded carbonatite pipe) of the intersecting sets of fractures forms the focus of the copper mineralisation (Heinrich, 1970).

2.2.2. Economic importance.

The Palabora Complex carbonatite body contains one of the world's largest copper deposits (Korobeinikov *et al.,* 1998) and is also a major source of commercial vermiculite (Muiambo *et al.,* 2010). Palabora Copper produces approximately 45 000 tons of copper per annum (PMC, 2017). The complex is not only a major copper deposit, but also yields by-products of zirconium, nickel, uranium, phosphorus, gold, platinum group elements, and tellurium (Cooper *et al.,* 1995).

Apatite is the main source of phosphate. The phosphate is recovered via flotation from the tailings (Giesekke and Harris, 1994). The apatite minerals are also rare earth bearing. However, no rare earths are extracted at present (Gupta and Krisnamurthy, 2005; Verplanck *et al.,* 2014).

The Loolekop copper orebody contains baddeleyite, which is a zirconium oxide with a trace of hafnium, and also uranothorianite, which is a variable oxide of uranium and thorium. Both of these minerals are economically recoverable (Frank and Edmond, 2001).

Magnetite grains occur as strings which accentuate the foliation within banded carbonatites. The result is a crude banding appearance. However, magnetite forms randomly situated coarse-grained blebs in the transgressive carbonatites (Heinrich, 1970). This mineral is also economically recoverable (Pell, 1994).

The large quantities of magnetite and sulphides is the reason why a revised IUGS classification, like that previously proposed by Gittins and Harmer (1997), is likely needed for Palabora carbonatites.

CHAPTER 3. METHODS

3.1. Sampling.

Seventy-three samples were obtained from the MT-01 drill hole (Figure 3.1), which is located in the central Loolekop pipe. The drill core was situated between the first and second lift at a depth of 864 m to 1185 m, with a dip of 41.26° (Appendix A). Samples were obtained from areas with visible sulphide and magnetite mineralisation.

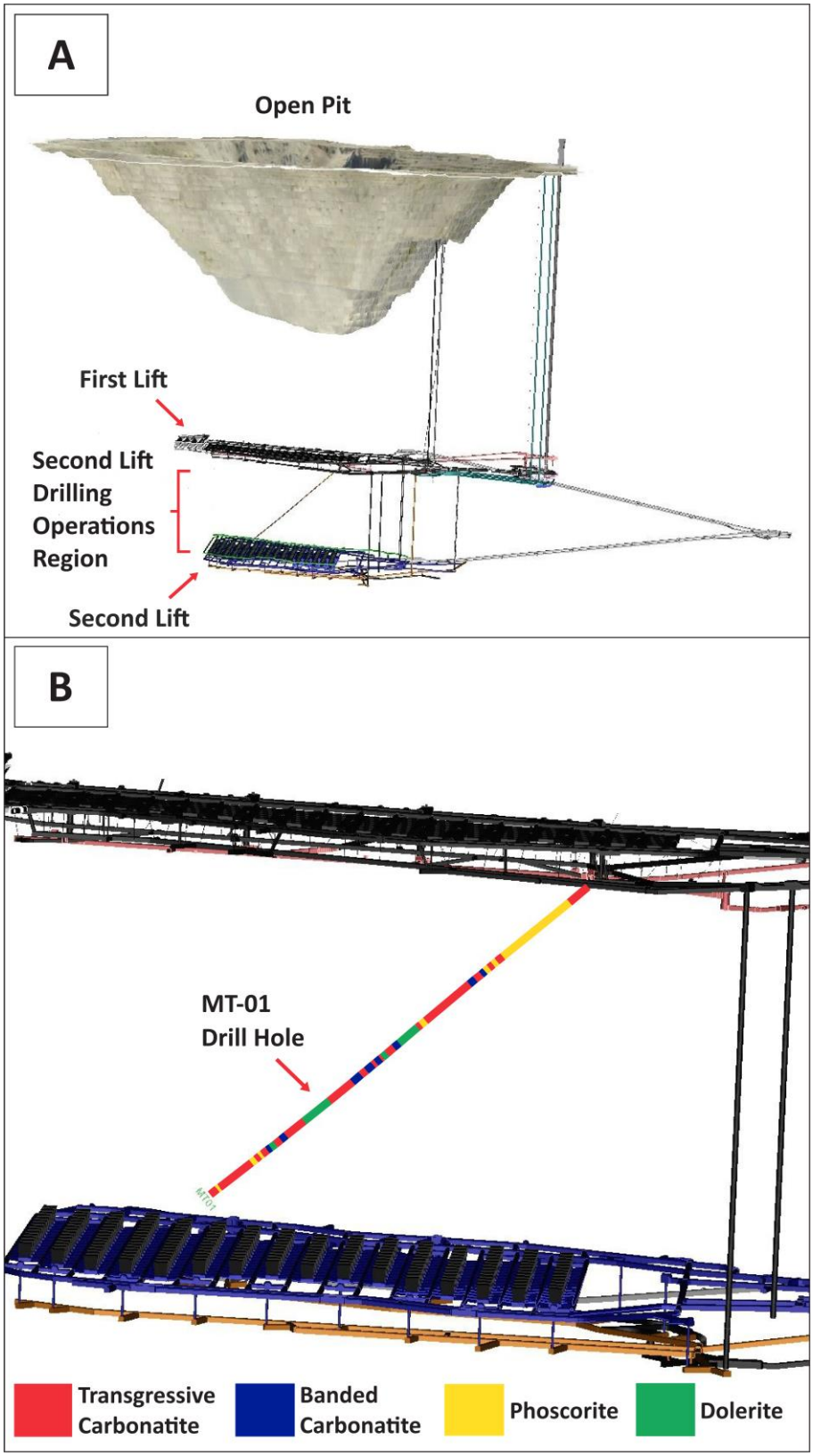

Figure 3.1: A) Oblique-section (E-W more or less) showing the position of the two lifts relative to the position of the open pit. B) Oblique-section (E-W more or less) showing the position of drill hole MT-01 (MET-01) between the first and second lift of Palabora underground mining operations (images modified after PMC Staff, 2018, supplied by geology staff, 22 June).

3.2. Sample preparation.

3.2.1. Sample preparation for transmitted light microscopy and reflected light microscopy.

For transmitted and reflected light microscopy, 46 representative thin sections were prepared from the 73 samples. The thin sections were prepared by cutting a 2 cm x 5 cm x 1 cm block from the samples. The grinded side of these blocks were glued to a glass plate afterwards and left to dry. These blocks were then grinded to the required thickness (±30 µm) and polished afterwards. This preparation method was performed at the Geology Department's polishing lab at the University of the Free State, South Africa.

3.2.2. Sample preparation for scanning electron microscopy.

The thin sections were carbon-coated with a thin layer of 15-100 nm carbon by using a Quorum Q150T fully automated, high vacuum sputter coater at the University of the Free State.

3.3. Analytical methods.

3.3.1. Transmitted light microscopy and reflected light microscopy.

Petrography was of immense importance for this study. Thus detailed petrographic interpretations were acquired for each relevant thin section.

Thin section observations were conducted under reflective and transmitted light with the use of a dual mode Olympus BX51 microscope at the University of the Free State. Mainly 2x, 4x, 10x and 20x magnification objective lenses were used, as well as a blue filter where necessary during sulphide mineral analysis. The microscope is equipped with an Altra 20 soft imaging system camera that was used for taking high resolution images (2048 x 1532 pixels) via Olympus Soft Imaging Solutions software.

Modal percentages were firstly estimated by dividing the minerals into two superclasses: transparent minerals and opaque minerals (at 2x magnification). Estimated percentages were then assigned to each of these superclasses. The total estimated percentage that was

assigned to the transparent minerals class was then divided between carbonates, phosphates, silicates, and sulfates (at 2x – 4x magnification). The total estimated percentage that was assigned to the opaque minerals was divided into two subclasses: oxides and sulphides (at 2x – 4x magnification). The estimated percentage that was assigned to the oxide class was divided between minerals that form part of the oxide group (at 10x – 20x magnification). The same procedure was followed with sulphide group minerals (at 10x – 20x magnification). Estimating mineral grain percentage charts were primarily used when comparing the percentages of carbonates, phosphates, silicates, and sulfates with one another.

An extensive amount of time had to be spent per thin section during reflected light microscopy in order to acquire as many as possible relevant spatial and textural associations for the different sulphide minerals. Paper copies were made for each thin section to be used as a blueprint. As many as possible associations were noted on these copies to indicate important locations for later scanning electron microscopy analysis. Numerous microscopic images were also taken primarily under reflected light, where areas of importance were noted on the copies for further study.

The microscopic images and petrographic descriptions also included the main carbonate-magnetite-sulphide associations for each thin section in order to make more sense of geochemical differences between different generations of the same phases later on, thus improving the accuracy of the paragenetic schemes.

3.3.2. Scanning electron microscopy (SEM).

With the relevant thin sections prepared for SEM analysis, the locations of importance were studied in much greater detail. Major and minor element compositions were determined via spot/point analysis on carbon-coated polished sections by energy dispersive spectroscopy (EDS) with the JOEL JSM 6610 Scanning Electron Microscope at the University of the Free State. The spectrometer that was used is a Thermo Scientific UltraDry Compact EDS Detector. Analyses were performed with a spot size of ±1 µm at an accelerating voltage of 20 kV.

The SEM was also used to obtain back-scattered electron images (with an image resolution of 512 x 384 pixels) and spectral images. Spectral imaging acquisition properties include: Map

Resolution: 256 x 192 pixels; Frame Time (s) = 50.0; Dwell time (µs) = 1017; Number of frames = 30; and Acquisition Time (s) = 1500.

For EDS-analyses, the mineral chemistry of the analysed minerals were compared to that of the minerals from the Handbooks of Mineralogy. The five volumes of the Handbooks of Mineralogy (Anthony, 1990; Anthony, 1995; Bideaux *et* al., 2000; Howie, 1998) compare the mineral chemistry of three to four examples of the same mineral type, thus giving a broad range of elemental weight percentages which can be used to define a specific mineral.

Certain precautions had to be taken into account in order to ensure accuracy during EDS-data collection. These precautions include:

a) Having thoroughly carbon coated the thin sections to ensure electrical conductivity. Thin sections lacking the proper amount of carbon coating will result in low resolution images as well as on-screen image drift. During image drift, a person might think that he/she is doing point analyses on a certain mineral, but in fact he/she is busy doing it on another mineral, or on the contact between the mineral he/she wants to study and a different one. This leads to faulty data capturing.

The improper setup of the carbon coater may form a carbon layer on the thin section that is too thin. Such a thin section should be carbon coated again until the user starts to see his/her reflection on the carbon coated area. This will indicate that the correct carbon coat thickness was more or less achieved.

b) Ensure that a proper amount of carbon tape connects the thin section to the sample holder. The sample holder has a positive charge. Connecting the two will also give the thin section a positive charge, thus increasing the attraction between the negative charged beam and the positive charged thin section. This will increase the accuracy of the beam, as the beam will now move true to the positive charged area which is marked for point analyses. If carbon tape is not used then the beam may bend as it is attracted by the positive charge sample holder. This will cause the beam to bend away from the points that have to be analysed. This also leads to faulty data capturing.

c) Know the beam size limits. Point analyses of grains that are too small, or doing point analyses too close to the boundary between different minerals will result in beam size overlap

between the mineral you want to analyse and the adjacent mineral(s). The result will be a combined analysis from both minerals. However, the beam size limit can be tested. For instance, a person can do point analyses at the outer reaches of a sphalerite grain with no chalcopyrite inclusions (containing no Cu) adjacent to chalcopyrite (containing Cu). A person will have more or less a sense of the capabilities of the beam if Cu analyses starts to show as the point analyses progress closer towards the edge of the sphalerite grain. This is also the reason why only two sets for covelline analyses (Appendix C, Table C.1) are presented in this study, seeing that other points of analyses would have been inaccurate due to the small size of the covelline grains. However, the used SEM exceeds all expectations and is even capable of obtaining pure analyses even from sphalerite grains with chalcopyrite inclusions (Appendix C, Table C.2, MT-23), showing no Cu overlap from the chalcopyrite inclusions in the process of data collection.

CHAPTER 4. RESULTS

4.1. Petrographic description of transgressive carbonatite sulphide mineralisation.

The following chapter describes the sulphide minerals of transgressive carbonatites, arranged from the most abundant to the least abundant as observed from data obtained through reflected light microscopy and scanning electron microscopy.

Table B.1 (Appendix B) lists the applicable thin sections and their estimated sulphide mineral modal compositions. The table is summarised in a fashion to give a sense of variations in sulphide mineralisation abundances (in percentages) per sample and associations with depth. The table was updated after scanning electron microscopy. Only the minerals identified during ore microscopy will be discussed in this part of the dissertation. Other sulphide minerals that needed identification via scanning electron microscopy will be discussed later on.

The author opines that it is not possible to assign smaller percentages than 1 modal % (e.g. 0, 32 modal %) to a specific sulphide mineral, seeing that such accurate estimations cannot be made just by observations with the naked eye alone. Thus, the minerals estimated to comprise less than 1 modal % of the total mineralisation of a sample were given ranks instead when comparing their abundances in that specific thin section. For example, a sample (thin section) may contain chalcopyrite, bornite, and chalcocite (as its only sulphide minerals) in which the total sulphide mineralisation is 12 modal % for that sample. The chalcopyrite and bornite may each show amounts clearly above 1 modal %, while the chalcocite shows amounts clearly less than 1 modal %. In this case, modal percentages will be assigned to the chalcopyrite and bornite while a rank of “3rd” will be assigned to the chalcocite, seeing that it is the 3rd most abundant sulphide mineral in that specific sample. Adding all these estimated modal percentages together, from all the samples for a certain sulphide mineral, makes it possible to compare the abundances for different sulphide minerals present within transgressive carbonatites. Comparisons are also possible for sulphide minerals that only have ranks but no modal percentages via the calculation of averages from the ranks, although certain aspects must be taken into account and will be discussed.

The data reveals that the optical properties of the different sulphide minerals, during microscopic observations, make them easily distinguishable from one another. In-depth descriptions focusing on textural relationships between different sulphide minerals are provided in Appendix F. These textural relationships will also be discussed later on.

4.1.1. Chalcopyrite (rank: 1st).

The most abundant sulphide mineral by far within the transgressive carbonatite samples is chalcopyrite (Figure 4.1). This sulphide mineral, with its superior volume and primarily subhedral to euhedral grain shape, is the most commonly replaced sulphide mineral in this study, although it replaced other sulphide minerals as well. Chalcopyrite is easily distinguishable from the other sulphide minerals due to its canary yellow colour under reflected light.

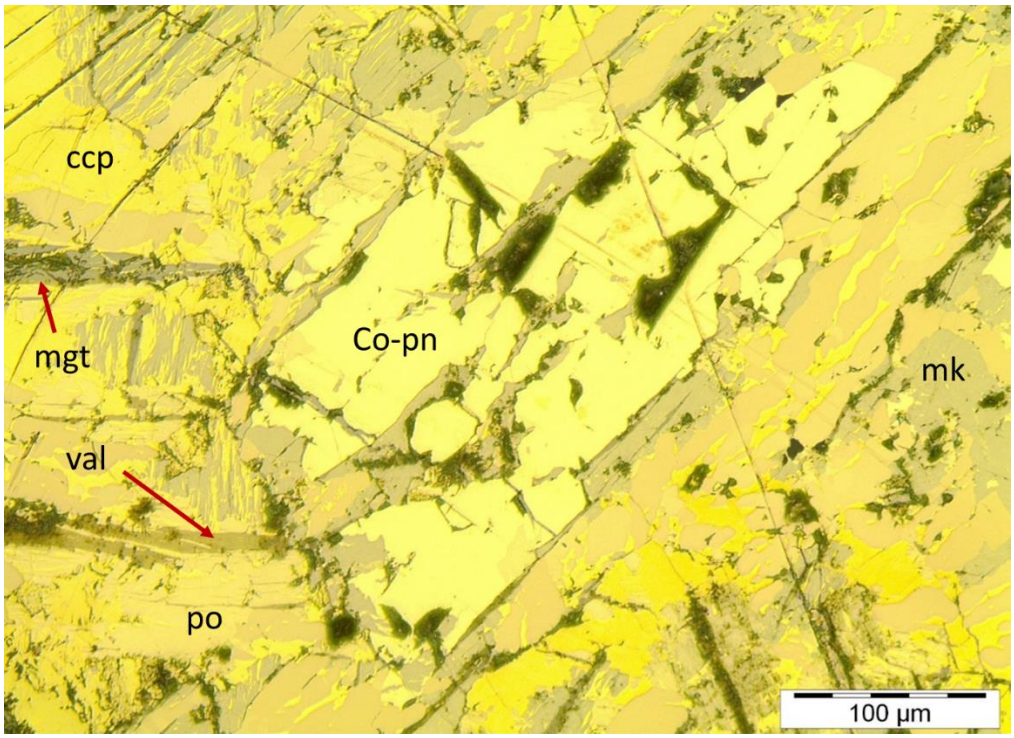

Figure 4.1: Cobalt pentlandite replaced by pyrrhotite, chalcopyrite, and mackinawite. Pyrrhotite replaced by chalcopyrite, mackinawite, and valleriite. Chalcopyrite replaced by mackinawite, magnetite, and valleriite. Mackinawite and magnetite replaced by valleriite. Reflected light (RL) image, sample MT-7.

4.1.2. Cubanite (rank: 2nd).

Cubanite is present as the second most abundant sulphide mineral within the transgressive carbonatite samples. It is not uncommon for cubanite to be found in larger amounts than chalcopyrite, especially where both sulphide minerals are present within the same sample.

Cubanite in transgressive carbonatite is found in two forms. Firstly, as cubanite laths produced from the exsolution of chalcopyrite (Figure 4.2; Figure 4.3), and secondly, as large relict replacement areas where the original chalcopyrite grain shape is still visible in the newly formed cubanite (Figure 4.2; Figure 4.3; Figure 4.4). The latter forms the bulk of cubanite mineralisation in this study. The light pink tint of cubanite under reflected light makes it easily distinguishable from chalcopyrite.

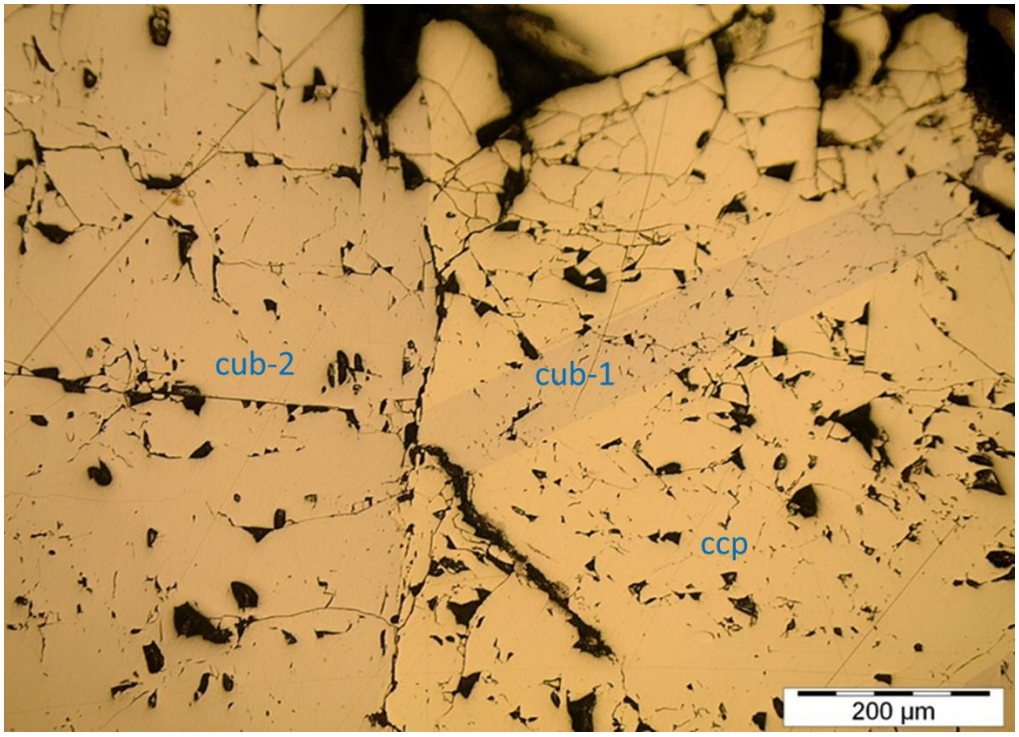

Figure 4.2: Chalcopyrite and first generation cubanite laths (cub-1) replaced by second generation cubanite (cub-2). RL image, sample MT-35.

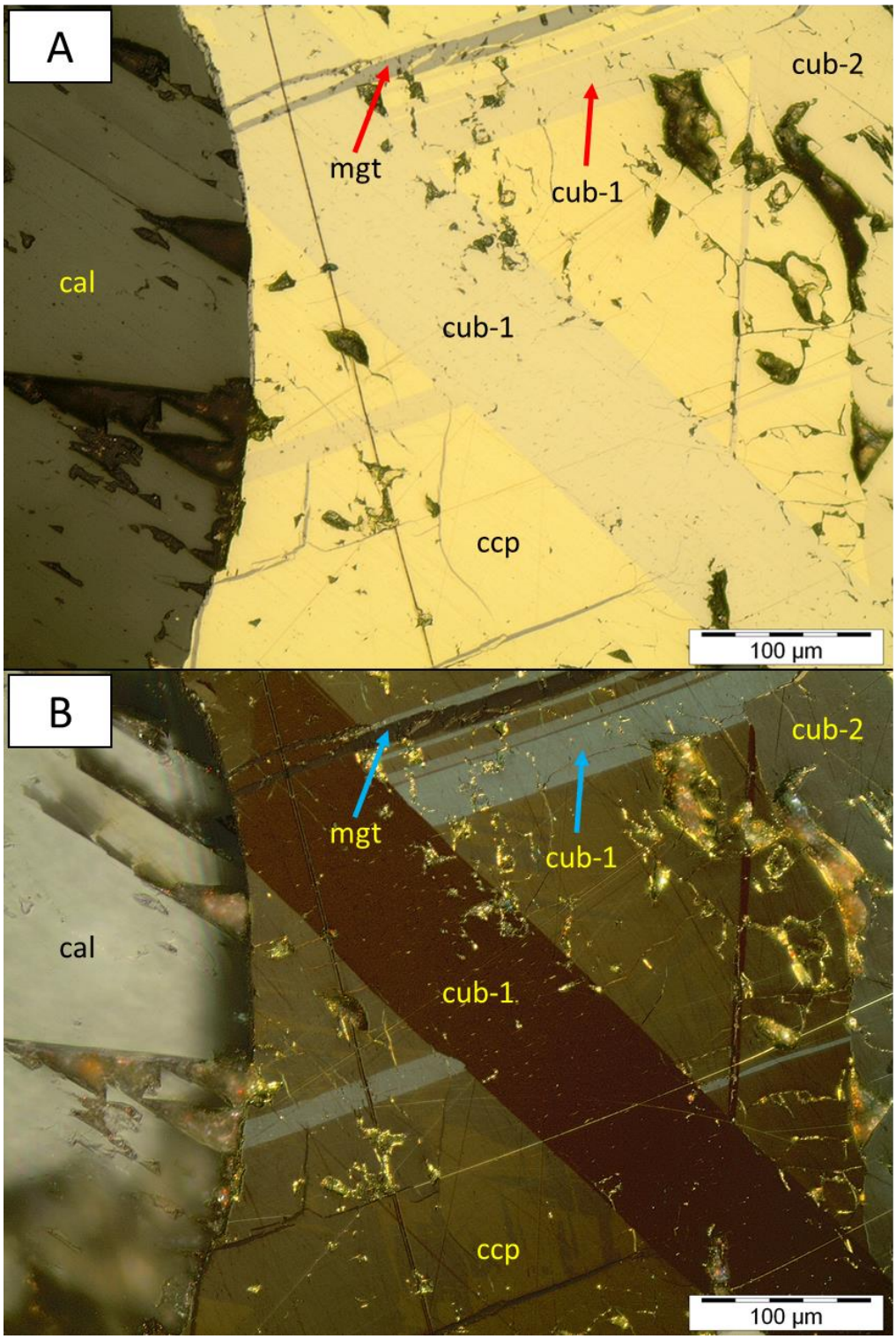

Figure 4.3: Chalcopyrite and first generation cubanite laths (cub-1) replaced by second generation cubanite (cub-2). RL image (A) under plane polarised light (PPL) and with crossed polarisers (B), sample MT-7.

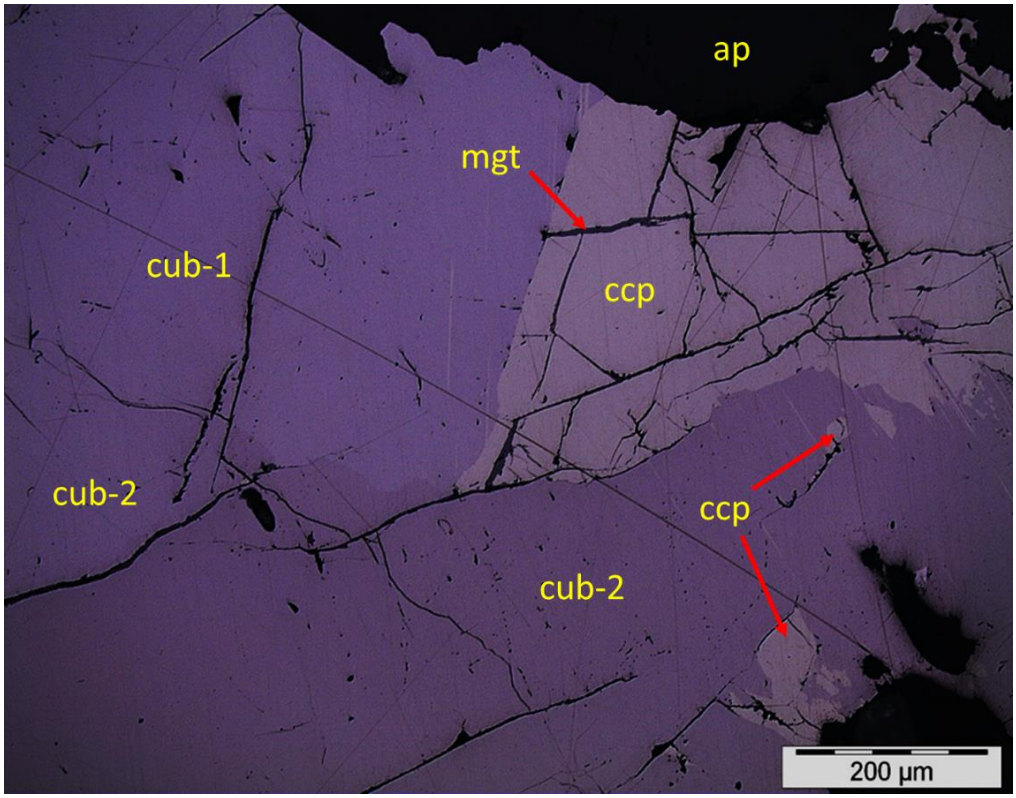

Figure 4.4: Chalcopyrite and first generation cubanite (cub-1) replaced by second generation cubanite (cub-2). RL image with blue lens, sample MT-3.

4.1.3. Bornite (rank: 3rd).

Bornite mineralisation in this study primarily occur as a replacement phase of chalcopyrite. This includes larger fabrics (Figure 4.5), smaller flames (Figure 4.6), and distorted bands (Figure 4.7). Additional textures are described later on.

Bornite is easily distinguishable from the other sulphide minerals due to its red-brown colour under reflected light. Sawkins (1990) affirms that chalcopyrite and bornite are two of the major sulphide minerals in the orebody.

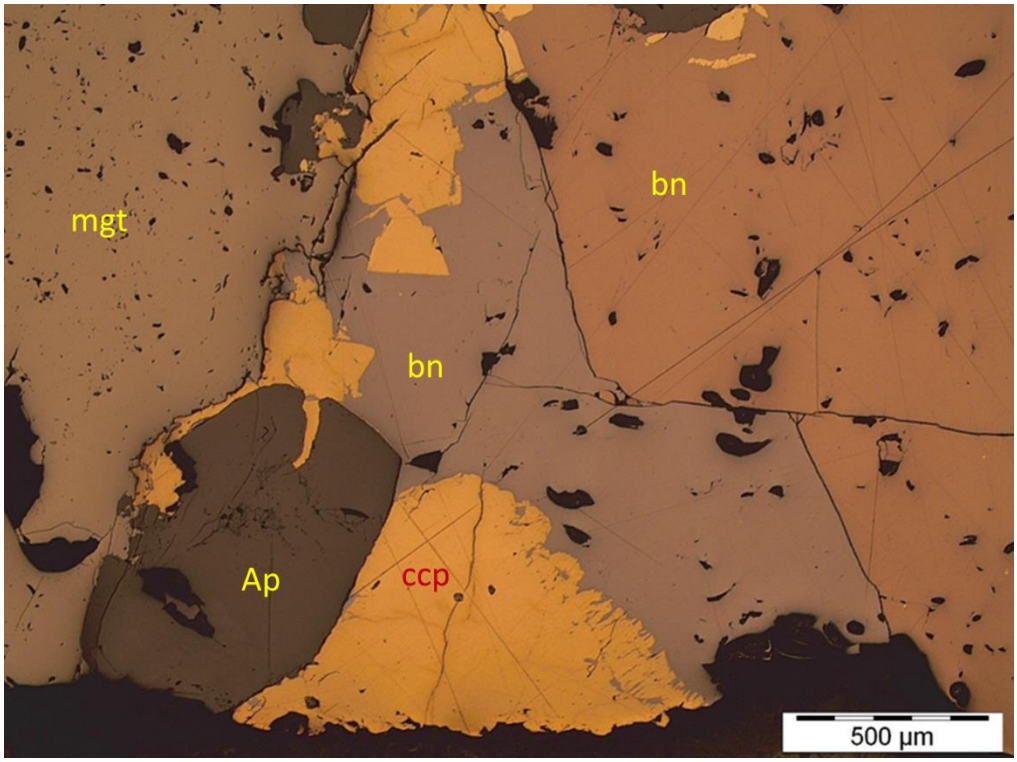

Figure 4.5: Euhedral to subhedral chalcopyrite grains replaced by bornite in large quantities. RL image, sample MT-19.

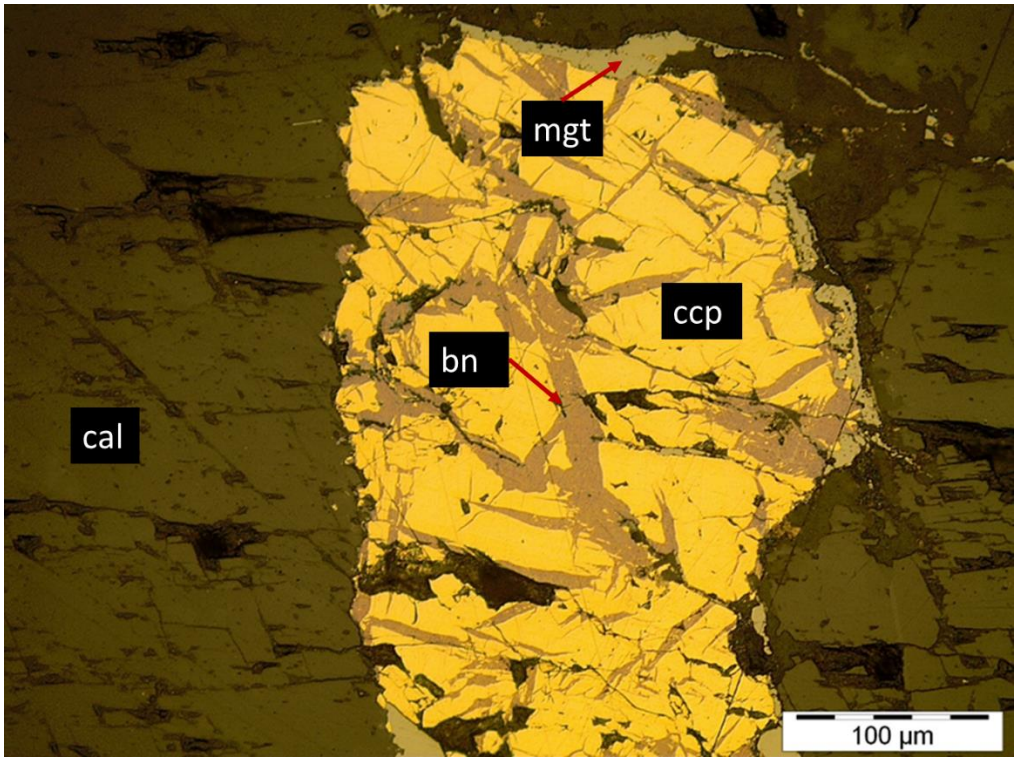

Figure 4.6: Chalcopyrite replaced by bornite flames. RL image, sample MT-40.

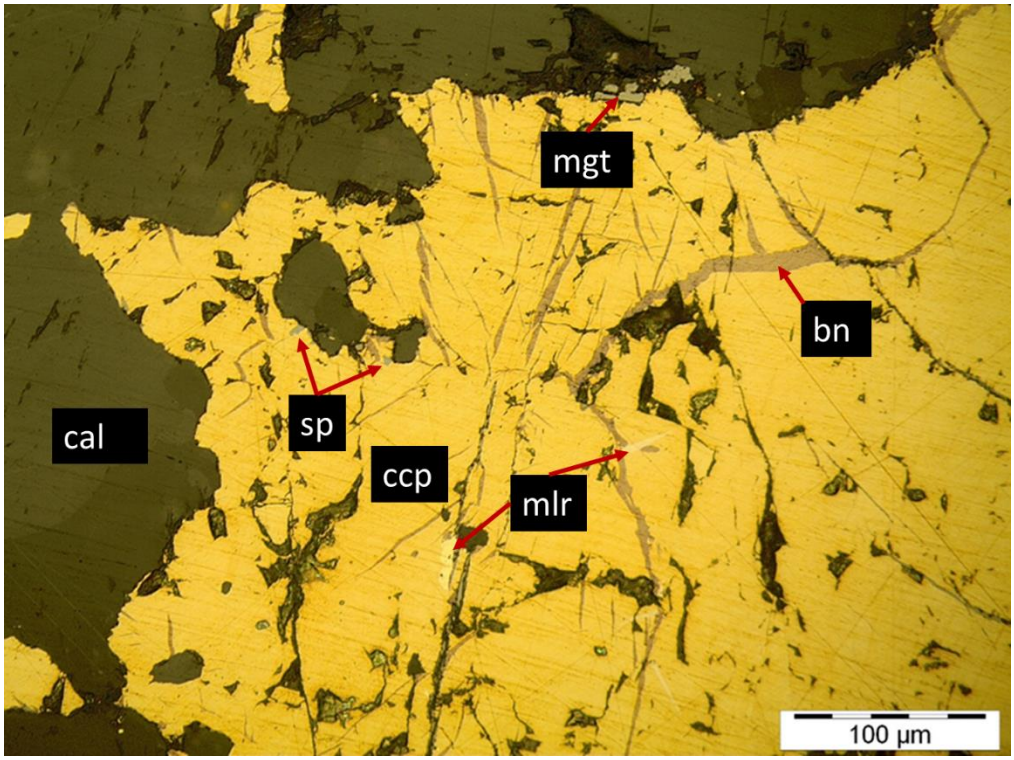

Figure 4.7: Distorted bornite bands (upper right-hand corner) and bornite flames that replaced chalcopyrite. RL image, sample MT-44.

4.1.4. Valleriite (rank: 4th).

Verwoerd (1986) describes valleriite as a graphite-like mineral containing between 18.9% and 22.9% copper. The mineral causes poor recovery due to its ability to coat other sulphide minerals, thus interfering with their flotation process (PMC Staff, 1976). Also, the recovery of pure valleriite by flotation is less than 20%, which is considerably lower than the recovery percentages of chalcopyrite (86%), cubanite (60-70%), bornite (90%), and chalcocite (90%) (Verwoerd 1986).

This late stage sulphide mineral (Figure 4.8) replaced the majority of transgressive carbonatite minerals in this study. It is also the most abundant sulphide replacement mineral. The most commonly replaced minerals by valleriite include carbonates, phlogopite, chondrodite, serpentine, magnetite, chalcopyrite, cubanite, phlogopite, and mackinawite. Minerals that show great resilience towards valleriite replacement include baddeleyite, thorianite, apatite, cobalt pentlandite, and pyrrhotite.

Certain samples (e.g. MT-27, MT-28, MT-32, MT-55, and MT-56) show extremely small amounts of sulphide mineralisation. Valleriite form the bulk of the sulphide mineralisation in these examples, with the valleriite replacing primarily gangue minerals or magnetite along cracks and fissures. Valleriite is present in both carbonatite types and in phoscorite. The yellow-brown colour of valleriite under reflected light makes it easily distinguishable from the other sulphide minerals.

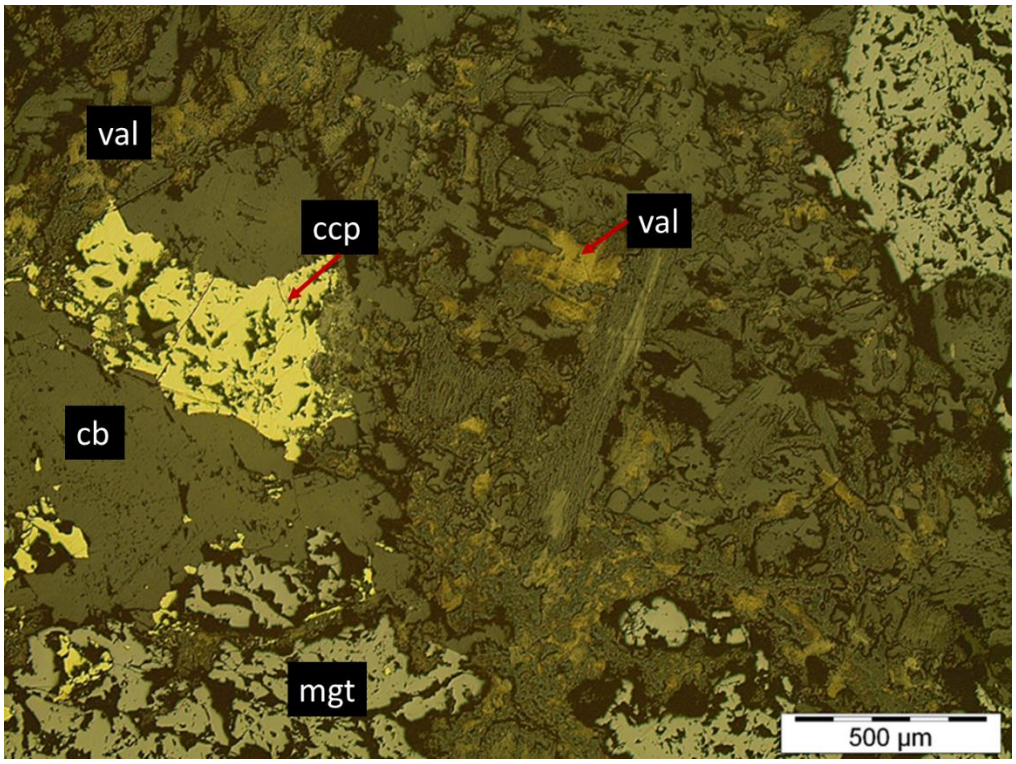

Figure 4.8: Magnetite, carbonates, and chalcopyrite replaced by valleriite. RL image, sample MT-20.

4.1.5. Cobalt pentlandite (rank: 5th).

Cobalt pentlandite (Figure 4.1) is present in the majority of the studied samples as euhedral to subhedral grains that are enclosed by chalcopyrite. The colour of these grains are light yellow under reflected light and have a higher reflectance than chalcopyrite, but they lack the intense canary yellow colour.

Cobalt pentlandite can be found sharing mutual grain boundaries with pyrrhotite, or can even be partially to completely enclosed by pyrrhotite (Figure 4.9). Cobalt pentlandite grains are also occasionally found clustered together (Figure 4.10). The association between cobalt pentlandite and pyrrhotite is the strongest of all the sulphide mineral associations found in this study, but a great deal of examples do exist were cobalt pentlandite grains occur without the presence of pyrrhotite.

This sulphide mineral shows a great manner of resilience towards replacement, which is indicated by its sharp crystal faces. However, the sharp crystal faces of this mineral may be deceiving in certain scenarios, seeing that fractures form parallel to the sharp crystal faces. This gives the impression of a “still euhedral” grain, even when chunks of the original grain have been removed. In almost all the observed grains, excluding the cobalt pentlandite grains being enclosed by pyrrhotite, chalcopyrite has cut the cleavages of this mineral.

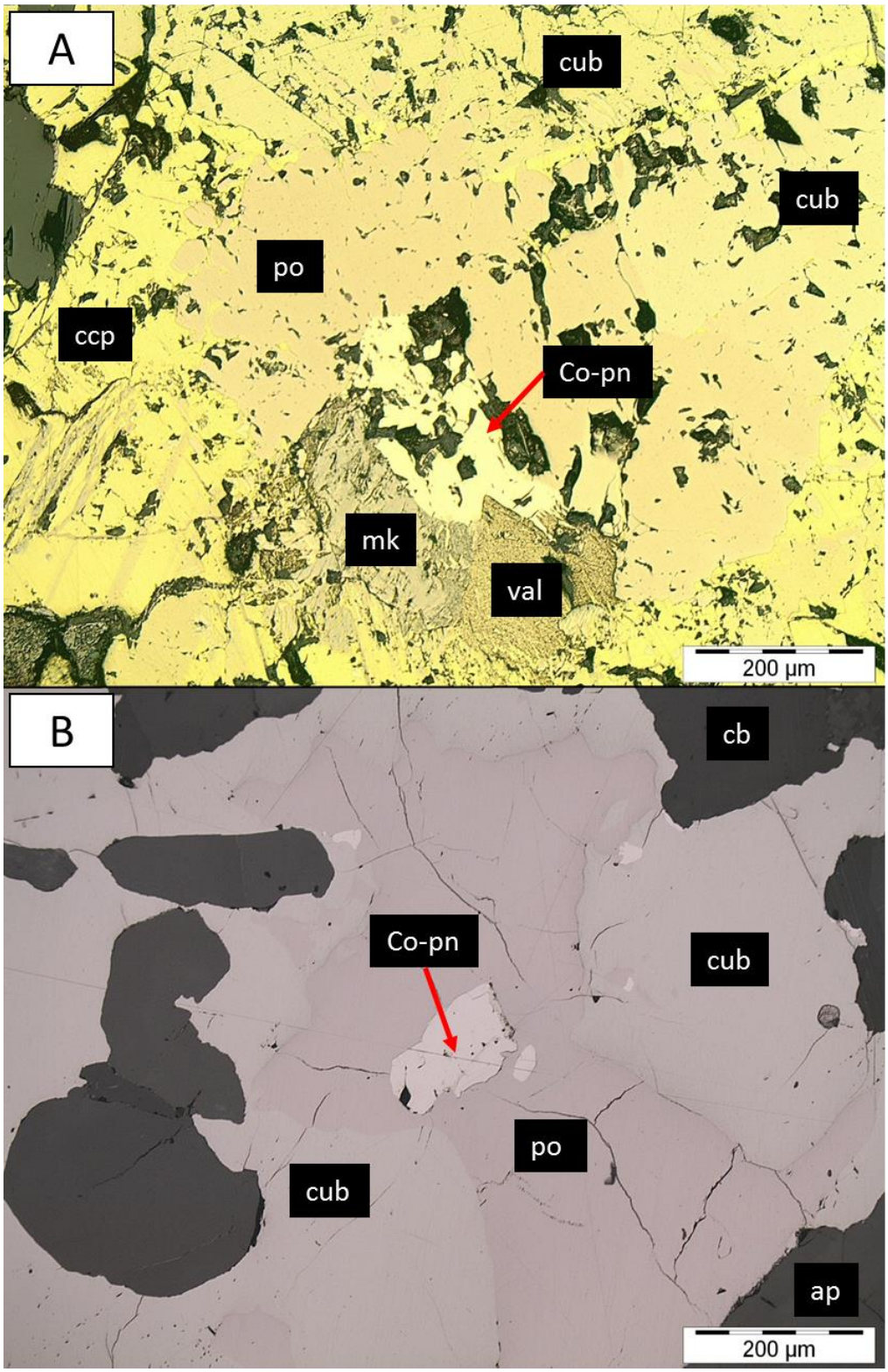

Figure 4.9: A) Cobalt pentlandite partially enclosed by pyrrhotite. Cobalt pentlandite replaced by mackinawite and chalcopyrite. Chalcopyrite replaced by mackinawite. Mackinawite replaced by valleriite. RL image, sample MT-7. B) Cobalt pentlandite completely enclosed by pyrrhotite. Cobalt pentlandite replaced by pyrrhotite. Cobalt pentlandite and pyrrhotite replaced by cubanite. RL image with blue lens, sample MT-3.

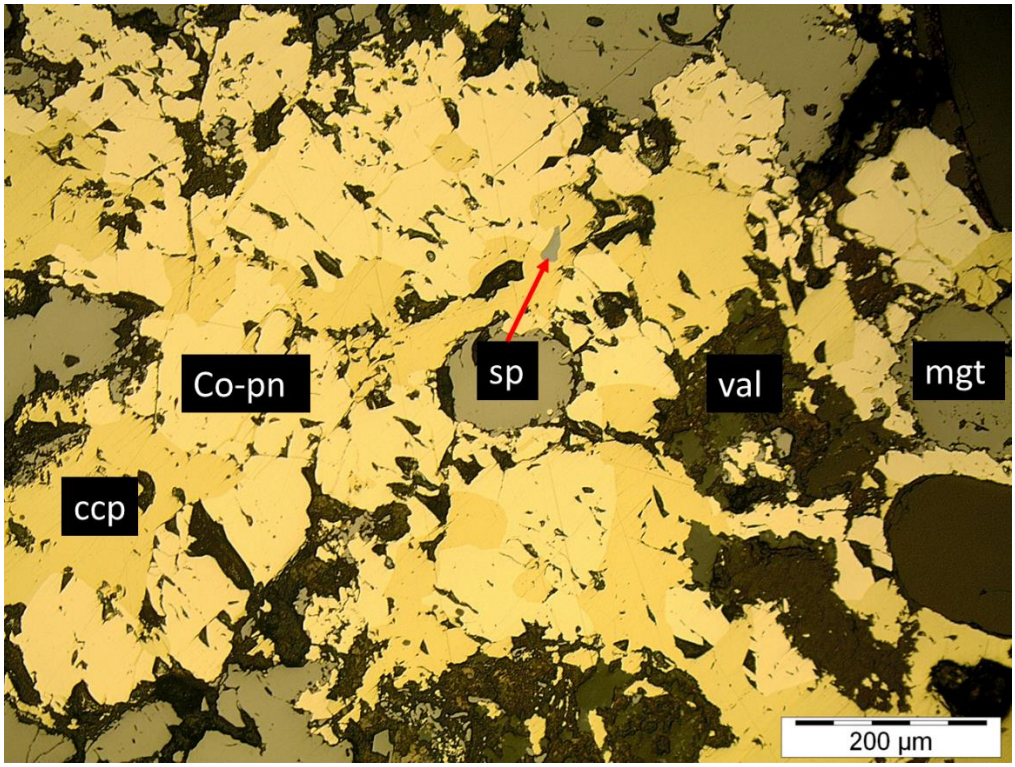

Figure 4.10: Cobalt pentlandite grains clustered together. Chalcopyrite crystallised from interstitial liquid. Magnetite replaced by cobalt pentlandite and chalcopyrite. Cobalt pentlandite, chalcopyrite, and magnetite replaced by valleriite. RL image, MT-58.

4.1.6. Pyrrhotite (rank: 6th).

Pyrrhotite grains are present in the majority of the samples as irregularly shaped granules that are enclosed by chalcopyrite (Figure 4.1; Figure 4.9, A). These grains are also occasionally clustered together (Figure 4.11). Pyrrhotite has a dark pink colour under reflected light, which makes it easily distinguishable from cubanite. It also exhibits stronger bireflectance compared to cubanite.

Pyrrhotite is rarely found not sharing any spatial relationship with cobalt pentlandite, unlike cobalt pentlandite that may be found on its own. This mineral also shows strong resistance towards replacement by other sulphide minerals. However, the replacement of pyrrhotite and cobalt pentlandite by cubanite (not lathed) is common in certain samples. Replacement by cubanite formed remnant streaks/bands of these two minerals as a result (Figure 4.12).

Pyrrhotite is mostly present in greater amounts than cobalt pentlandite, where both minerals are present in the same sample. However, cobalt pentlandite is more commonly found within the samples compared to pyrrhotite, thus giving cobalt pentlandite a higher rank than pyrrhotite.

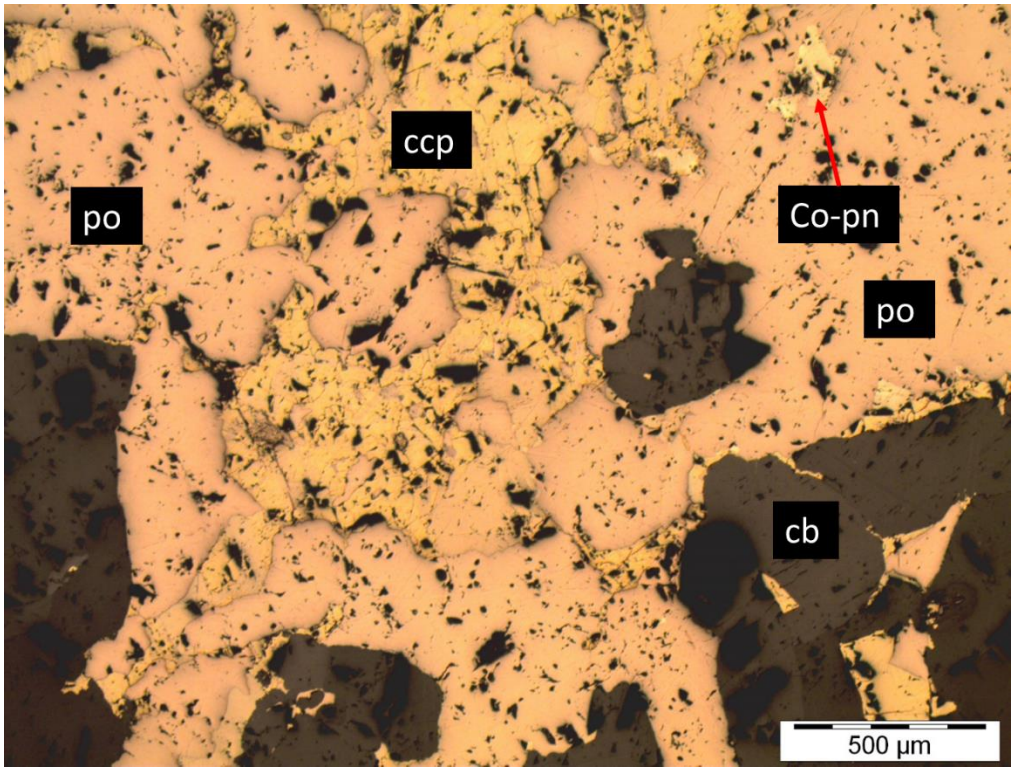

Figure 4.11: Pyrrotite grains clustered together. Chalcopyrite crystallised from interstitial liquid. RL image, MT-5.

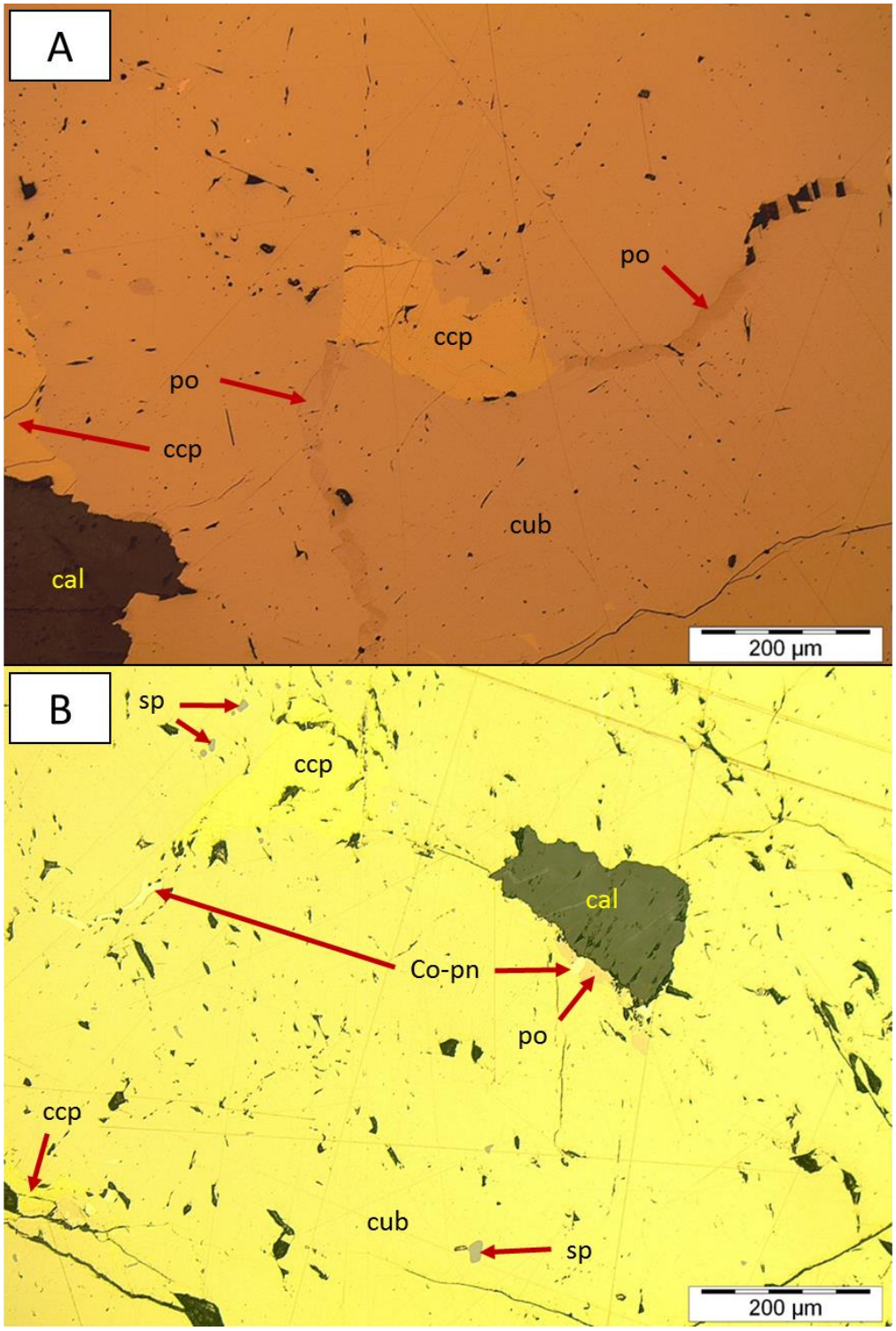

Figure 4.12: A) Pyrrhotite streaks formed due to cubanite replacement. RL image, sample MT-35. B) Remnant pyrrhotite and cobalt pentlandite formed as a result of cubanite replacement. Also showing the formation of anhedral sphalerite grains. RL image, sample MT-38.

4.1.7. Chalcocite (rank: 8th).

Chalcocite shows a very strong association with bornite. The mineral replaced bornite in very small amounts at grain boundaries as very small anhedral bodies (Figure 4.13). Chalcocite also formed symplectic intergrowths (Figure 4.14) with bornite. In less common associations, this sulphide mineral occurs as veins of varying sizes that formed from sulphide-non-sulphide grain boundaries, or from fractures within the sulphide mineral fabric. The mineral is rarely present as a replacement product of chalcopyrite. The light blue colour of chalcocite under reflected light makes it very easily distinguishable from the other sulphide minerals.

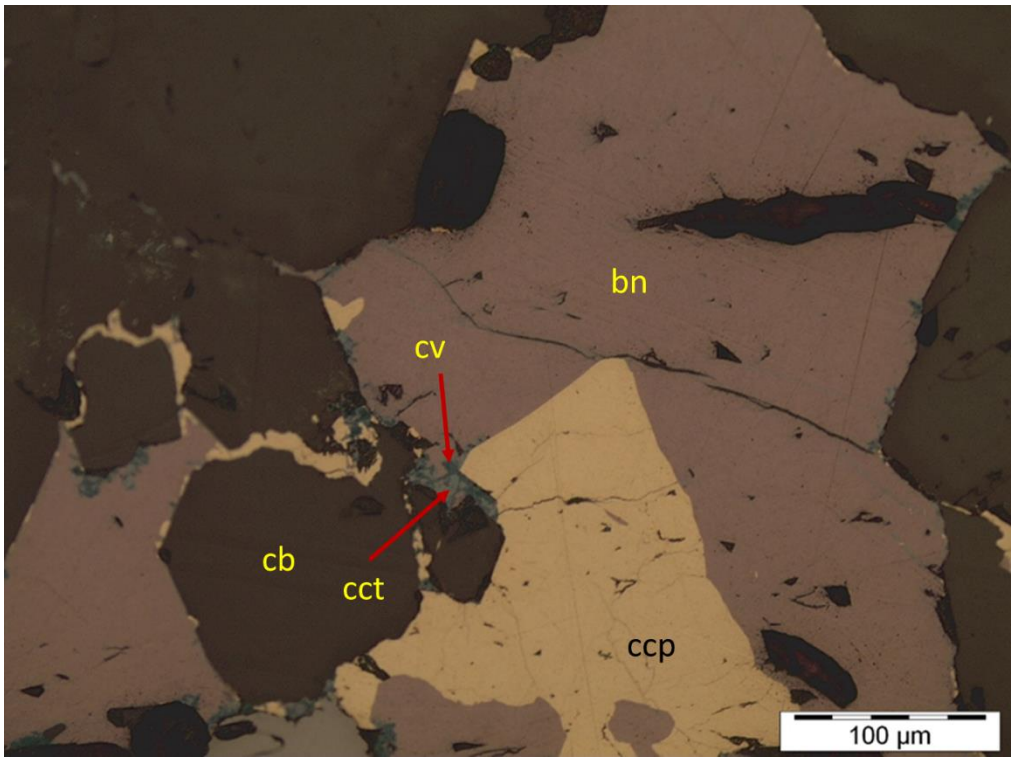

Figure 4.13: Showing the replacement of bornite by chalcocite (light blue), and the replacement of chalcocite by covelline (dark blue). RL image, sample MT-16.

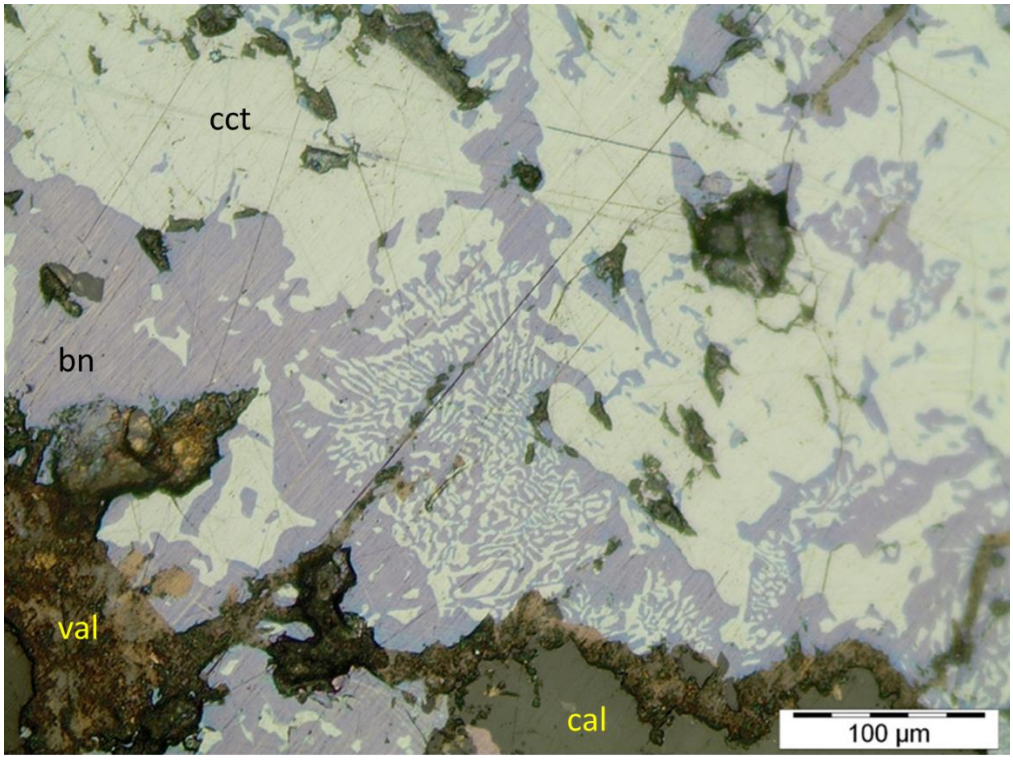

Figure 4.14: Symplectic intergrowth texture between bornite and chalcocite. RL image, sample MT-55.

4.1.8. Sphalerite (rank: 9th).

Two variations of sphalerite are present in this study. This less common sulphide mineral either exists as larger euhedral to subhedral grains, with or without chalcopyrite inclusions (Figure 4.15), and as smaller anhedral grains with no chalcopyrite inclusions (Figure 4.12). The smaller grains show a very strong association towards cubanite laths, and it mainly formed from pitted areas. The larger grains do not show any association towards a specific sulphide mineral. Instead, it only shows a spatial relationship towards sulphide-non-sulphide grain boundaries from which it formed. The dark blue-grey colour of sphalerite makes it easily distinguishable from other sulphide minerals.

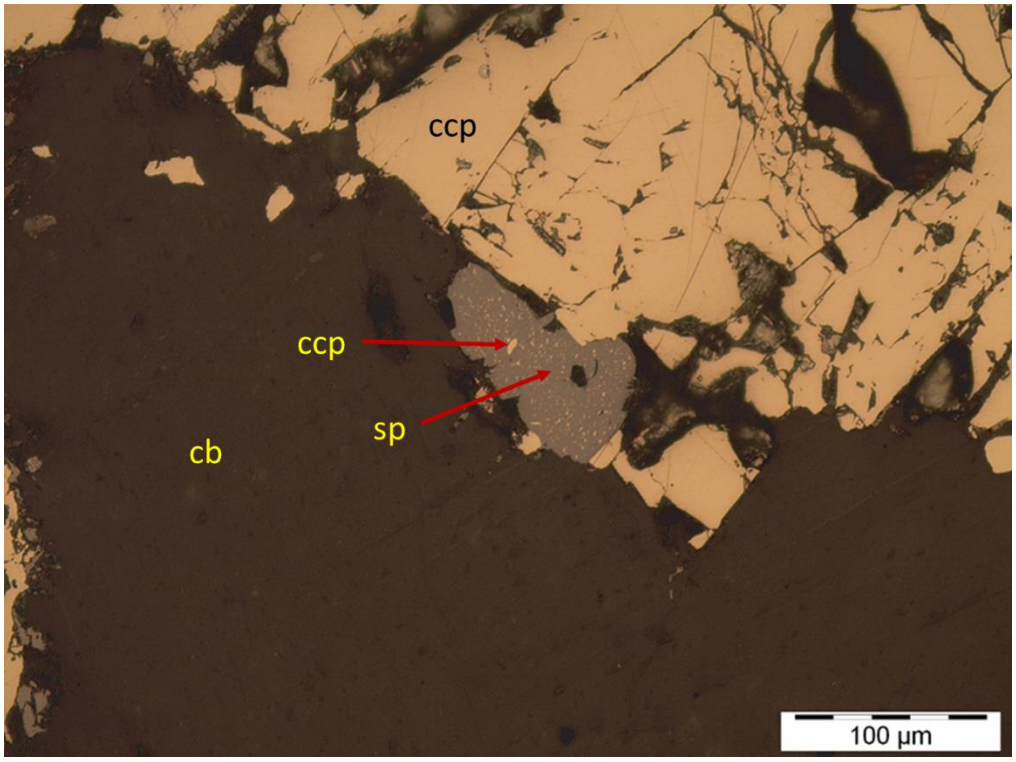

Figure 4.15: Subhedral to euhedral sphalerite grain with chalcopyrite inclusions. RL image, sample MT-23.

4.1.9. Mackinawite (rank: 10th).

Mackinawite was first discovered in platinum-bearing basic and ultrabasic rocks of the Bushveld Complex (Transvaal Basin, South Africa) (Schot *et al.,* 1972). This less common, mostly anhedral sulphide mineral (Figure 4.1; Figure 4.9, A) shows a strong replacement association towards pentlandite. Replacement of chalcopyrite by mackinawite is also common, while cobalt pentlandite replacement is rarer. The mineral is rarely found not showing any association towards fractured zones. Mackinawite is easily distinguishable from other sulphide minerals due to its purple colour under reflected light. The mineral also exhibits strong bireflectance.

4.1.10. Millerite (rank: 11th).

Millerite exists as a subhedral to anhedral replacement phase of chalcopyrite and bornite (Figure 4.16) at fracture zones associated with magnetite veinlets. Its cream to light yellow

bireflectance and strong yellow to blue anisotropy makes it easily distinguishable from the other sulphide minerals.

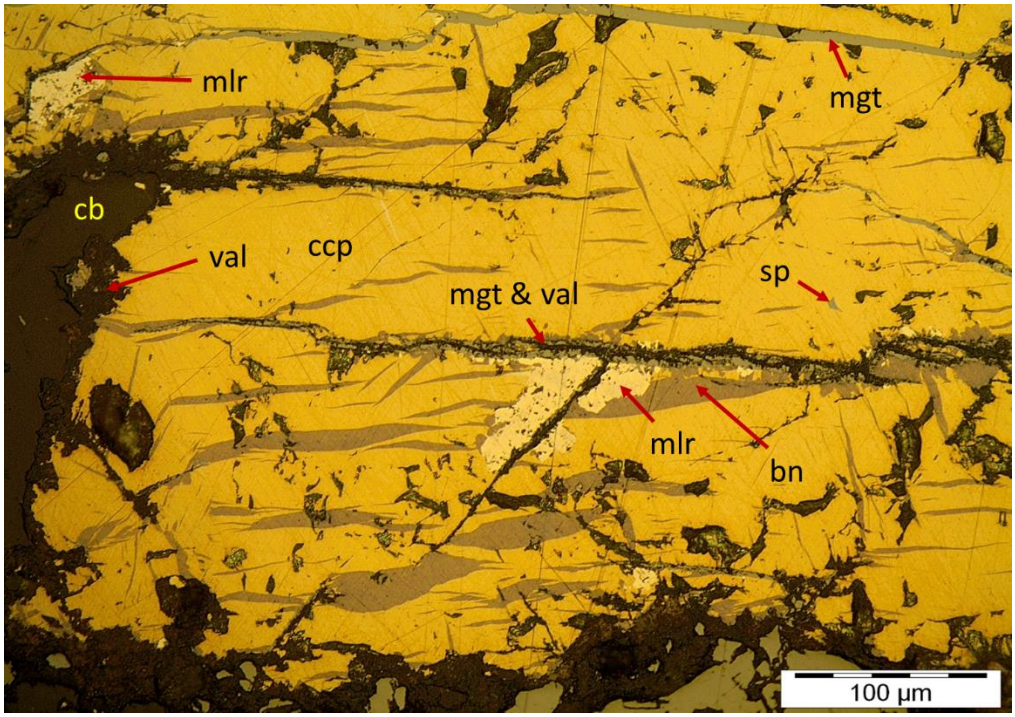

Figure 4.16: Millerite replacing bornite from magnetite-filled fractures. RL image, sample MT-44.

4.1.11. Covelline (rank: 14th). Covelline only exists as a replacement product of small anhedral chalcocite grains (Figure 4.13). The chalcocite in this chalcocite-covelline association only replaced bornite at bornite-chalcopyrite, or bornite-non-sulphide grain boundaries. The dark blue colour of covelline under reflected light and its orange anisotropy under cross-polarised light makes it easily distinguishable from the other sulphide minerals.

4.2. Scanning electron microscopy results.

In this study, which links and compares mineral chemistry with different textures of sulphide minerals of the same and different kind, a thorough SEM-EDS investigation was needed to identify the slightest differences.

Appendix C represents the mineral chemical compositions obtained via SEM-EDS for each sulphide mineral identified via reflected light microscopy. Additional textural data is provided in brackets in certain cases in order to compare the mineral chemistry of texturally similar and different sulphide minerals.

4.2.1. Sulphide minerals primarily identified via scanning electron microscopy.

Some uncertainty remained during the identification of certain sulphide minerals during the reflected light microscopy stage. These minerals were carefully studied via SEM-EDS. This method, combinded with the optical properties of these sulphide minerals, provided the necessary information in order to update Table B.1.

a) X-bornite (rank: 7th):

X-bornite (Appendix C, Table C.3) represents an intermediate phase between chalcopyrite and bornite. It exists as exsolution flames that are restricted to bornite (Figure 4.17). In many cases these flames can be larger than bornite flames. Its strong association towards the third most abundant sulphide mineral does not make it too uncommon. This texture is present in both carbonatite types. The orange colour of x-bornite under reflected light makes it easily distinguishable from the other sulphide minerals.

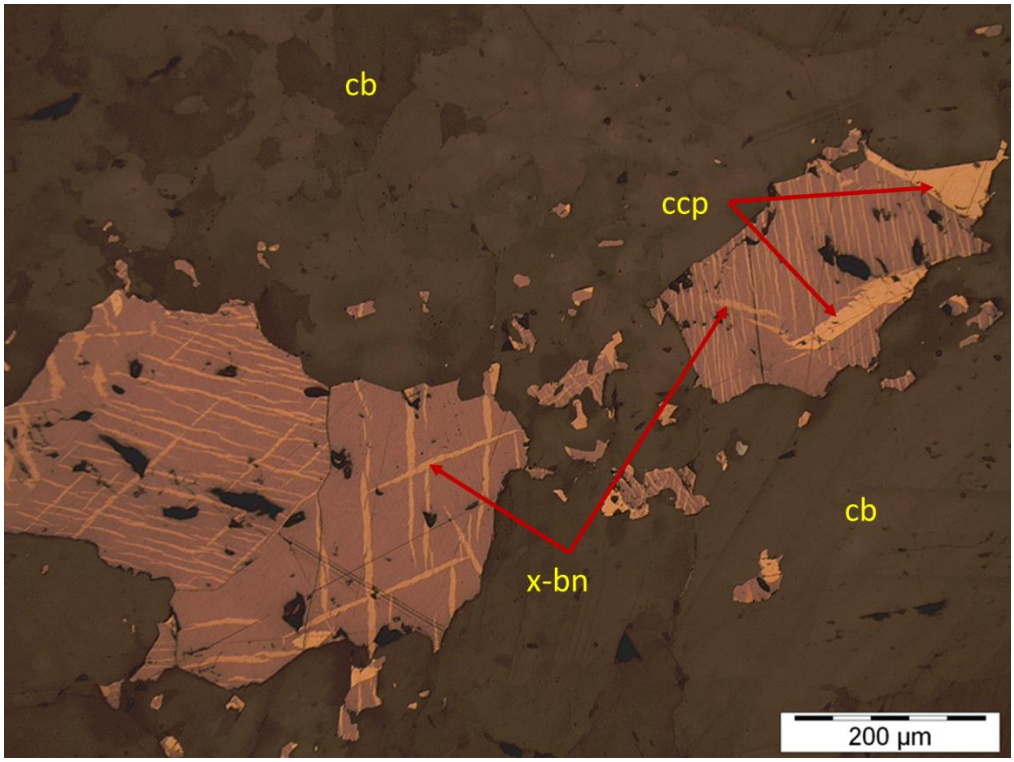

Figure 4.17: X-bornite exsolution flames in bornite. Bornite replaced chalcopyrite. RL image, sample MT-52.

b) Pentlandite (rank: 12th):

This uncommon flame-like sulphide mineral (Appendix C, Table C.4) shows a very strong association towards fractured areas within the sulphide mineral fabric, just like mackinawite and millerite. As mentioned before, a strong replacement association exists between this mineral and mackinawite, with mackinawite being the replacing phase (Figure 4.18). The light cream colour of pentlandite under reflected light makes it easily distinguishable from the light yellow colour of cobalt pentlandite. Its isotropic nature makes it easily distinguishable from millerite.

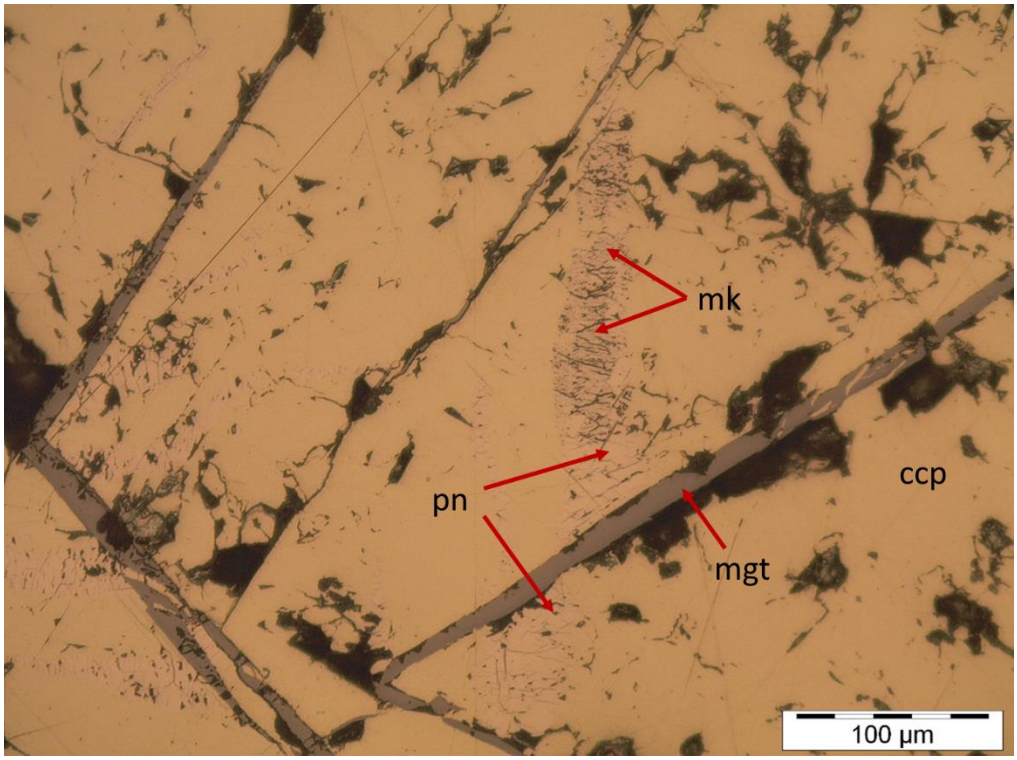

Figure 4.18: Flame-shaped pentlandite grains replaced by mackinawite. RL image, sample MT-23.

c) Galena (rank: 13th):

Galena is an extremely rare, Pb-rich sulphide mineral with respect to the studied samples. Galena (Appendix C, Table C.1) exists in very small amounts between the boundaries of bornite and chalcopyrite grains in the majority of cases (Figure 4.19). The existence of the mineral at chalcopyrite-non-sulphide grain boundaries (Figure 4.20) is even rarer, although these grains are larger than those found at chalcopyrite-bornite grain boundaries. The bornite in this association exists as a replacement phase of chalcopyrite. The white to light-grey colour of galena under reflected light and its isotropic nature makes it easily distinguishable from the other sulphide minerals.

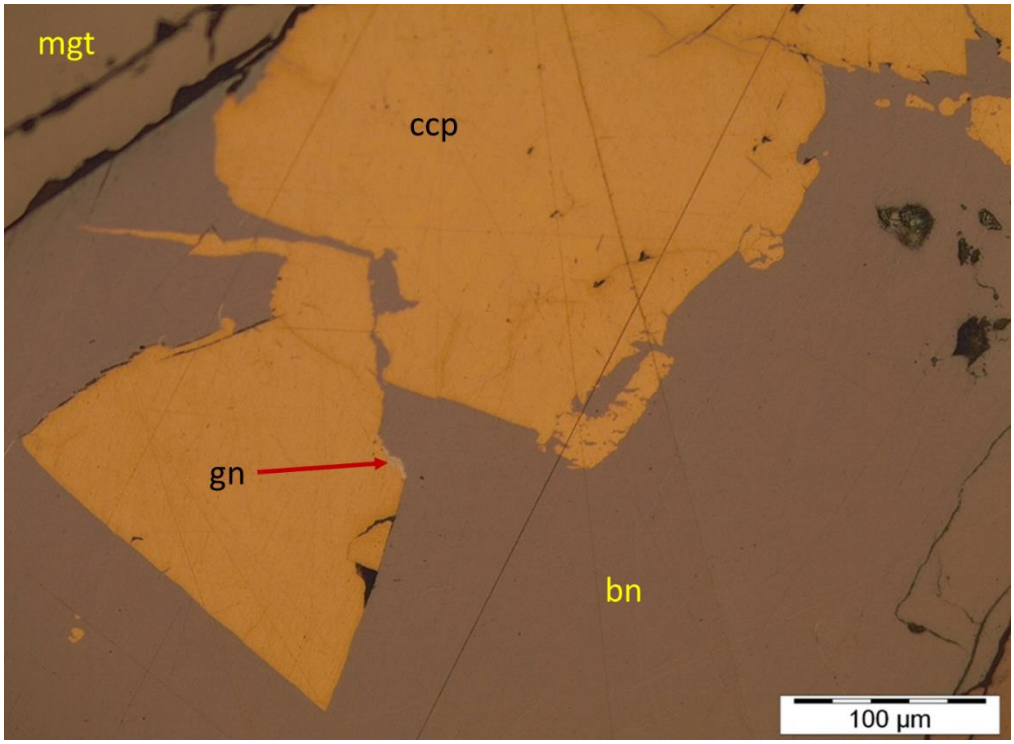

Figure 4.19: Galena formation at chalcopyrite-bornite boundary. RL image, sample MT-19.

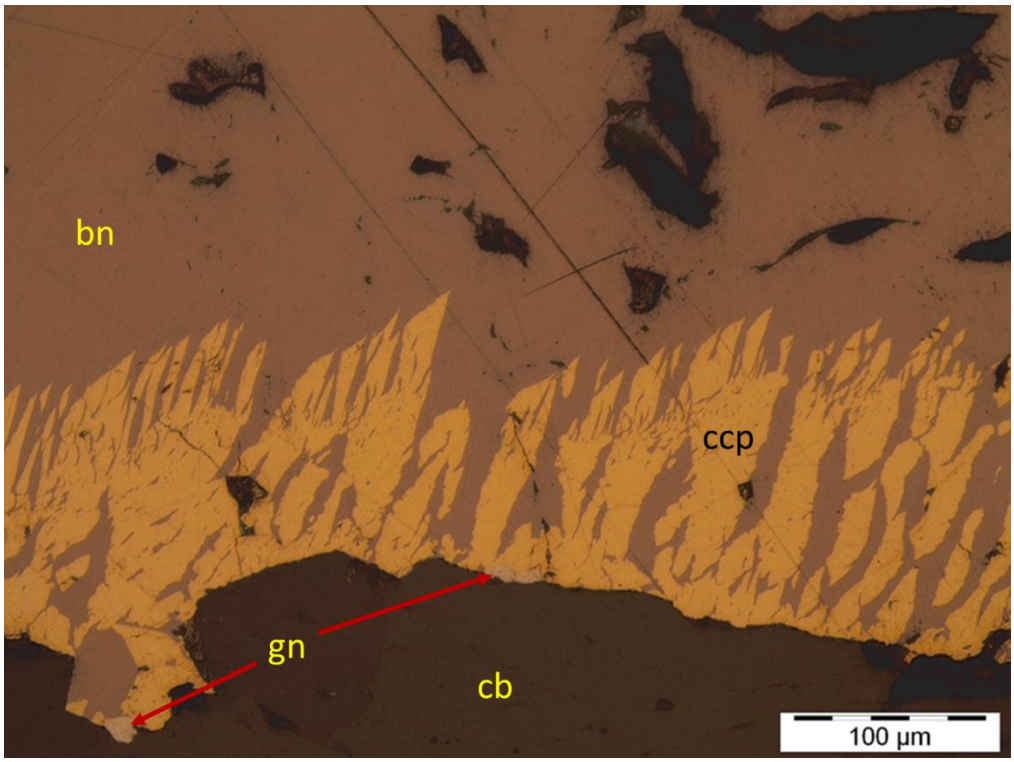

Figure 4.20: Galena formation at sulphide-non-sulphide grain boundaries. RL image, sample MT-19.

d) Heazlewoodite (rank: 15th):

Heazlewoodite (Appendix C, Table C.1) is extremely rare. Only a handful of grains were found in one sample (MT-58) during this study. These grains show some relationship to the fractures in which magnetite veinlets occur (Figure 4.21). However, these grains are cut by the magnetite veinlets. Heazlewoodite can also be found completely isolated, just surrounded by chalcopyrite. This sulphide mineral is light yellowish-creamy under reflected light. The strong brown to bluish-grey anisotropy of heazlewoodite makes it easily distinguishable from millerite.

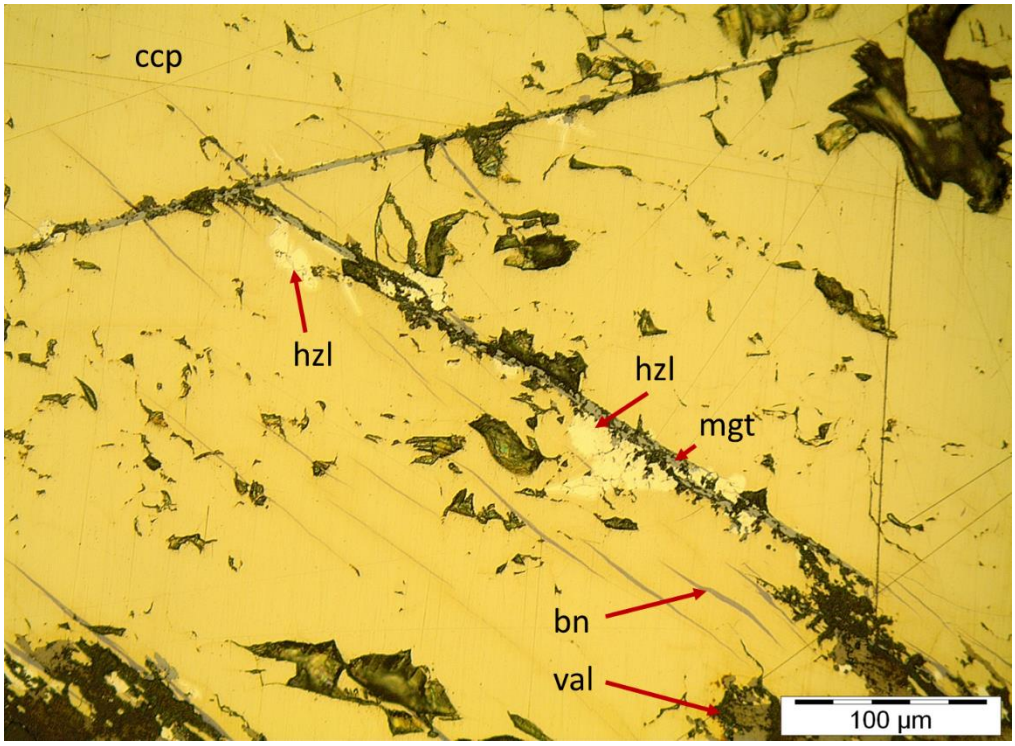

Figure 4.21: Chalcopyrite replaced by heazlewoodite in close proximity to magnetite veinlets. RL image, sample MT-58.

e) Shandite (16th):

Shandite (Appendix C, Table C.1) is even rarer than heazlewoodite. Only two grains were found in this study (MT-15). Both grains are pseudocubic and strongly euhedral. The grains only show a formational association within large chalcocite veins (Figure 4.22; Figure 4.23 and Figure 4.24). To the best of our knowledge, neither heazlewoodite nor shandite have previously been reported from this area.

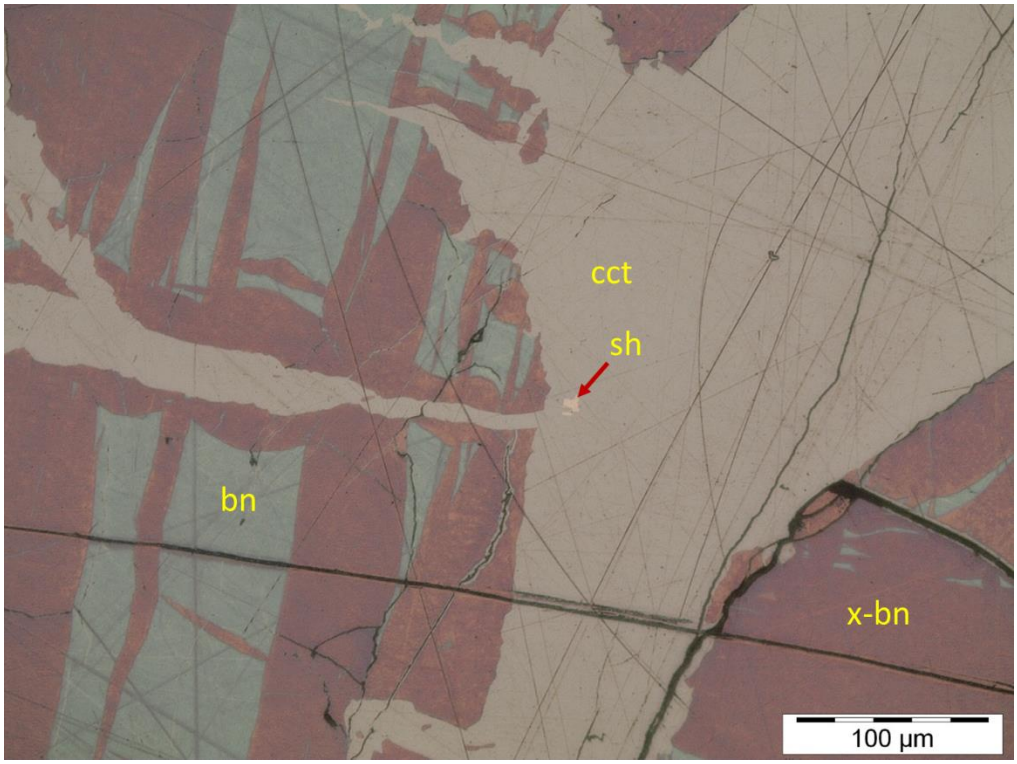

Figure 4.22: Shandite within a large chalcocite vein. X-bornite exsolution intergrowths within bornite. Bornite and x-bornite replaced by chalcocite. Bornite replaced by x-bornite. RL image, sample MT-15.

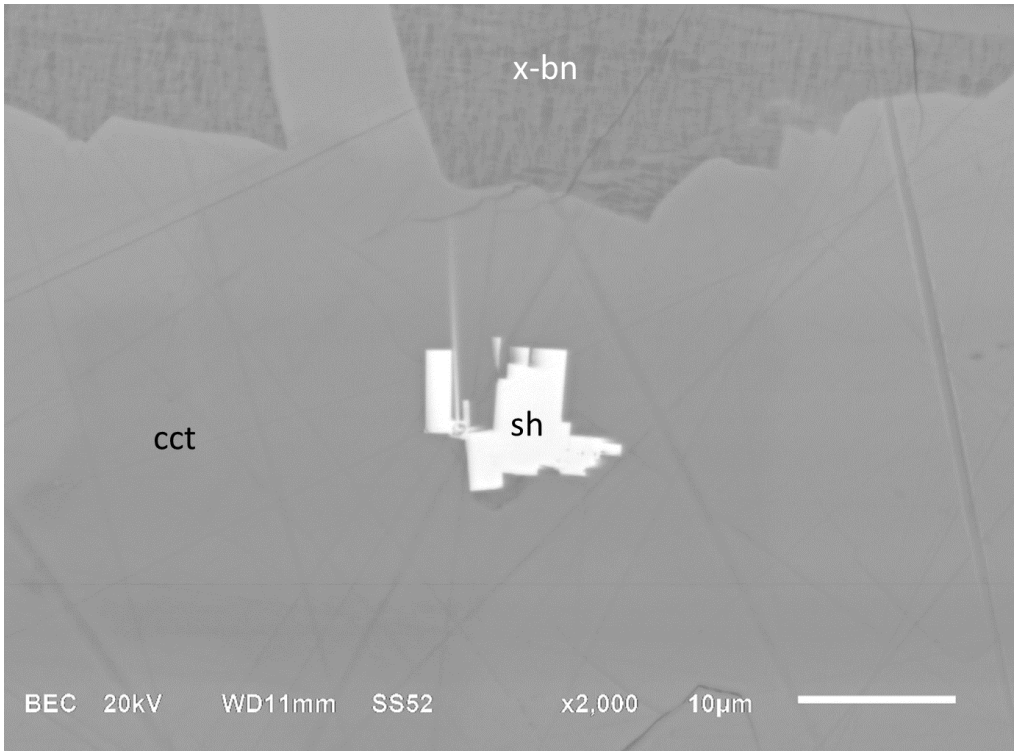

Figure 4.23: Image showing the euhedral shape of a shandite grain. Back-scattered electron (BSE) image, sample MT-15.

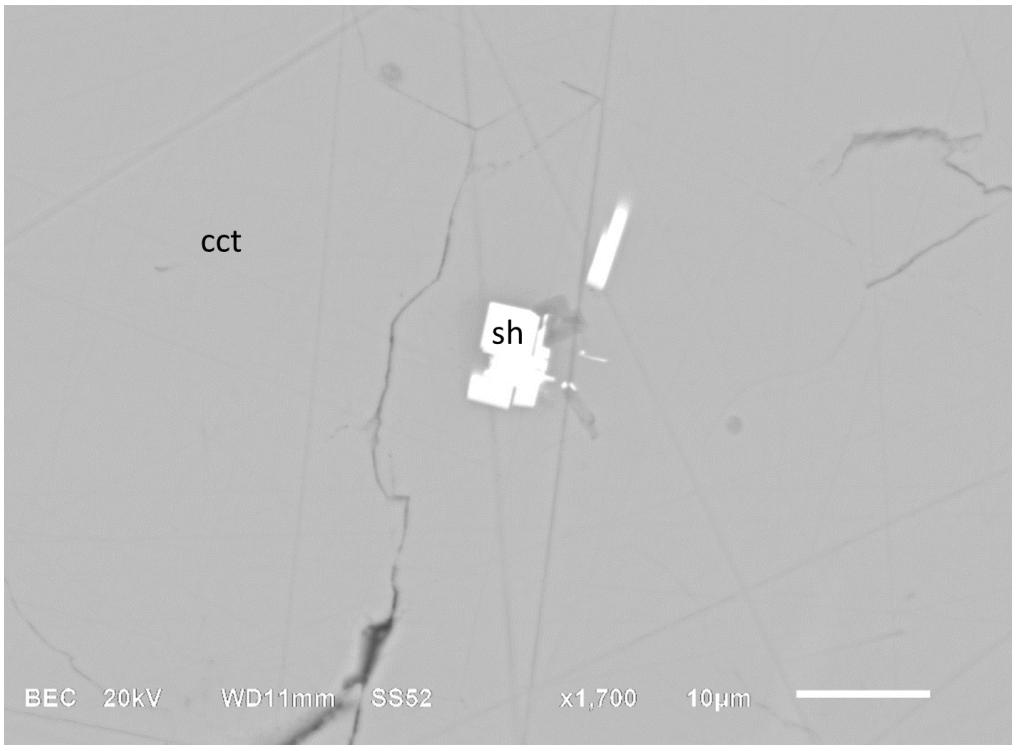

Figure 4.24: The euhedral, pseudocubic shape of a shandite grain. BSE image, sample MT-15.

4.2.2. Geochemical and textural data obtained via SEM.

An attempt was made to gather SEM-EDS data in order to identify the variations in major and minor elemental percentages/concentrations of the same type of mineral(s), with the same or with differing textural and physical properties. These distinguishable features will be categorised later on.

The majority of the chalcopyrite analyses (Appendix C, Table C.5) remained constant for a wide range of samples, with Cu falling within a range of 32.20 wt.% to 33.50 wt.% . However, anomalies/outliers were detected from MT-16, MT-19, and MT-49. These samples indicated two different "shadings" of chalcopyrite (lighter and darker using SEM) relative towards each other (Figure 4.25). The "darker" chalcopyrite exsolved from the "lighter" chalcopyrite.

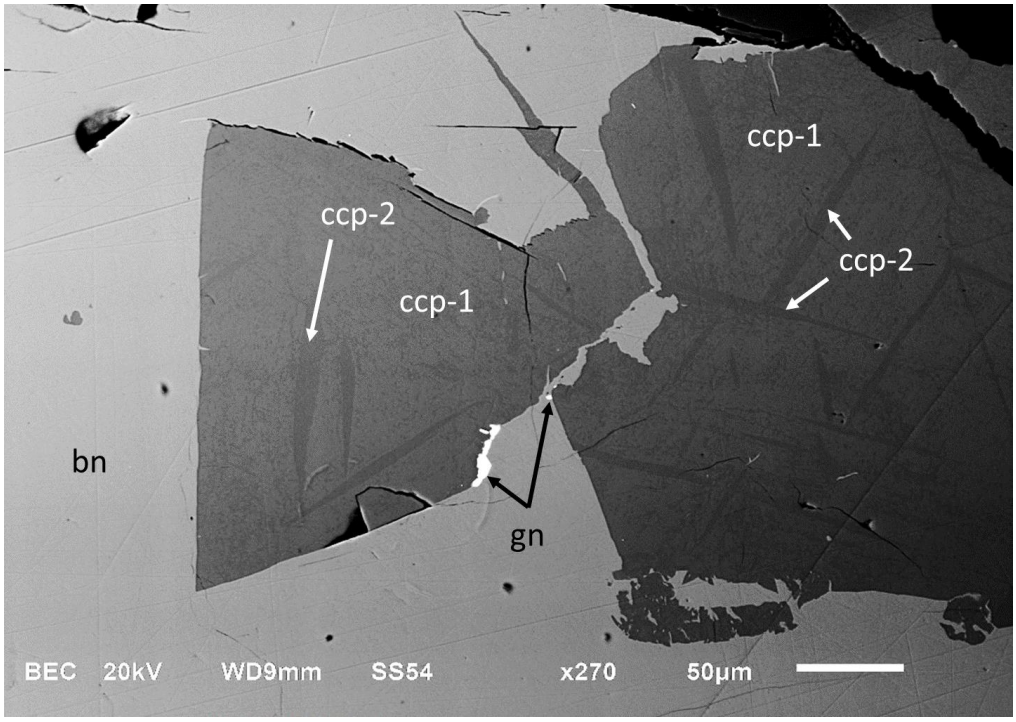

Figure 4.25: Chalcopyrite exsolution (ccp-2; darker using SEM) from chalcopyrite (ccp-1; lighter using SEM). Chalcopyrite replaced by bornite. Galena formed at bornite-chalcopyrite boundaries. BSE image, sample MT-19.

The different shadings are also coupled to noticeable variations in major elemental amounts (Figure 4.26), with the "lighter" chalcopyrite (35.98 wt.% to 37.26 wt.% Cu) having higher

amounts of Cu compared to the “darker” chalcopyrite (33.21 wt.% to 33.87 wt.% Cu). This led to the conclusion that two variations of chalcopyrite were identified in this study, with both phases showing contents which would categorise them as chalcopyrite. The “darker” exsolution of another chalcopyrite phase can, however, not reflect an early stage of bornite formation, seeing that a decrease in Cu was observed, instead of an increase. These two variations of chalcopyrite are not distinguishable via reflected light microscopy.

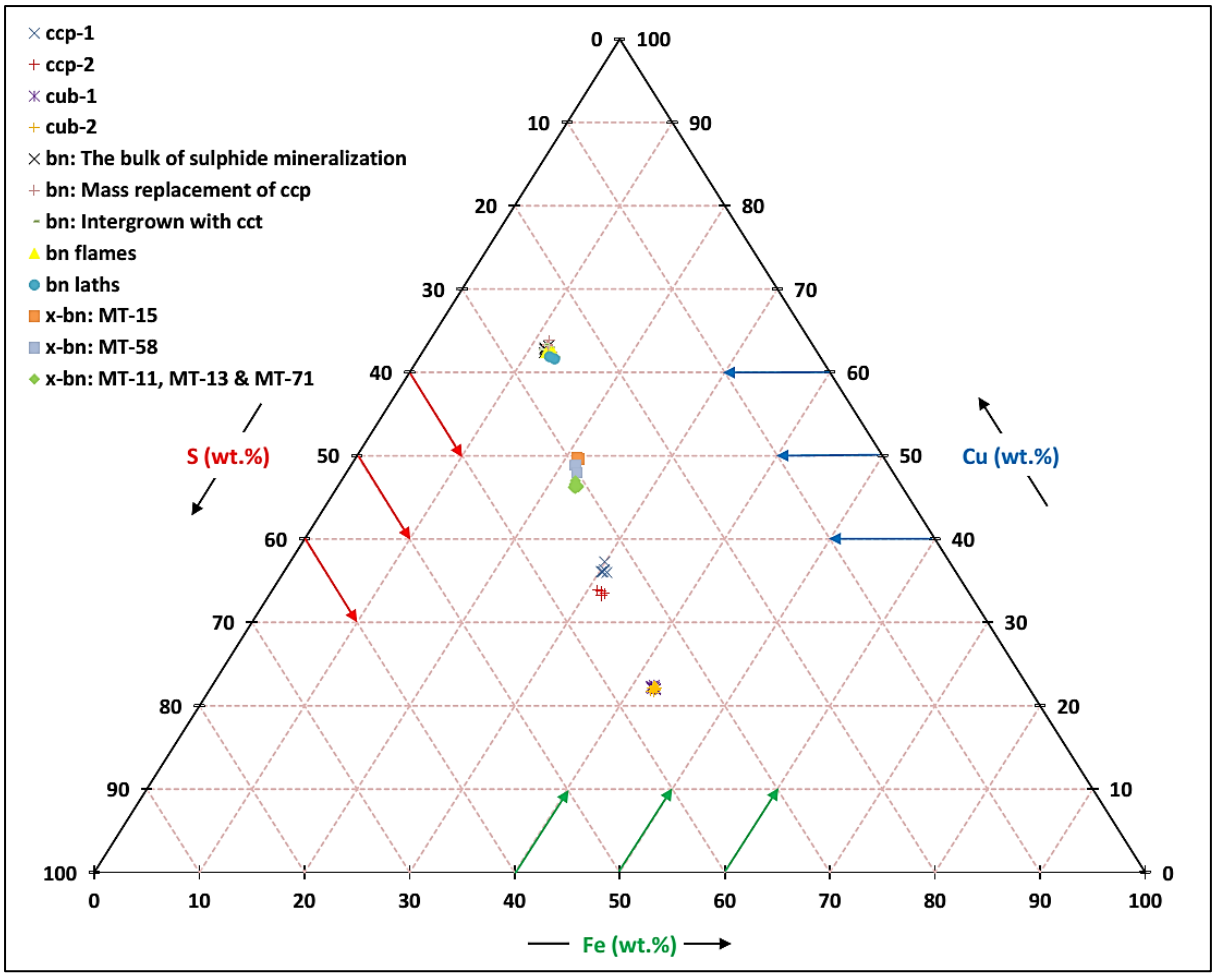

Figure 4.26: Compositions of chalcopyrite (first (ccp-1) and second (ccp-2) generation), cubanite (first (cub-1) and second (cub-2) generation), bornite, and x-bornite from transgressive carbonatite. The guideline arrows (green, blue, and red) are also applicable to the other ternary diagrams.

A similar anomaly and noticeable variations in major elemental amounts were identified within certain pyrrhotite grains (Appendix C, Table C.6), e.g. MT-3 and MT-58. However, in this case, the “lighter” pyrrhotite replaced the “darker” pyrrhotite by dissecting it into wave-formed bands (Figure 4.27).

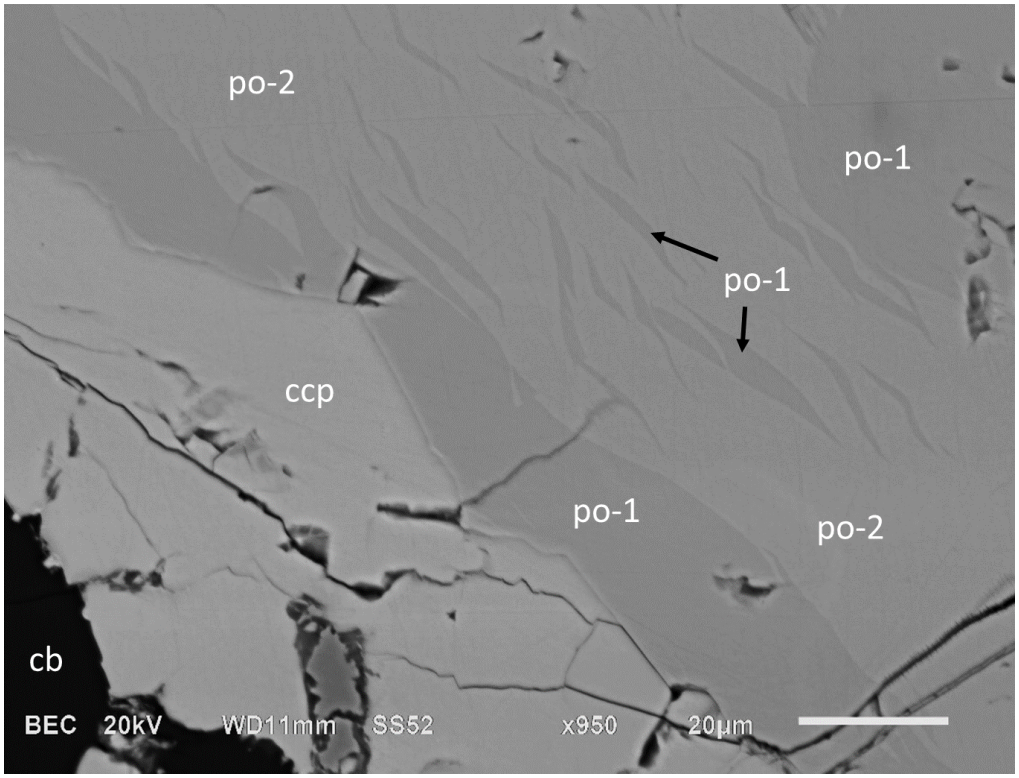

Figure 4.27: Pyrrhotite (po-1; darker using SEM) replaced by pyrrhotite (po-2; lighter using SEM). BSE image, sample MT-60.

“Lighter” pyrrhotite (63.79 wt.% to 64.07 wt.% Fe) has more Fe compared to “darker” pyrrhotite (61.74 wt.% to 61.81 wt.% Fe; Figure 4.28). The former also replaced chalcopyrite by breaking the chalcopyrite up into linear segments (Figure 4.29). The two variations of pyrrhotite are difficult to detect via reflected light microscopy alone. In fact, the texture might even be overlooked as bireflectance.

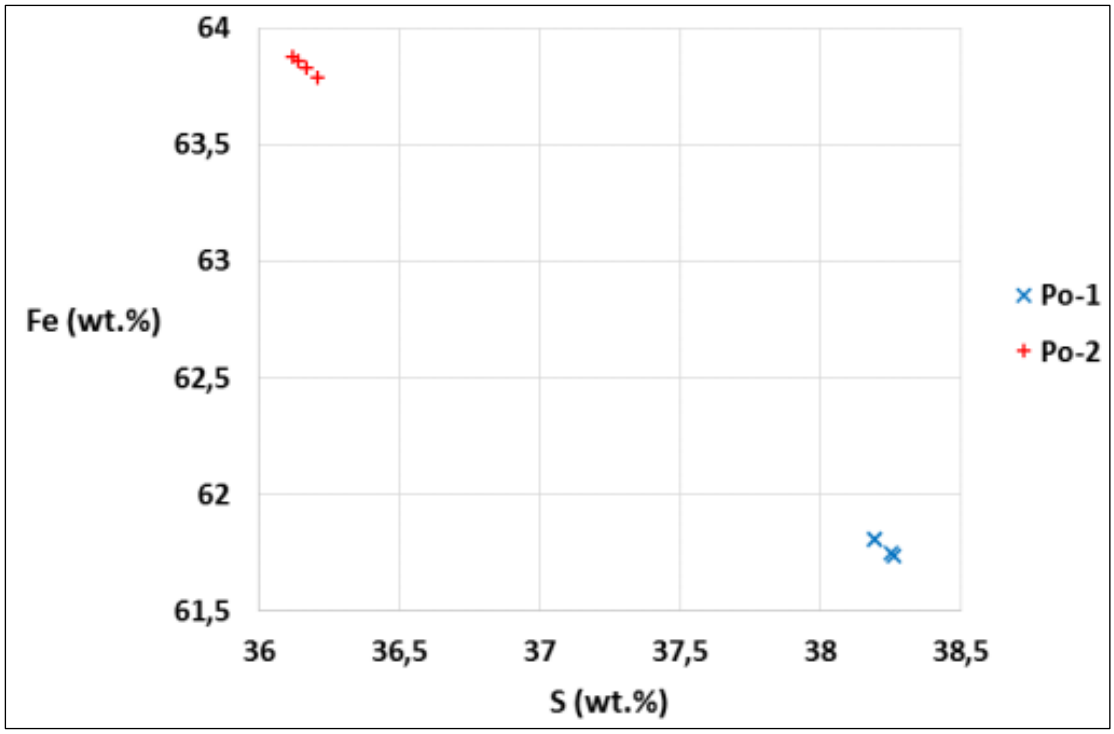

Figure 4.28: Compositions of first (po-1) and second (po-2) generation pyrrhotite from transgressive carbonatite.

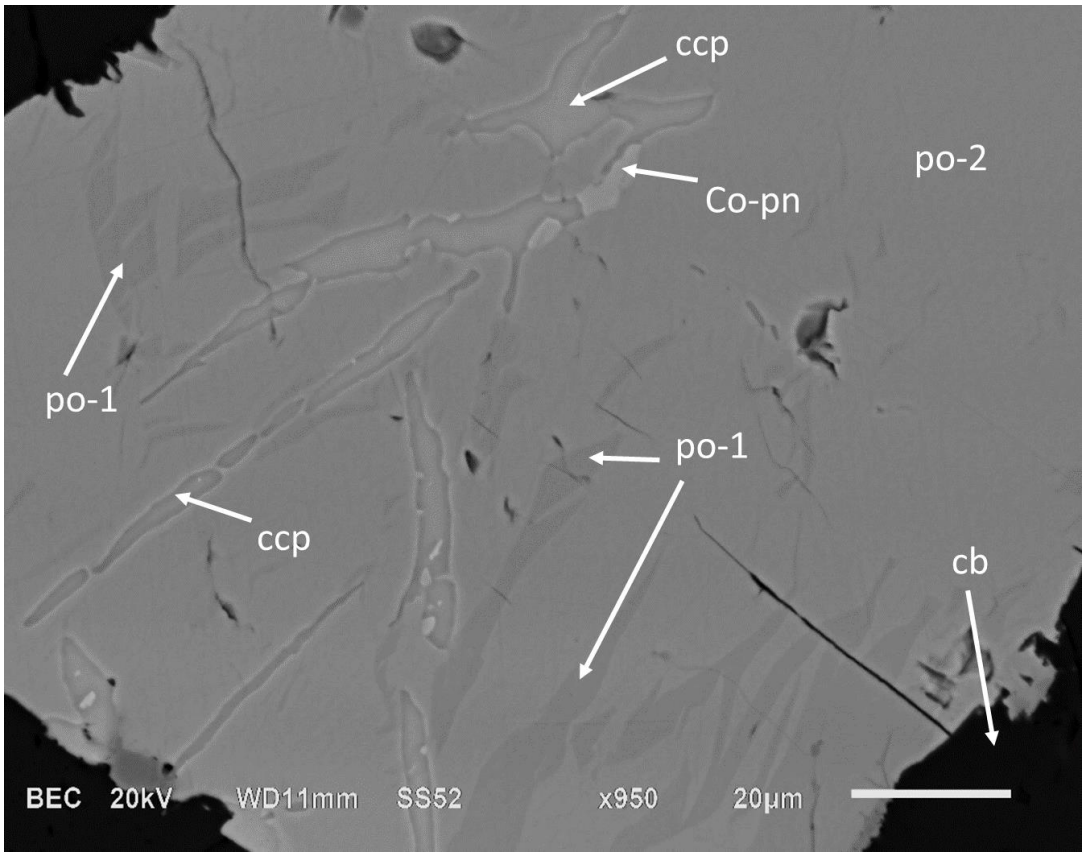

Figure 4.29: Chalcopyrite and pyrrhotite (po-1) replaced by recrystallised pyrrhotite (po-2). BSE image, sample MT-60.

This texture may be indicative of the recrystallisation of pyrrhotite, with the recrystallised phase showing signs of having replaced chalcopyrite. Just like the chalcopyrite analyses, the analyses from the pyrrhotite show great consistency. Even the anomalous analyses show consistency. Another phase that can also be easily overlooked via reflected light microscopy is the presence of extremely small Cu-rich veinlets (Figure 4.30; Figure 4.31; Appendix D, Spectral Image 1), which occurs more in samples obtained from shallower depths.

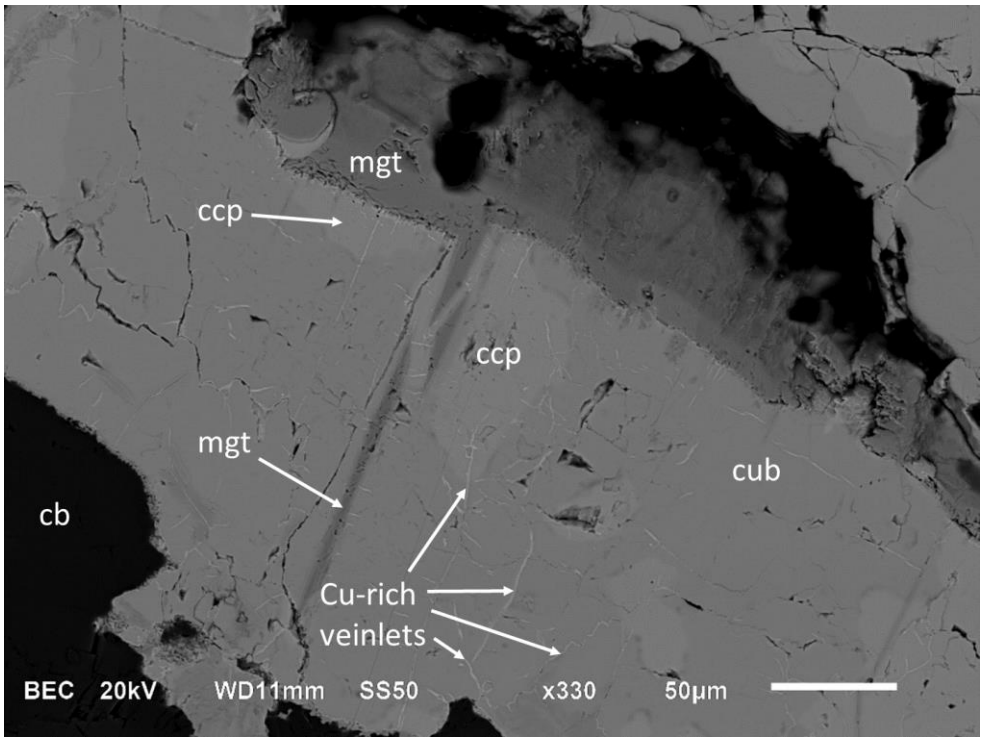

Figure 4.30: Fractures in cubanite filled by extremely small Cu-rich veinlets, and also filling chalcopyrite-cubanite boundaries. BSE image, sample MT-7.

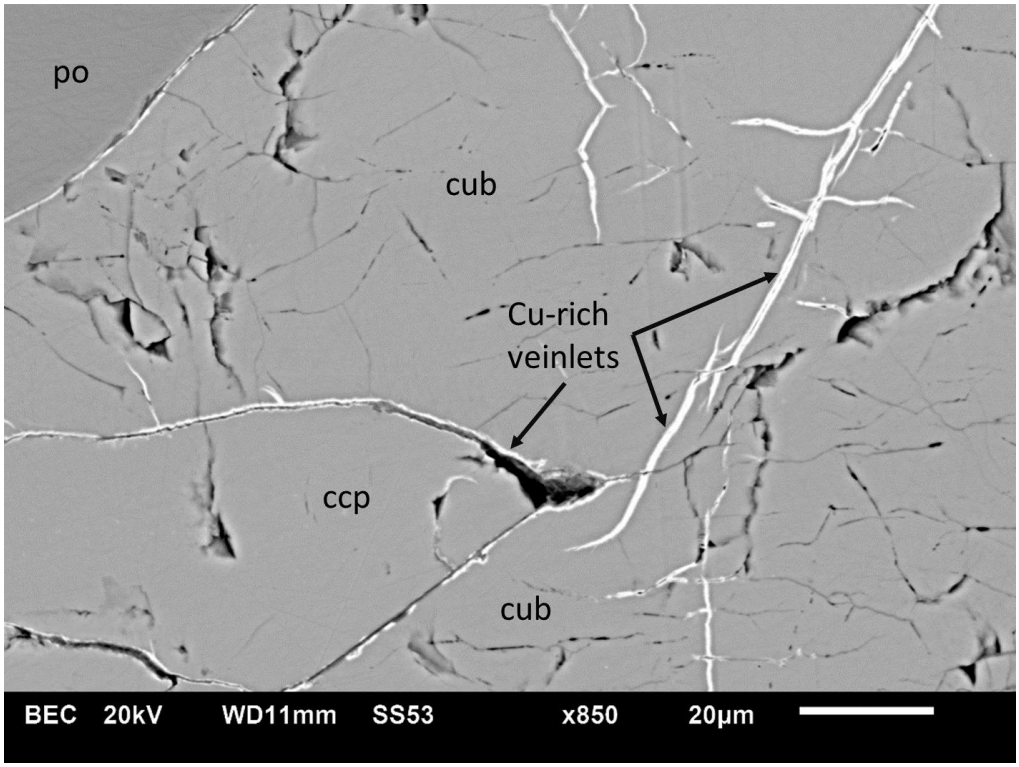

Figure 4.31: Chalcopyrite replaced by Cu-rich veinlets from chalcopyrite-pyrrhotite boundary. BSE image, sample MT-5.

The geochemically distinguishable features present within sulphide minerals (chalcopyrite and pyrrhotite) with such homogeneous optical properties, lead to the assumption that more differences/anomalies would arise when comparing the mineral chemistry of larger cubanite laths (between 30 µm and 200 µm in width), smaller cubanite laths (less than 30 µm in width), and cubanite that replaced cobalt pentlandite, pyrrhotite, and chalcopyrite in large quantities (well over 200 µm in width, engulfing large areas). However, these three distinguishable features do not show any significant variations in their mineral chemistry, at least not in major or minor elemental amounts (Appendix C, Table C.7; Figure 4.26). Analyses obtained from cubanite remained more or less constant throughout the study, with no outliers to detect which will differ from the average weight percentages, even with these three distinguishable features being present.

Although no distinguishable differences in mineral chemistry are indicated by cubanite analyses, the analyses are still quite helpful in indicating the great consistency and accuracy of the used SEM-EDS. Take cubanite analyses from sample MT-7 from Appendix C, Table C.7

as an example. Two representative average analyses per cubanite grain are indicated in the table for five different cubanite grains. The combined average difference in Cu weight percentages for these five different cubanite grains is only ±0.23 wt.%. So if a multitude of EDS point analyses are provided per mineral, and a representative average weight percentage analysis differs greatly from the combined average analysis for that mineral (e.g. that found in chalcopyrite and pyrrhotite analyses), then the outlier representative average weight percentage analysis cannot be overlooked, especially if that average weight percentage analysis is represented by another texture type.

Cubanite is very easily distinguishable from chalcopyrite during reflected light microscopy. However, special care must be taken when trying to identify this mineral during scanning electron microscopy, seeing that its molecular weight compared to that of chalcopyrite is more or less the same. This property may result in similar “grey shades” for both minerals during back-scattered electron imaging.

A great amount of contrast in the imaging system must thus be added to the settings of the SEM in order to make it possible to distinguish between these two minerals, even when the contacts between the grains are visible. Although these contacts may not be very clear as well. Only at large enough magnifications of about 1000x to 1800x is it possible to clearly see the existence of two different phases in the majority of cases, although the shadings of the two phases still do differ that much. The unclear contact between these minerals will only be visible at these great amounts of magnification as well.

If a high enough contrast for the imaging system of the SEM is not possible, it would be possible to distinguish between chalcopyrite and cubanite via their differences in mineral surfaces. Cubanite formed more of a pitted surface, while chalcopyrite formed more of a smoother surface (Figure 4.32).

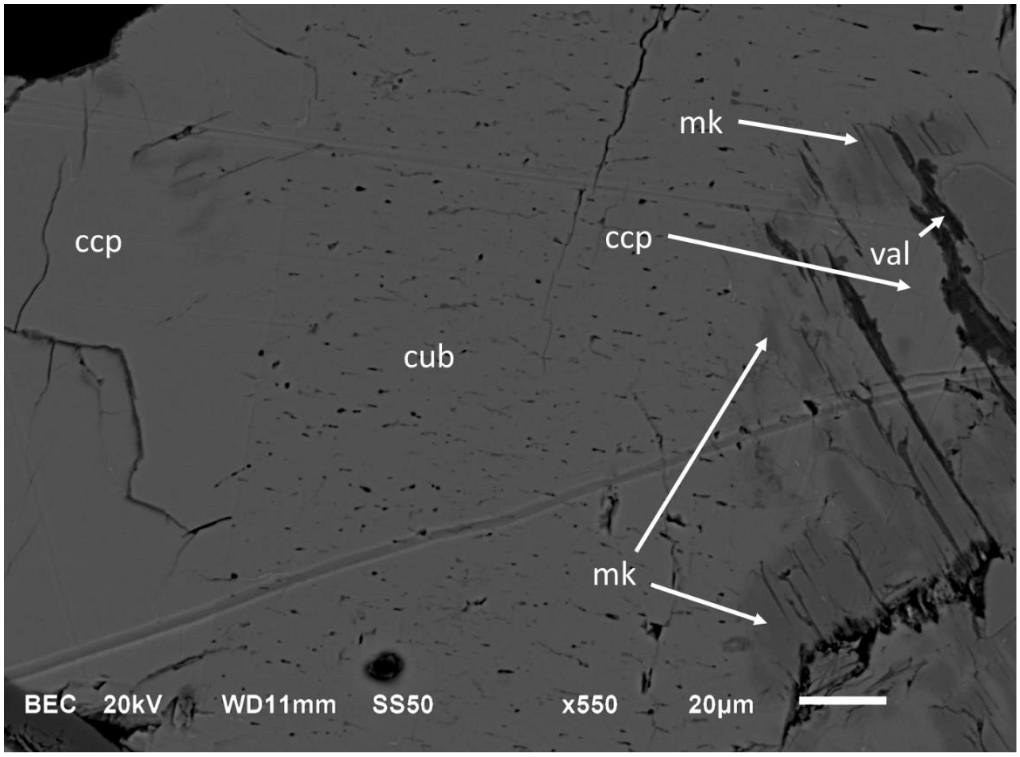

Figure 4.32: Large pitted cubanite lath rimmed by mackinawite. Mackinawite replaced chalcopyrite. BSE image, sample MT-7.

Weak areas also formed at the boundaries of certain cubanite laths and chalcopyrite over time. These weaker zones became fractured and intruded by magnetite. The magnetite formed veinlets, which outlined the cubanite laths in the process (Figure 4.33). The same "outlining effect" was produced after mackinawite replaced chalcopyrite adjacent to cubanite (Figure 4.32).

Mackinawite proper (Appendix C, Table C.1) showed no evidence of replacing pyrrhotite, even after the study of this sulphide mineral under extremely high magnification. However, it favoured the replacement of cobalt pentlandite under rare occasions (Figure 4.34).

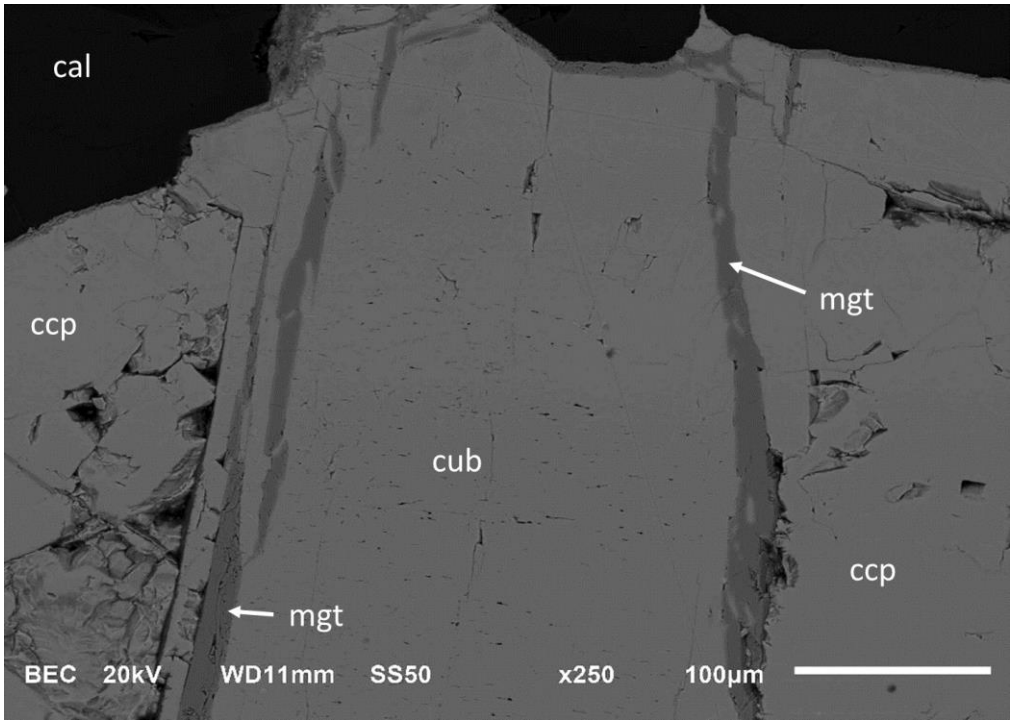

Figure 4.33: Large pitted cubanite lath outlined by magnetite veinlets. BSE image, sample MT-7.

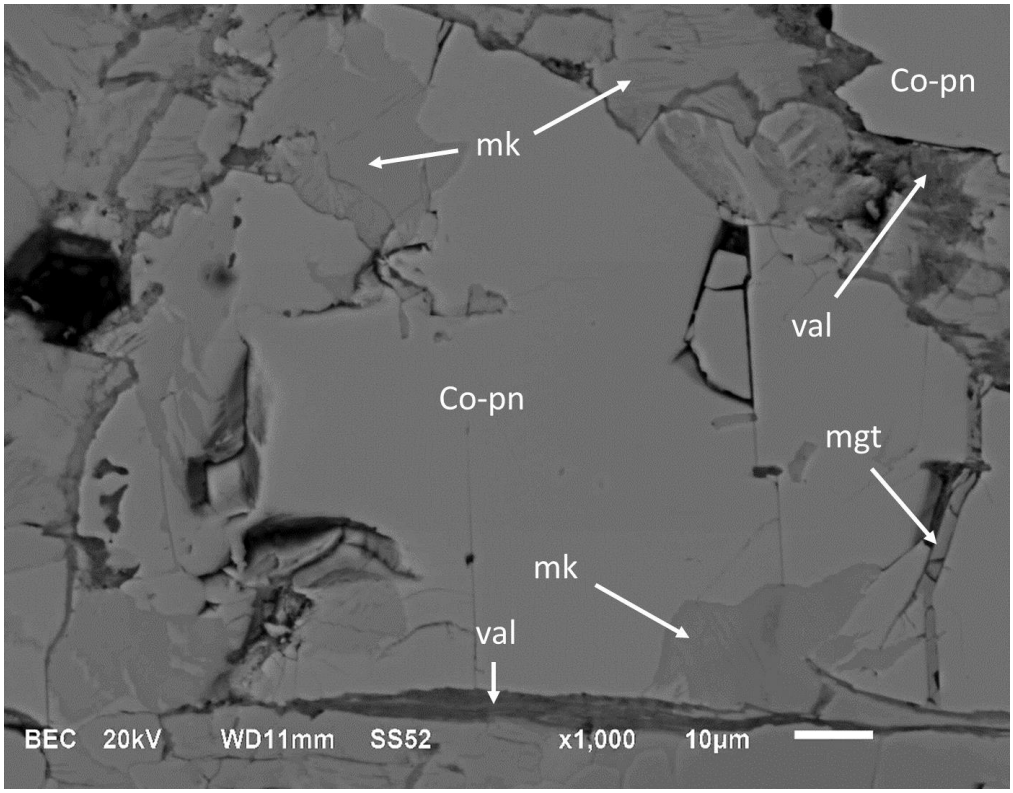

Figure 4.34: Cobalt pentlandite replaced by mackinawite. BSE image, sample MT-7.

Mackinawite was replaced by valleriite very often, showing an extremely strong replacement association towards this mineral even in areas where mackinawite is surrounded by other sulphides, while the other sulphides might show no signs of replacement by valleriite. Due to the mineral almost always showing replacement associations with valleriite and pentlandite in this study, and because beamsize overlap was an issue due to the small size of mackinawite grains, prevented the collection of more data than that presented in Table C.1.

Mackinawite that replaced pentlandite (4.87 wt.% to 5.27 wt.% Ni) has a higher Ni content compared to mackinawite that replaced chalcopyrite (4.13 wt.% to 4.18 wt.% Ni; Figure 4.35). This is due to higher amounts of Ni in pentlandite than in chalcopyrite.

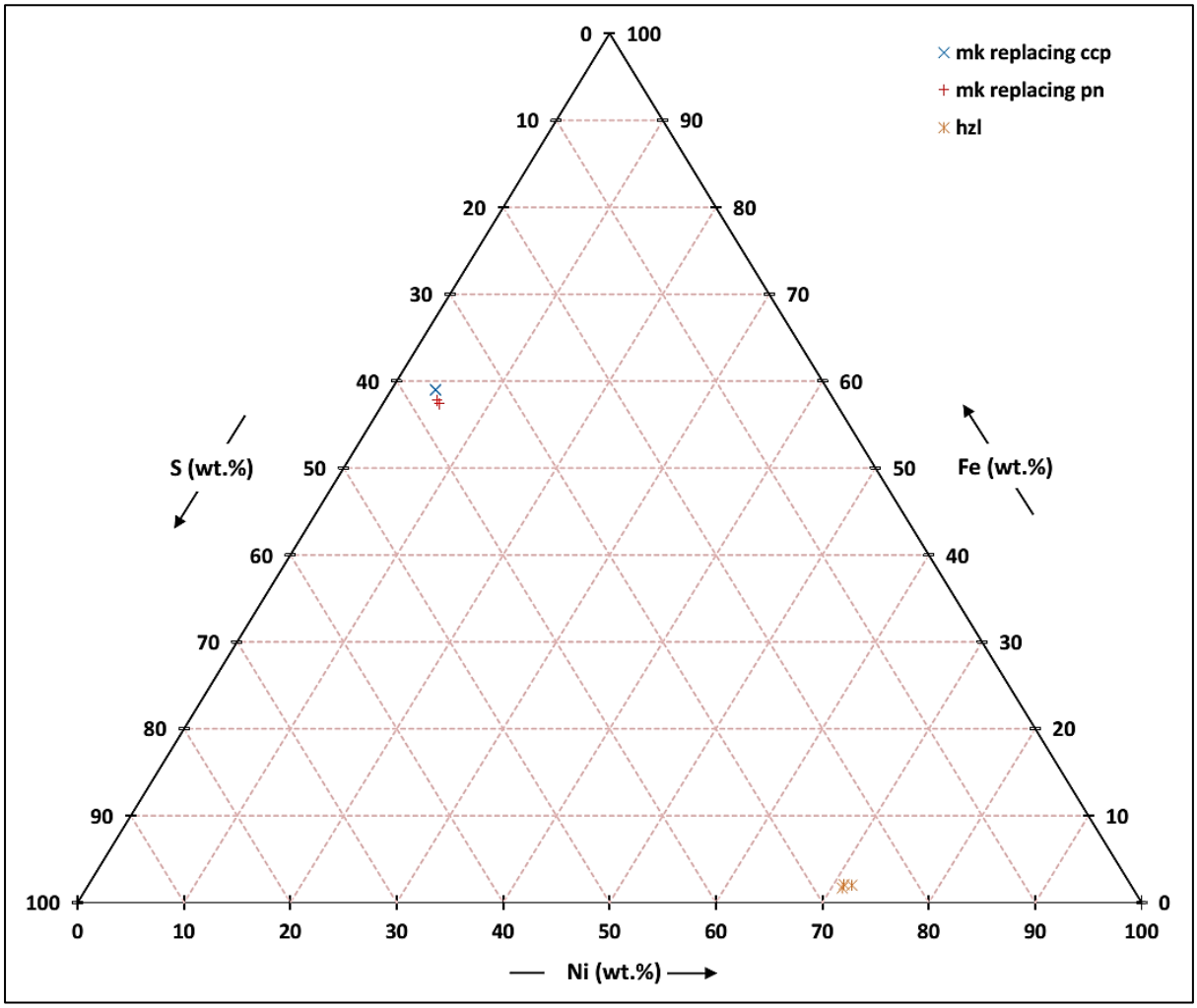

Figure 4.35: Compositions of mackinawite and heazlewoodite from transgressive carbonatite.

Just like cubanite, the mineral chemistry of bornite with various textural features are similar in major elemental amounts (Appendix C, Table C.8; Figure 4.26). The higher x-bornite (that replaced bornite) Cu analyses obtained from MT-15 and MT-58, may be linked to the fact that these samples also show some of the highest bornite Cu analyses in this study (Appendix C, Table C.3; Figure 4.26). Aldous (1980) sustain that x-bornite is a separate phase than bornite, with 0.4% more sulphur compared to bornite, and that bornite values can lie between Cu_3FeS_3 and Cu_9FeS_6.

Sphalerite mineral chemistry (Appendix C, Table C.2; Figure 4.36) can be coupled to its physical properties. The larger euhedral to subhedral grains (62.41 wt.% to 66.31 wt.% Zn) have significantly larger amounts of Zn compared to the smaller anhedral grains (55.15 wt.% to 58.26 wt.% Zn). It is important to also consider the fact that the larger euhedral to subhedral grains primarily replaced bornite, chalcocite, and x-bornite, whereas the smaller anhedral sphalerite grains replaced chalcopyrite and cubanite. Both chalcopyrite and cubanite have higher Fe contents compared to bornite, chalcocite, and x-bornite. This may be the cause for higher Fe contents in the smaller anhedral sphalerite grains. Also, the smaller anhedral sphalerite grains that replaced cubanite (9.45 wt.% to 11.78 wt.% Fe) have higher amounts of Fe compared to the anhedral sphalerite grains that replaced chalcopyrite (8.02 wt.% to 8.93 wt.% Fe). This may be due to the cubanite having higher Fe contents compared to chalcopyrite.

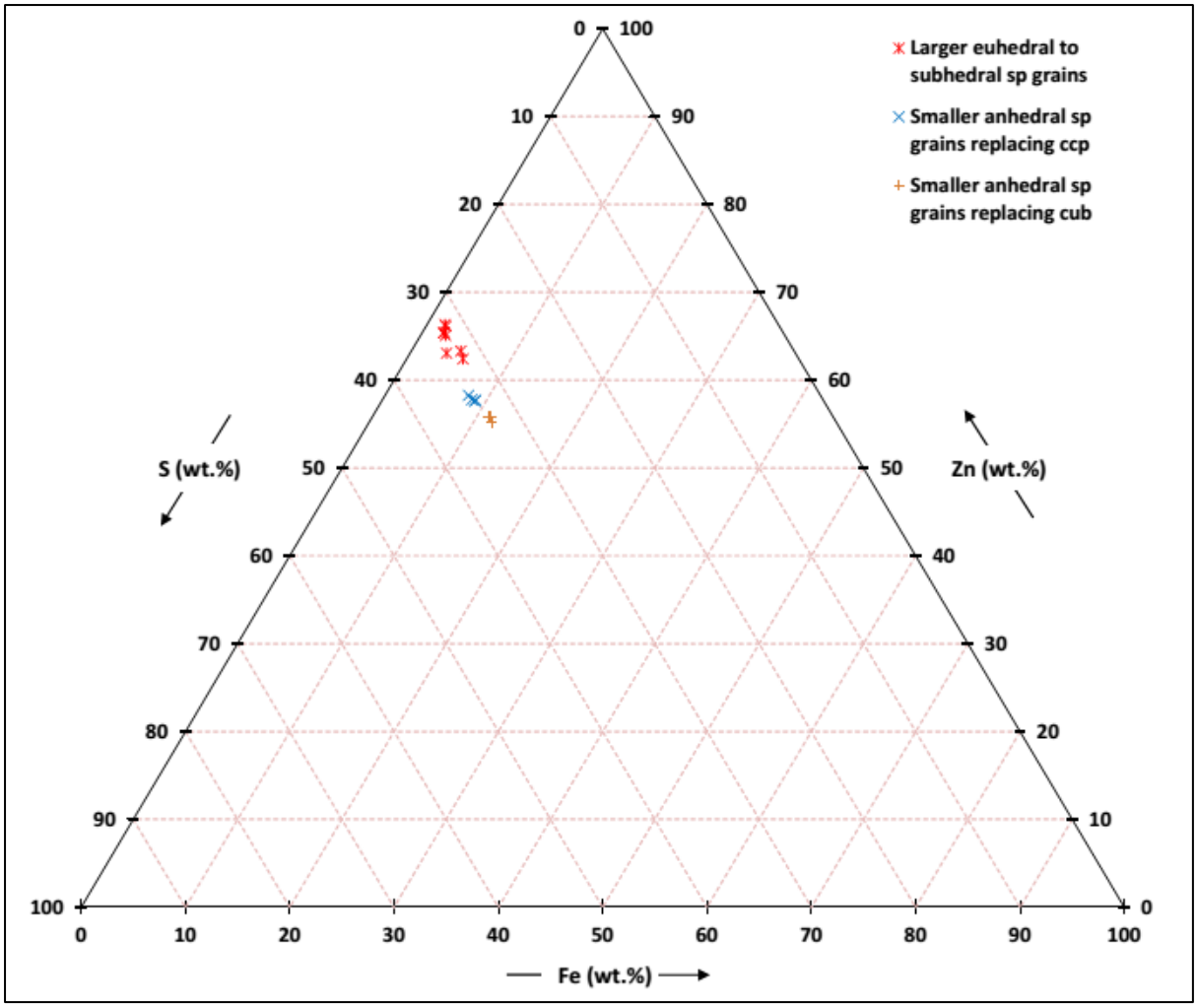

Figure 4.36: Compositions of sphalerite from transgressive carbonatite.

A broad range of Co contents was detected for grains that are classified within the pentlandite group (Appendix C, Table C.4 and Table C.9; Figure 4.37). Harris and Nickel (1972) conducted a study on pentlandite-group samples that show variations in Co, Ni, and Fe contents and classified these pentlandites based on their Co contents. Normal pentlandite is shown to have up to 10 wt.% Co. Cobaltian pentlandites have a cobalt content between 12 wt.% and 14 wt.%, and cobalt pentlandites have more than 20 wt.% Co. However, EDS-analyses from MT-60 indicate that cobalt pentlandite grains that have the same optical properties, size, and are found within a very close spatial relationship can have cobalt contents lower than 20 wt.%. The highest cobalt contents for cobalt pentlandite for this study have values as high as ±45 wt.%. The cobalt in cobalt pentlandite shows a negative correlation with Fe and Ni.

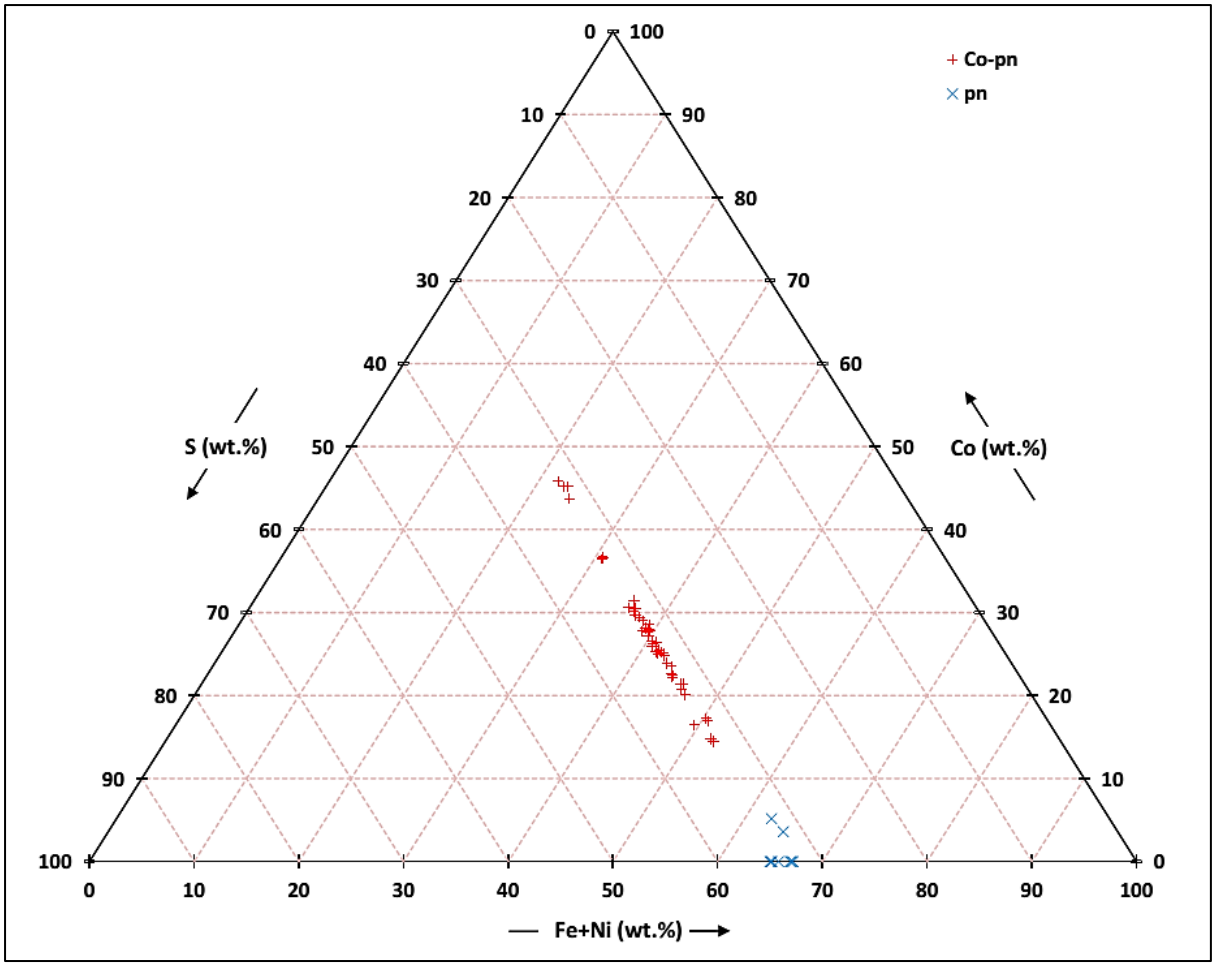

Figure 4.37: Compositions of cobalt pentlandite and pentlandite from transgressive carbonatite.

Cobalt pentlandite grains show no distinguishable compositions that can be linked to their physical properties so far. The analyses are too random. Later categorisation of all sulphide minerals may prove to be a means in order to find some pattern in the randomness of its contents.

Pentlandite proper (having no Co impurities accommodated in its structure) is present in MT-23 and MT-38, and have more or less constant Fe and Ni contents, except for analyses obtained from MT-26, which contains more or less between 3 wt.% and 10 wt.% Co.

The intergrowth and replacement phases of chalcocite have similar compositions (Appendix C, Table C.10; Figure 4.38). Both phases can have more than 0.8 wt.% Fe, or can be absent of

Fe. Covelline (Appendix C, Table C.1; Figure 4.38) contains even larger amounts of Fe compared to chalcocite (up to 2.25 wt.% Fe)

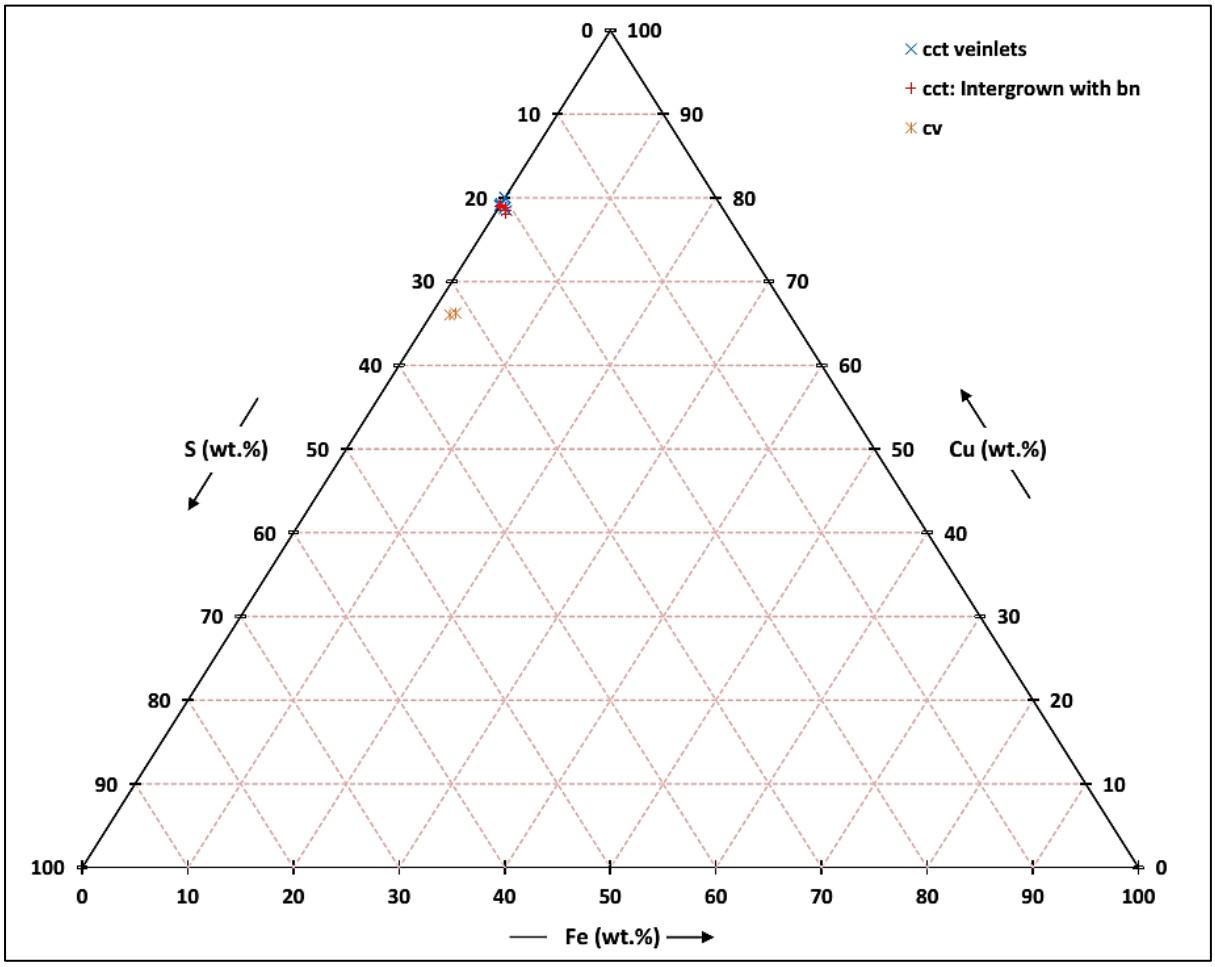

Figure 4.38: Compositions of chalcocite and covelline from transgressive carbonatite.

Galena and shandite (Appendix C, Table C.1; Figure 4.39) are the only sulphide minerals observed in this study that contain measurable quantities of Pb. Heazlewoodite (Appendix C, Table C.1; Figure 4.35) contains the highest amount of Ni (up to 71.78 wt.% Ni) compared to shandite, cobalt pentlandite, pentlandite, and mackinawite.

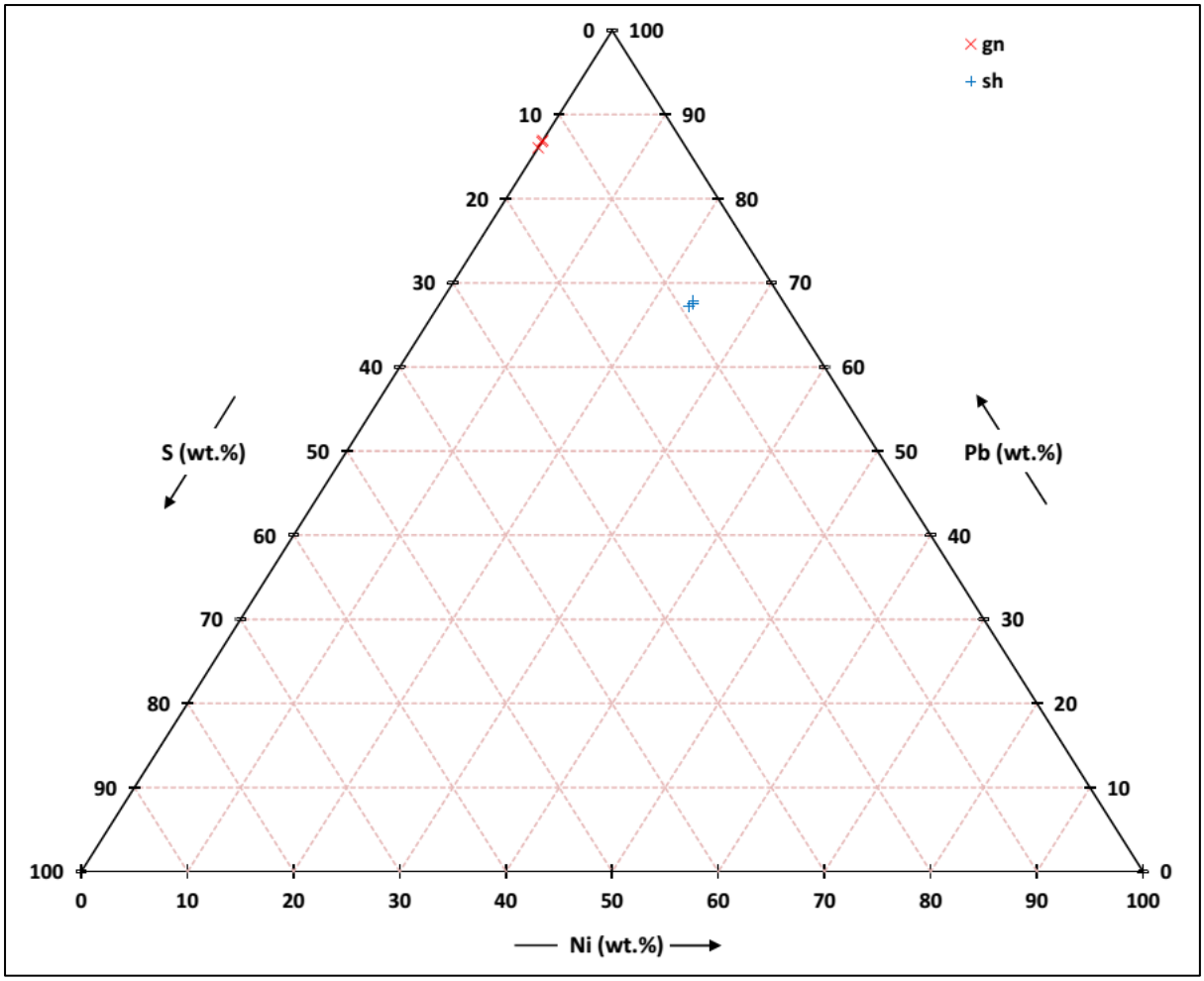

Figure 4.39: Compositions of galena and shandite from transgressive carbonatite.

4.3. The petrographic description of phoscorite sulphide mineralisation.

According to Lee *et al.* (2003), phoscorite is defined as a plutonic, ultramafic phosphate-oxide-silicate rock that occurs in spatial and temporal association with carbonatite. This study has revealed noticeable differences between sulphide mineral textures of phoscorite and carbonatite (both banded and transgressive), even though just two phoscorite samples (MT-56 and MT-65) have been studied.

Bornite, chalcocite, and valleriite are the most abundant sulphide minerals within the phoscorite samples. Chalcocite and bornite also formed symplectic intergrowths (Figure 4.40), just like the bornite and chalcocite in both carbonatite types (Figure 4.14). However, it is very common to find individually formed bornite and chalcocite fabrics in the phoscorite samples (Figure 4.41; Figure 4.42). This is rare in carbonatite samples, seeing that the

chalcocite in carbonatite samples always show an association with bornite. Also, chalcocite replaced cobalt pentlandite (Figure 4.43) in the phoscorite samples, a texture that is not present within the carbonatite samples.

Bornite replaced chalcopyrite within both carbonatite types (Figure 4.17; Figure 4.25). However, chalcopyrite replaced bornite in the phoscorite samples (Figure 4.40; Figure 4.44). Chalcopyrite also replaced cobalt pentlandite and formed relict grains in the process (Figure 4.45). This is a texture (the relict grains of cobalt pentlandite) that is not present in transgressive carbonatite samples. Cobalt pentlandite and millerite are the least abundant minerals.

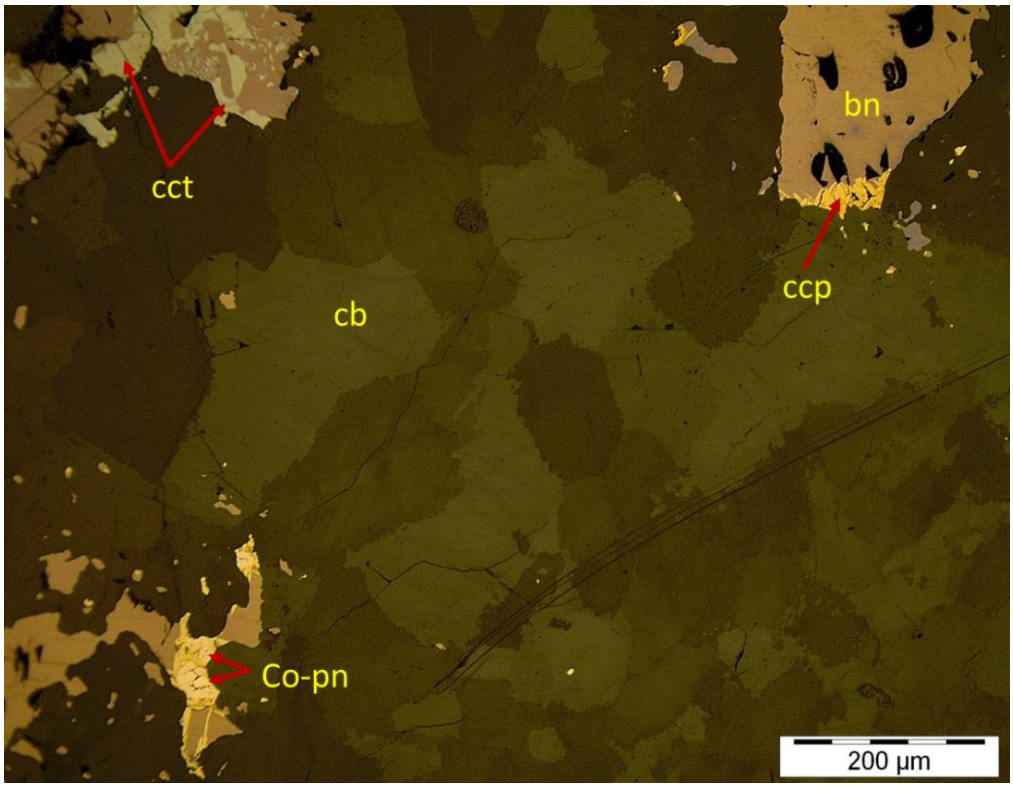

Figure 4.40: Symplectic intergrowth between chalcocite and bornite. Bornite fabric replaced by chalcopyrite (upper right-hand corner and lower left-hand corner). Cobalt pentlandite replaced by chalcopyrite (lower left-hand corner). RL image, sample MT 56.

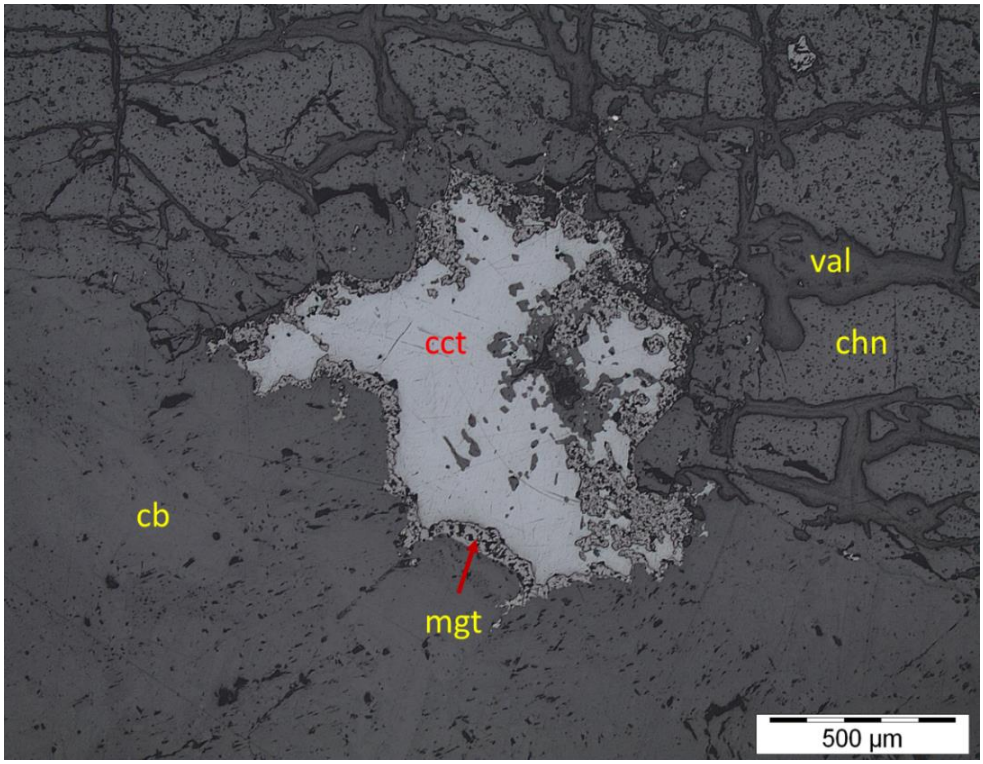

Figure 4.41: Chondrodite and carbonates replaced by chalcocite. Chalcocite replaced by magnetite. Carbonates, chondrodite, and magnetite replaced by valleriite. RL image, sample MT-65.

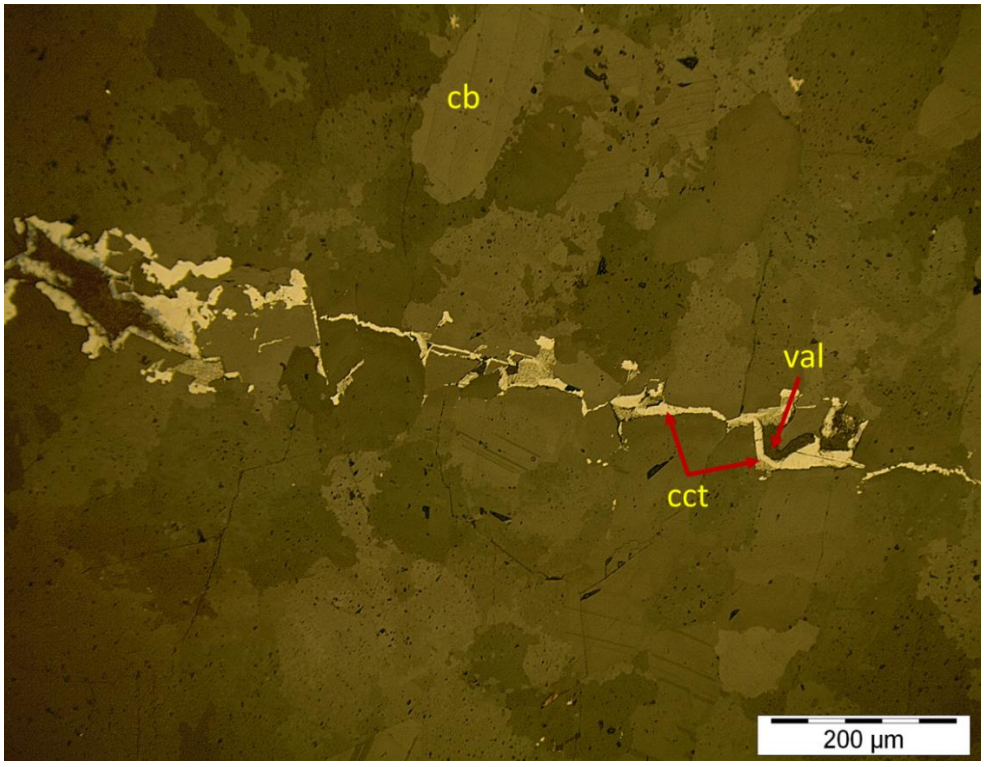

Figure 4.42: Grain boundaries within the carbonate fabric filled with chalcocite. RL image, sample MT-56.

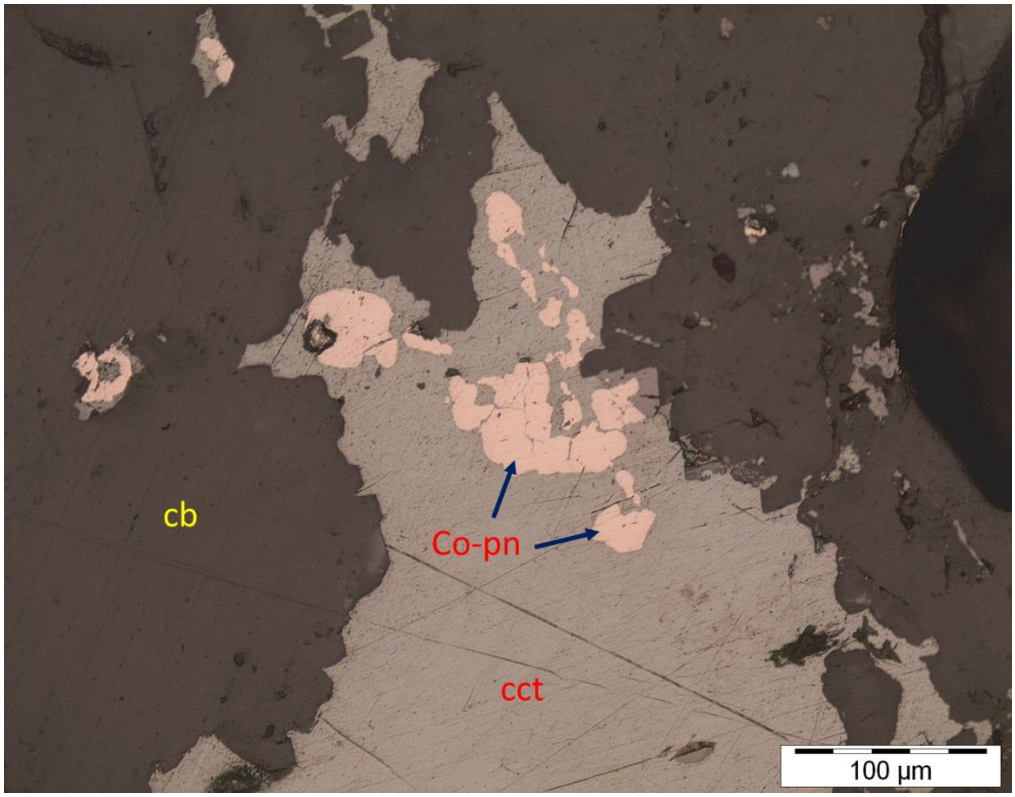

Figure 4.43: Cobalt pentlandite replaced by chalcocite. Carbonates replaced by sulphides. RL image, sample MT-65.

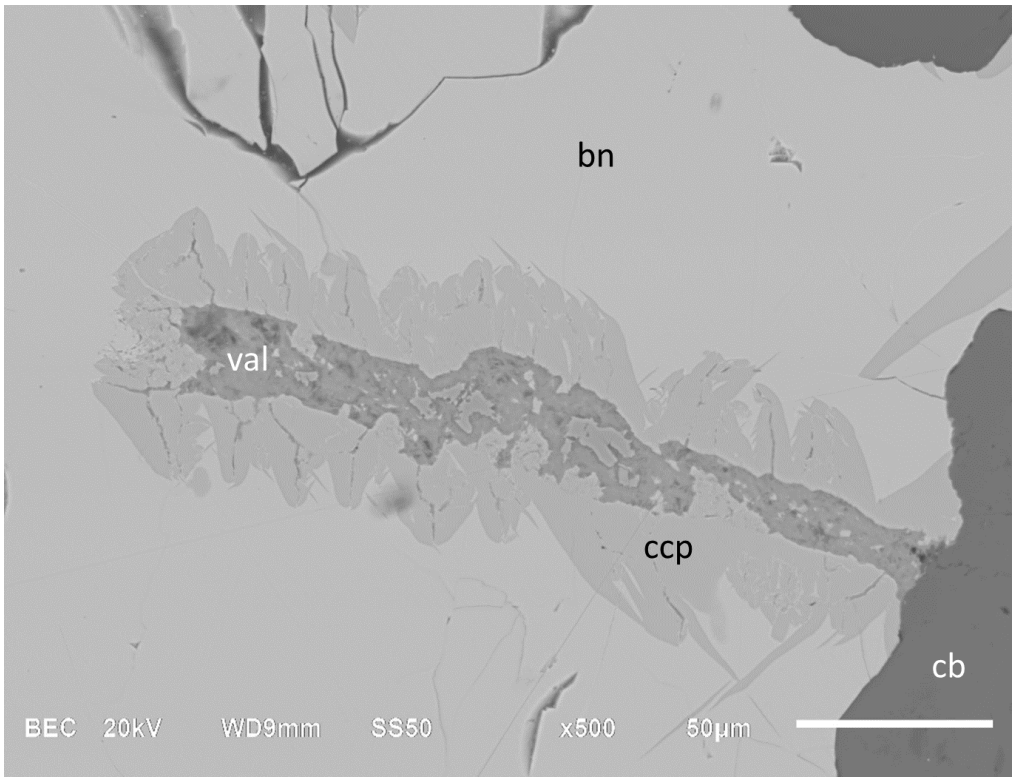

Figure 4.44: Bornite replaced by chalcopyrite. Chalcopyrite replaced by valleriite. BSE image, sample MT-56.

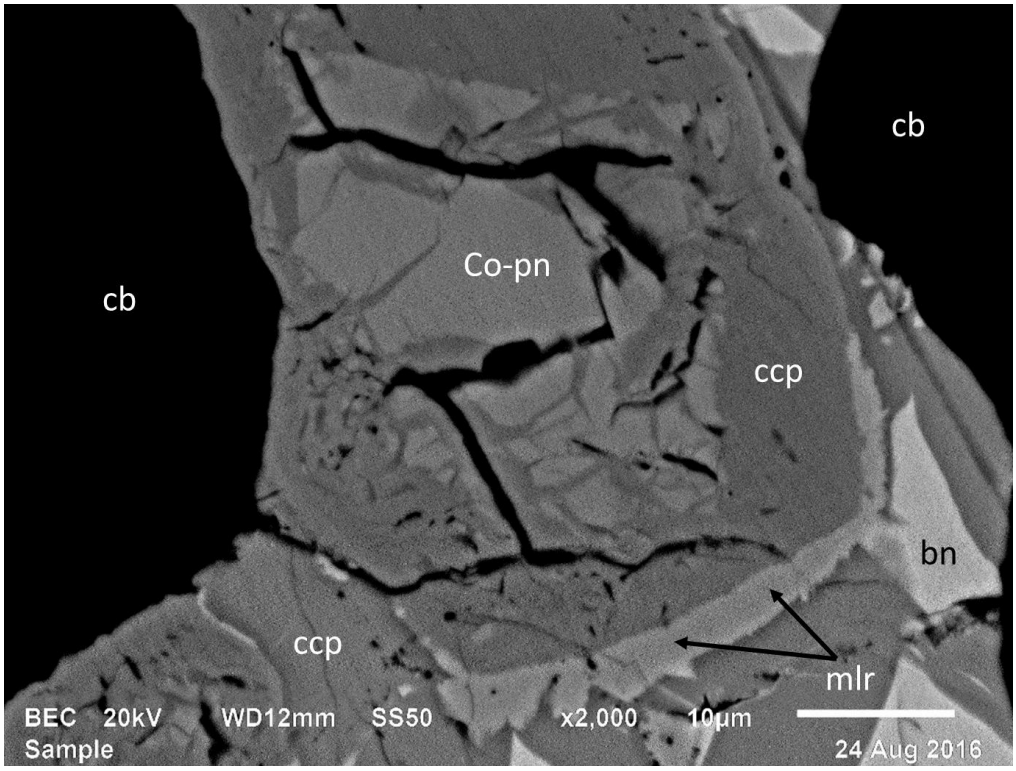

Figure 4.45: Relict cobalt pentlandite grain. Cobalt pentlandite and bornite replaced by chalcopyrite. Chalcopyrite and bornite replaced by millerite. BSE image, sample MT-56.

4.4. Petrographic description of common non-sulphide minerals in transgressive carbonatites.

The following gives a generalised textural description of the primary non-sulphide minerals and commonly found accessory minerals (Appendix E, Table E.1). The crystallinity of all the samples is holocrystalline. The main minerals within banded and transgressive carbonatites are calcite, dolomite, phlogopite, and apatite, with variable amounts of magnetite and sulphides. The main minerals within phoscorite is chondrodite, magnetite, and apatite, with variable amounts of phlogopite, carbonates, and sulphides.

4.4.1. Carbonate minerals.

The majority of the carbonatite samples have a carbonate content which varies between 60% and 80%. The carbonatite bodies of both carbonatite types form idiomorphic to hypidiomorphic textures.

Some of the carbonatite samples are indicative of sulphides and/or magnetite enrichment. This results in carbonate minerals contributing to only a smaller percentage (e.g. below 40%) of the estimated modal percentages. However, this does not classify these carbonatites as phoscorites, seeing that the phoscorite samples have small amounts of sulphide mineralisation and still have carbonate contents lower than 30%, and as previously mentioned. Also, the phoscorite samples are easily distinguishable just by the identification of their sulphide mineral assemblages.

a) Calcite:

The calcite crystals in the carbonatites are euhedral to anhedral in shape and mostly medium-grained. Coarse-grained (up to 6 mm long) and medium-grained calcite crystals frequently replace and/or enclose baddeleyite, uranothorianite, olivine, and apatite in a subpoikilic to poikilitic fashion. Fine-grained calcite crystals usually form overgrowth textures, replacement textures, or interstitial intergrowths with these minerals rather than poikilitic type textures.

The mosaic texture produced by the interlocked coarse-grained (Figure 4.46) or medium-grained calcite crystals (Figure 4.47) indicates equilibrium under sub-solidus conditions (Bouabdellah *et al.,* 2010).

The calcite crystals may appear “stained/dirty” under transmitted light. These calcite alteration zones show a strong association towards regions of valleriitisation at calcite-magnetite (- or sulphide) boundaries (Figure 4.48; Figure 4.49).

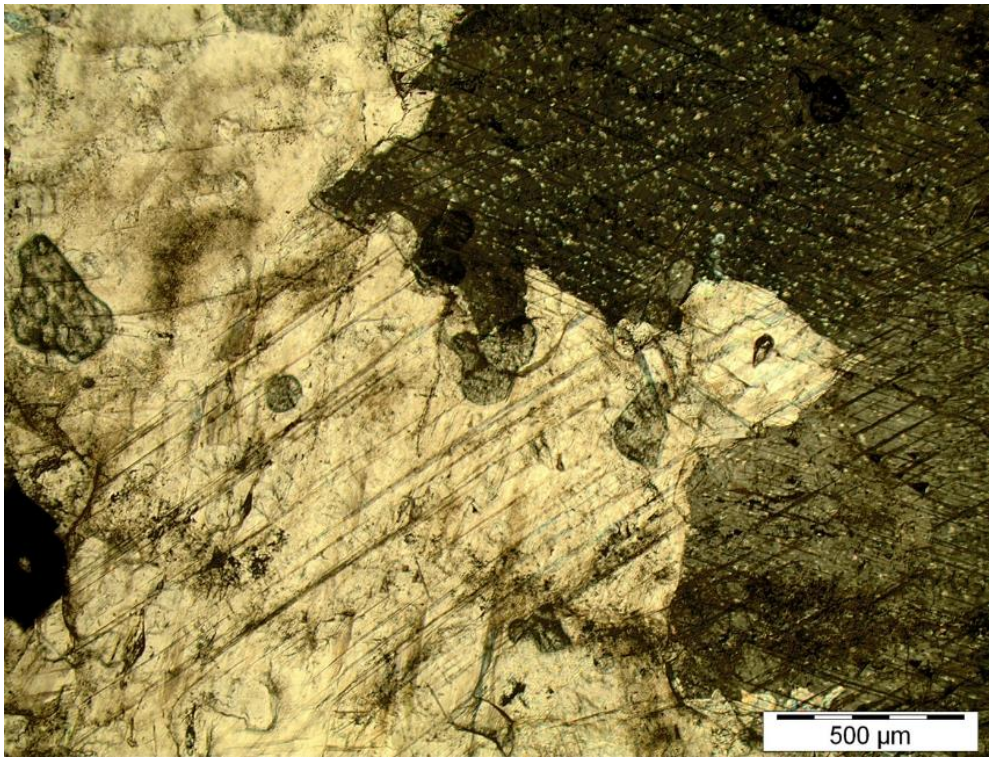

Figure 4.46: Consertal texture produced by interlocked coarse-grained calcite crystals. TL image with crossed polarisers, sample MT-38.

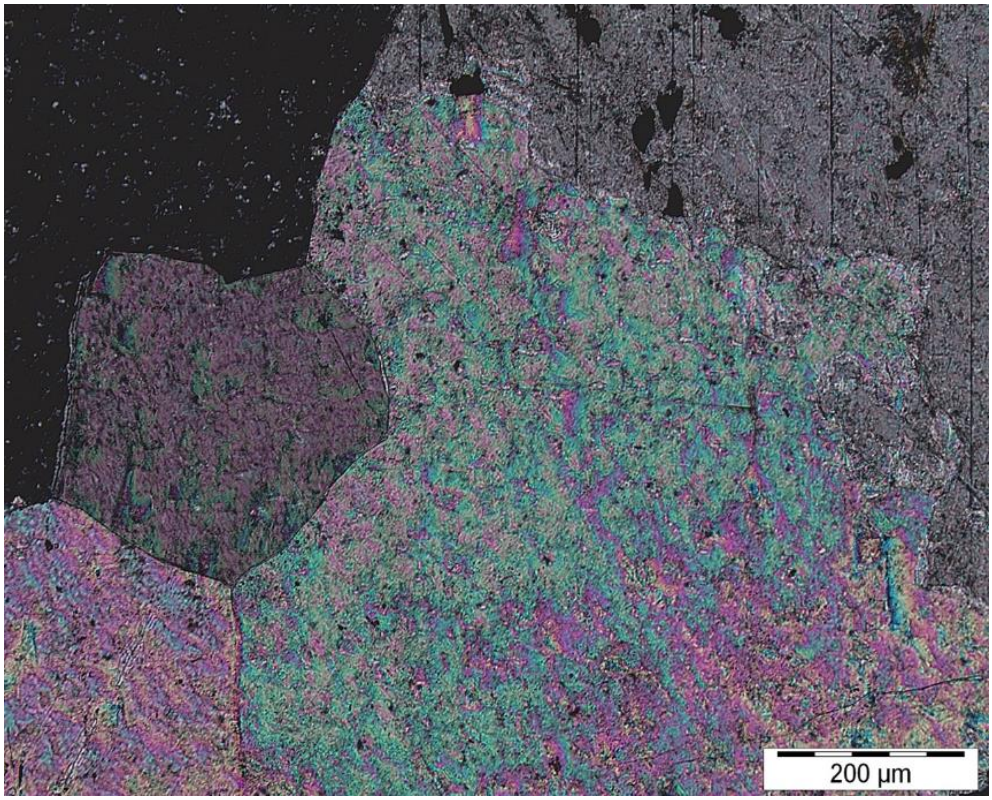

Figure 4.47: Triple-junction produced by interlocked medium-grained calcite crystals. TL (transmitted light) image with crossed polarisers, sample MT-3.

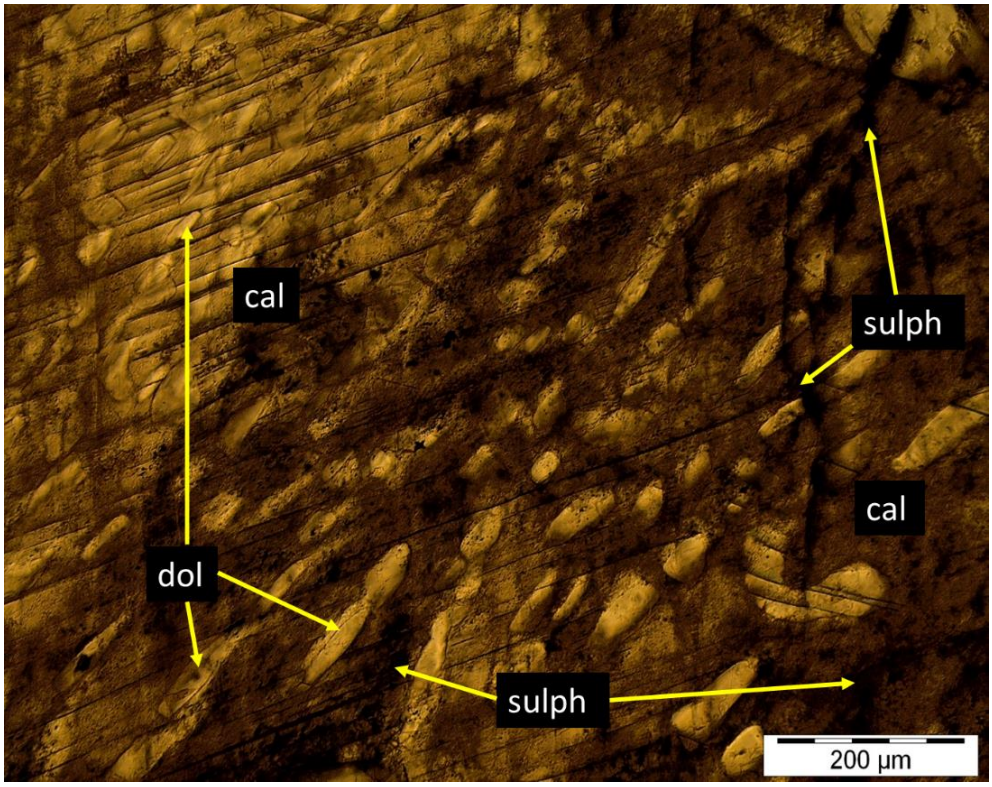

Figure 4.48: “Stained” coarse-grained calcite with dolomite exsolution. TL image, sample MT-40.

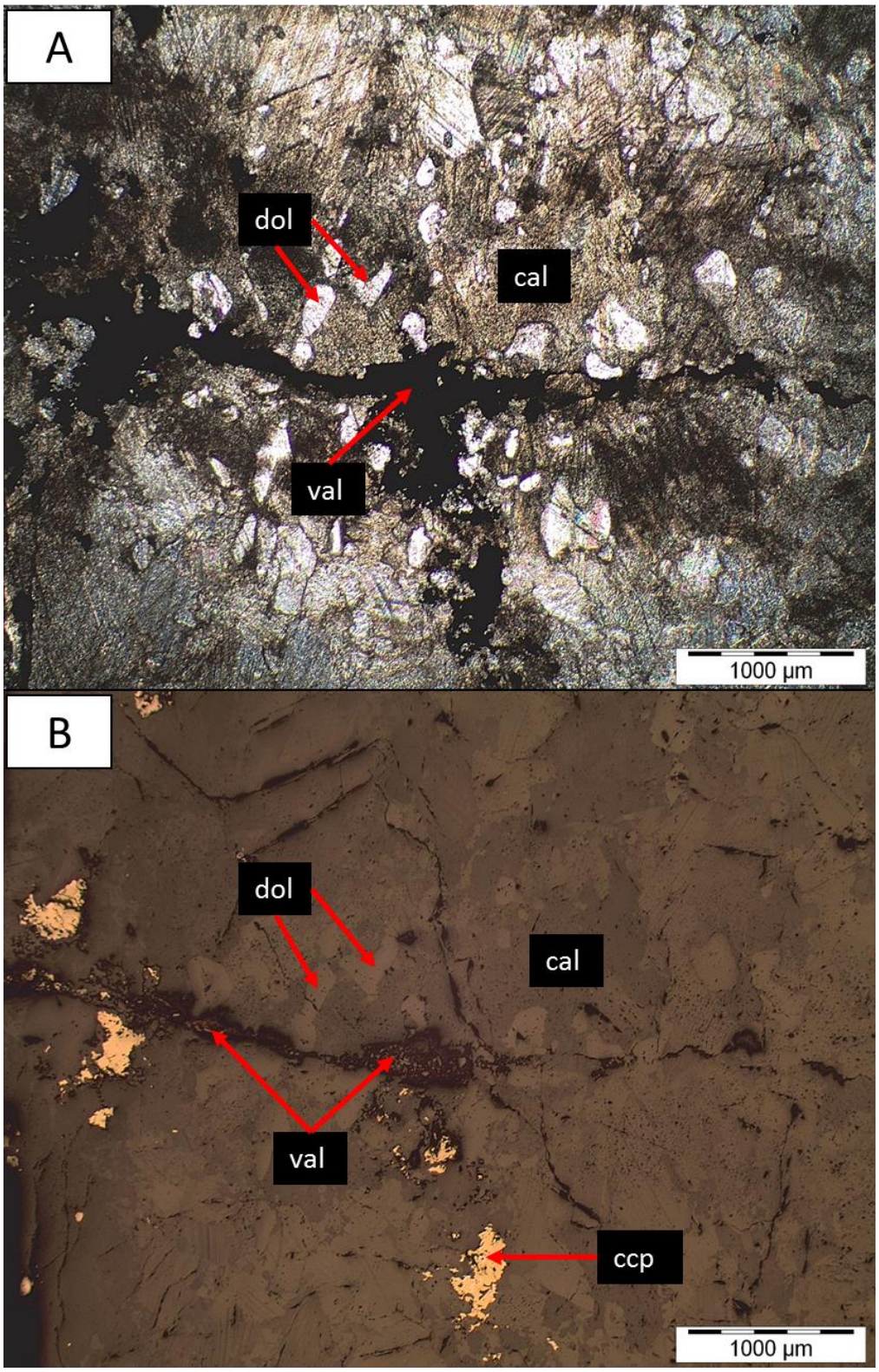

Figure 4.49: Carbonate alteration zone parallel to valleriite veinlet. TL image (A) and RL image (B), sample MT-60.

b) Dolomite:

Dolomite constitutes an average of 3 modal % within both carbonatite types. It is very common for calcite crystals to share mutual grain boundaries with first generation dolomite and also to contain exsolved rod-shaped/vermicular or rounded dolomite grains (second generation) that are usually equally distributed within the calcite matrix (Figure 4.50). Figure 4.50 also indicates the coalescence between dolomite blebs (lower left-hand side) which then resulted in the formation of larger blebs, the coalescence of a larger dolomite bleb with a rod-shaped dolomite crystal (upper left-hand side), as well as the coalescence of dolomite rods that resulted in the appearance of long dolomite lamellae (right-hand side).

Both dolomite and calcite are very easily distinguishable from other minerals under reflected light and scanning electron microscopy, due to the formation of triangular pits in these carbonate minerals (Figure 4.50). They are also easily distinguishable from each other during scanning electron microscopy even though both minerals look very similar under transmitted light.

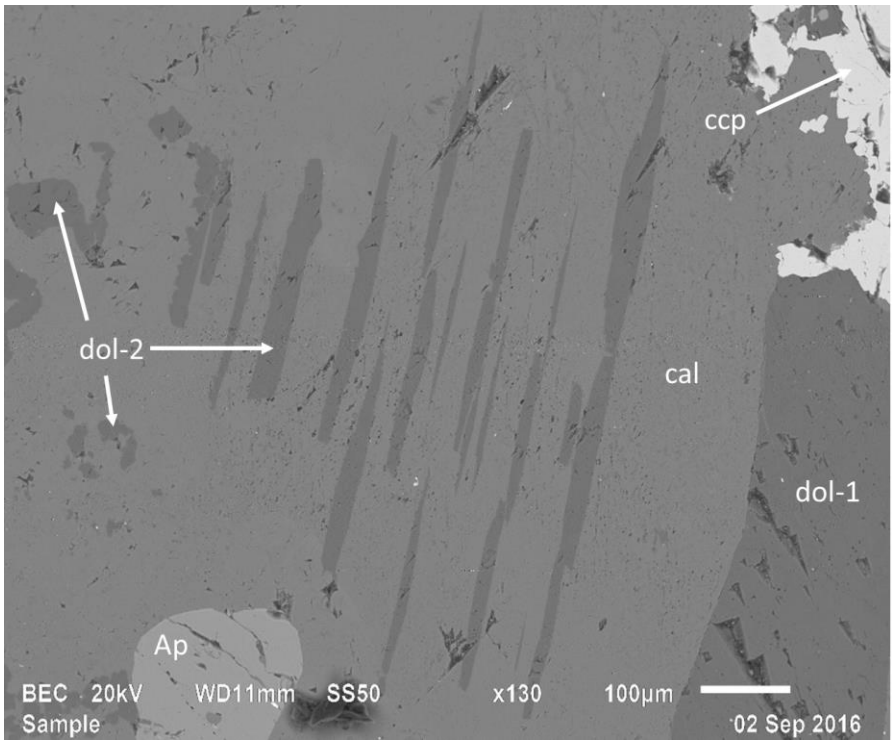

Figure 4.50: Orientated rods of dolomite (dol-2) exsolved from calcite. Image also shows a mutual grain boundary between dolomite (dol-1) and calcite. Notice the triangular pits in dolomite (lower right-hand corner). BSE image, sample MT-44.

c) Recrystallised carbonate minerals:

The recrystallisation of dolomite and calcite replaced minerals from the carbonate group (Figure 4.51; Figure 4.52), silicate group (Figure 4.53; Figure 4.54), sulphide group, and oxide group (Figure 4.55). The vein-like appearance of recrystallised carbonates make them easily distinguishable from earlier formed carbonate minerals.

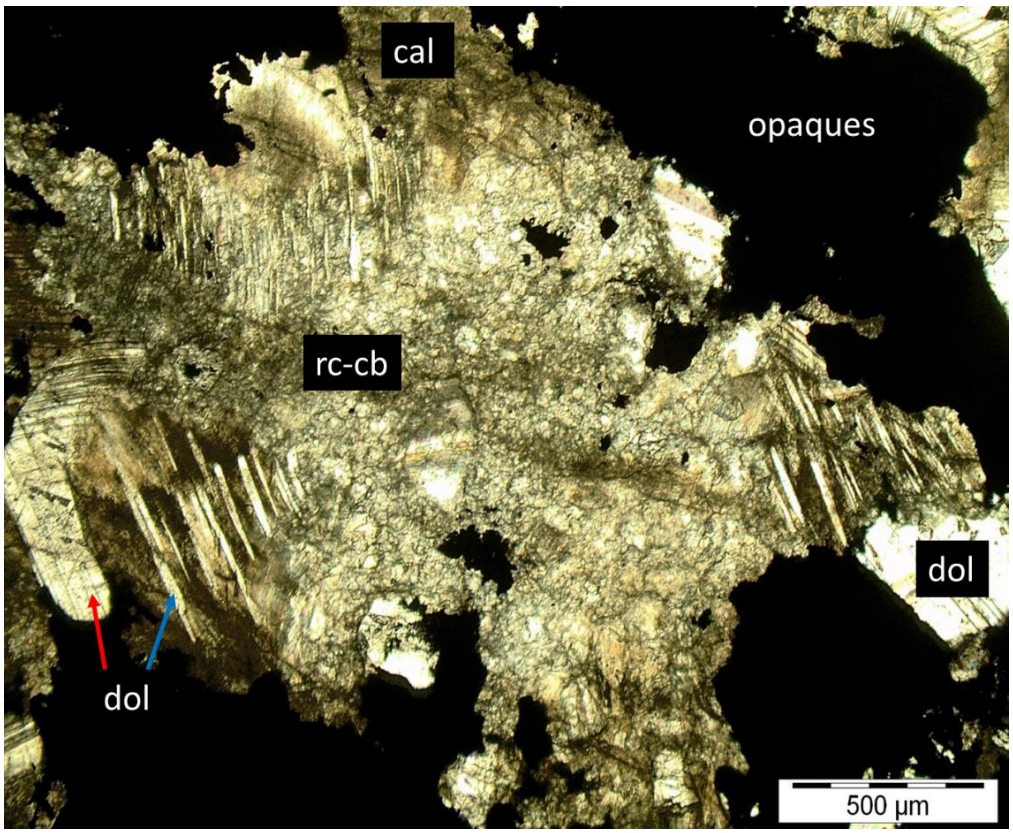

Figure 4.51: Calcite, first generation dolomite (red arrow), and second generation dolomite (blue arrow) replaced by recrystallised carbonates (rc-cb). Notice its vein-like appearance. TL image, sample MT-44.

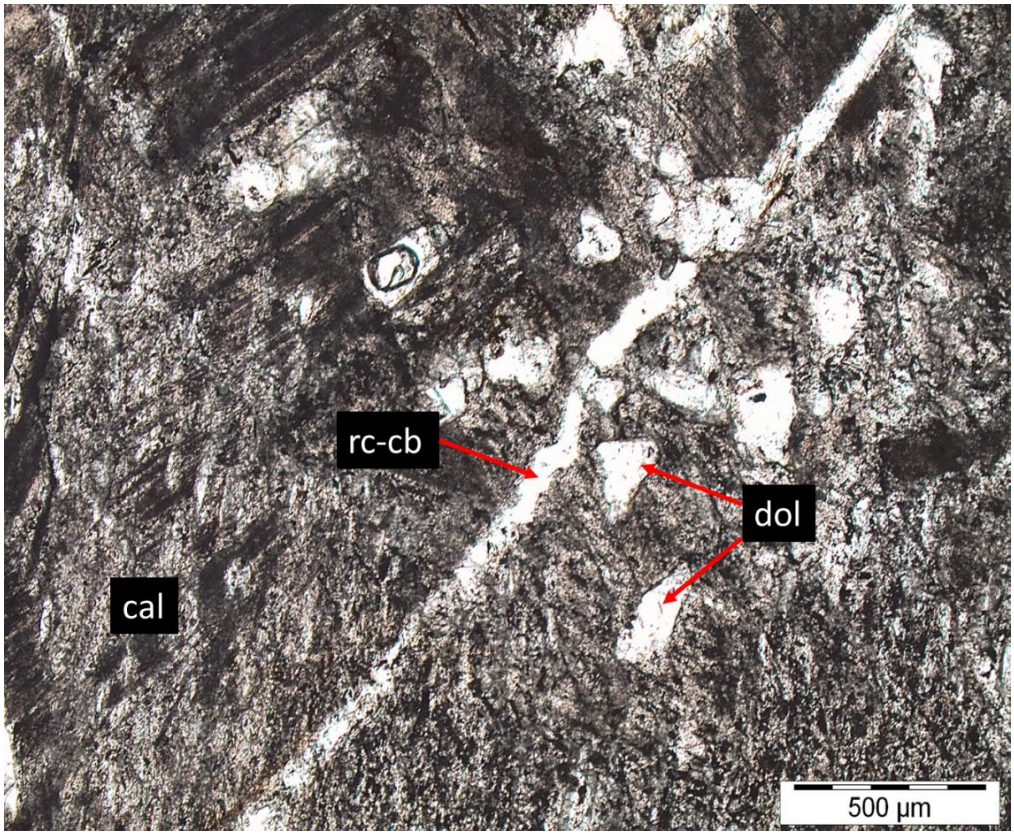

Figure 4.52: Calcite and dolomite replaced by recrystallised carbonate with a vein-like appearance. TL image, sample MT-14.

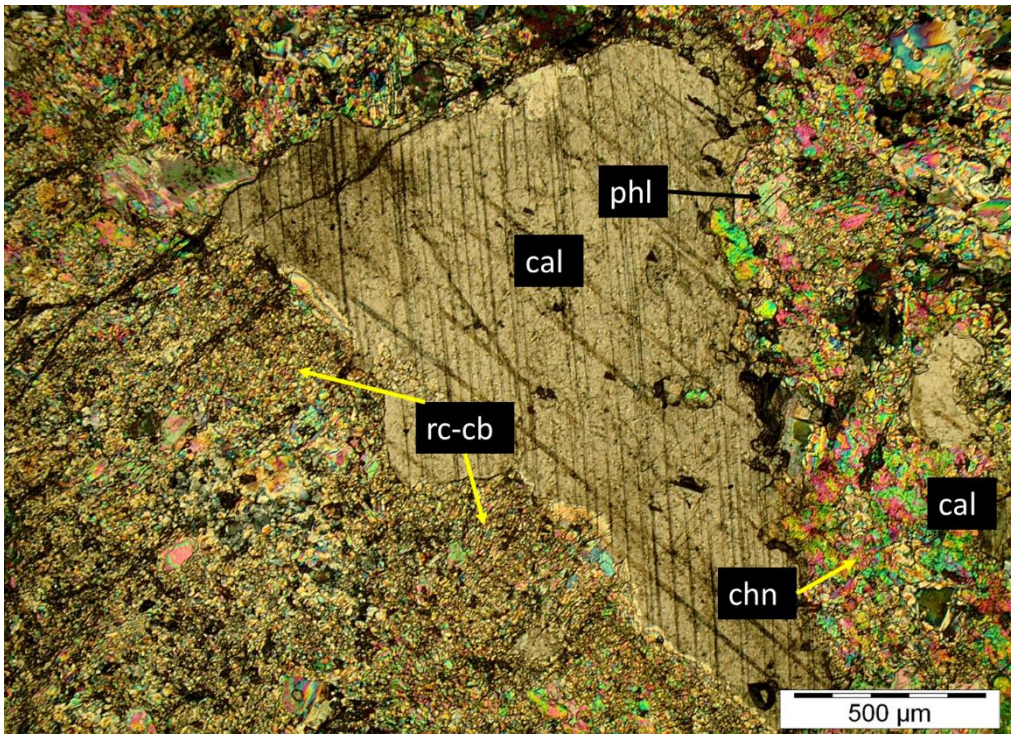

Figure 4.53: Calcite, phlogopite, and chondrodite replaced by recrystallised carbonates. TL image with crossed polarisers, sample MT-8.

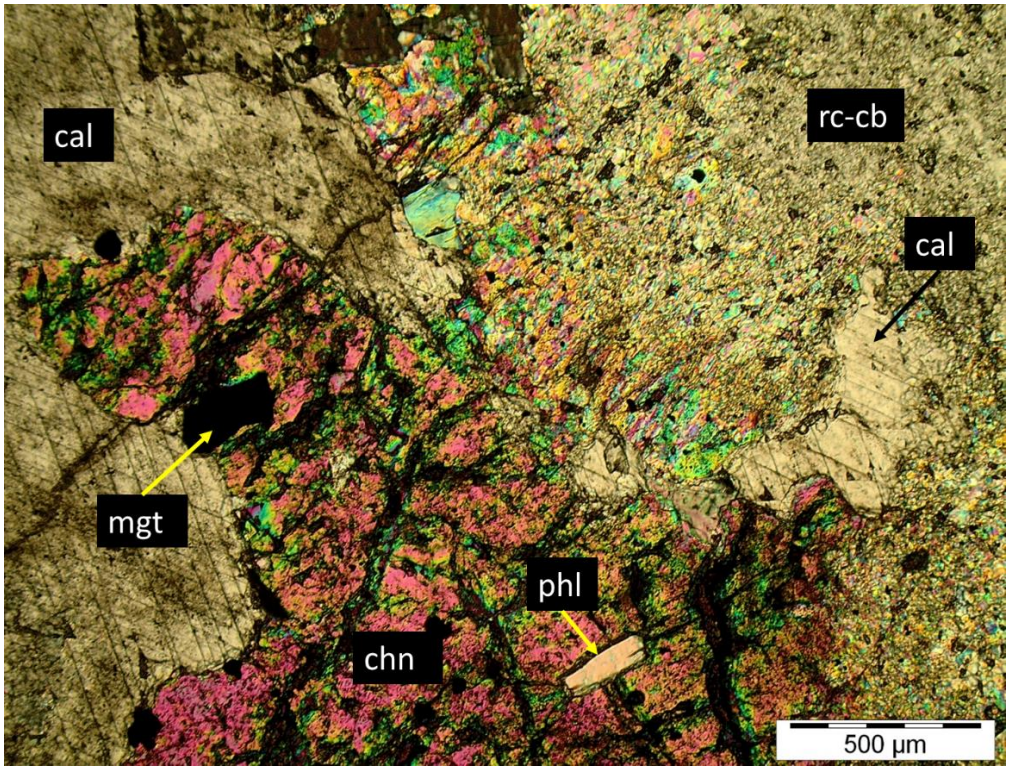

Figure 4.54: Calcite and chondrodite replaced by recrystallised carbonates. Calcite and phlogopite replaced by chondrodite. TL image with crossed polarisers, sample MT-8.

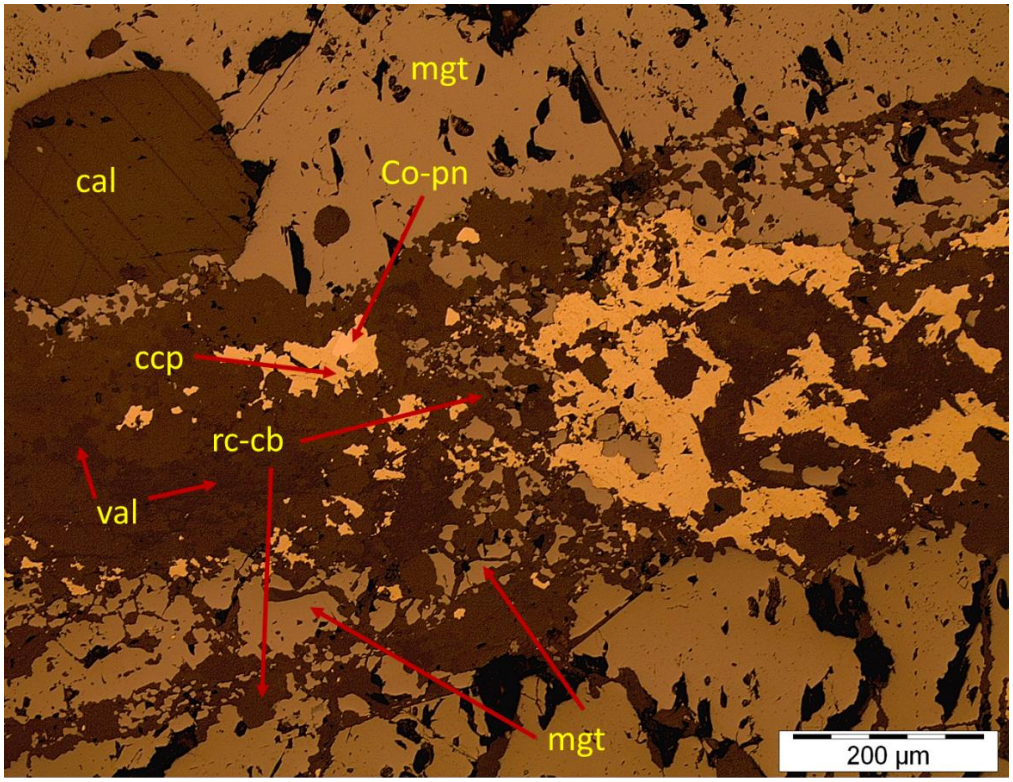

Figure 4.55: Magnetite and chalcopyrite replaced by recrystallised carbonates. Recrystallised carbonates replaced by valleriite. RL image, sample MT-49.

4.4.2. Oxides: Magnetite, ilmenite, spinel, baddeleyite and uranothorianite.

a) Magnetite:

The most common and abundant oxide mineral in both transgressive and banded carbonatites is magnetite. Three generations of magnetite crystallisation have been identified in transgressive carbonatite samples.

First and second generation magnetite is observed as coarse-grained to medium-grained masses that are mostly euhedral to subhedral in shape. First generation magnetite formed before the main calcite and dolomite crystallisation phase (Figure 4.56; Figure 4.57). This resulted in the replacement of first generation magnetite by these carbonate minerals. However, second generation magnetite formed after the main calcite and dolomite crystallisation phase and thus resulted in vice versa replacement associations between these carbonate minerals and second generation magnetite (Figure 4.58).

Both first and second generation magnetite formed before sulphide mineralisation, while third generation magnetite formed after sulphide mineralisation (Figure 4.59). Third generation magnetite formed well-defined veinlets in fractures of the sulphide masses and rims at sulphide-non-sulphide grain boundaries.

Both first and second generation magnetite can constitute more than 40 modal % each. However, second generation magnetite is more common than first generation magnetite within the observed samples. Third generation magnetite constitutes only minor amounts within the samples and is the least common magnetite generation within the observed samples. Figure 4.60, Figure 4.61 (A), Figure 4.62, and Figure 4.63 compare the calcite-sulphide-magnetite assemblages of the three magnetite generations. It is possible for a sample to host more than one magnetite generation, e.g. MT-40 and MT-71 (Figure 4.64). Recrystallised carbonates show textural evidence of forming after all three magnetite generations and sulphides (Figure 4.55).

The boundaries of all three generations show signs of being easily modified by valleriite replacement. This may cause the euhedral to subhedral magnetite grains to appear anhedral and also give the impression of valleriite-veinlet formation in areas where magnetite veinlets

are replaced. The grey colour of magnetite under reflected light makes it easily distinguishable from sulphide minerals.

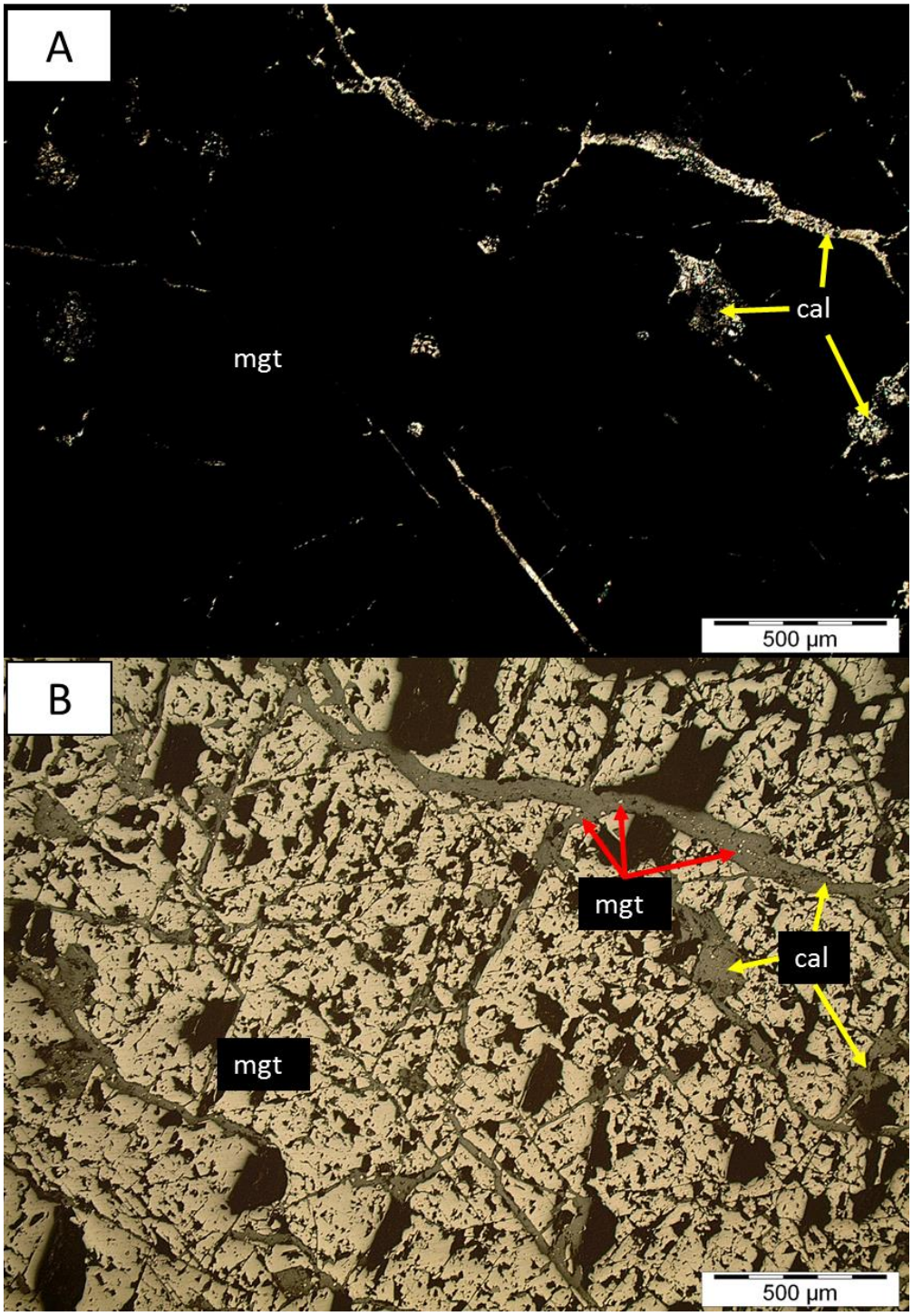

Figure 4.56: Strained first generation magnetite replaced by calcite at cracks and fractures. Image also shows residual islands of first generation magnetite in calcite (red arrows). TL image with crossed polarisers (A) and RL image (B), sample MT-27.

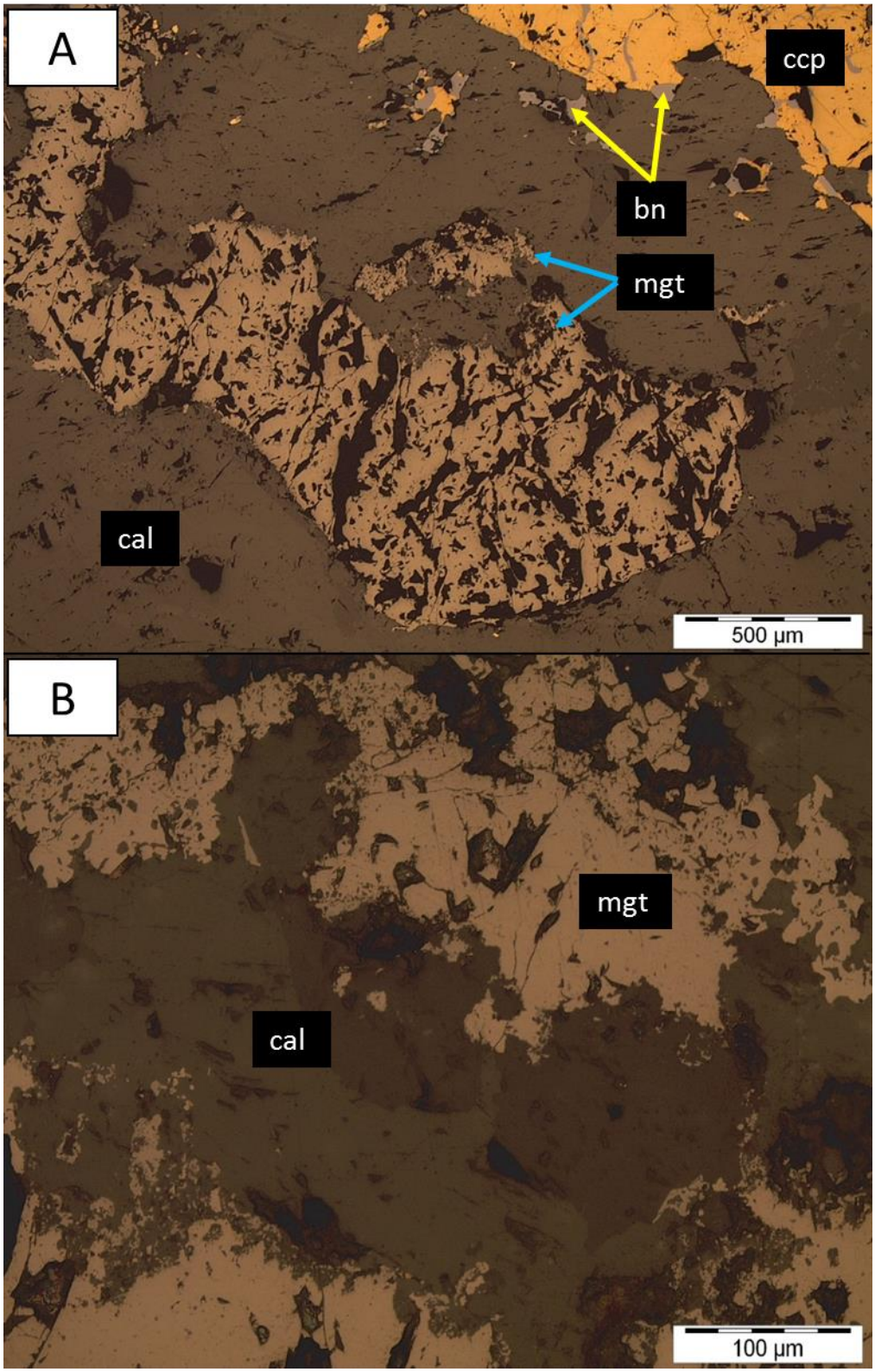

Figure 4.57: A) First generation magnetite mass replaced by calcite. B) Magnified image of the same area (blue arrows; rotated slightly clockwise). RL images (A & B), sample MT-19.

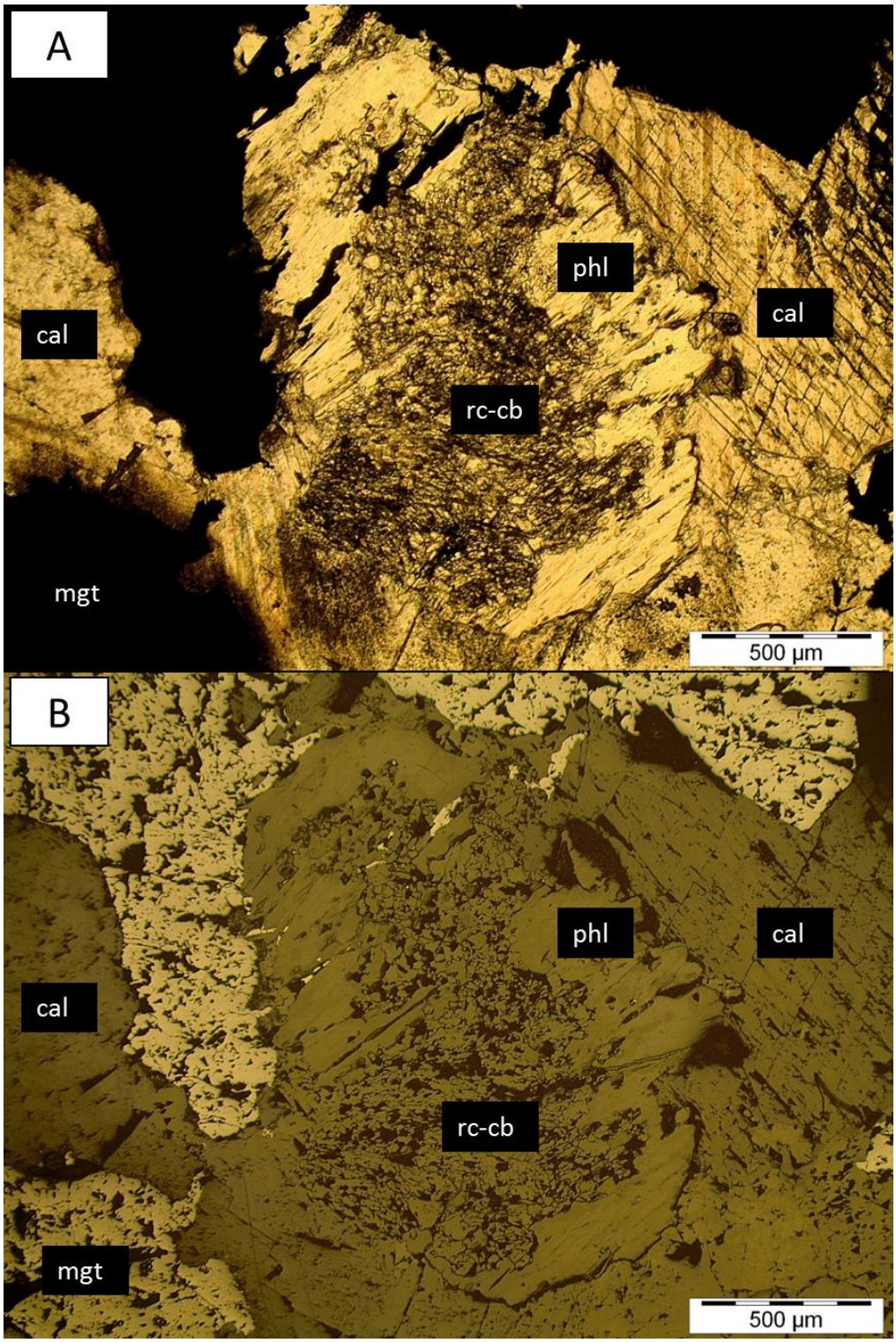

Figure 4.58: Calcite replaced by second generation magnetite. Phlogopite and calcite replaced by recrystallised carbonates. Notice how the magnetite dissected the calcite fabric (lower left-hand corner). TL image (A) and RL image (B), sample MT-20.

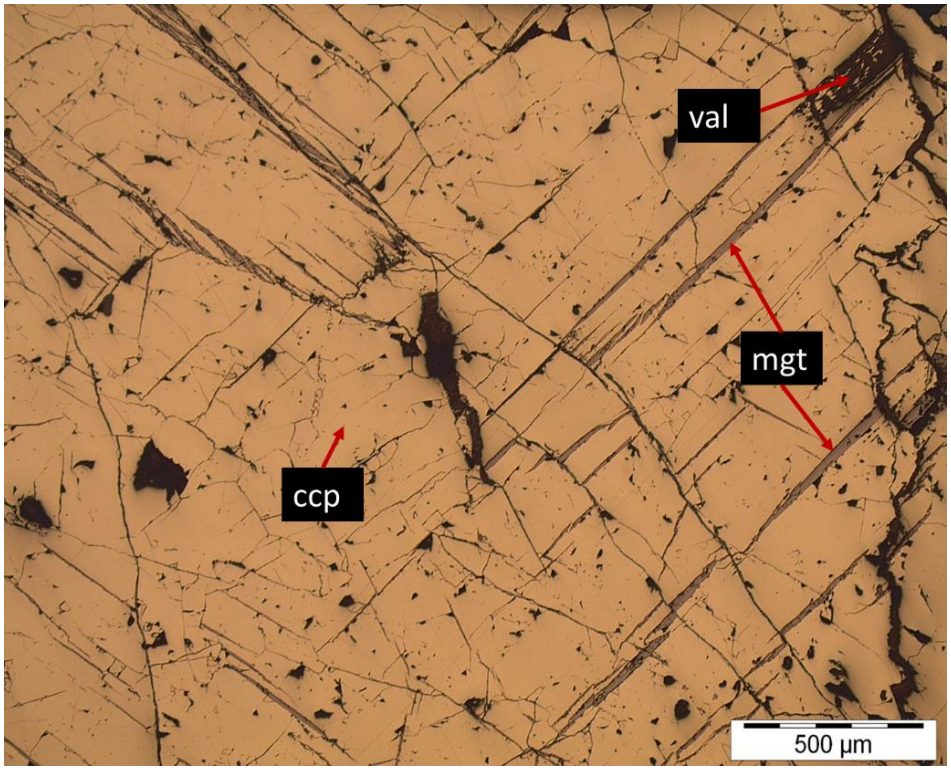

Figure 4.59: Third generation magnetite veinlets in chalcopyrite fabric. RL image, sample MT-23.

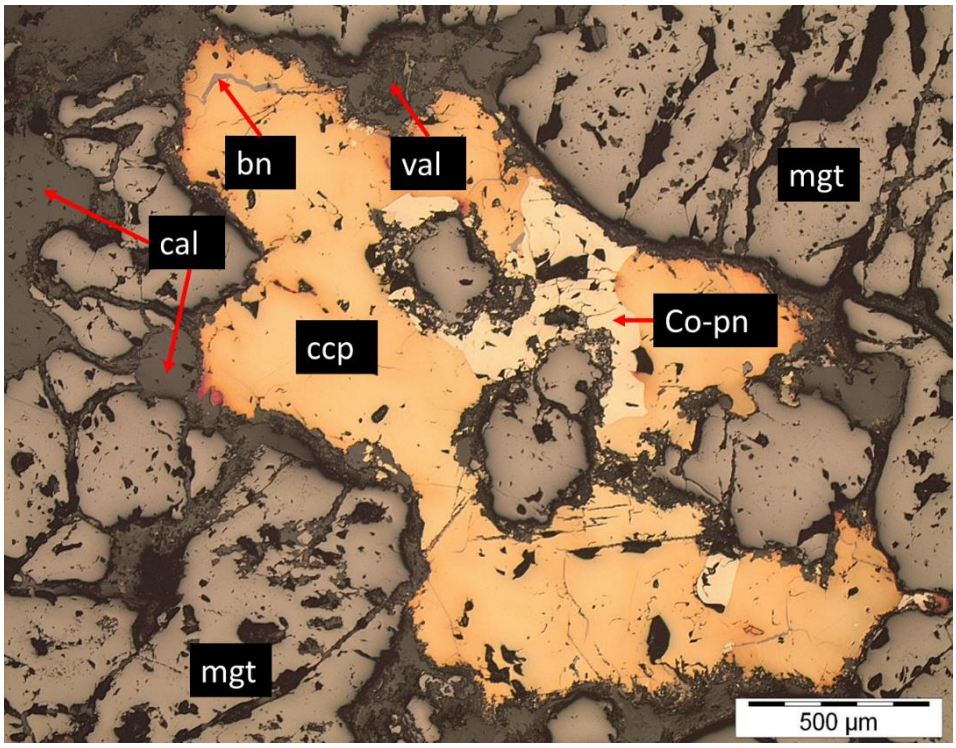

Figure 4.60: First generation magnetite-calcite-sulphide association. Magnetite grains (left-hand side) dissected by calcite. Magnetite and calcite replaced by sulphides. RL image, sample MT-58.

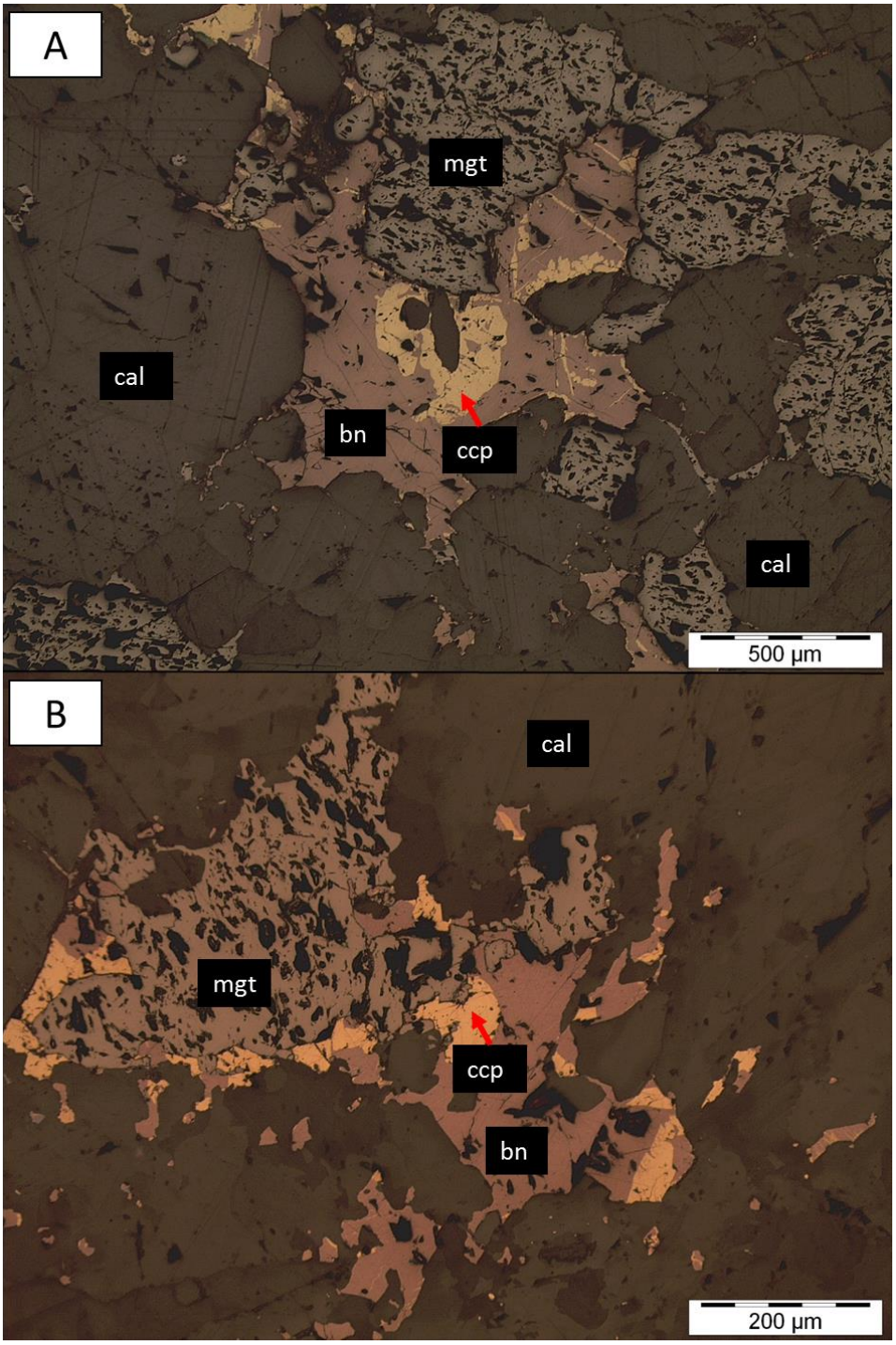

Figure 4.61: A) Second generation magnetite-calcite-sulphide association. Magnetite dissected calcite grains (right-hand side). Magnetite and calcite replaced by sulphides. RL image, sample MT-16 (TCB). B) The same magnetite-calcite-sulphide association present within BCB, RL image, sample MT-52.

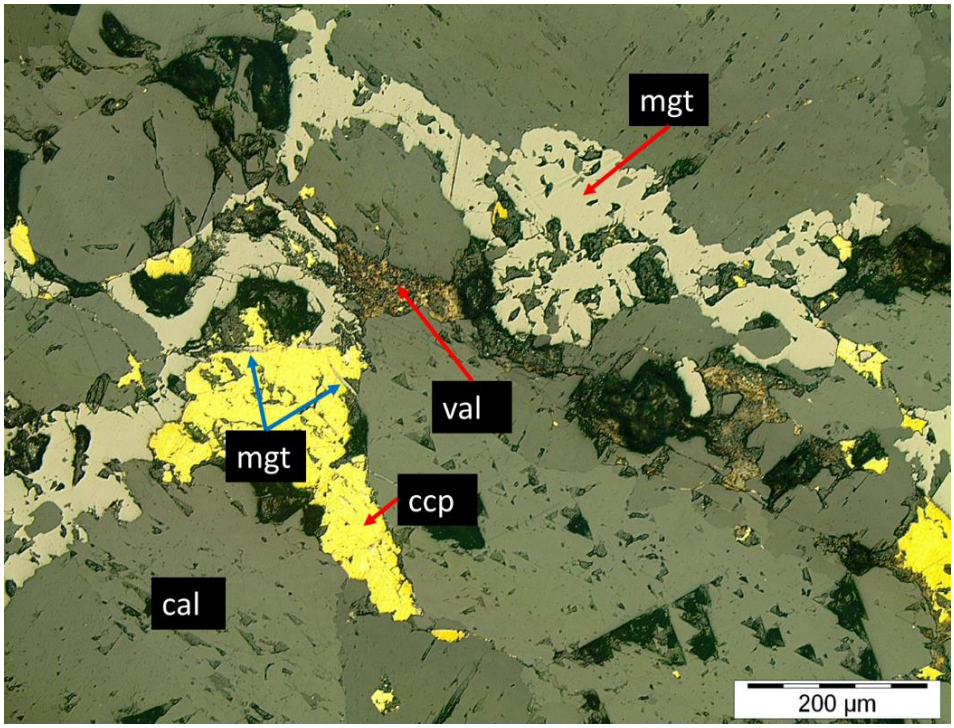

Figure 4.62: Third generation magnetite-calcite-sulphide association. Magnetite formed at calcite-sulphide boundaries (left-hand side) and also in chalcopyrite (blue arrows). RL image, MT-7.

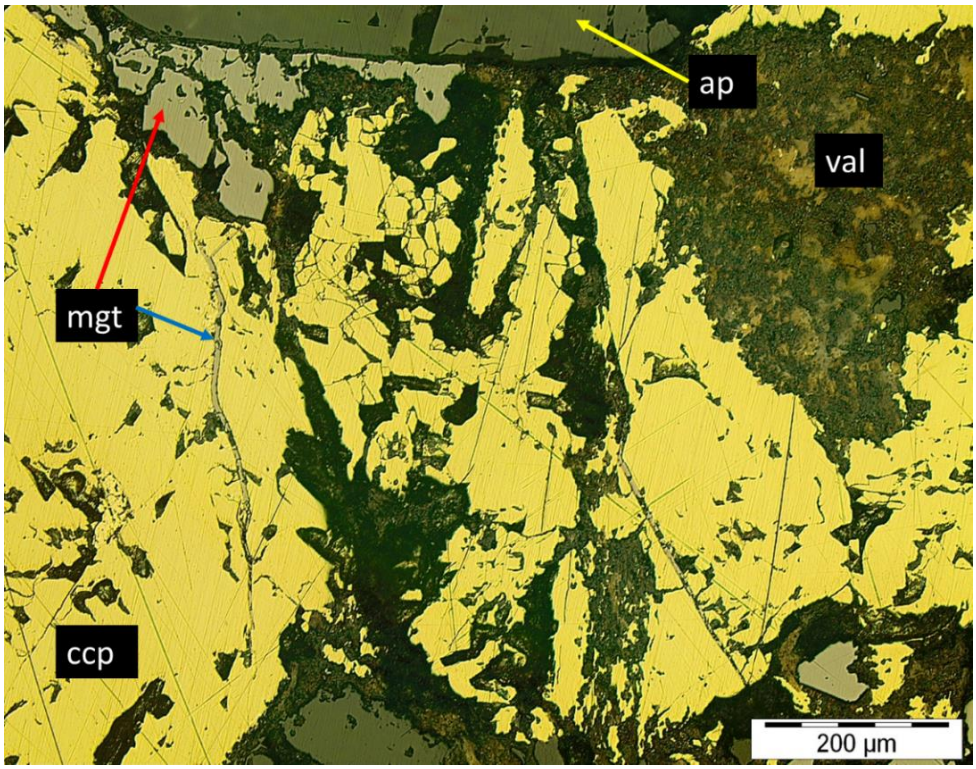

Figure 4.63: Third generation magnetite formed at apatite-sulphide boundary (red arrow). Magnetite veinlets also formed in chalcopyrite (blue arrow). RL image, sample MT-20.

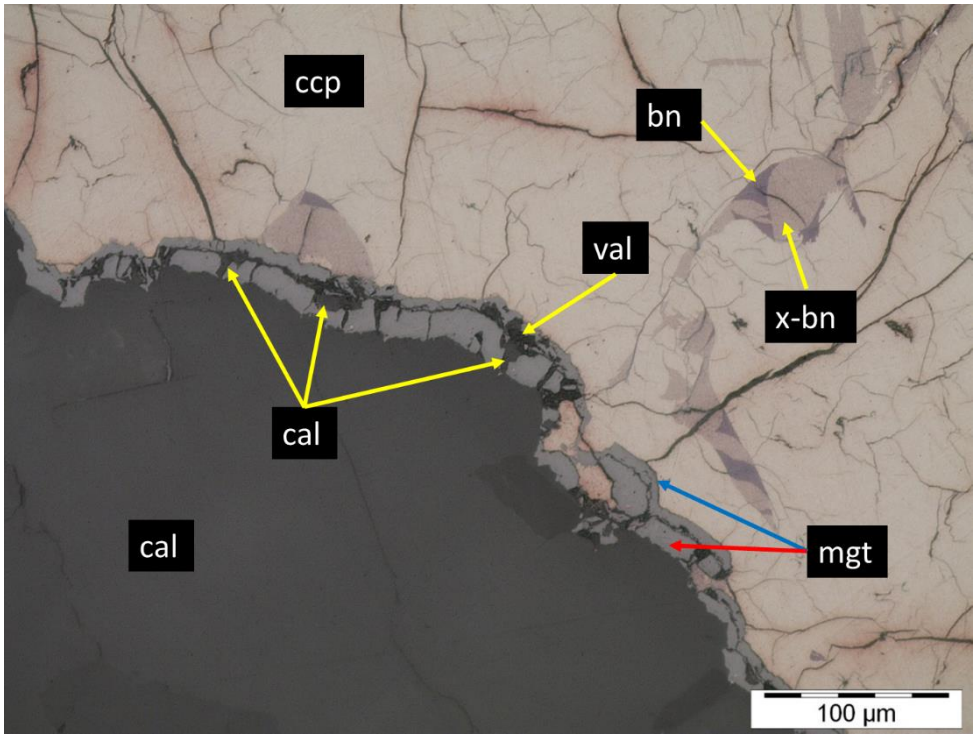

Figure 4.64: Third generation magnetite rim (blue arrow) between first generation magnetite (red arrow) and sulphides. First generation magnetite replaced by calcite. Both magnetite generations and calcite are replaced by valleriite. RL image, sample MT-71.

b) Ilmenite:

Two very easily distinguishable generations of ilmenite formation are present within both banded and transgressive carbonatites. Firstly, as fine-grained, euhedral to subhedral grains that formed during the first stage of magnetite crystallisation (Figure 4.65; Figure 4.66), and secondly, as ilmenite exsolution laths within first stage magnetite (Figure 4.67).

First generation ilmenite forms mutual grain boundaries with magnetite and occurs at magnetite-non-sulphide grain boundaries (Figure 4.65), or completely enclosed by magnetite (Figure 4.66). Both generations occur only in first generation magnetite and show textural evidence of forming prior to calcite crystallisation (Figure 4.68; Figure 4.69; Figure 4.70). The pink tint of ilmenite under reflected light makes it easily distinguishable from magnetite, baddeleyite, and uranothorianite.

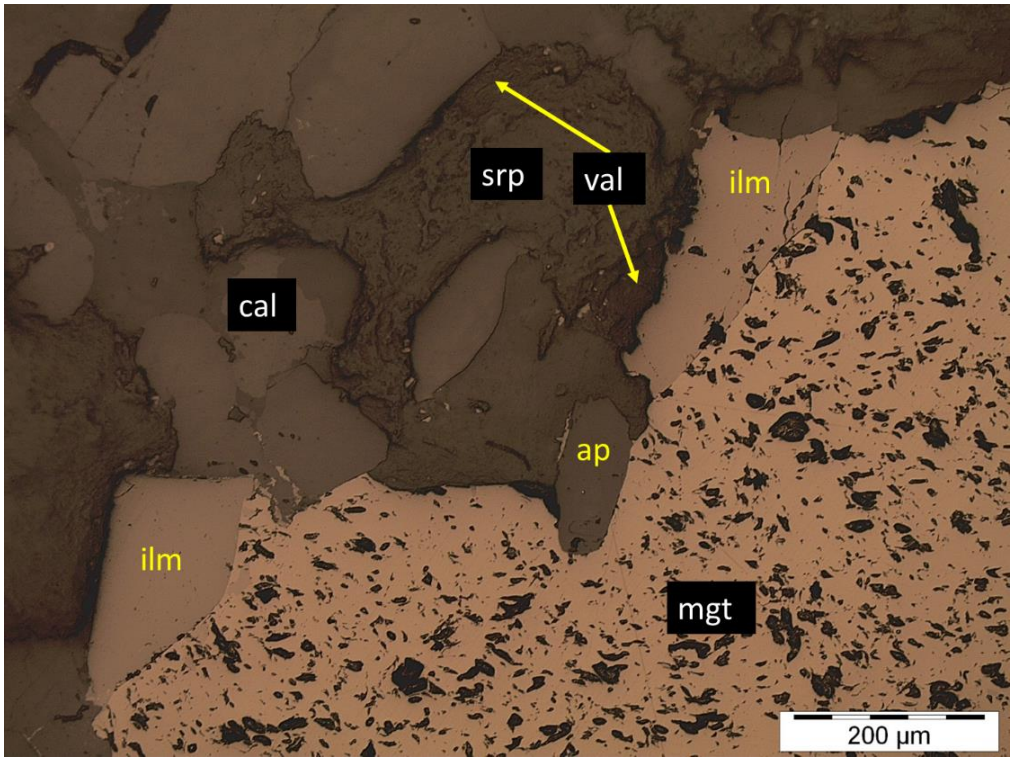

Figure 4.65: Mutual grain boundaries between magnetite and first generation ilmenite. RL image, sample MT-67.

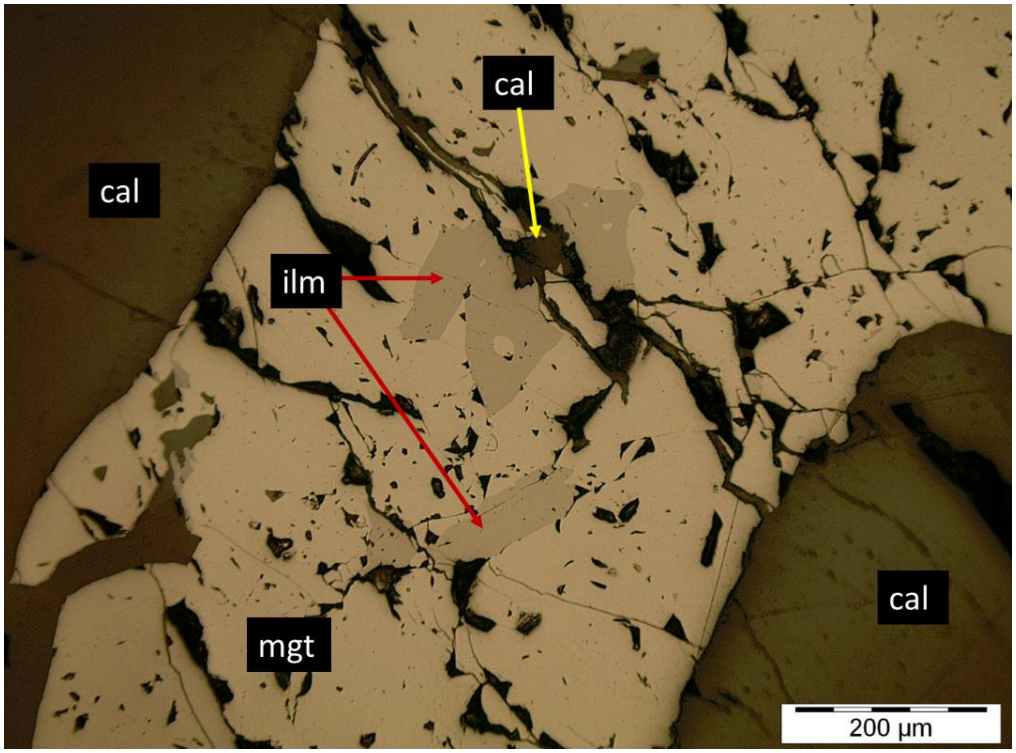

Figure 4.66: Euhedral ilmenite grains included in first generation magnetite. Ilmenite replaced by calcite (yellow arrow). RL image, sample MT-11.

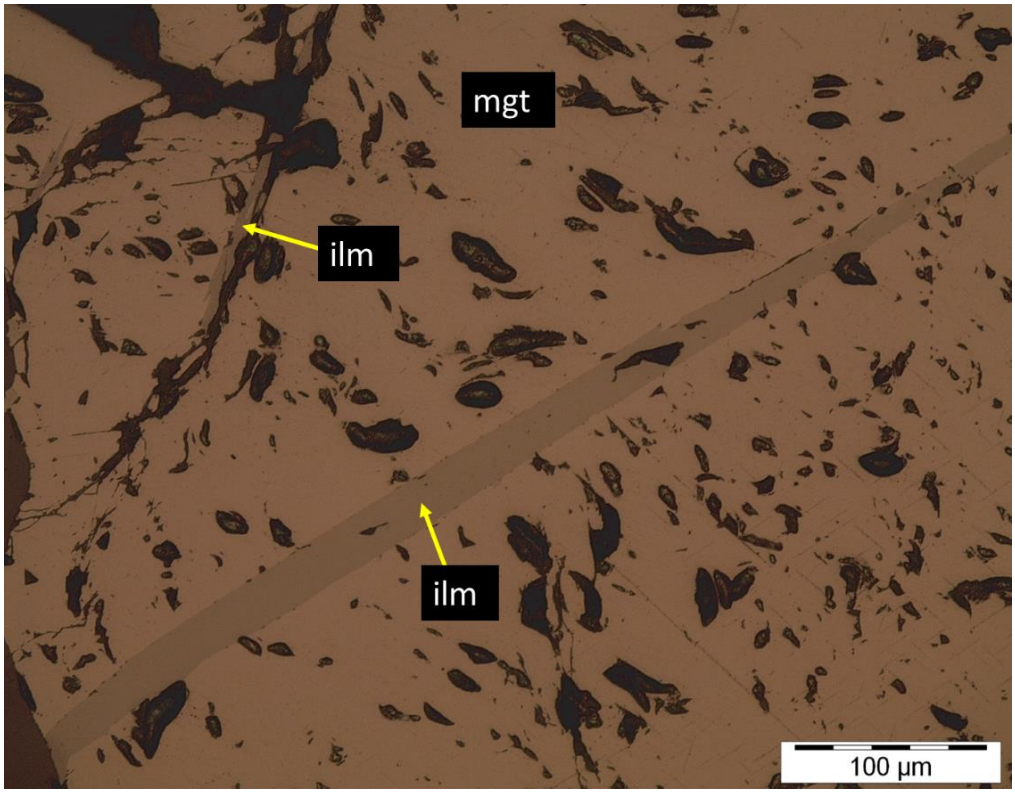

Figure 4.67: Ilmenite exsolution lath in first generation magnetite. RL image, sample MT-67.

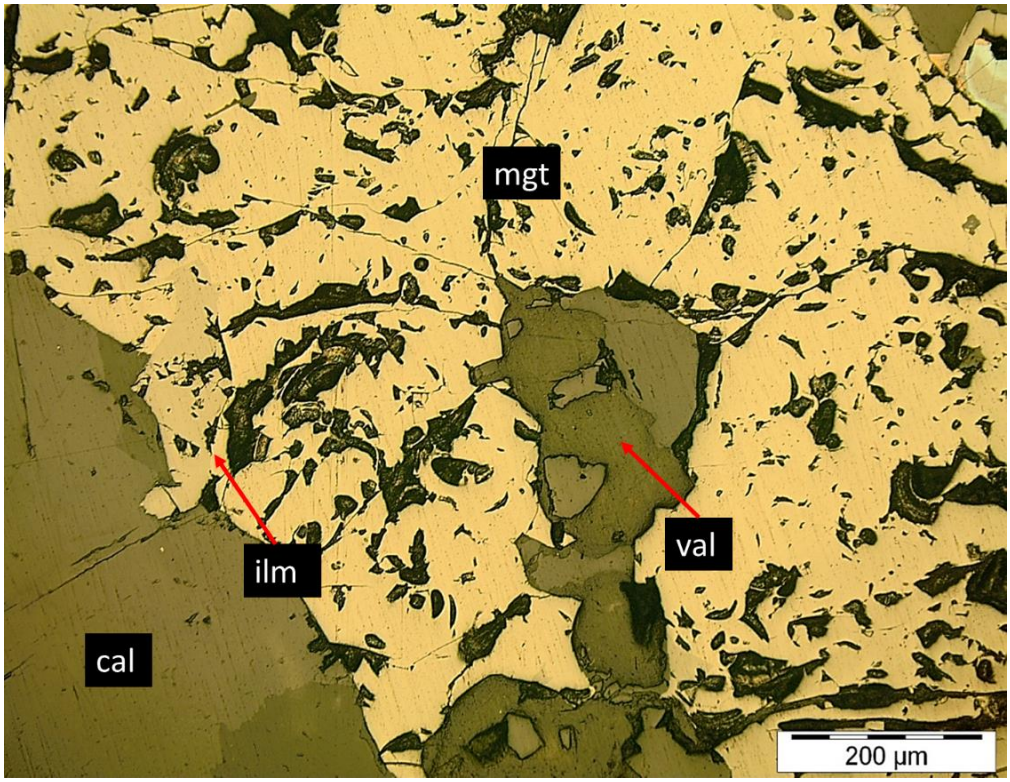

Figure 4.68: First generation ilmenite and first generation magnetite replaced by calcite. RL image, sample MT-11.

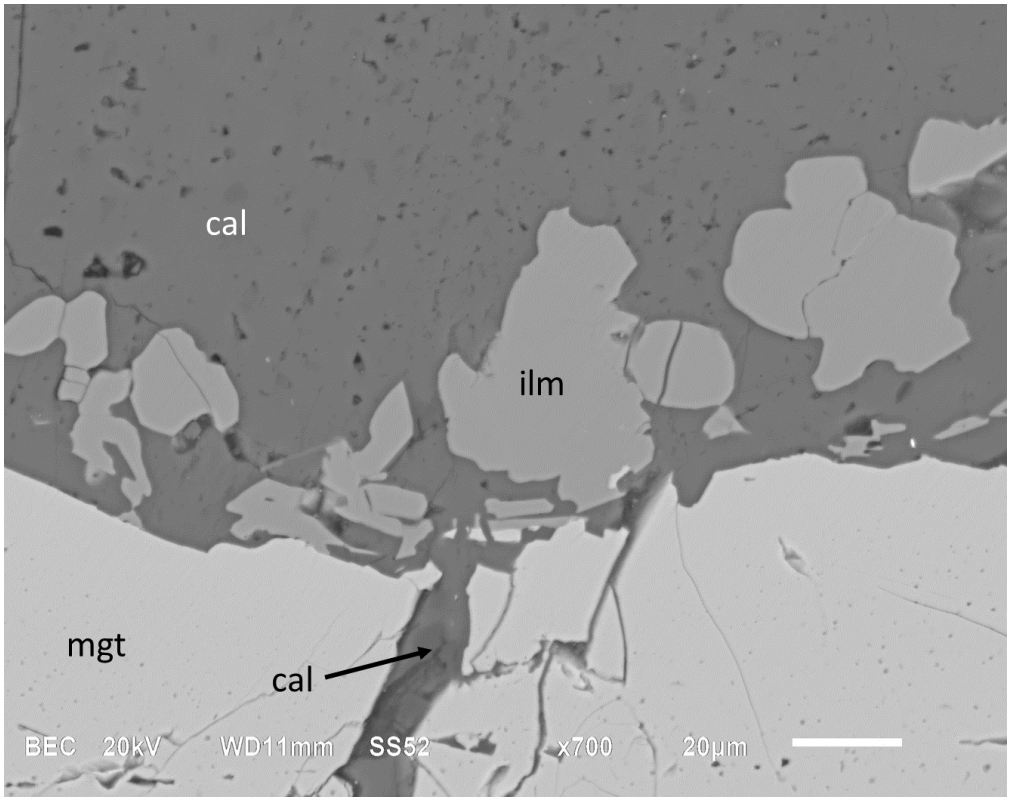

Figure 4.69: First generation magnetite and first generation ilmenite replaced by calcite. BSE image, sample MT-11.

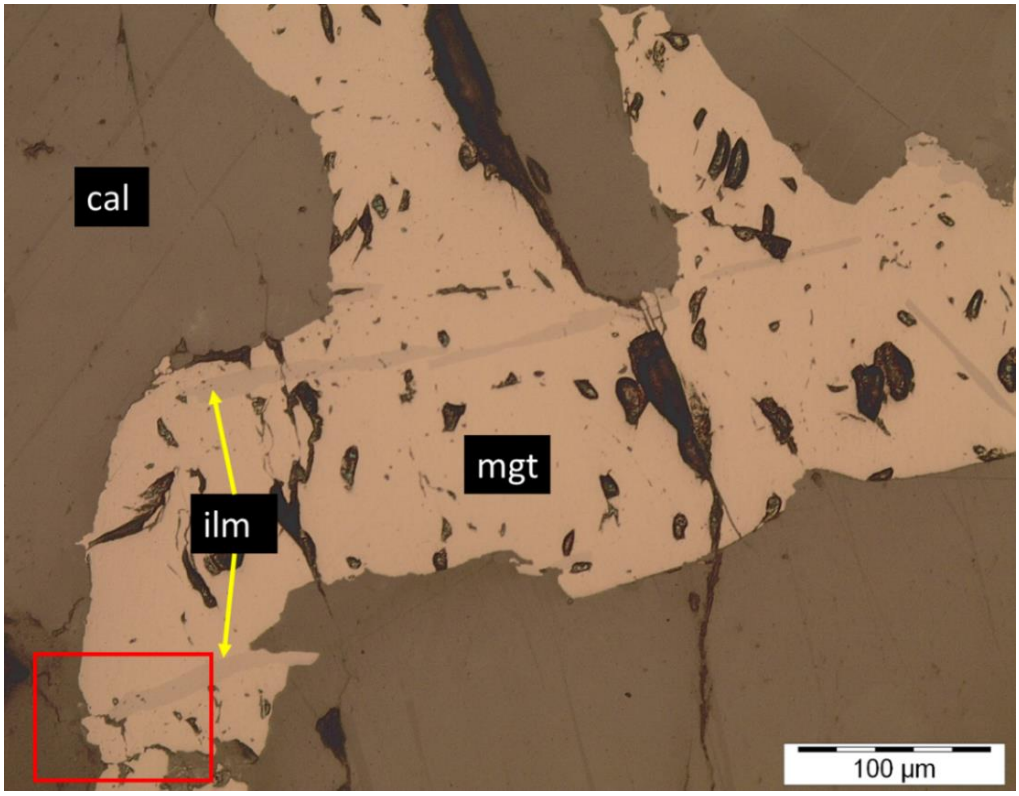

Figure 4.70: First generation magnetite and second generation ilmenite replaced by calcite (red rectangle). RL image, sample MT-67.

c) Spinel:

Ilmenite is not the only exsolved phase observed in magnetite. Euhedral to subhedral cubic grains (5 µm – 150 µm) may be distributed throughout the large magnetite masses. However, it is absent from third generation magnetite. According to Giebel *et al.* (2017), these grains are spinel (Figure 4.71; Figure 4.72).

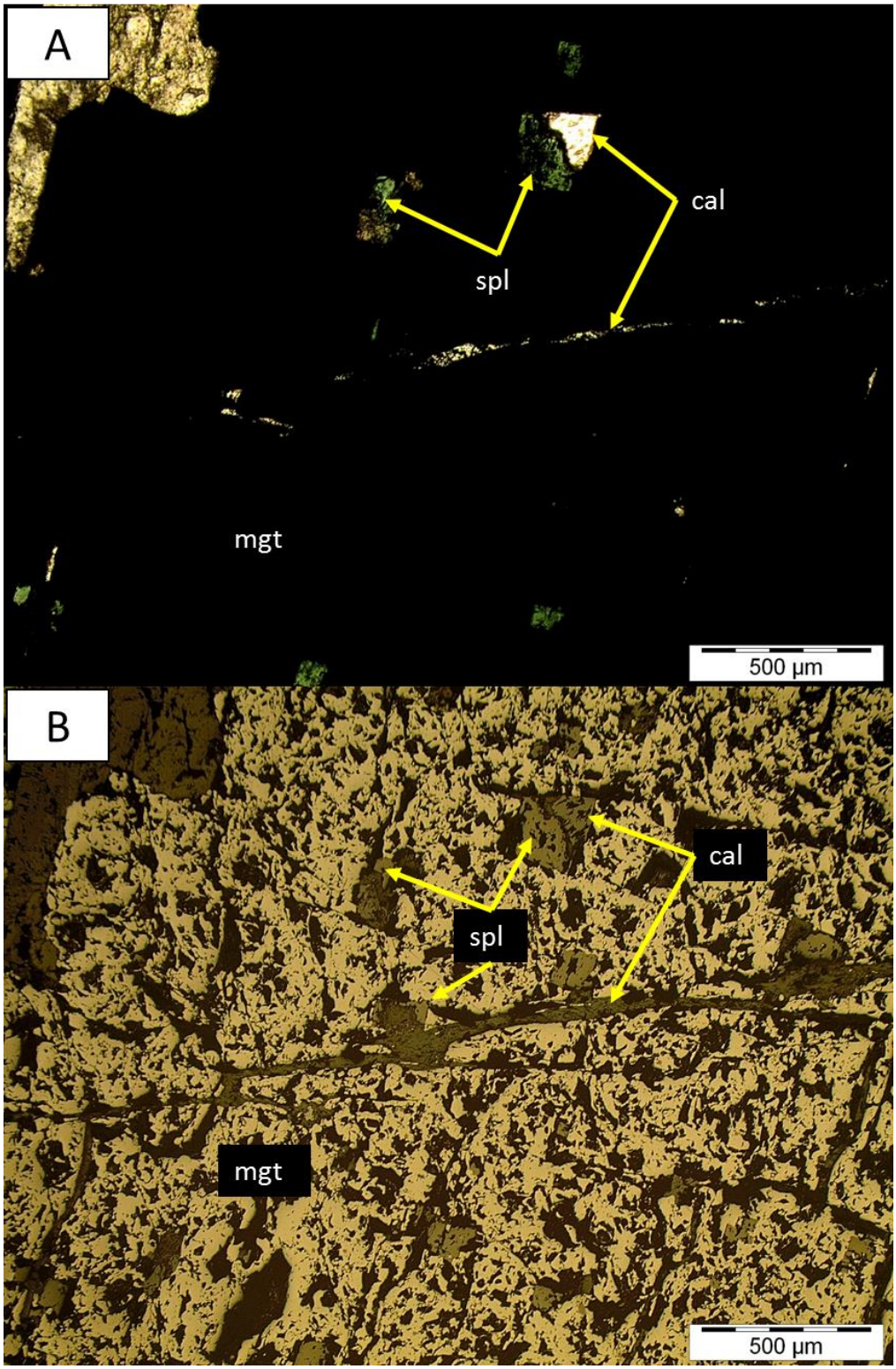

Figure 4.71: Exsolved spinel and first generation magnetite replaced by calcite. TL image (A) and RL image (B), sample MT-40.

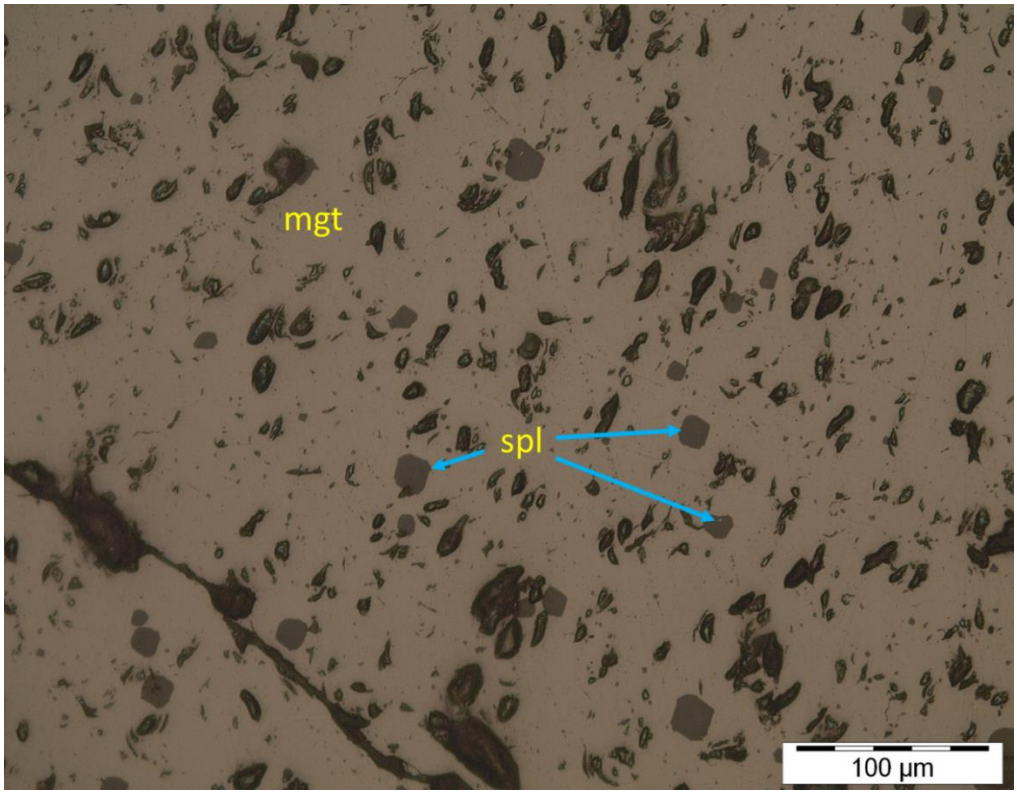

Figure 4.72: Spinel exsolved from first generation magnetite. RL image, sample MT-16.

d) Baddeleyite:

Baddeleyite is a frequently occurring accessory mineral in both carbonatite types. It is also present in one of the two phoscorite samples.

The mineral primarily forms euhedral prismatic crystals that are dark-brown under transmitted light and grey under reflected light (Figure 4.73). However, baddeleyite has a lower reflectance than magnetite under reflected light. It is also common for baddeleyite to form cruciform twins (Figure 4.74), thus making it easier to distinguish from opaque minerals. Baddeleyite formed before sulphide mineralisation (Figure 4.73, B), first stage magnetite (Figure 4.75), and apatite (Figure 4.76).

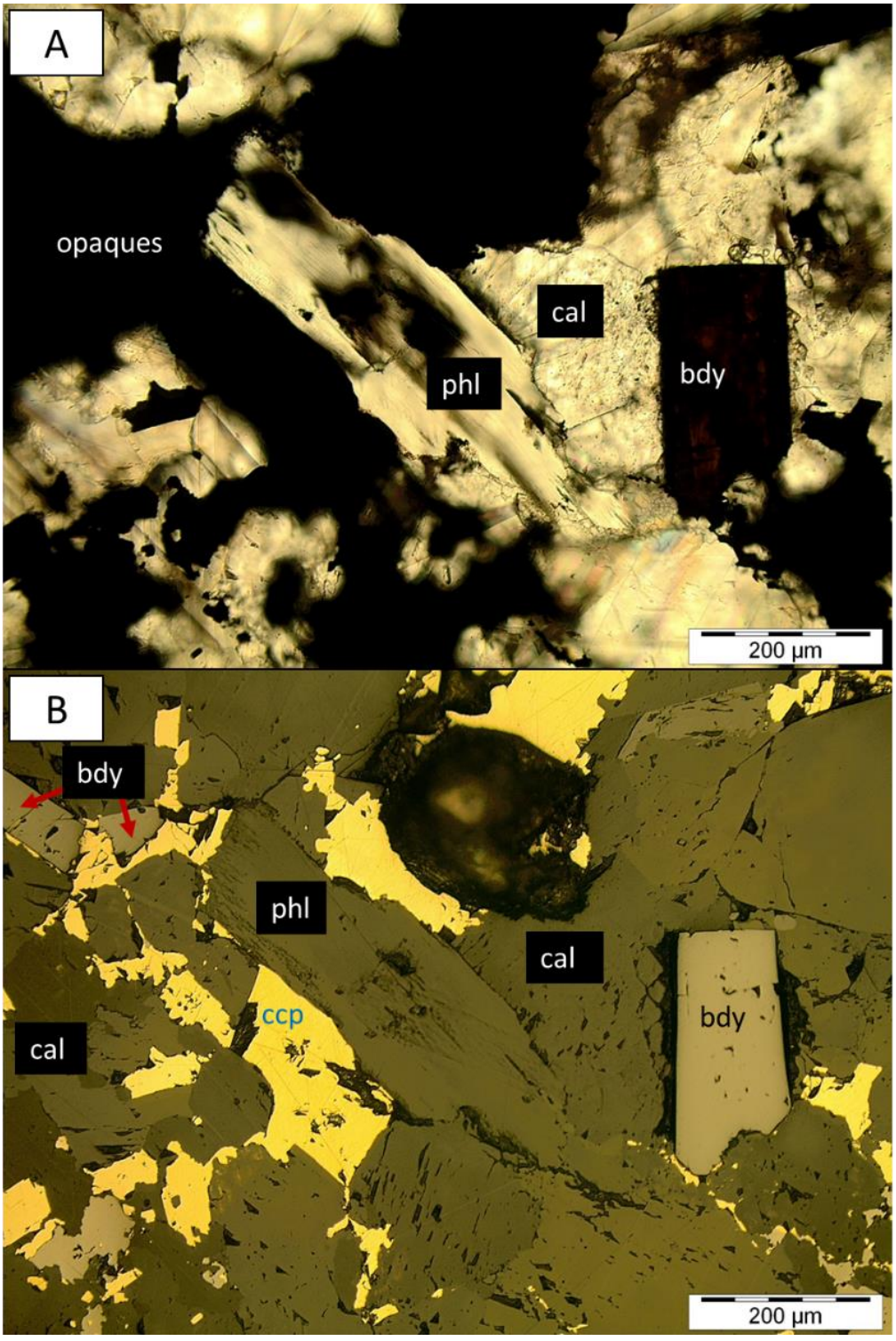

Figure 4.73: A) Dark-brown, euhedral baddeleyite grain (elongated) enclosed by calcite. B) Baddeleyite replaced by chalcopyrite (red arrows). TL image (A) and RL image (B), sample MT-38.

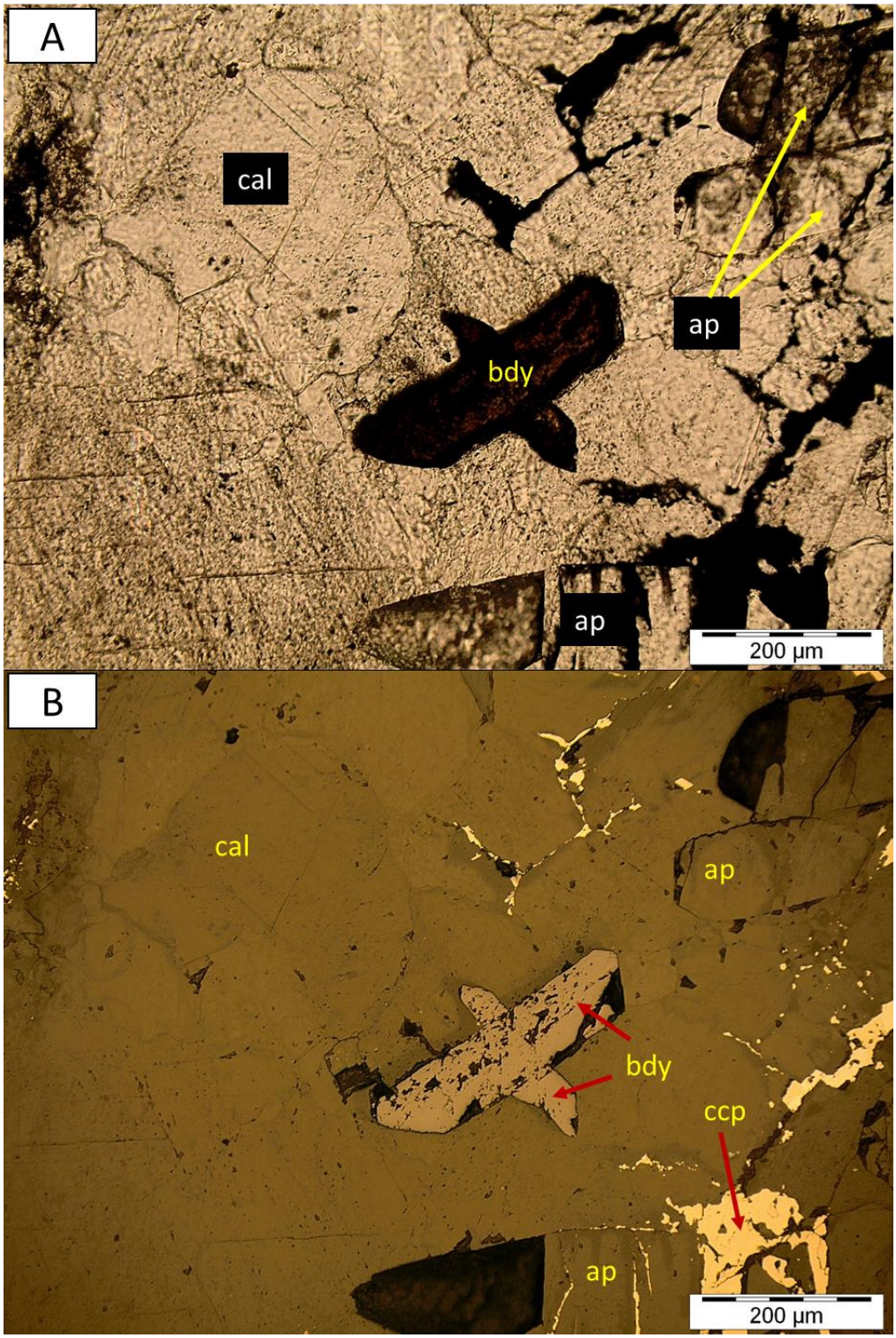

Figure 4.74: Cruciform twinning of baddeleyite.TL (A) image and RL (B) image, sample MT-48.

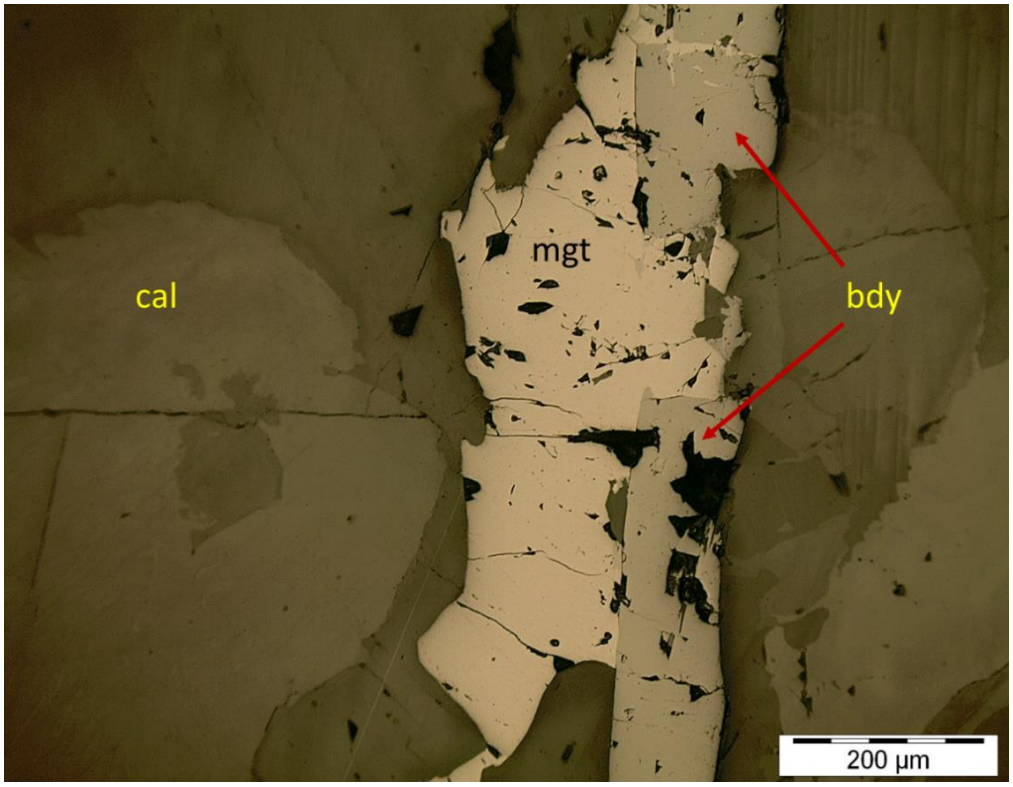

Figure 4.75: Elongated baddeleyite grains replaced by first generation magnetite. RL image, sample MT-11.

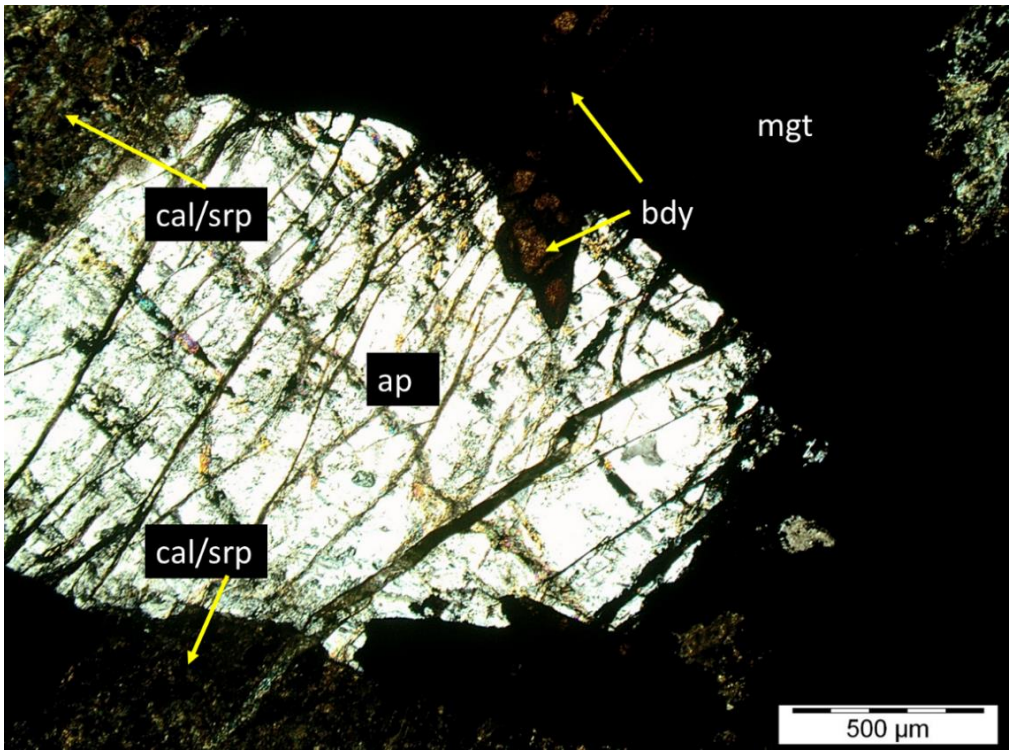

Figure 4.76: Baddeleyite subpoikilitically enclosed by coarse-grained apatite. TL image with crossed polarisers, sample MT-55.

e) Uranothorianite:

Uranothorianite primarily forms strongly euhedral cubic grains (Figure 4.77). Uranothorianite and baddeleyite have similar colours under reflected light. However, the presence of radiation halos (Figure 4.77, A; Figure 4.78) makes uranothorianite easily distinguishable under transmitted light. Also, uranothoriantie is opaque under transmitted light, while baddeleyite is dark-brown. According to Eriksson (1984), the Palabora Complex has been dated by U-Pb analysis of baddeleyite and uranothorianite.

Baddeleyite and uranothorianite form intergrowths (Figure 4.79). Thus, it is interpreted that these minerals formed approximately in the same time period. Just like baddeleyite, uranothorianite shows signs of being poikilitically enclosed by apatite (Figure 4.80). This is indicative of uranothorianite and baddeleyite formation prior to apatite formation.

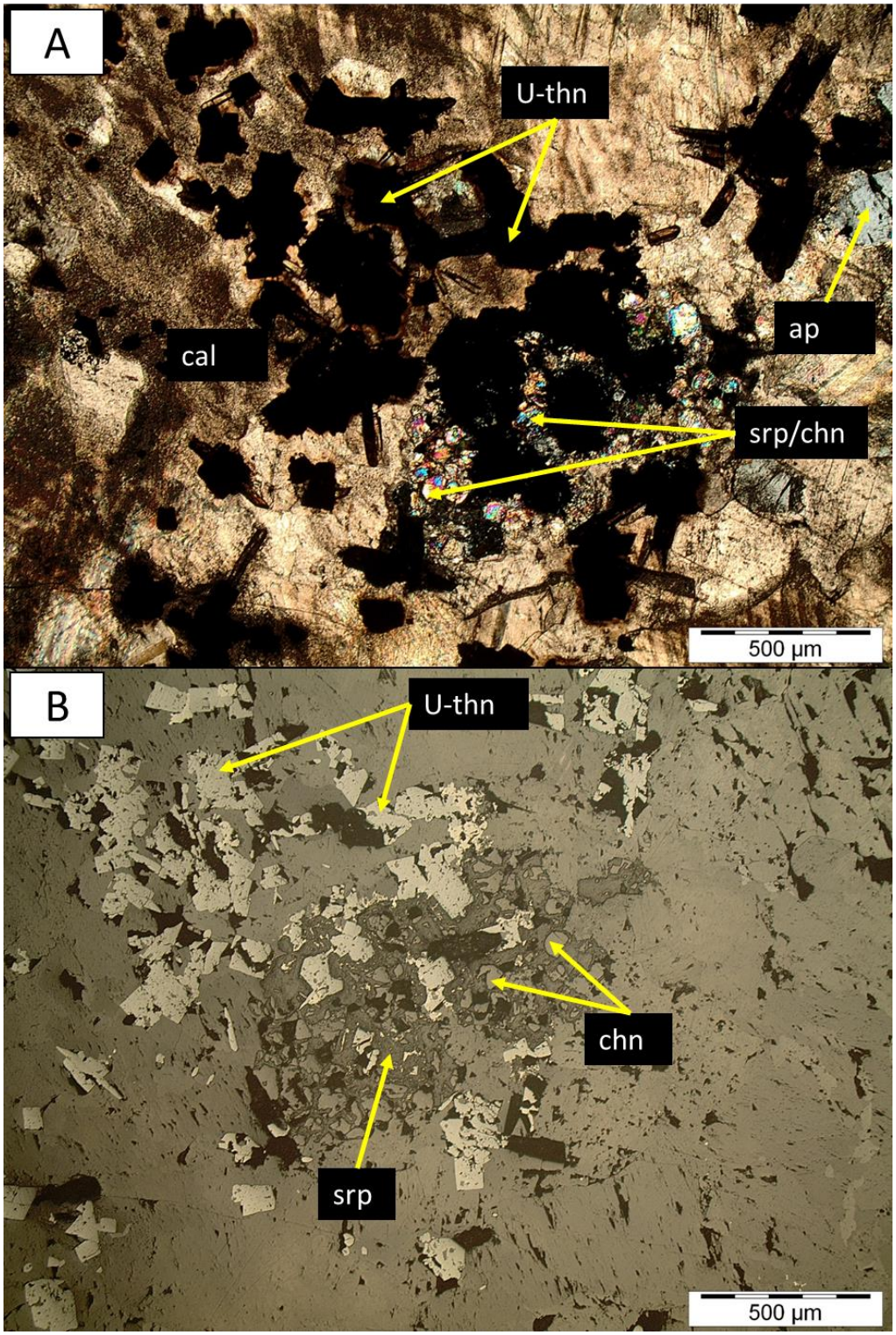

Figure 4.77: Cubic uranothorianite grains enclosed by calcite. Image also shows uranothorianite enclosed by first generation magnetite. TL image with crossed polarisers (A) and RL image (B), sample MT-32.

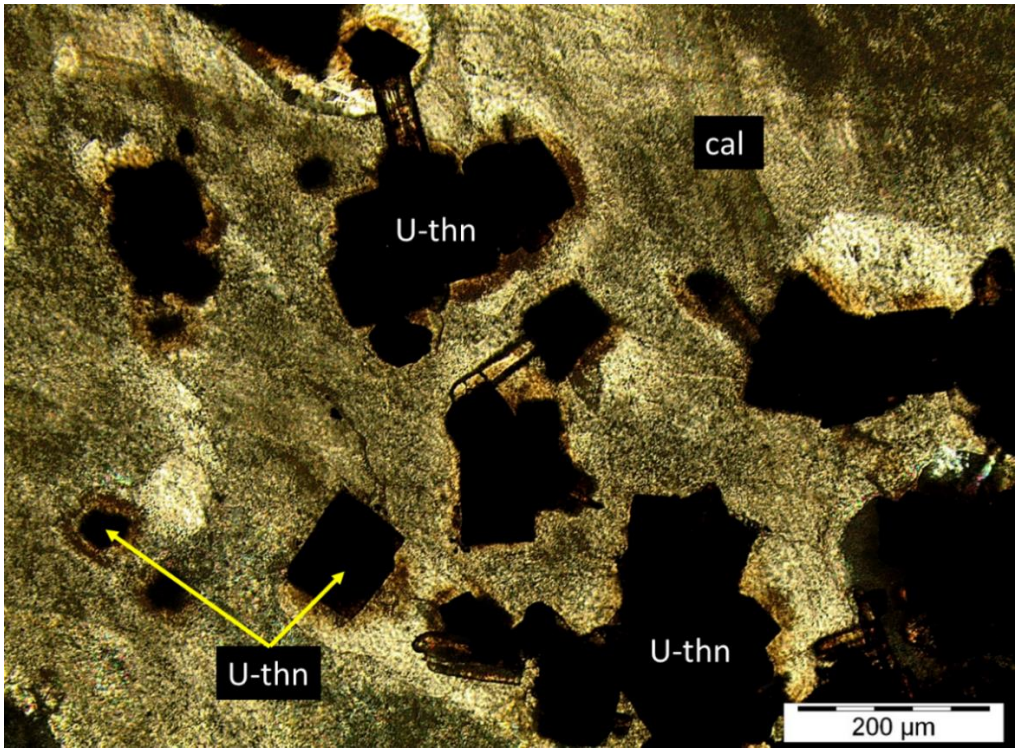

Figure 4.78: Euhedral uranothorianite grains rimmed by dark-brown radiation halos. TL image with crossed polarisers, sample MT-32.

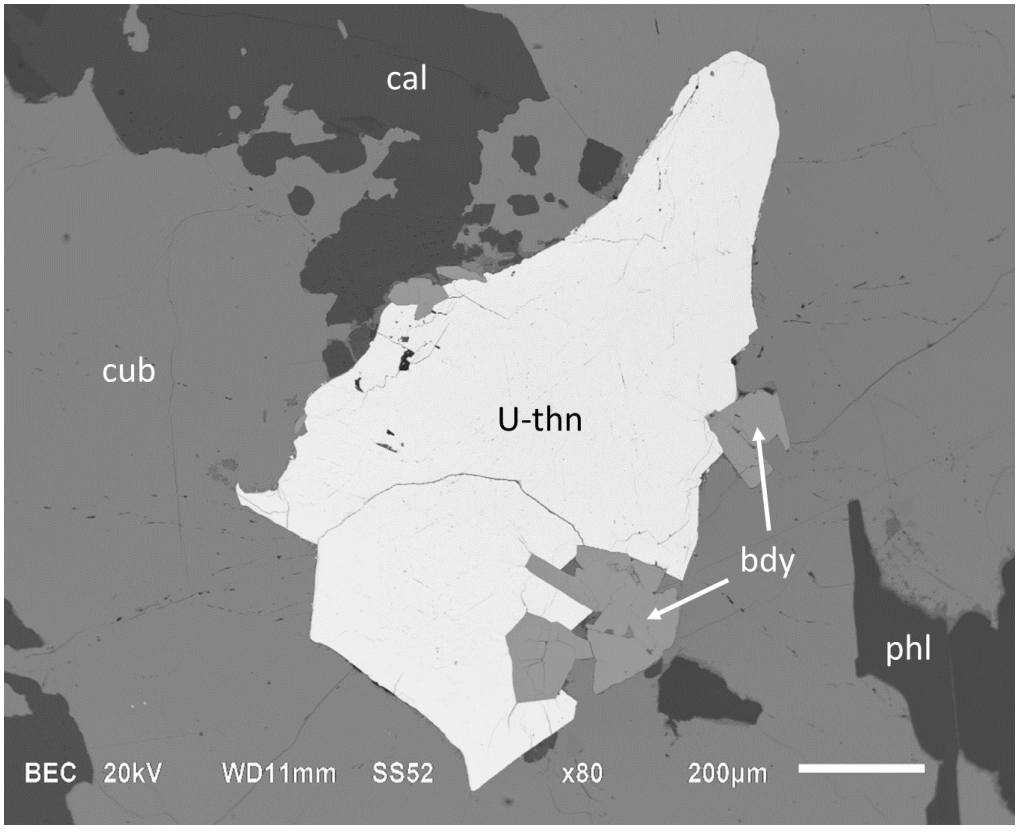

Figure 4.79: Intergrowth of baddeleyite and uranothorianite. BSE image, sample MT-3.

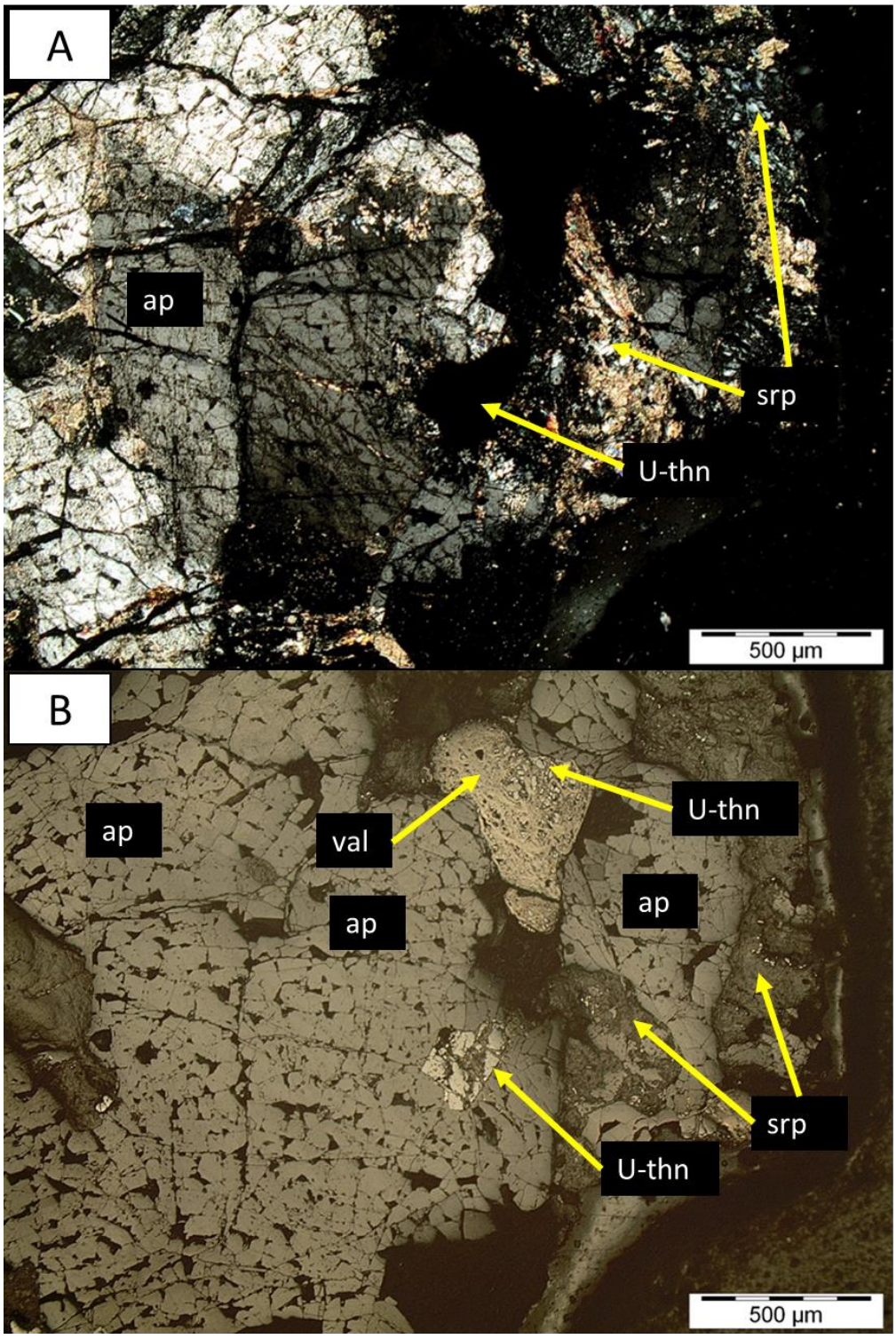

Figure 4.80: Cubic uranothorianite grain that is poikilitically enclosed by coarse-grained apatite and also partially replaced by valleriite. TL image with crossed polarisers (A) and RL image (B), sample MT-32.

4.4.3. Phosphates.

a) Apatite:

Apatite is abundant in both carbonatite types (up 9 modal % within banded carbonatite samples and 20 modal % within transgressive carbonatite samples) and in phoscorite (up to 22 modal %). The mineral shows a hexagonal shape perpendicular to the c-axis and has a distinguishable grey colour under cross-polarised light.

Five varieties of apatite, with respect to grain sizes and shapes, have been identified in both carbonatite types: 1) coarse-grained apatite, 2) medium-grained apatite, 3) fine-grained apatite, 4) larger aphanitic acicular apatite needles (compared to 5), and 5) smaller aphanitic acicular apatite needles (compared to 4). Coarse- to fine-grained apatite is mostly equally distributed within the carbonate matrix. Only coarse-grained apatite crystals are present in the phoscorite samples.

Apatite primarily occurs as coarse-grained (Figure 4.81; Figure 4.82) and medium-grained (Figure 4.83), elongated/prismatic crystals that are euhedral to subhedral in shape. These grains may show signs of extensive straining (Figure 4.82). Subparallel alignment of coarse- to medium-grained crystals is common (Figure 4.81 and 4.83). Brassinnes *et al.* (2005) speculates that this might be interpreted as a magmatic flow texture. The fine-grained apatite crystals are observed as rounded prisms and can be subhedral to anhedral in shape.

It is common to find apatite crystals that are poikilitically enclosed by olivine in both carbonatite types (Figure 4.84; Figure 4.85). Figure 4.85, B also shows minor replacement of magnetite by serpentine. The magnetite forming liquid must have intruded along cracks that formed inside the olivine grains. Serpentinisation then replaced the magnetite as well. Also notice the anhedral shape of the magnetite fabric that encloses the serpentinised olivine grain. The magnetite lost its euhedral to subhedral form due to serpentine replacement at the magnetite-olivine boundary.

Apatite also occurs as very rare, isolated euhedral acicular needles that are also poikilitically enclosed by olivine (Figure 4.86; Figure 4.87). However, the smallest acicular apatite needles are randomly distributed in a serpentine matrix that shows no association towards serpentinisation of olivine (Figure 4.88; Figure 4.89). Instead, the serpentine matrix is

indicative towards the mass replacement of carbonate minerals. It is proposed that these acicular needles formed due to the introduction of a hydrothermal fluid.

Thus two generations of apatite formation exist: 1) the formation of larger acicular apatite needles and coarse-grained to fine-grained apatite crystals before the formation of olivine and serpentine, and 2) the formation of smaller acicular apatite needles during serpentinisation.

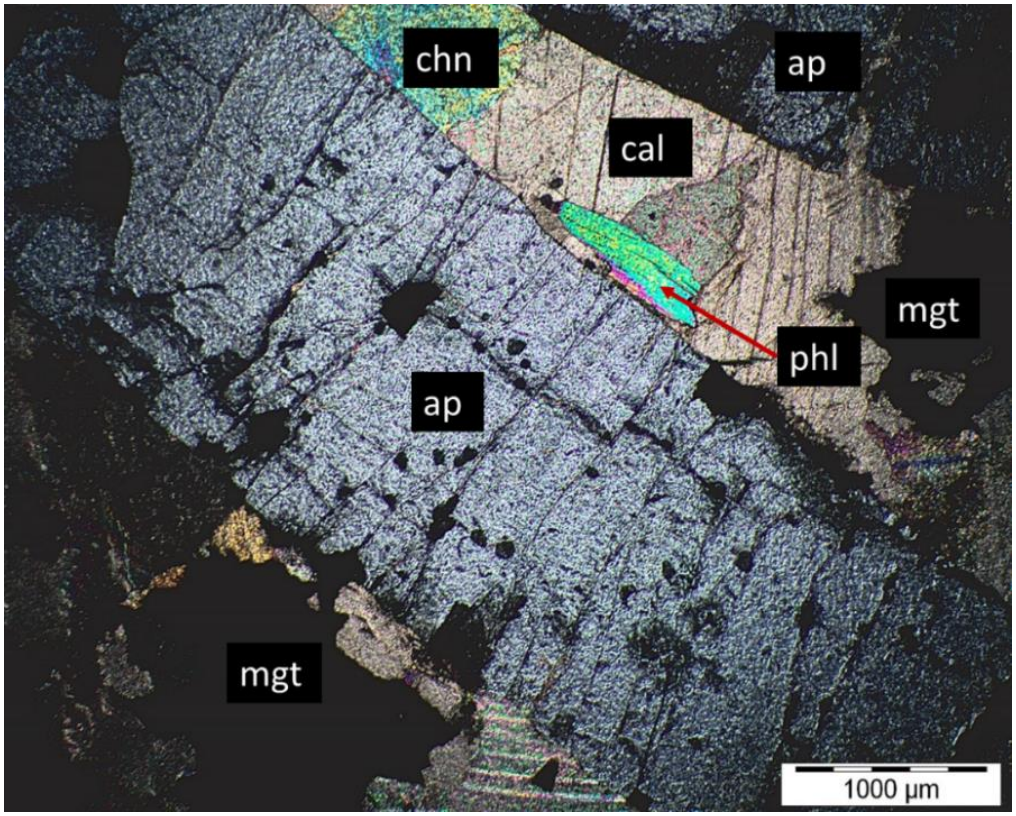

Figure 4.81: Elongated apatite grains with approximately the same orientation. Intercumulate liquid crystallised calcite. TL image with crossed polarisers, sample MT-13.

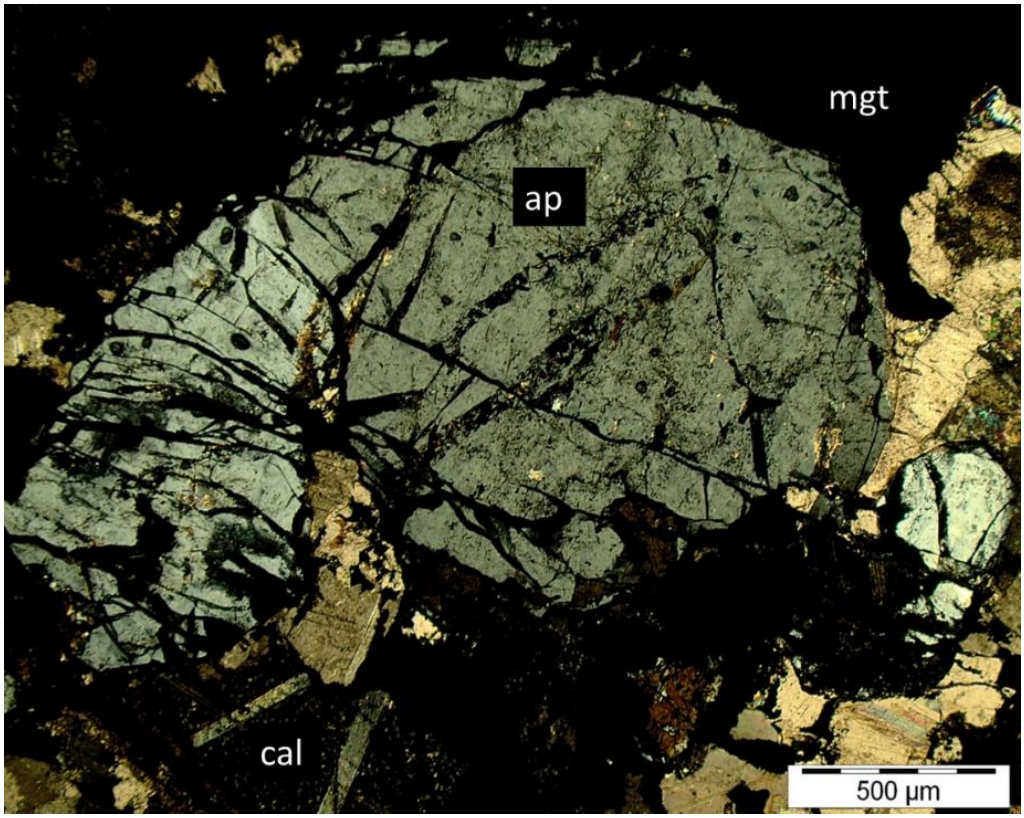

Figure 4.82: Coarse-grained apatite replaced by calcite and magnetite. TL image with crossed polarisers, sample MT-55.

First generation apatite shows signs of replacement by calcite (Figure 4.82) and serpentine (Figure 4.90), while the smaller acicular needles do not. If the tiny acicular grains (which are always embedded in serpentine) did form in the same period as the larger grains then they would have been completely replaced by serpentine, thus they must be from a younger generation of apatite formation, seeing that they are so well preserved in an environment of extensive replacement.

Speculation thus exists when wondering why the larger acicular apatite needles are not also second generation apatite like the smaller acicular apatite needles, seeing that both are acicular (which sets them aside from the other apatite shapes) and well preserved in an environment of extensive replacement. The reason why the first generation acicular apatite needles are so well preserved is probably due to olivine being a good preserving medium (at least in areas with little serpentinisation). Second generation apatite needles are not preserved by olivine at all. They exist in areas of mass replacement where the replacing phase, serpentine, even replaced magnetite, and yet they are smaller than first generation apatite

needles and are still well preserved. Thus they must be from a separate generation, a generation that probably formed due to the remobilisation of first generation apatite elemental components.

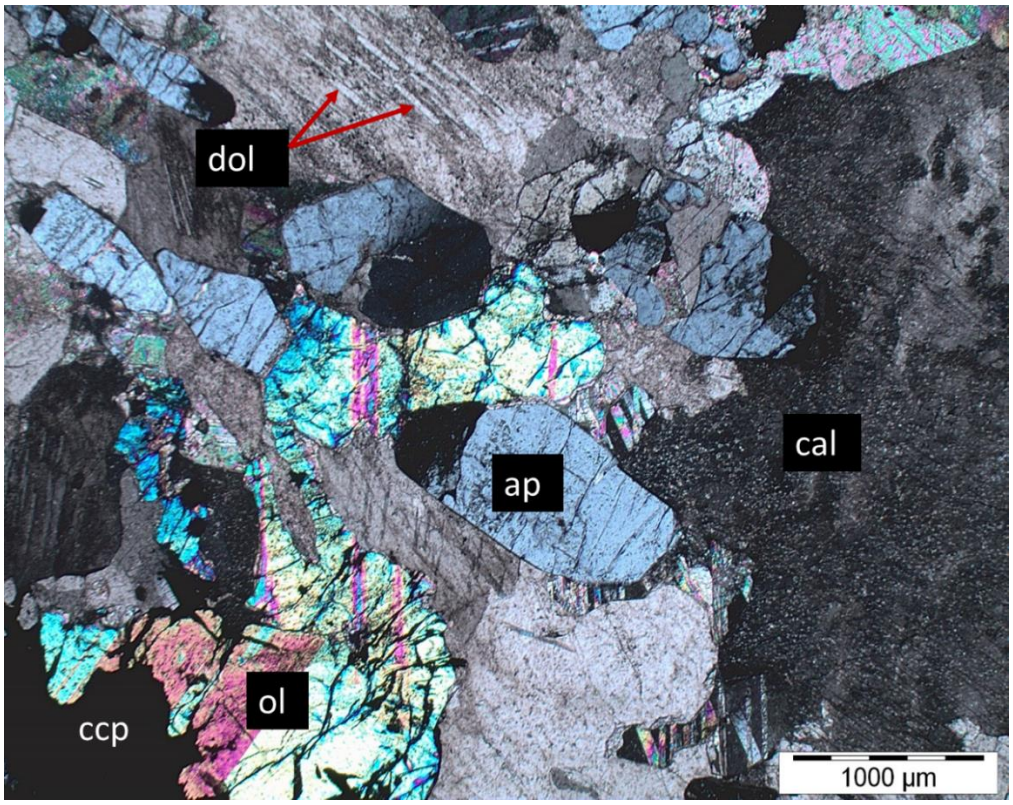

Figure 4.83: Subparallel alignment of medium-grained apatite. TL image with crossed polarisers, sample MT-3.

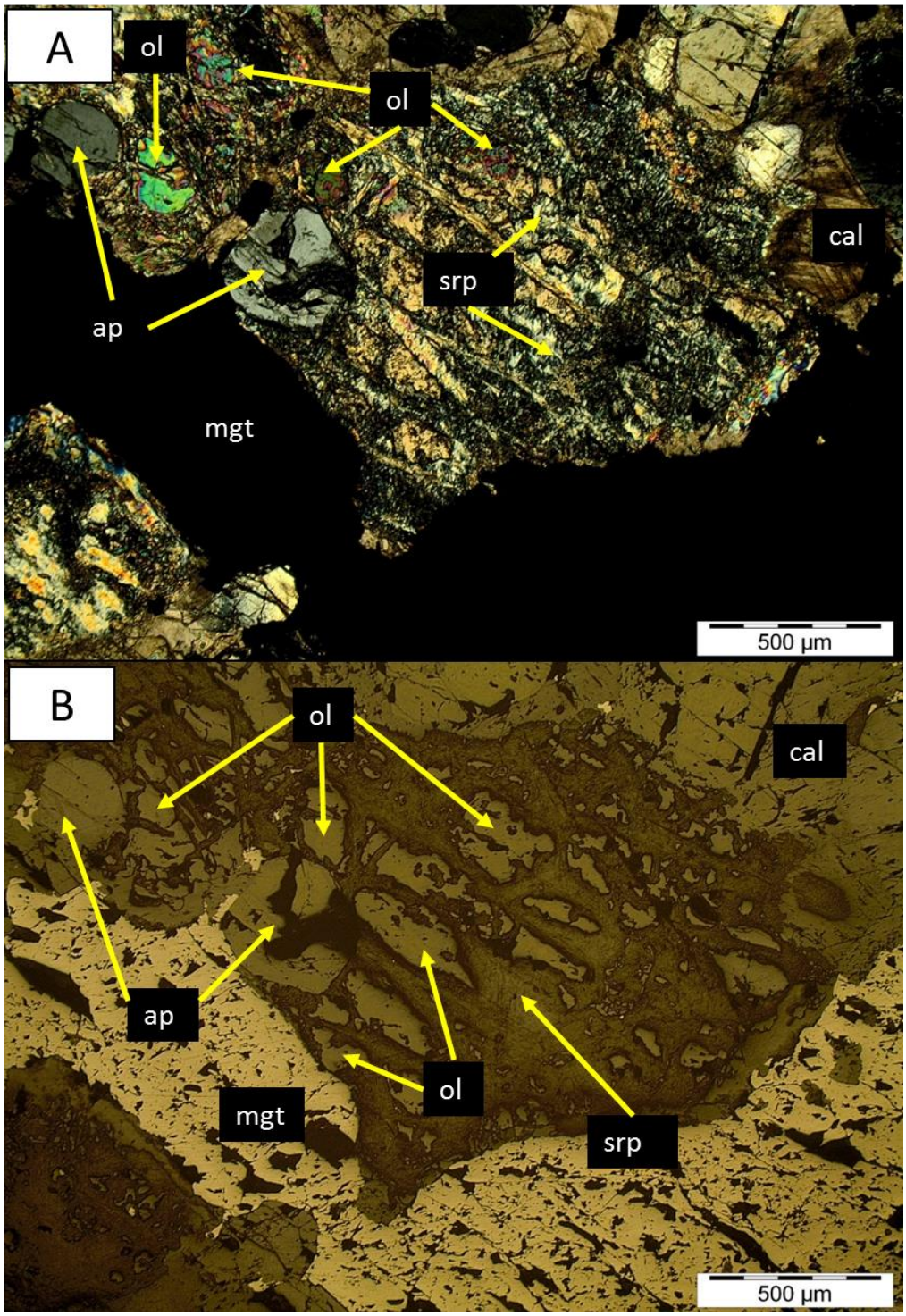

Figure 4.84: A) Apatite poikilitically enclosed by heavily serpentinised olivine. TL image with crossed polarisers. B) Olivine and calcite replaced by second generation magnetite (left-hand side). RL image, sample MT-28.

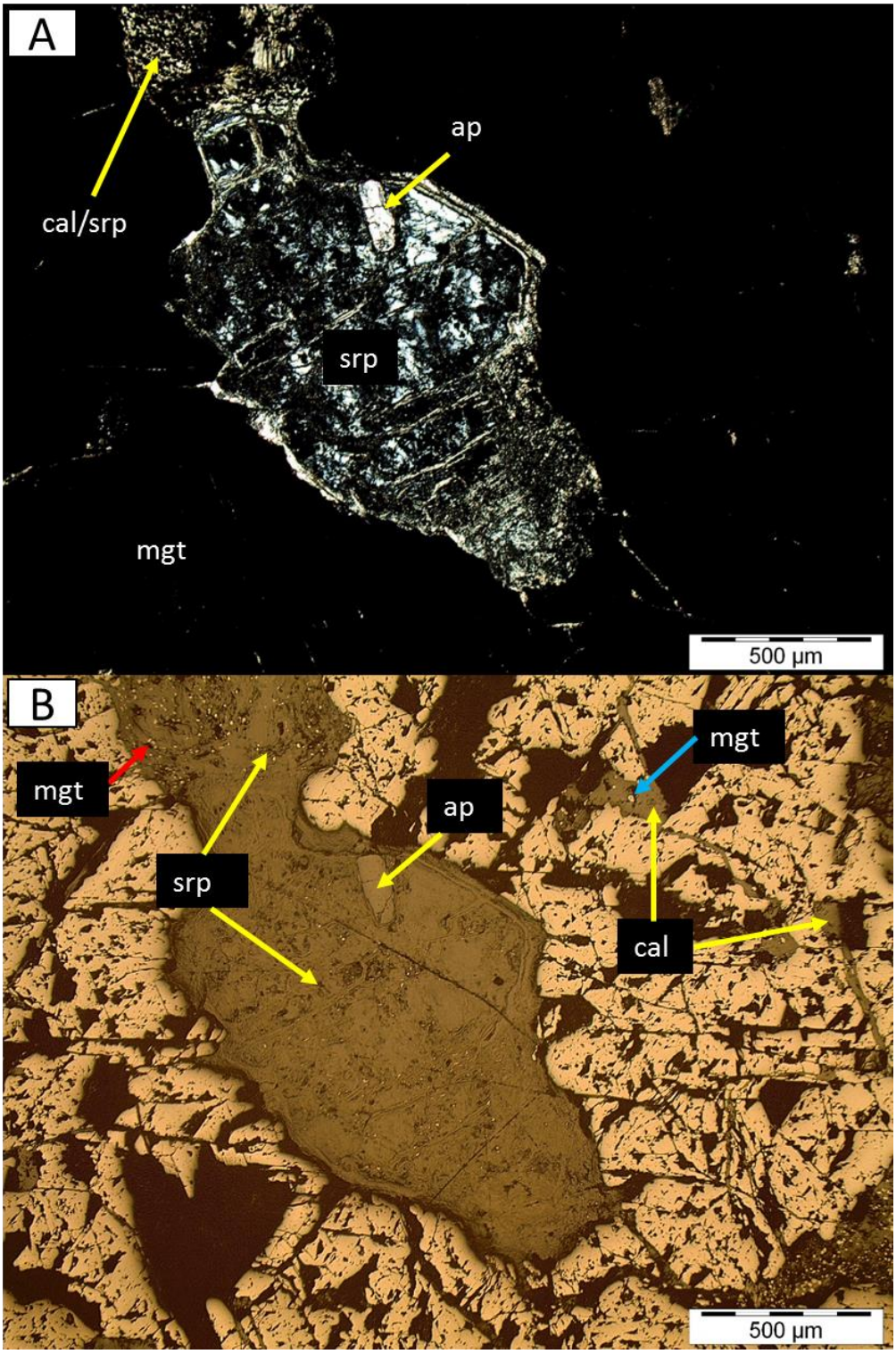

Figure 4.85: A) Apatite poikilitically enclosed by completely serpentinised olivine (mesh texture). TL image with crossed polarisers. B) Magnetite replaced by serpentine (red arrow) and calcite (blue arrow). RL image, sample MT-27.

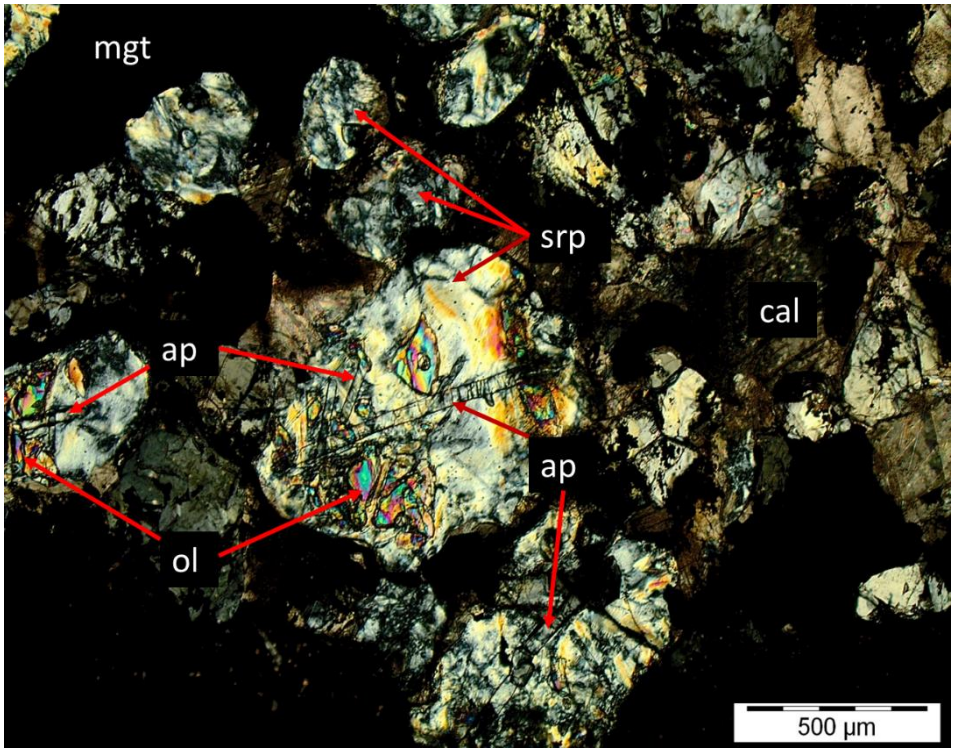

Figure 4.86: Acicular apatite needles poikilitically enclosed by partly serpentinised olivine grains. TL image with crossed polarisers, sample MT-2.

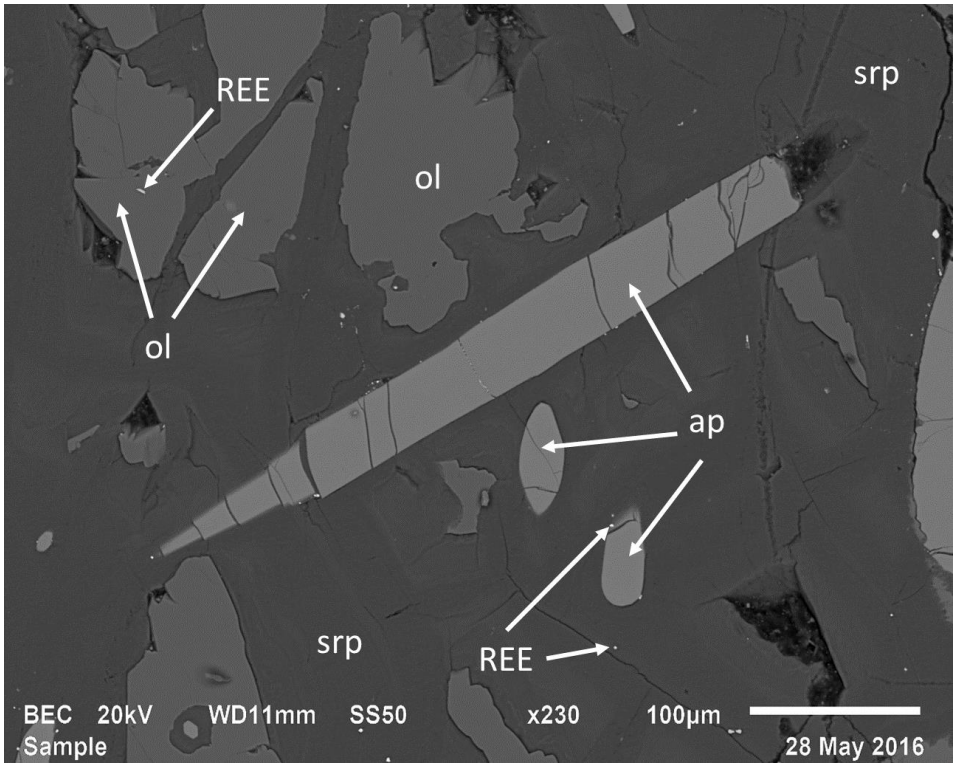

Figure 4.87: Acicular apatite needles that are poikilitically enclosed by partly serpentinised olivine (REE = rare earth element bearing mineral). Image also shows minor replacement of apatite by serpentine. BSE image, sample MT-2.

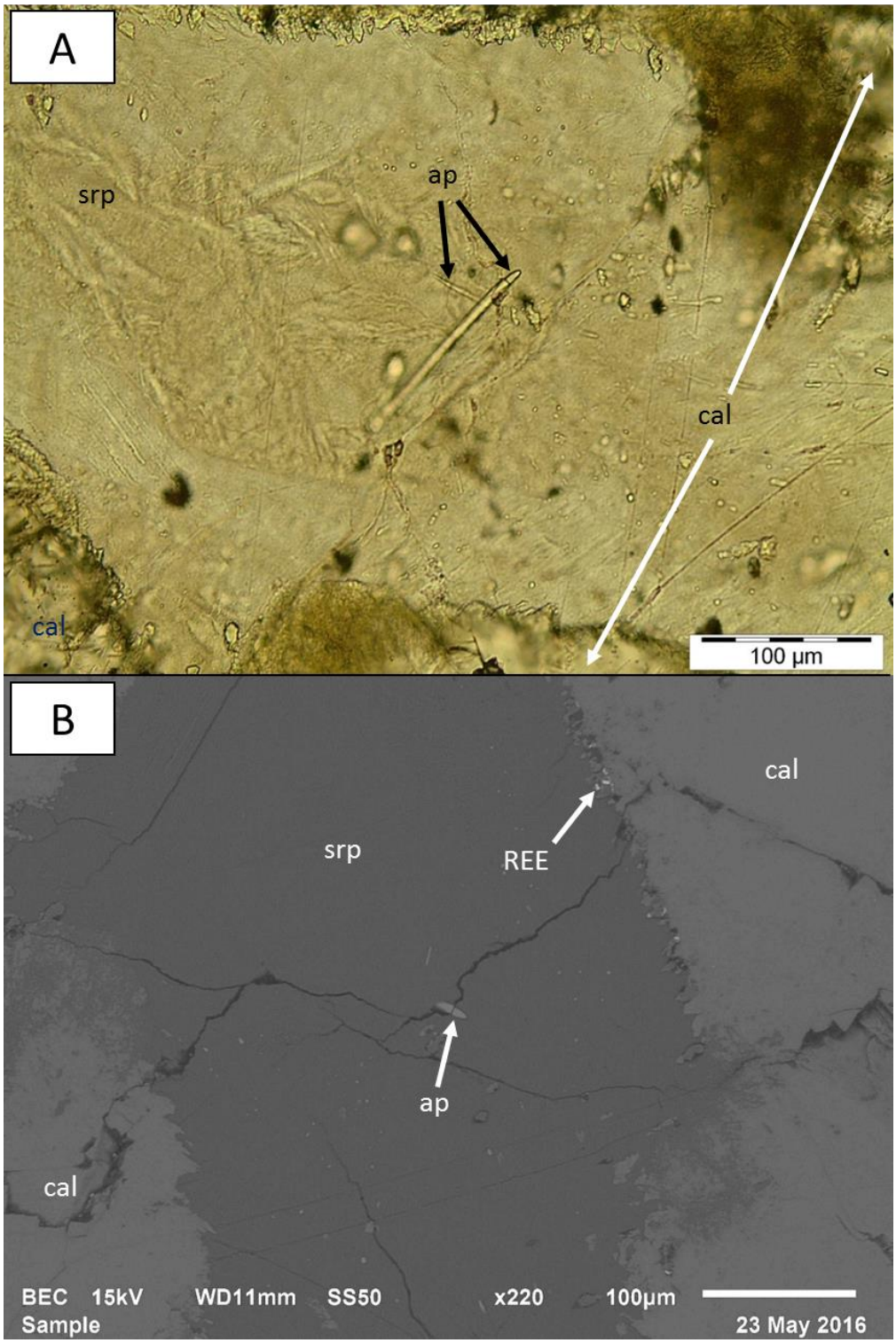

Figure 4.88: Acicular apatite needle enclosed by serpentine. Image also shows the replacement of calcite by serpentine. Notice the discoloured calcite grains (A). TL image (A) and BSE (B) image, sample MT-53.

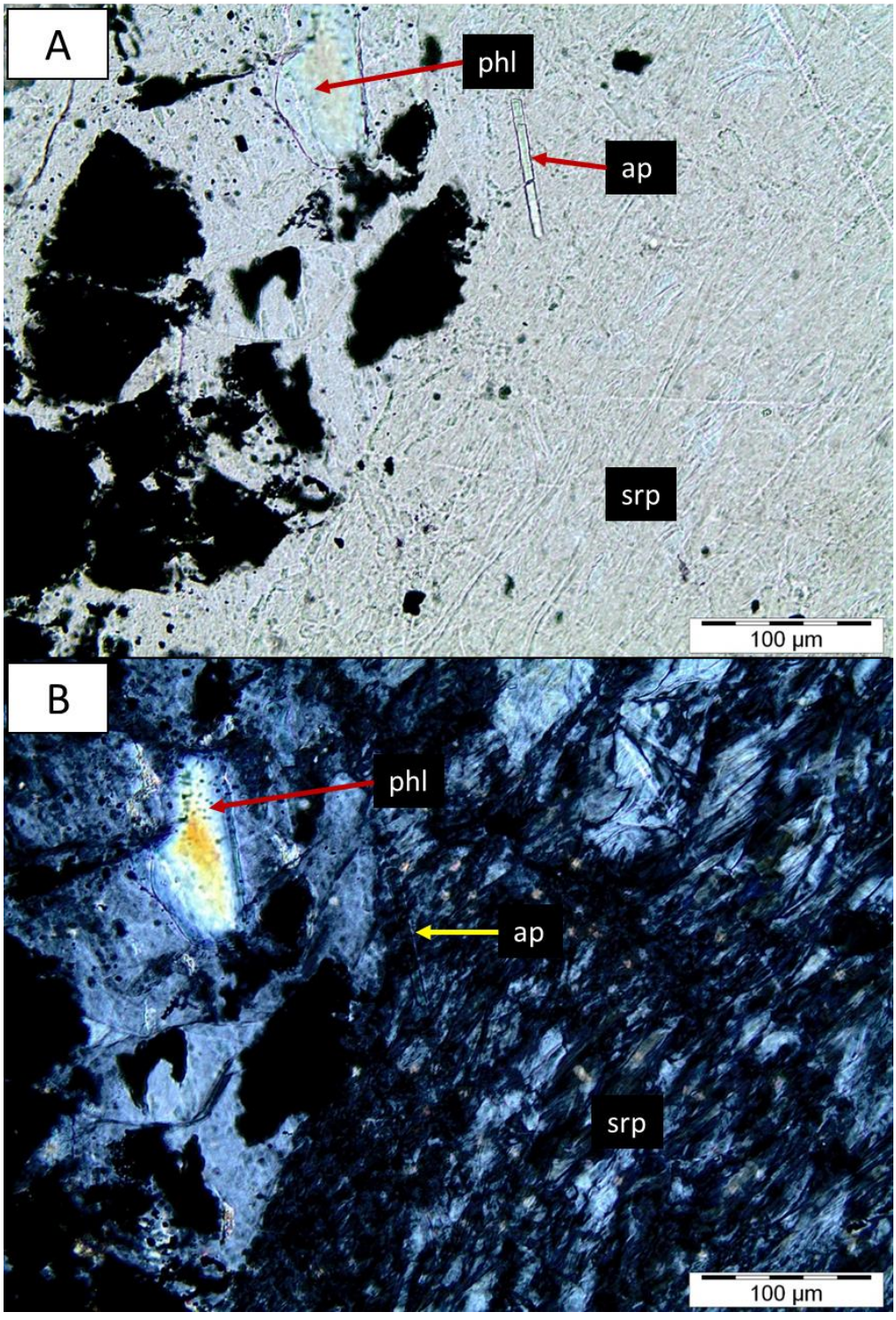

Figure 4.89: Second generation apatite included in serpentine. Phlogopite replaced by serpentine. TL image under plane polarised light (A) and with crossed polarisers (B), sample MT-55.

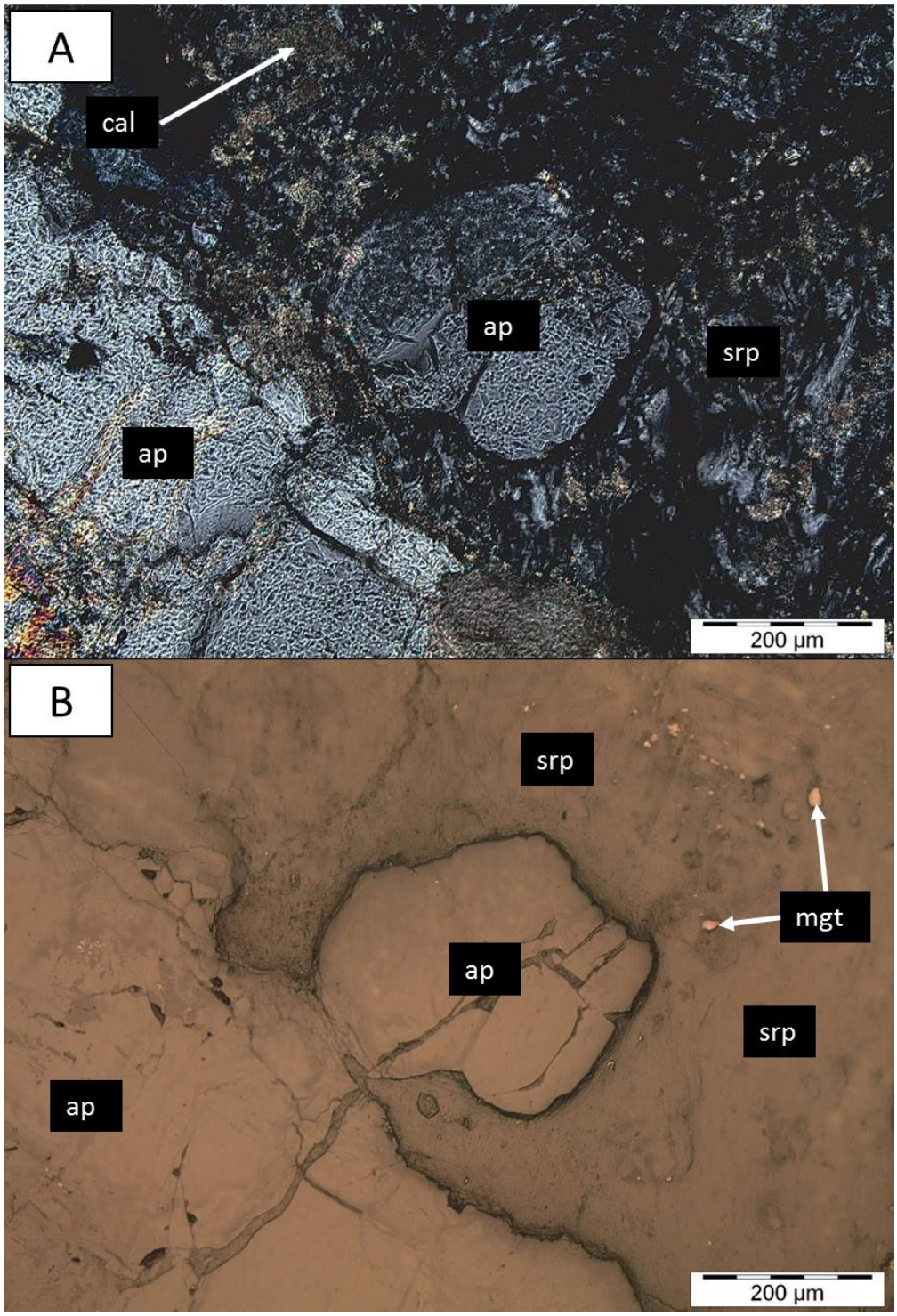

Figure 4.90: First generation apatite and calcite replaced by serpentine. TL image with crossed polarisers (A) and RL image (B), sample MT-22.

4.4.4. Silicates: Olivine, chondrodite, serpentine, chlorite and phlogopite.

a) Olivine:

Olivine is observed as rounded, medium- to fine-grained crystals in both carbonatite types (Figure 4.86). Textural evidence suggests that olivine formed after baddeleyite and apatite (Figure 4.91).

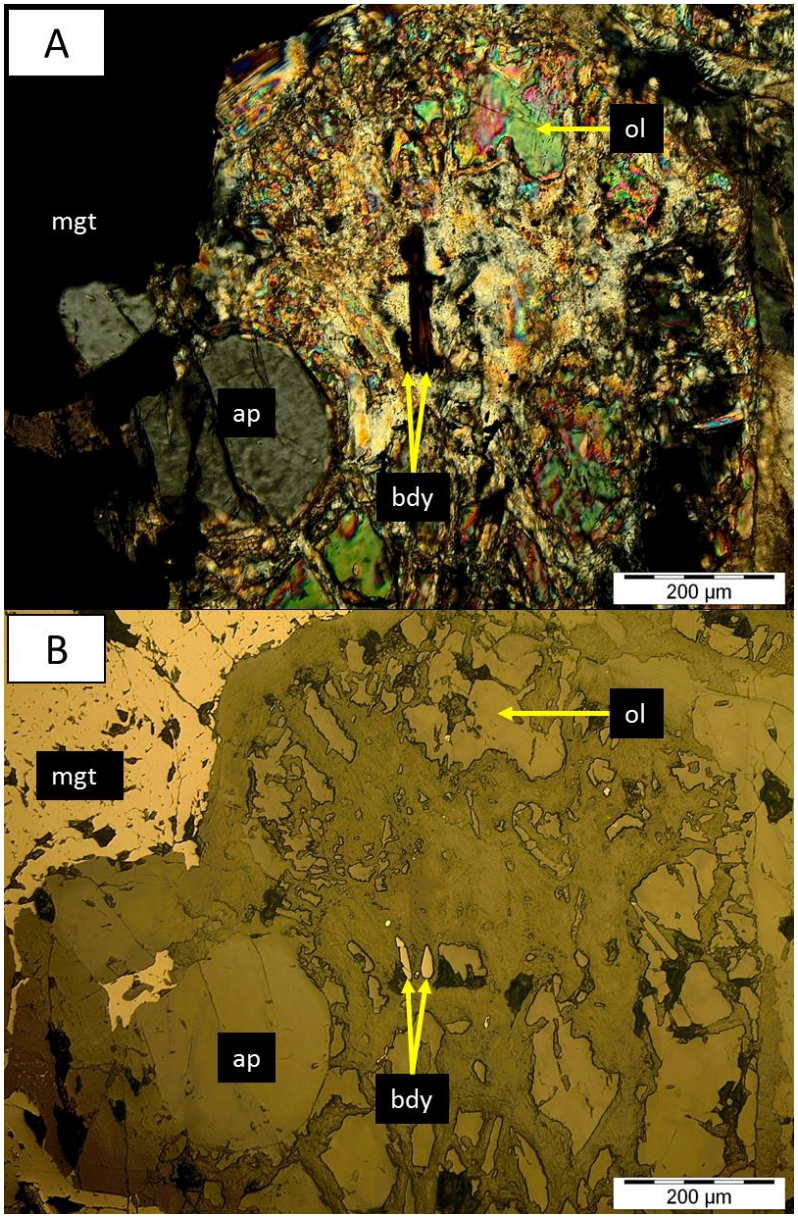

Figure 4.91: Baddeleyite poikilitically enclosed by olivine. Apatite subpoikilitically enclosed by olivine. Olivine replaced by serpentine. TL image with crossed polarisers (A) and RL image, sample MT-28.

b) Chondrodite:

Chondrodite primarily occurs as rims that formed due to the alteration of olivine (Figure 4.92; Figure 4.93). They can also occur as anhedral grains that show no signs towards olivine alteration (Figure 4.94). However, these occurrences are very rare. The mineral is found in larger amounts in phoscorite than in both carbonatite types.

Chondrodite shows textural evidence of forming after phlogopite but before second generation magnetite (Figure 4.95). Chondrodite is also highly effected by the serpentinisation process, seeing that the mineral shows a strong association towards olivine (Figure 4.96).

The main difference between olivine and chondrodite is that olivine tends to form rounded grains, while chondrodite is mostly irregularly shaped. Also, chondrodite can be colourless or have a yellow-green tint under plane polarised light, while olivine can be colourless or have a pink tint.

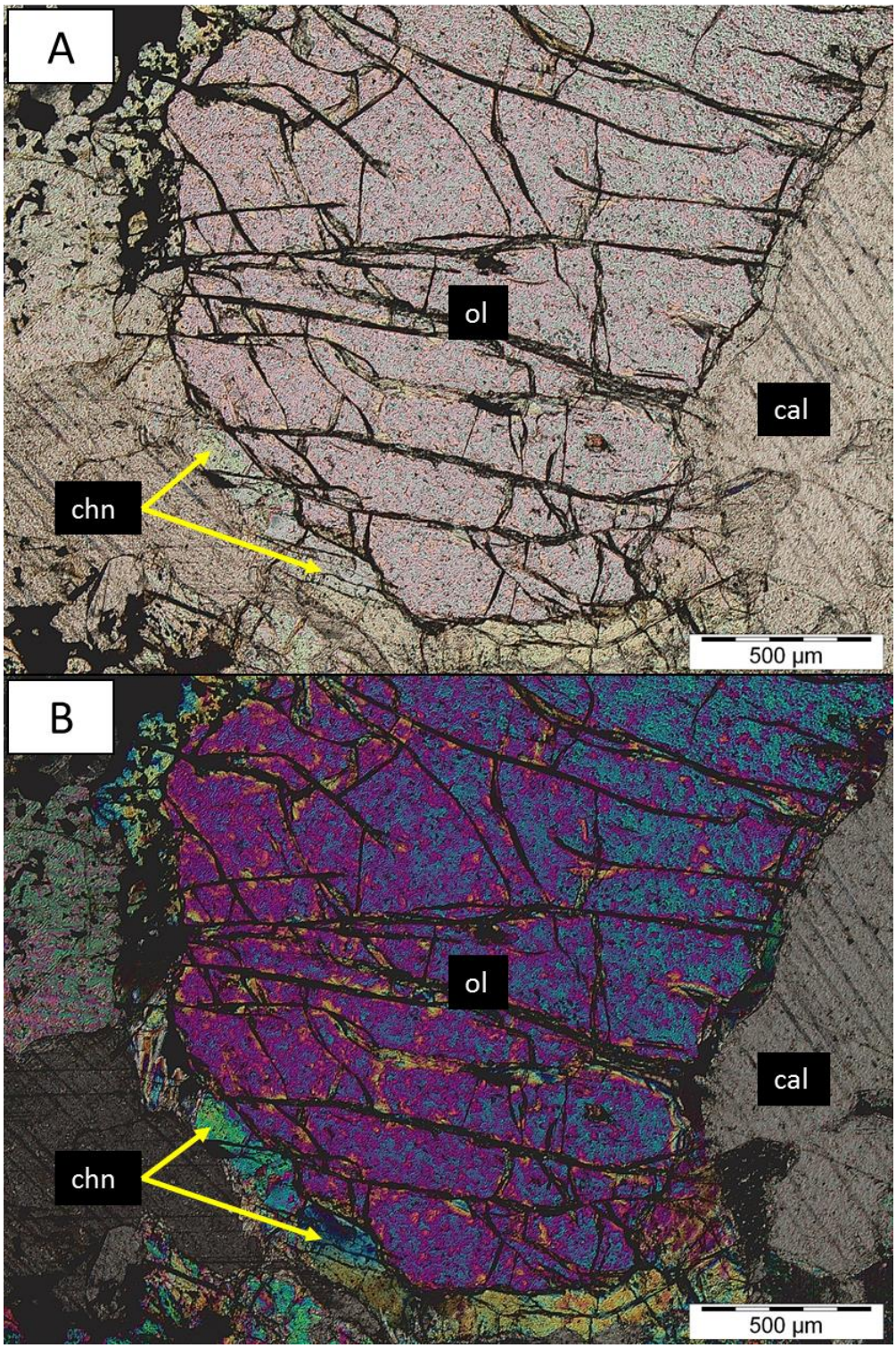

Figure 4.92: Chondrodite alteration rim around olivine. Olivine and calcite replaced by chondrodite. Image showing early stage of replacement by chondrodite. TL image under plane polarised light (A) and with crossed polarisers (B), sample MT-13.

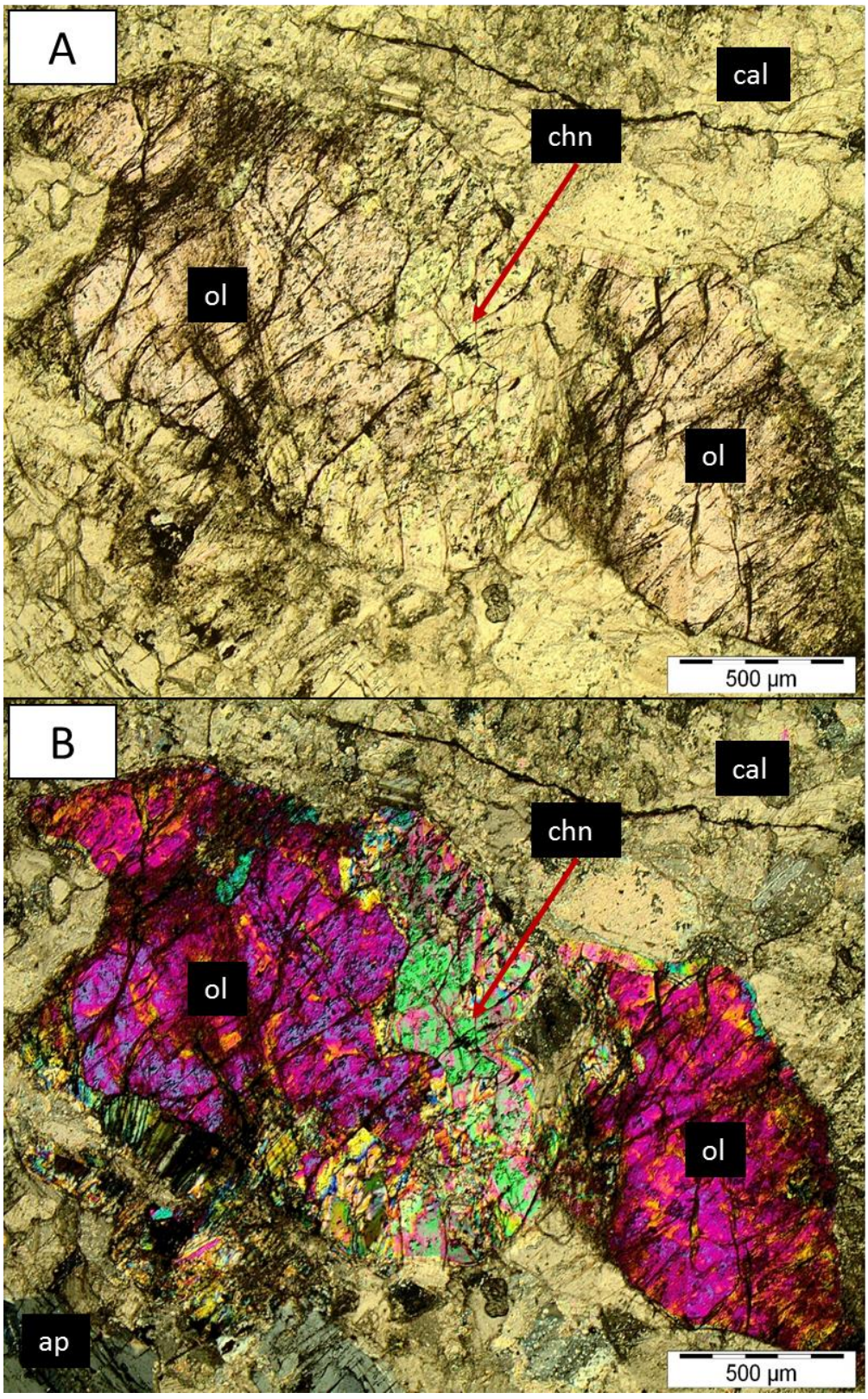

Figure 4.93: Advanced stage of olivine replacement by chondrodite. TL image under plane polarised light (A) and with crossed polarisers (B), sample MT-53.

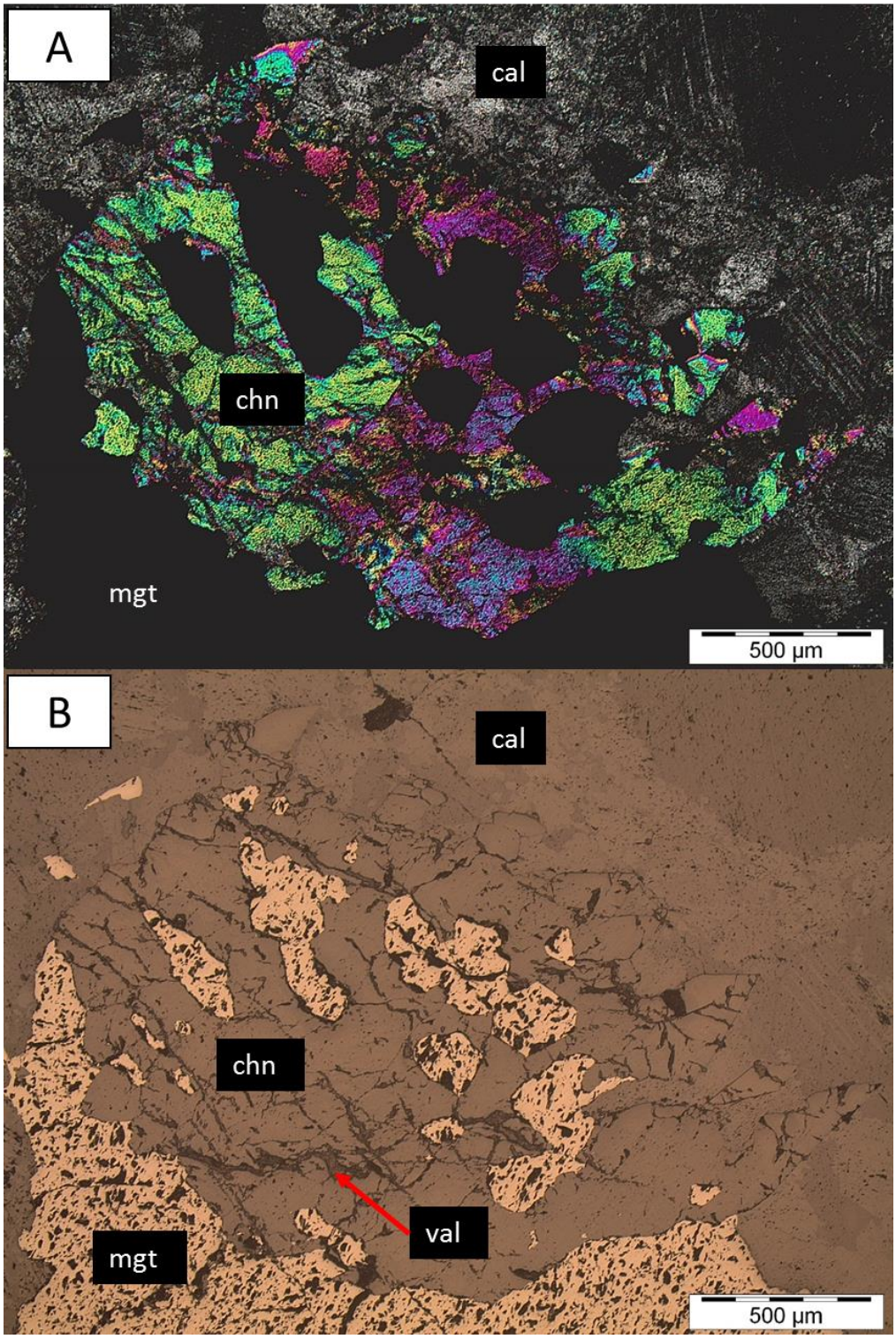

Figure 4.94: Anhedral chondrodite grain. Calcite and chondrodite replaced by second generation magnetite. TL image with crossed polarisers (A) and RL image (B), sample MT-68.

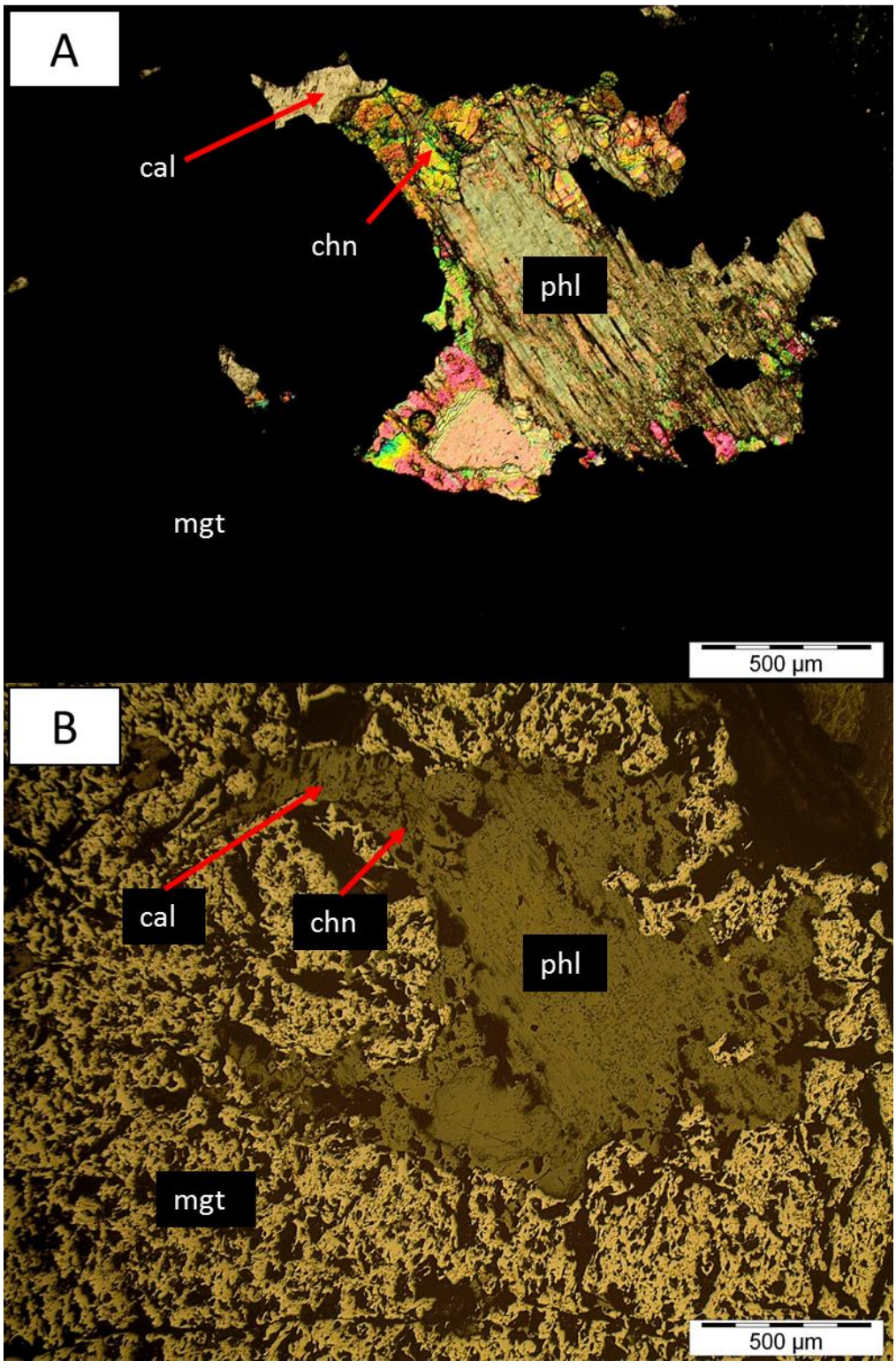

Figure 4.95: Chondrodite, phlogopite, and calcite replaced by second generation magnetite. Phlogopite replaced by chondrodite. TL image with crossed polarisers (A) and RL image (B), sample MT-8.

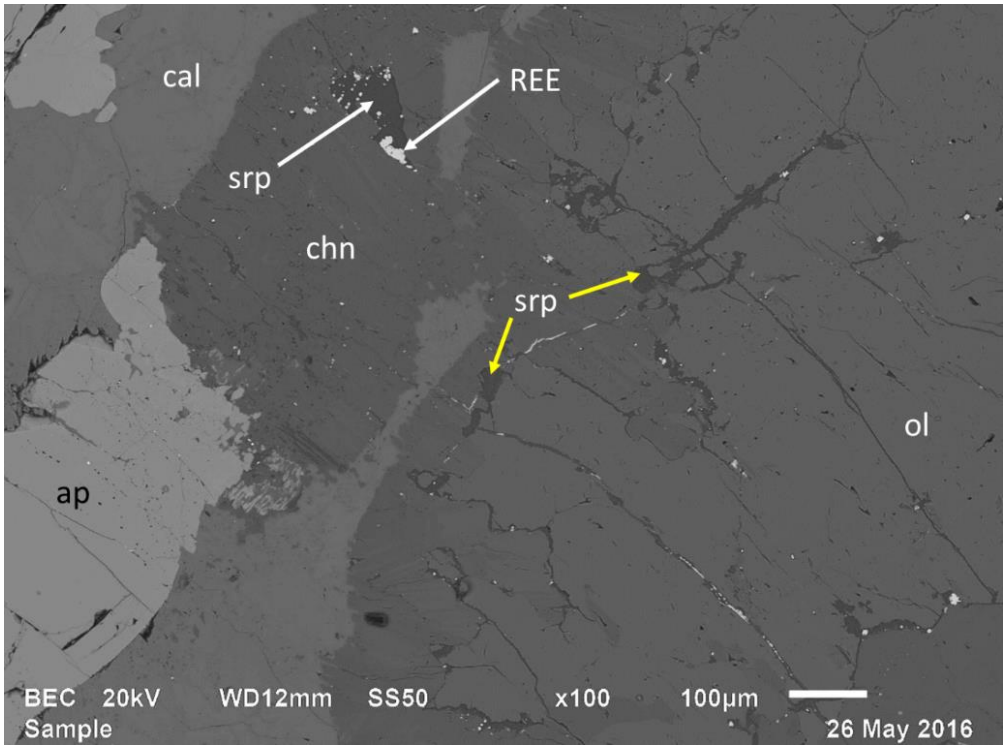

Figure 4.96: Olivine, calcite, and apatite replaced by chondrodite. Chondrodite and olivine replaced by serpentine at olivine-chondrodite boundary (yellow arrows). BSE image, sample MT-53.

c) Serpentine:

Serpentine typically forms a mesh texture where it replaced olivine and chondrodite (Figure 4.85; Figure 4.97). However, the serpentinisation process is not confined to chondrodite and olivine alone, as it has progressed to the replacement of the carbonate fabric as well (Figure 4.97). An hourglass texture is produced where serpentine replaced carbonate minerals (Figure 4.98).

Serpentine shows textural evidence of forming after the sulphide minerals (Figure 4.99; Figure 4.100) and recrystallised carbonates (Figure 4.101), but prior to valleriite formation (Figure 4.99; Figure 4.102). The grey colour of serpentine under cross-polarised light, as well as its low relief and fibrous texture, makes it very easily distinguishable from other minerals.

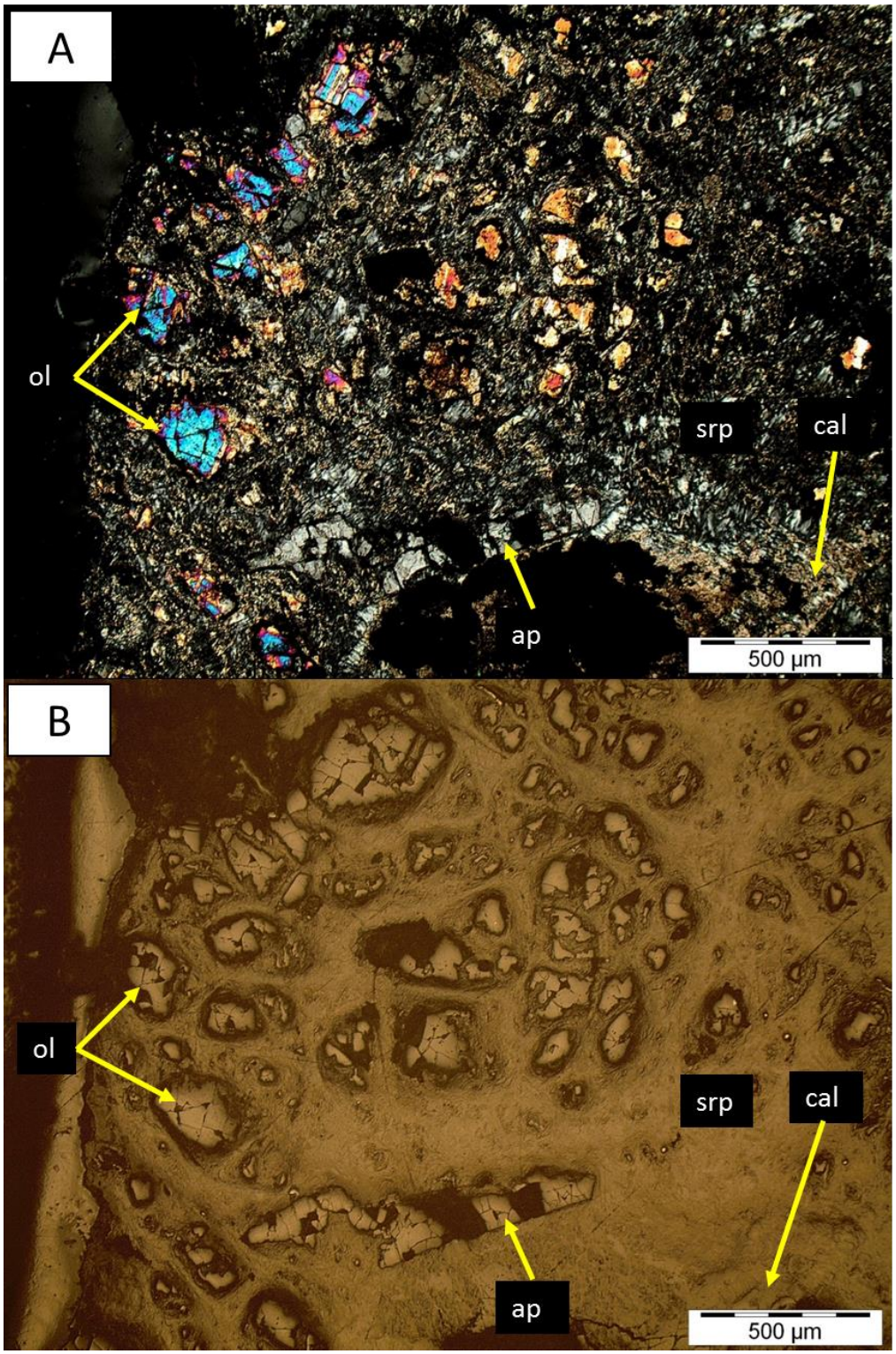

Figure 4.97: Serpentine mesh texture produced by the replacement of olivine. Apatite and calcite are also replaced by serpentine. TL image with crossed polarisers (A) and RL image (B), sample MT-27.

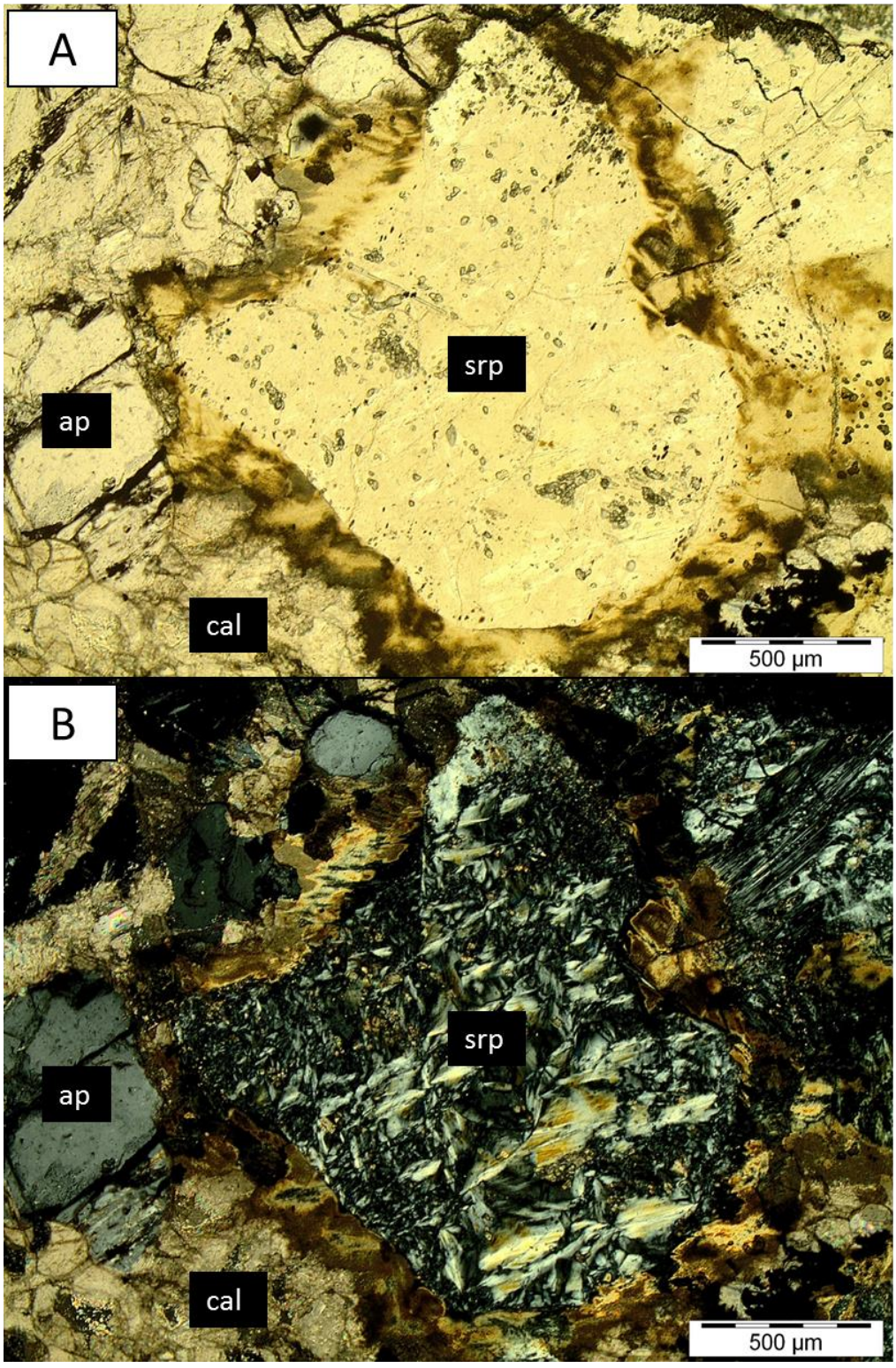

Figure 4.98: Serpentine hourglass texture. Calcite replaced by serpentine. TL image under plane polarised light (A) and with crossed polarisers (B), sample MT-53.

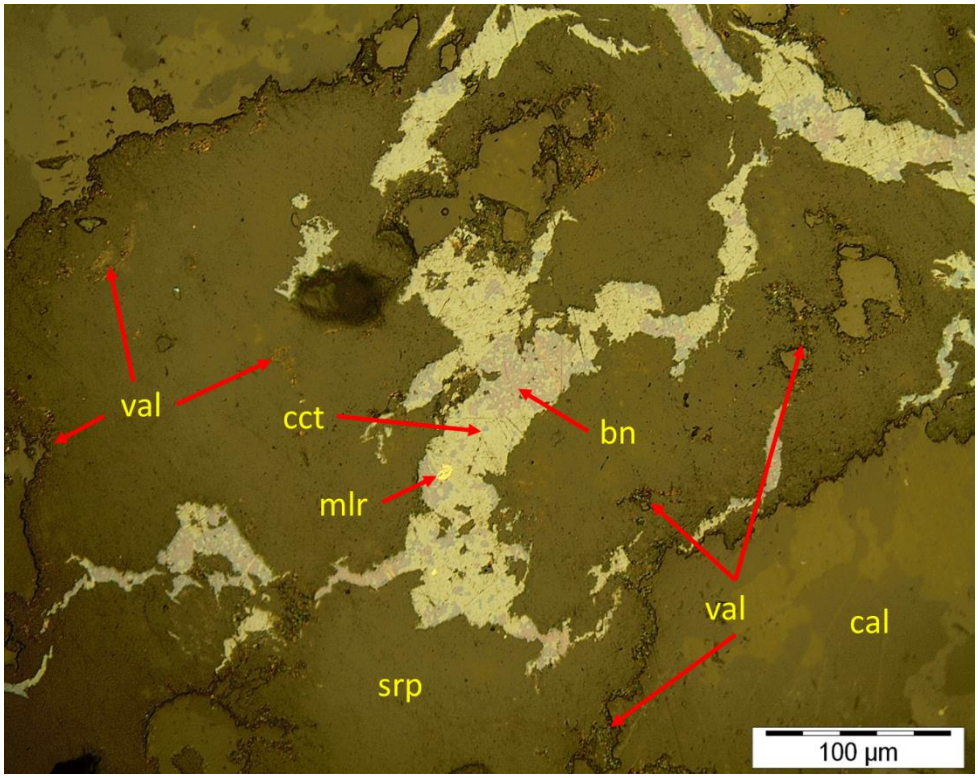

Figure 4.99: Calcite, bornite, and chalcocite replaced by serpentine. Calcite, bornite, chalcocite, and serpentine replaced by valleriite. RL image, sample MT-44.

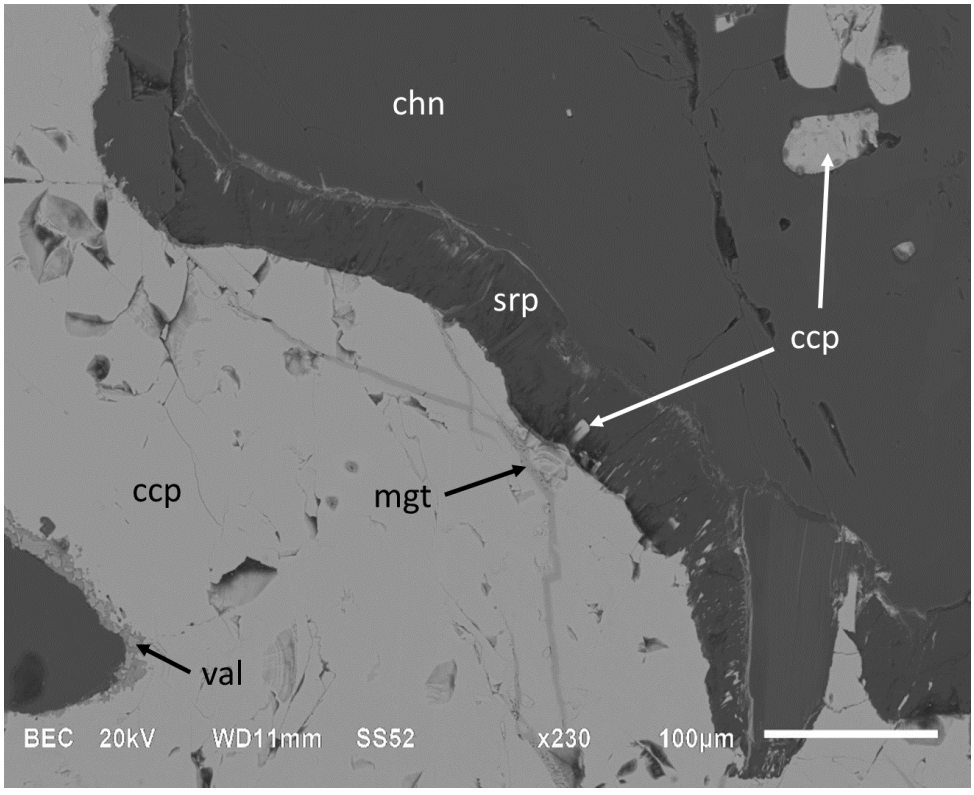

Figure 4.100: Chondrodite, chalcopyrite, and third generation magnetite replaced by serpentine rim. Notice the alteration rim formed by serpentine. BSE image, sample MT-48.

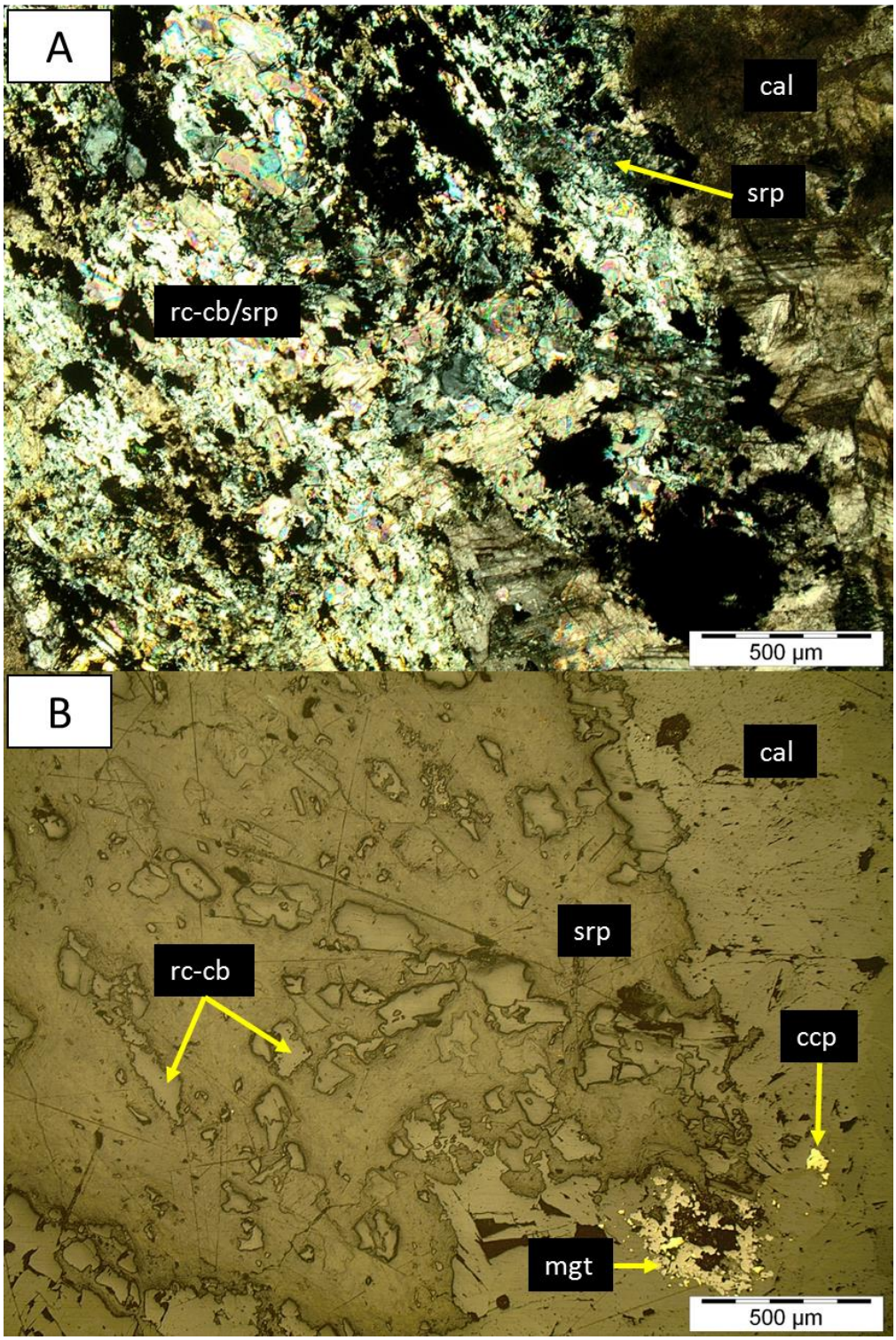

Figure 4.101: Recrystallised carbonate minerals and first generation calcite replaced by serpentine. TL image with crossed polarisers (A) and RL image (B), sample MT-38.

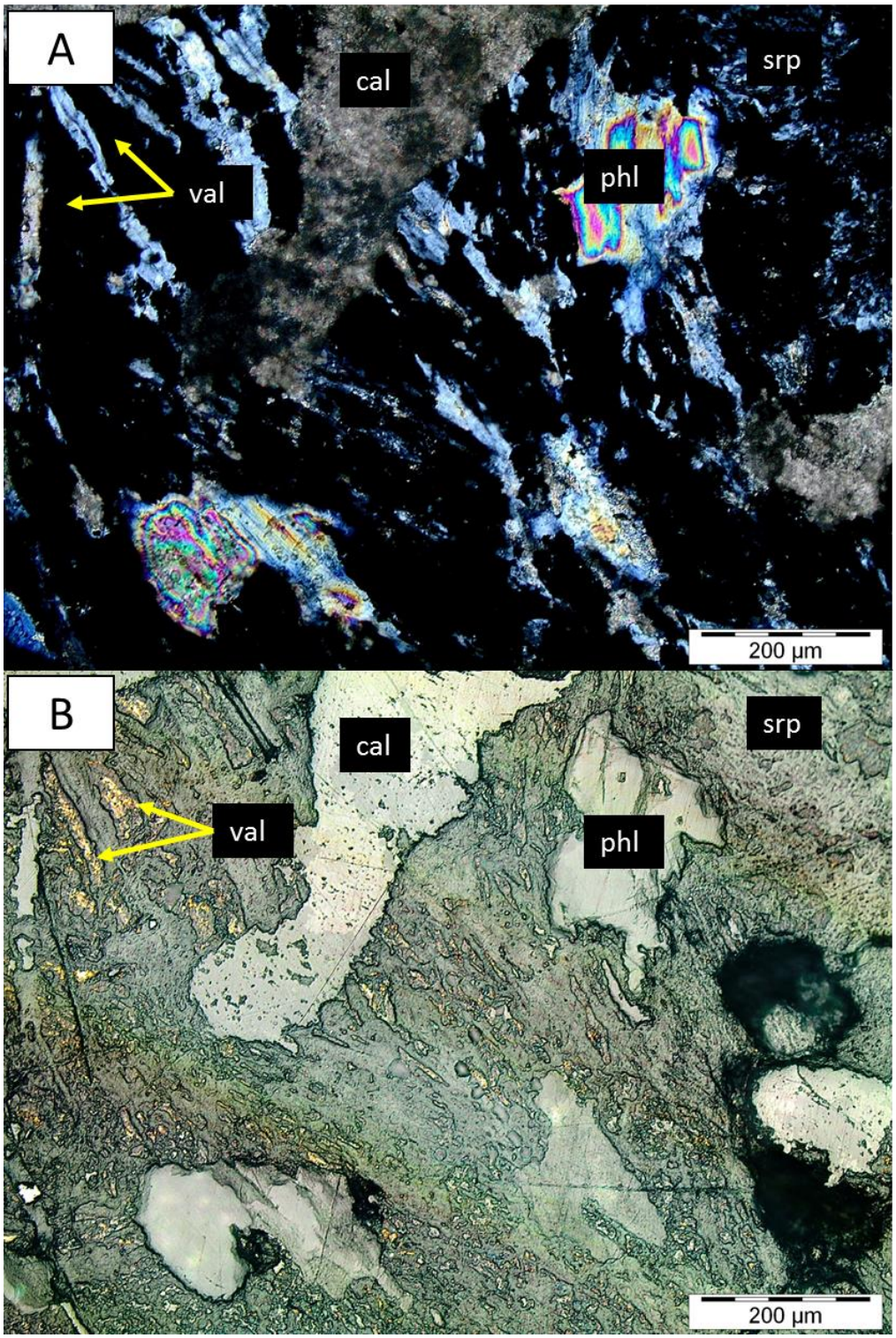

Figure 4.102: Phlogopite and calcite replaced by serpentine. Serpentine replaced by valleriite. TL image with crossed polarisers (A) and RL image (B), sample MT-55.

d) Chlorite:

Not only did the process of serpentinisation cause the replacement of olivine, but the process of chloritisation cause replacement of olivine as well (Figure 4.103). The iconic apple green colour of chlorite makes it very easily distinguishable from other minerals.

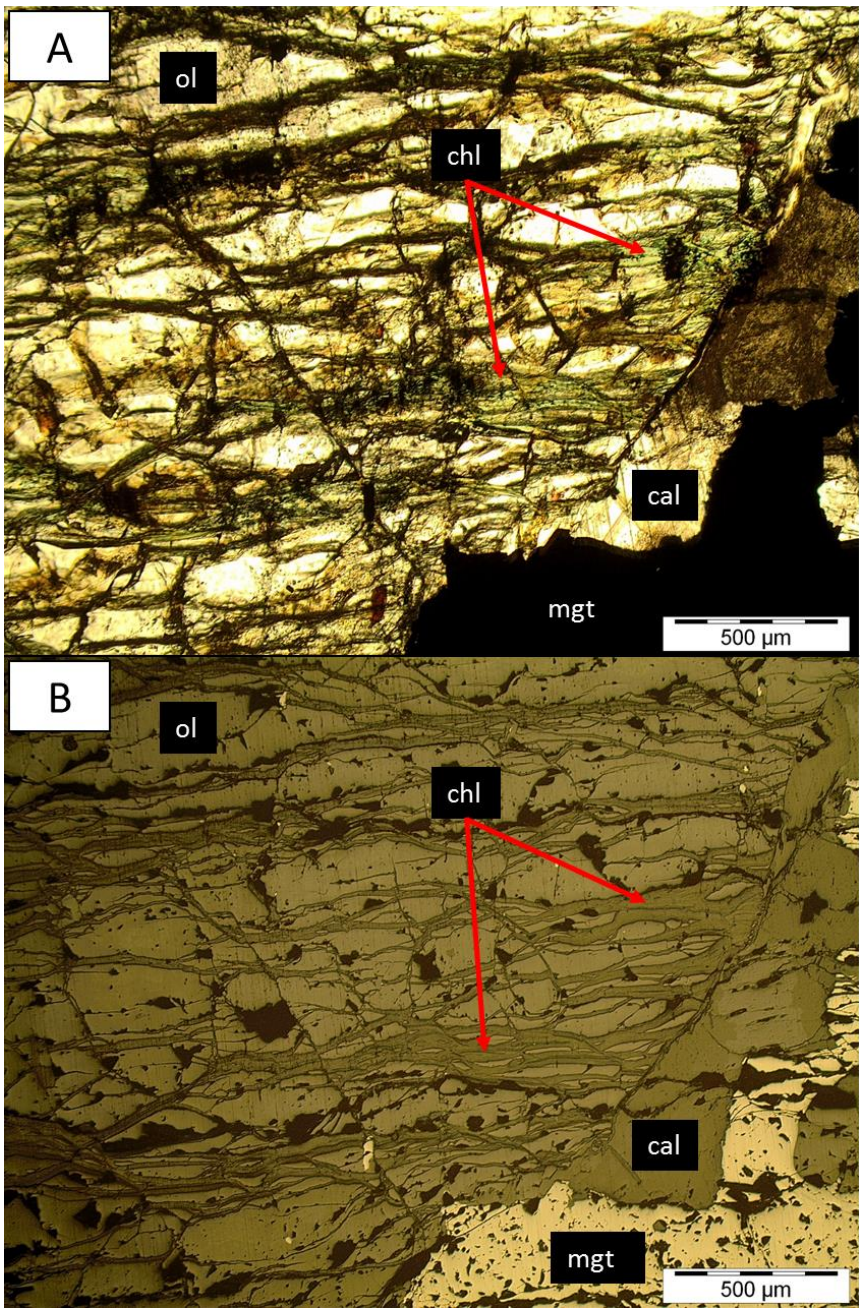

Figure 4.103: Olivine replaced by chlorite (commenced at olivine-calcite boundary). Olivine and chlorite replaced by second generation magnetite. TL image (A) and RL image (B), sample MT-11.

e) Phlogopite:

Phlogopite is a coarse-grained to medium-grained layered silicate mineral that is euhedral to subhedral in shape. The mineral's well-defined shape was mostly compromised by chondrodite (Figure 4.104) and serpentine (Figure 4.89) replacement.

Minerals that formed after phlogopite (especially magnetite and sulphide minerals) caused straining. This resulted in bent cleavage planes of the phlogopite (Figure 4.105). Phlogopite shows textural evidence of forming after apatite (Figure 4.106) and olivine (Figure 4.107), but before first generation magnetite. The mineral's flaky texture makes it easily distinguishable from other minerals.

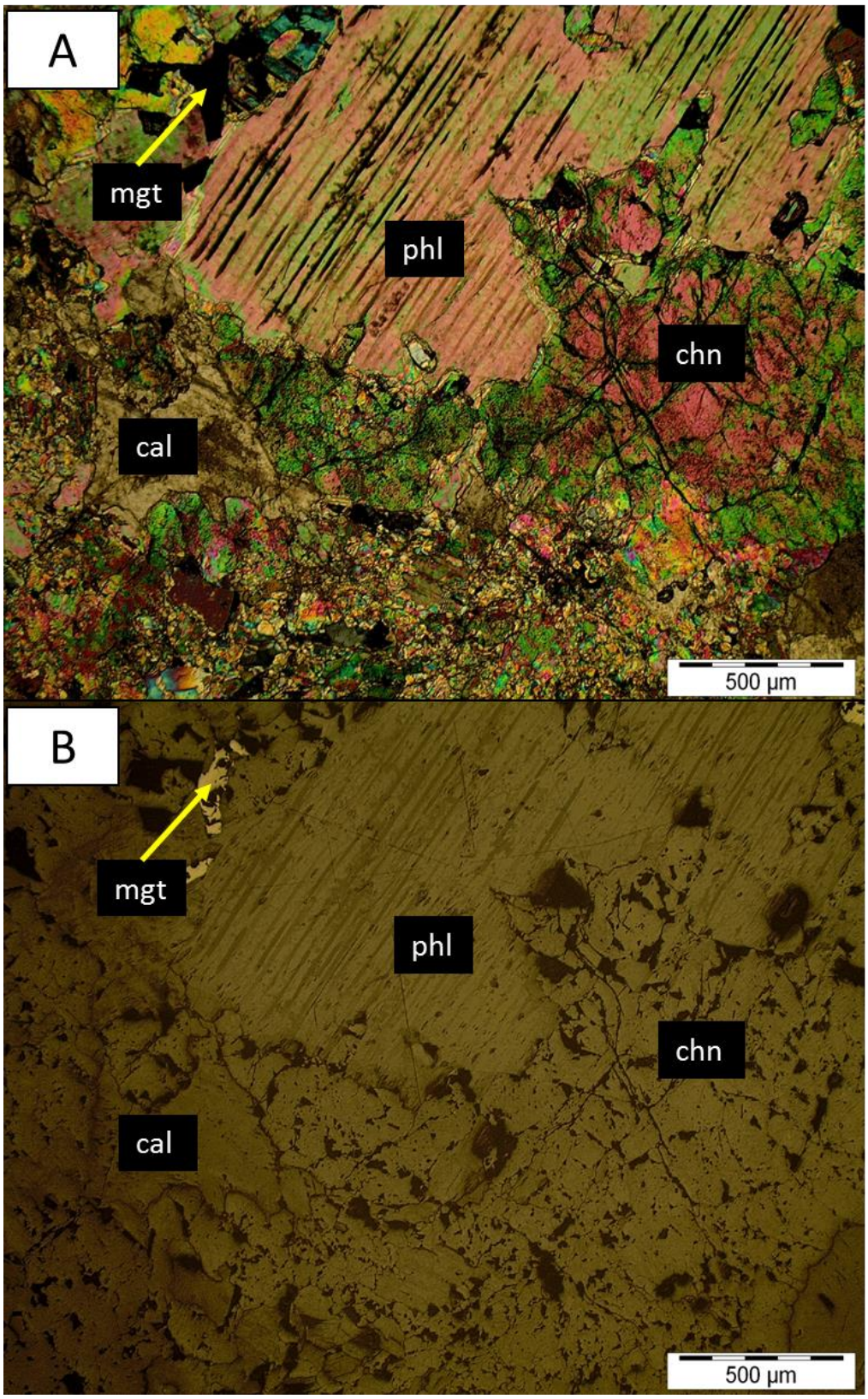

Figure 4.104: Phlogopite and calcite replaced by chondrodite. TL image with crossed polarisers (A) and RL image (B), sample MT-8.

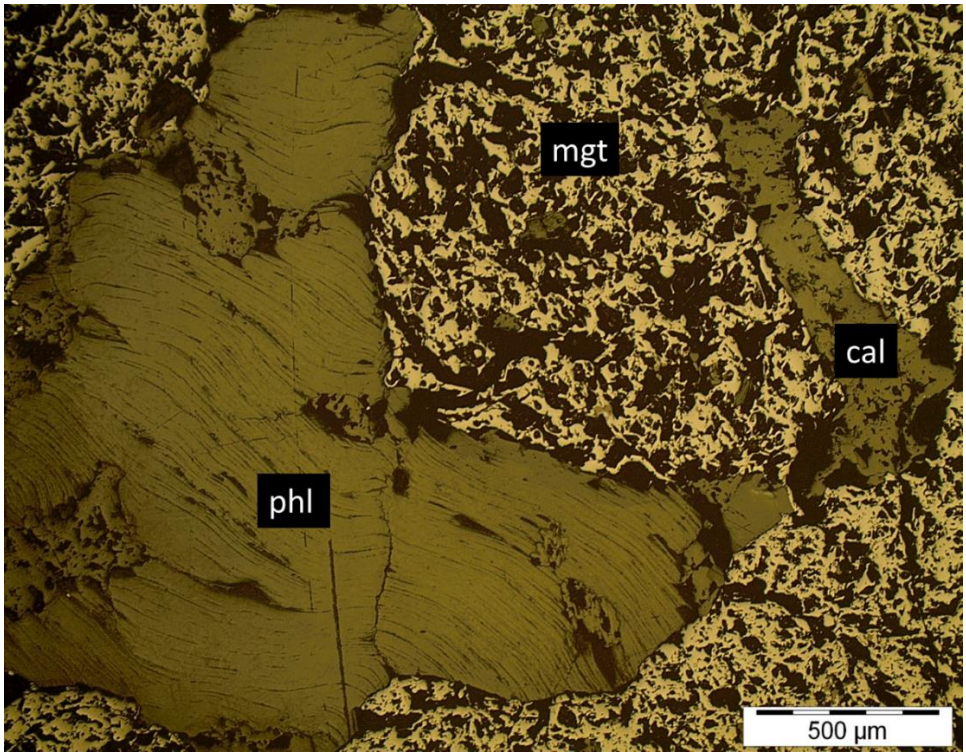

Figure 4.105: Bent phlogopite cleavage planes due to straining that was caused by second generation magnetite formation. Phlogopite and calcite replaced by magnetite. RL image, sample MT-8.

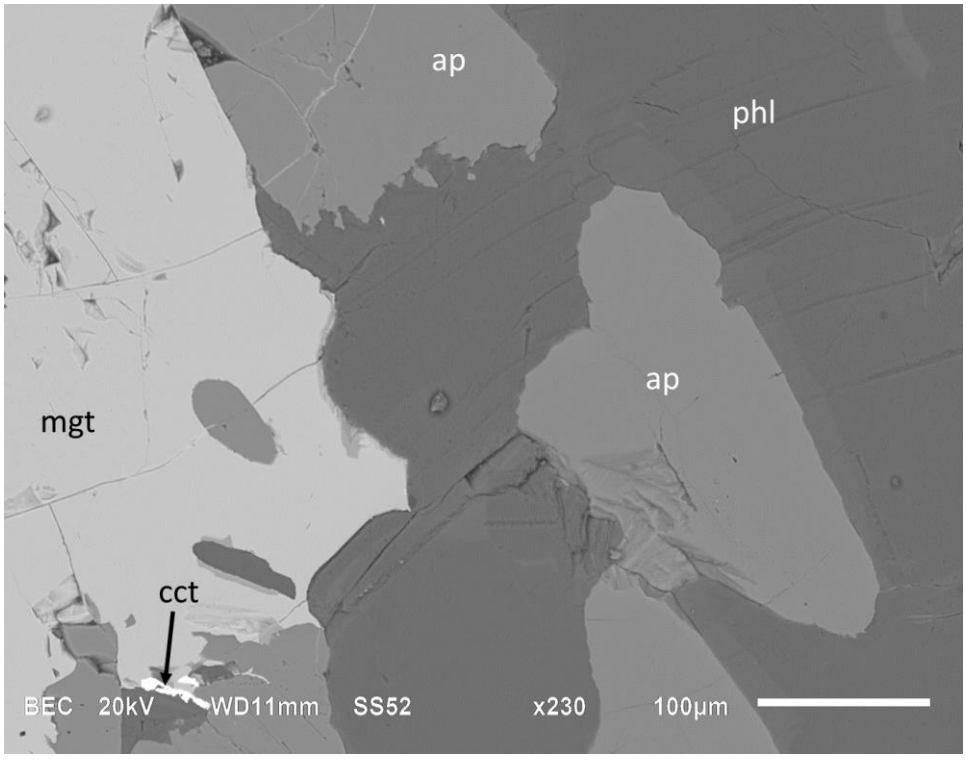

Figure 4.106: Apatite replaced by phlogopite. Phlogopite replaced by first generation magnetite. BSE image, sample MT-15.

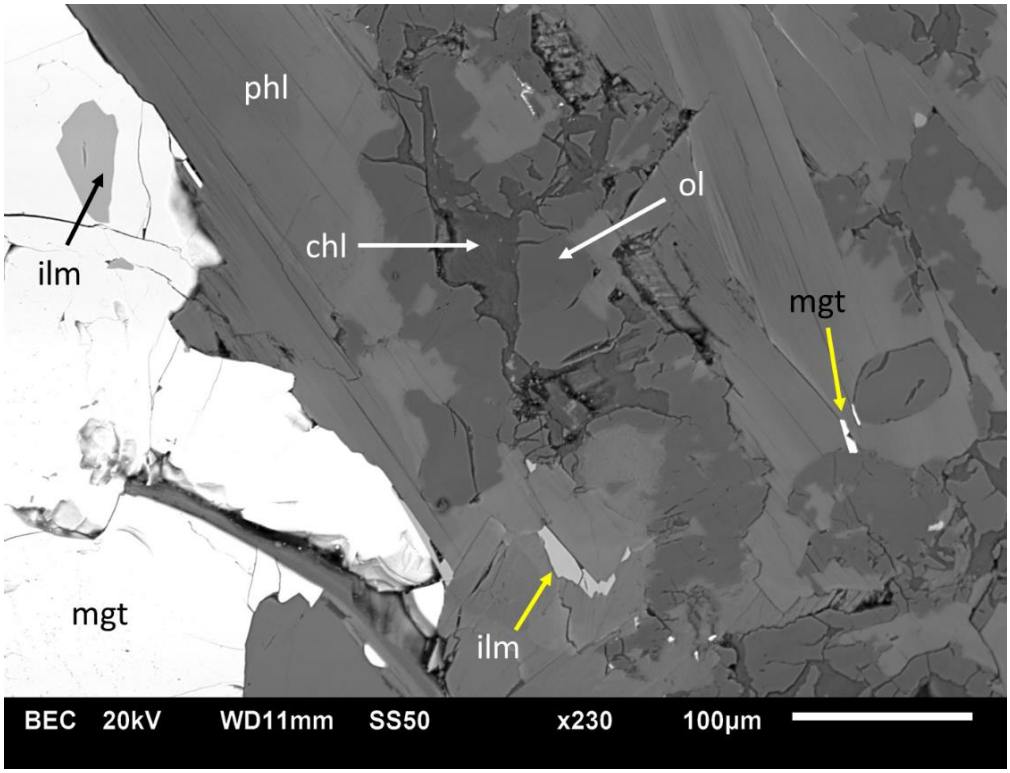

Figure 4.107: Olivine replaced by phlogopite and chlorite. Phlogopite replaced by first generation magnetite. The formation of first generation magnetite and first generation ilmenite in the cleavage planes of phlogopite (yellow arrows). BSE image, sample MT-11.

4.4.5. Sulfates.

a) Baryte:

Baryte occurs solely in the form of well-defined veinlets (Figure 4.108). The mineral is easily distinguishable from recrystallised carbonate veinlets, seeing that the carbonate veinlets show pale, high order interference colours under cross-polarised light, while baryte displays a variety of colours (primarily blue, yellow, and/or pink). Baryte shows textural evidence of forming prior to carbonate mineral recrystallisation (Figure 4.109) and the process of serpentinisation (Figure 4.110).

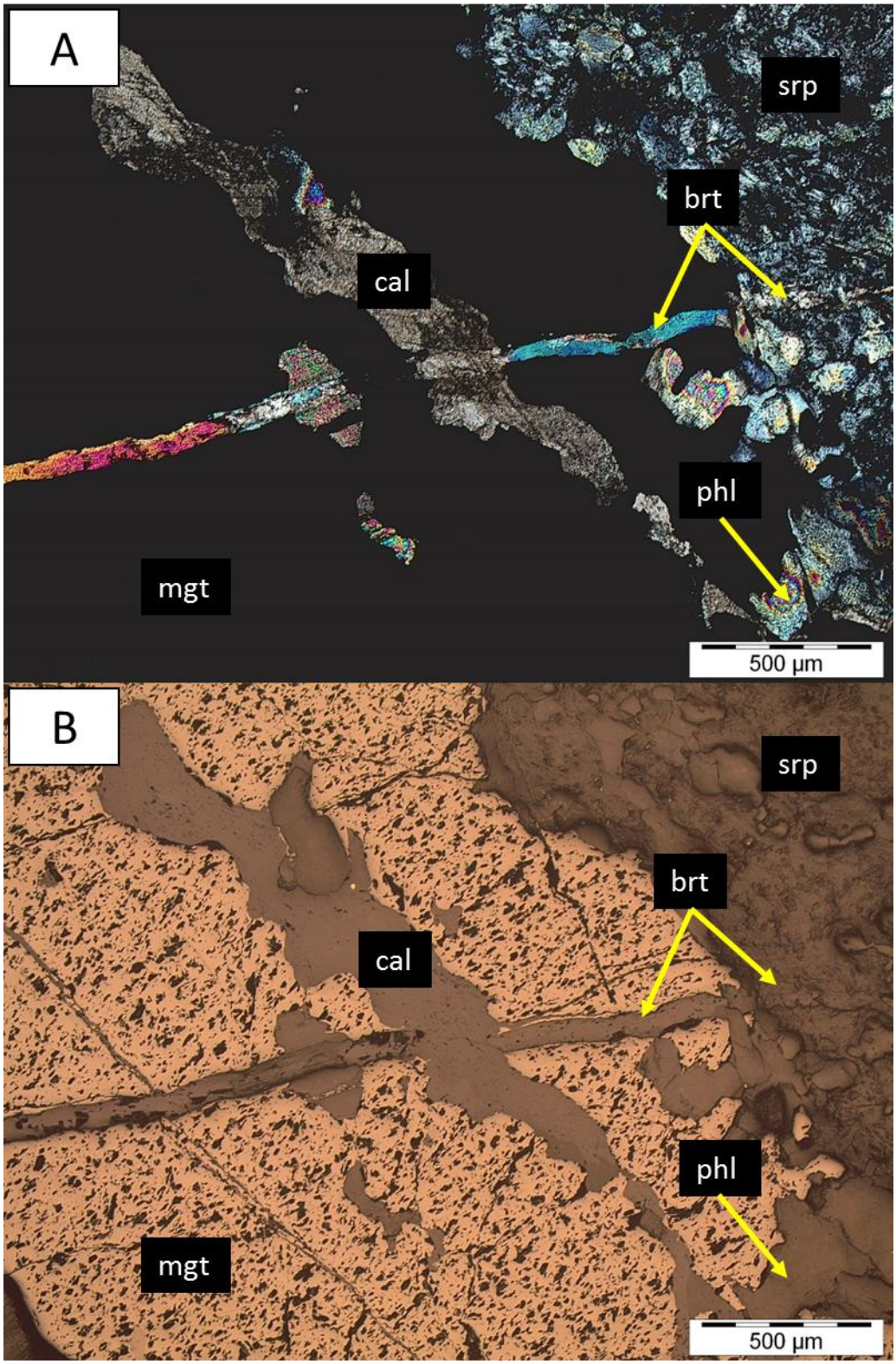

Figure 4.108: Second generation magnetite and phlogopite cut by baryte veinlet. Phlogopite and baryte veinlet partially replaced by serpentine. TL image with crossed polarisers (A) and RL image (B), sample MT-22.

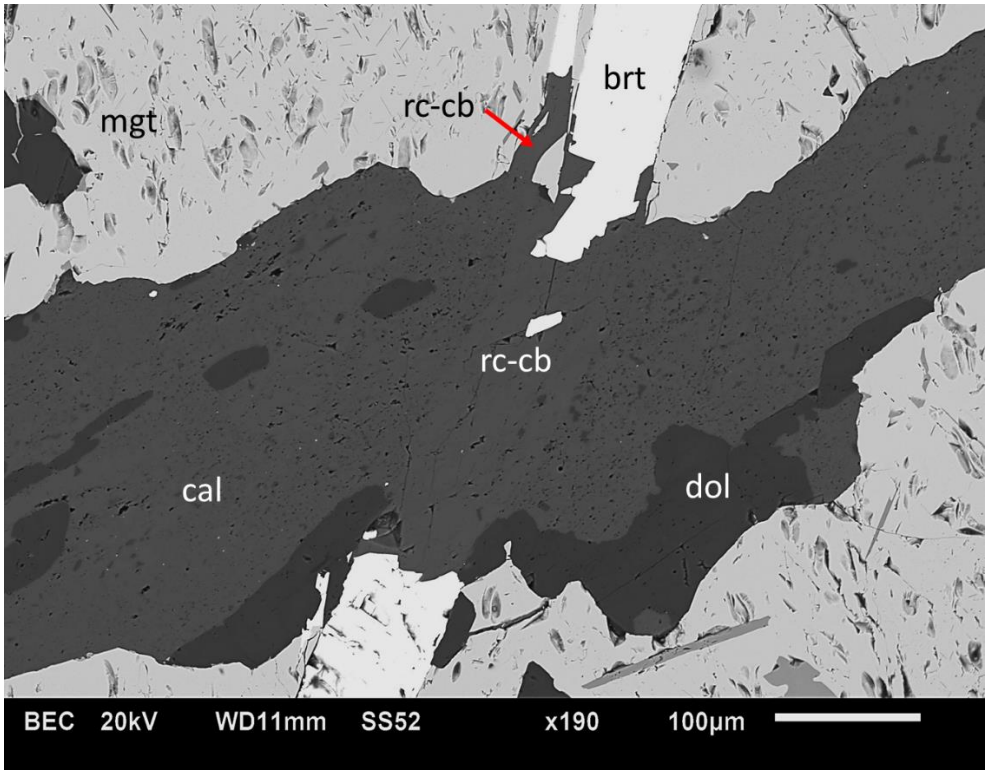

Figure 4.109: Frist generation magnetite, calcite, and dolomite replaced by baryte. Calcite, dolomite, and baryte replaced by recrystallised carbonates. BSE image, sample MT-22.

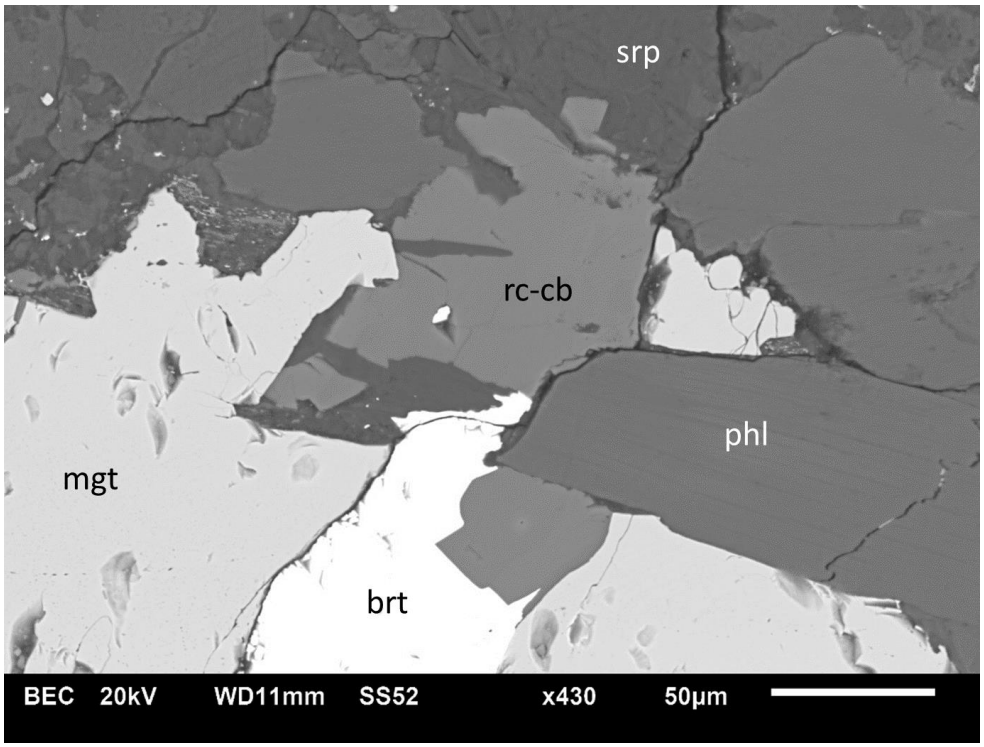

Figure 4.110: First generation magnetite and phlogopite replaced by baryte. Baryte replaced by recrystallised carbonates. Recrystallised carbonates, baryte, and phlogopite replaced by serpentine. BSE image, sample MT-22.

CHAPTER 5. DISCUSSION

5.1. The sulphide mineral assemblages in transgressive carbonatite.

Extensive observation of transgressive carbonatite samples indicated distinguishable recurring combinations/assemblages for the sulphide group minerals. Thus, it was decided to create individual groups for each assemblage (Appendix F, Table F.1) and to classify the samples into these main groups in order to make more sense of the paragenetic sequences of sulphide mineralisation in transgressive carbonatites.

Table F.1 makes use of a with-without regime in order to compare samples that were classified within the same group. Valleriite is excluded from the main groups seeing that it is a late-stage sulphide hybrid phase which replaced the majority of the minerals (sulphides and non-sulphides) in the observed transgressive carbonatite samples.

The main groups are primarily based on samples that show the greatest differences of sulphide mineral assemblages. The main groups are (arranged from most common to least common group): 1) the cobalt pentlandite-pyrrhotite-chalcopyrite-cubanite group (Group A), 2) the cobalt pentlandite-chalcopyrite(1)-chalcopyrite(2)-bornite group (Group B), 3) the bornite-x-bornite-chalcocite-cobalt pentlandite group (Group C), 4) the chalcopyrite-bornite-flames-and-laths group (Group D), 5) the bornite-chalcocite-cobalt pentlandite group (Group E), and 6) the chalcopyrite-millerite group (Group F). Therefore, similar sulphide mineral assemblages of the MT-samples were linked via the classification of the samples into these groups.

The group names indicate which sulphide minerals are most likely to be found in close proximity to one another. The main sulphide minerals in each group name are also arranged in their sequence of formation. The same mineral name present within different groups does not necessarily mean that those minerals are cogenetic, seeing that their sequences of emplacement may differ, as well as the way they were emplaced.

It is important to point out that the absence of a certain sulphide mineral(s) does not necessarily exclude the sample from a certain group. A sample (Sample-A) may contain a specific sulphide mineral which might be present within another sample (Sample-B) as well. Sample-A might show more or less the same sulphide mineral assemblage as Sample-B, but it

might be a possibility that the latter sample shows an absence of certain sulphide mineral(s), which is actually present within Sample-A. That specific mentioned sulphide mineral can be used to link both samples (Sample-A and Sample-B) to the same group, even though there is an absence of certain sulphide minerals within Sample-B. For example, it is initially difficult to classify MT-23 into one of the main groups. The sample does show a combination of cobalt pentlandite, chalcopyrite, cubanite, and mackinawite, but pyrrhotite is absent. In addition, pentlandite and sphalerite are also present. Creating a separate group for this type of combination might be considered as a more logical option, but when observing MT-26 it is found that this sample fits into the cobalt pentlandite-pyrrhotite-chalcopyrite-cubanite-mackinawite group, having all those minerals present in the sample like that of MT-5 and MT-7. However, this particular sample also contains pentlandite, like that found in MT-23. Thus, it is possible that MT-23 and MT-26 can be linked due to the presence of pentlandite in both of them, and that these samples can be linked to the main cobalt pentlandite-pyrrhotite-chalcopyrie-cubanite-mackinawite group due to the presence of pyrrhotite in MT-26, even though no pyrrhotite is found in MT-23. Thus MT-23 and MT-26 are extensions of MT-5 and MT-7 by showing that sphalerite and pentlandite can also form part of the mentioned main group.

A few samples show a combination of assemblages (transitional samples). However, these different assemblages are always apart, seeing that they form part of separate sulphide mineral fabrics. Also, the different assemblages never show any signs of replacement towards one another.

5.1.1. Cobalt pentlandite-pyrrhotite-chalcopyrite-cubanite group (Group A).

Group A has many textural features which makes it easily distinguishable from the other groups. When observing samples that are classified into this group, the most common features are the close association between pyrrhotite and cobalt pentlandite, as well as the presence of cubanite and mackinawite (Figure 4.1; Figure 4.9). Mackinawite, pentlandite, and Cu-rich veinlets are only present within Group A (Figure 4.18; Figure 4.30; Figure 4.31; Figure 5.1).

Pyrrhotite grains in this group became recrystallised. This is indicative of two generations of pyrrhotite (Figure 4.27; Figure 4.29). However, the presence of recrystallised pyrrhotite grains is extremely rare. The two pyrrhotite generations are geochemically distinctive due to the fact that first generation pyrrhotite has a lower Fe content compared to second generation pyrrhotite (Figure 4.28).

Two generations of cubanite form part of Group A (Figure 4.26). First generation cubanite exists as laths that exsolved from chalcopyrite, while second generation cubanite exists as a replacement phase of cobalt pentlandite, pyrrhotite (Figure 4.12), chalcopyrite (Figure 4.4), and first generation cubanite (Figure 4.2; Figure 4.3). A strong association exists between later formed Cu-rich veinlets and chalcopyrite-cubanite boundaries (Figure 4.30).

This group also shows the existence of two generations of cobalt pentlandite. First generation cobalt pentlandite (Figure 4.1; Figure 4.9) is very common and is the cobalt pentlandite generation that is found in the majority of the other groups as well. However, in this particular group, the first generation cobalt pentlandite grains are commonly enclosed by pyrrhotite (Figure 4.9), or replaced by chalcopyrite (Figure 4.1) and mackinawite (Figure 4.34). Second generation cobalt pentlandite (Figure 5.2) is extremely rare. It formed well-shaped flames that replaced chalcopyrite and cubanite at pyrrhotite-chalcopyrite boundaries.

Two sphalerite generations are present within this group. First generation sphalerite is euhedral to subhedral in shape and contains chalcopyrite inclusions (Figure 4.15), with the chalcopyrite inclusions being indicative of its formation in more or less the same period as chalcopyrite crystallisation. These sphalerite grains are extremely rare in Group A, because they occur only in one sample (MT-23). However, second generation sphalerite is very common in Group A and occurs as smaller anhedral grains. These grains caused the replacement of chalcopyrite and cubanite from fractured and pitted zones (Figure 4.12, B; Figure 5.3; Figure 5.4). They also exist as rims that formed at cobalt pentlandite-cubanite (or chalcopyrite) boundaries (Figure 5.5). The two sphalerite generations are geochemically distinctive due to the fact that first generation sphalerite has a higher Zn content compared to second generation sphalerite (Figure 4.36). MT-35 and MT-38 may indicate that the replacement of cobalt pentlandite and pyrrhotite by second generation cubanite occurred only at deeper depths. Samples from shallower depths (e.g. MT-5 and MT-7) do not contain any residual island of cobalt pentlandite and pyrrhotite.

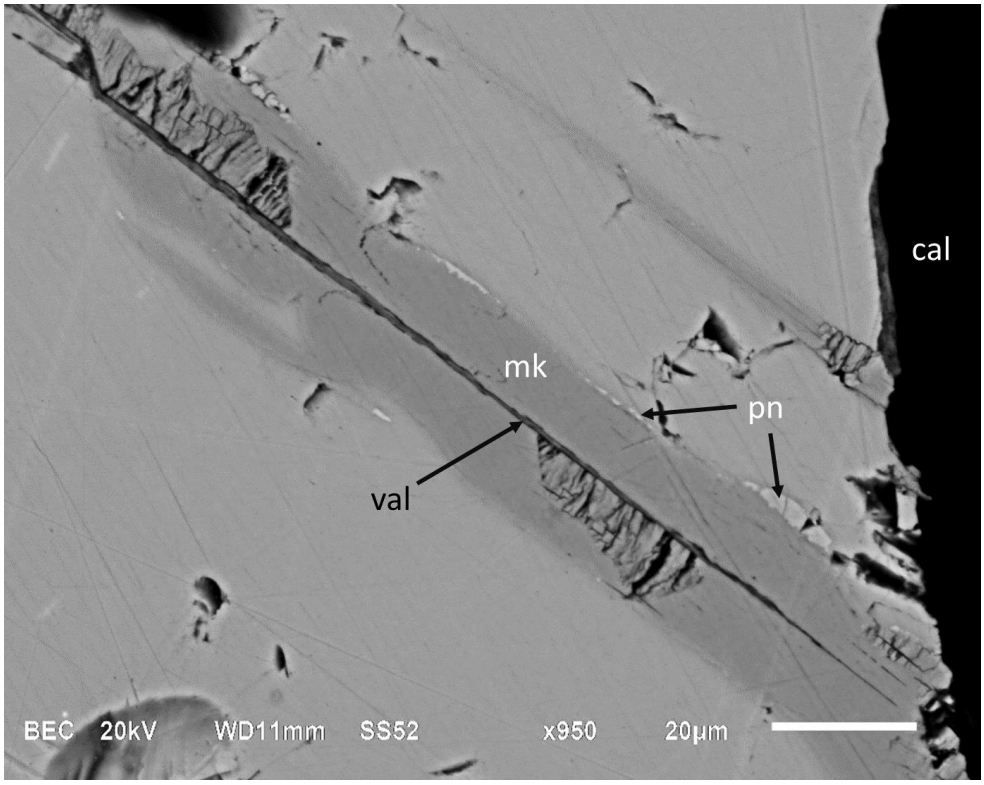

Figure 5.1: Chalcopyrite replaced by pentlandite and mackinawite. Pentlandite replaced by mackinawite. Mackinawite replaced by valleriite. BSE image, sample MT-38.

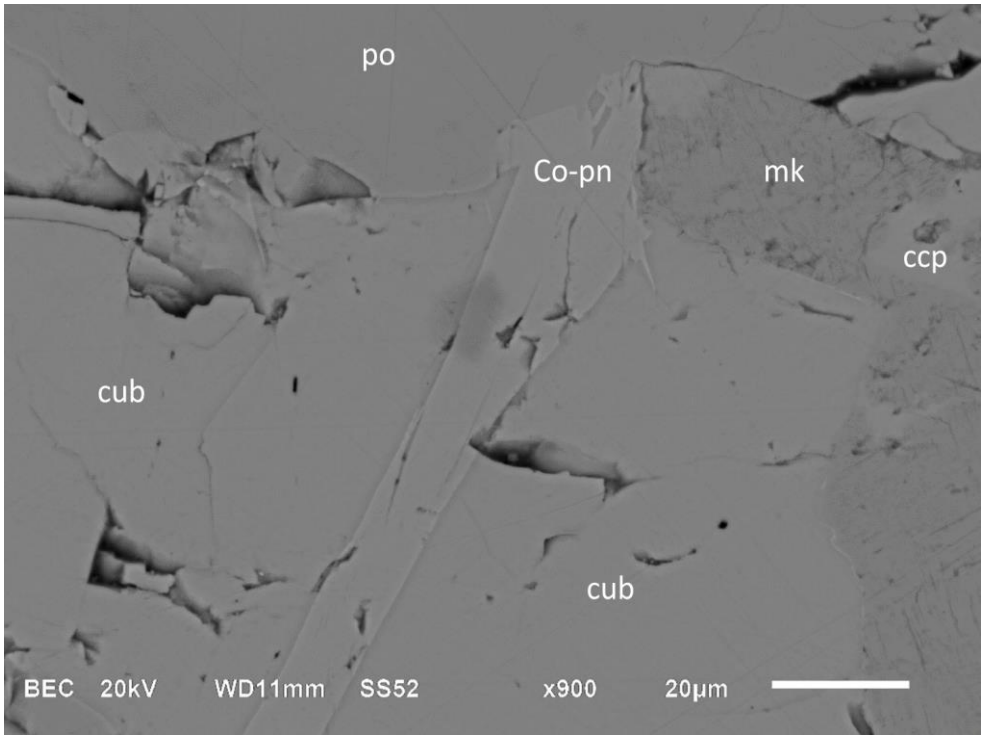

Figure 5.2: Second generation cobalt pentlandite flames replaced by mackinawite. Chalcopyrite, pyrrhotite, and second generation cubanite replaced by second generation cobalt pentlandite. BSE image, sample MT-5.

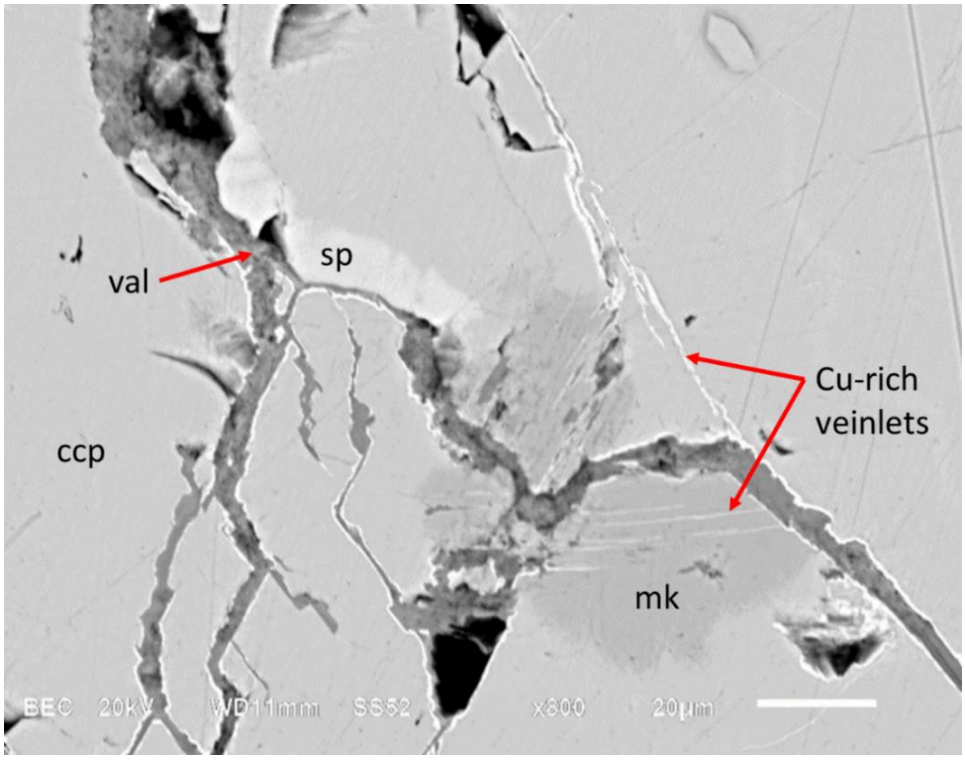

Figure 5.3: Sphalerite (second generation), mackinawite, and chalcopyrite replaced by Cu-rich veinlets at fractured zones. Sphalerite replaced by mackinawite. Third generation magnetite replaced by valleriite. Valleriite rimmed by Cu-rich veinlets. BSE image, sample MT-14.

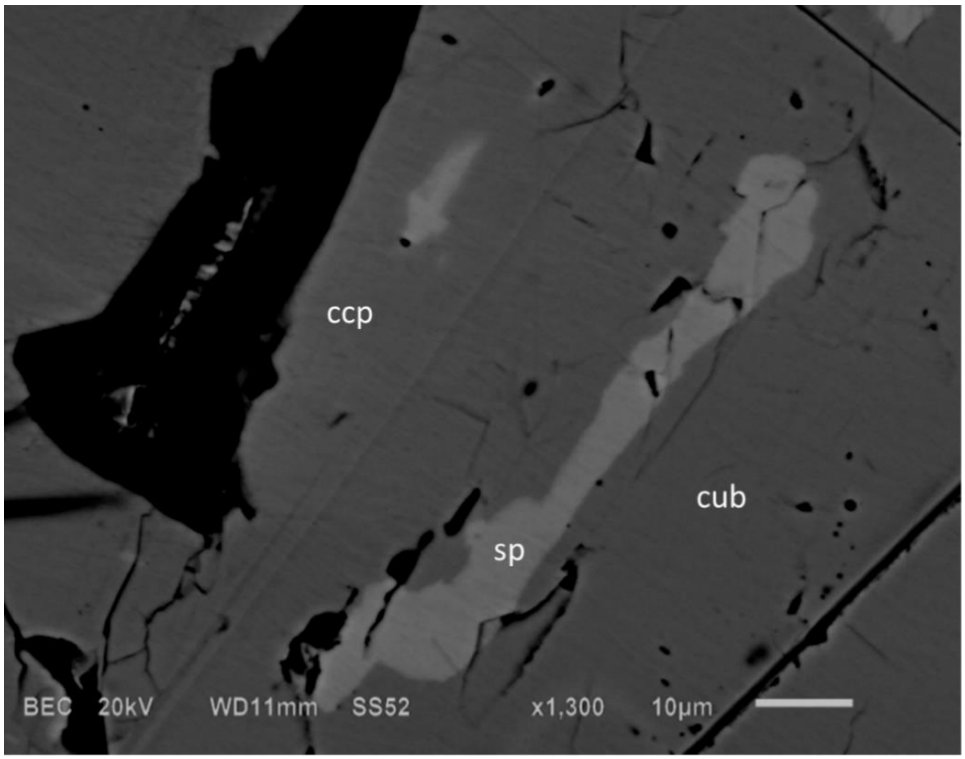

Figure 5.4: Chalcopyrite and first generation cubanite replaced by second generation sphalerite from pitted surfaces. BSE image, sample MT-23.

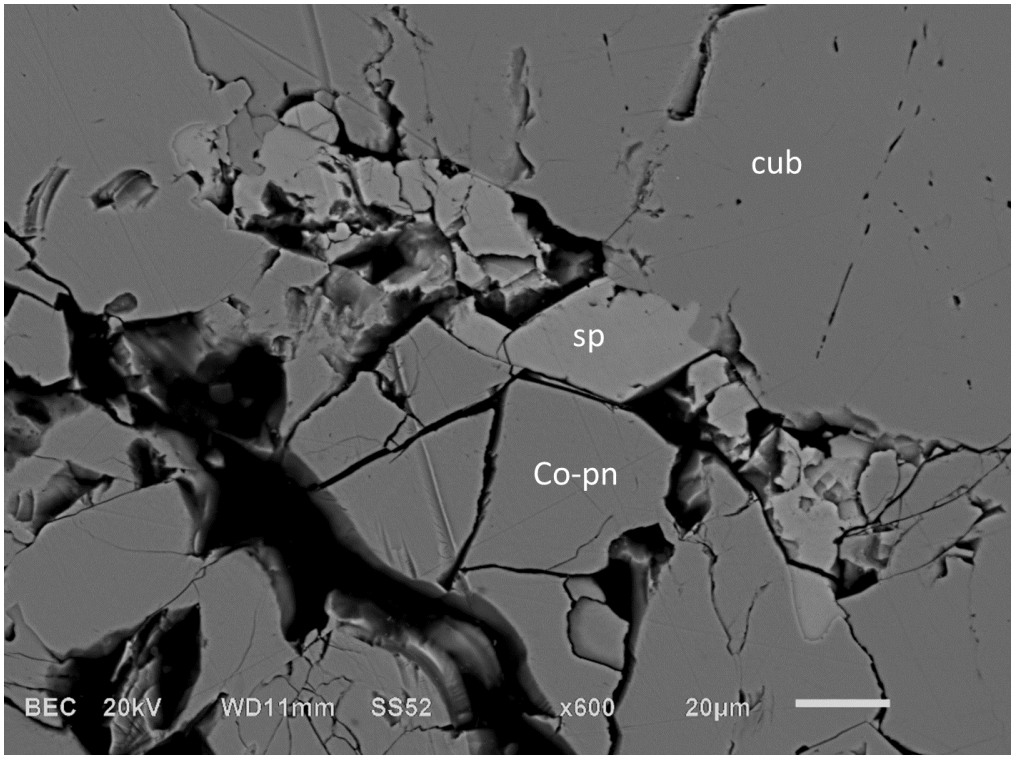

Figure 5.5: Cobalt pentlandite and second generation cubanite replaced by sphalerite. BSE image, sample MT-38.

5.1.2. Cobalt pentlandite-chalcopyrite(1)-chalcopyrite(2)-bornite group (Group B).

Group B is characterised by the occurrence of two generations of chalcopyrite (Figure 4.25) and by the mass replacement of both chalcopyrite generations by bornite (Figure 4.5; Figure 4.19; Figure 4.20; Figure 4.25). The two chalcopyrite generations are geochemically distinctive due to the fact that first generation chalcopyrite has a higher Cu content compared to second generation chalcopyrite (Figure 4.26).

Initially, the euhedral to subhedral (mostly) chalcopyrite grains formed mutual grain boundaries. Bornite replacement mainly commenced at chalcopyrite-non-sulphide grain boundaries afterwards, which progressed further between chalcopyrite grain boundaries, outlining the shape of the chalcopyrite grains with irregularly shaped bornite “threads” that are connected to the larger bornite replacement bodies. Advanced stages or replacement includes the remains of smaller irregularly shaped grains of chalcopyrite that were completely enclosed by bornite (Figure 5.6). Bornite also caused the total replacement of chalcopyrite grains in certain areas. This may appear as bornite grains forming an interlocking framework

with chalcopyrite, but it is in fact relict chalcopyrite forming part of the interlocking framework (Figure 4.5; Figure 4.13). It might be that bornite replacement at this scale and fashion only took place where this particular chalcopyrite(1)-chalcopyrite(2) exsolution association existed, seeing that bornite was prone to replace second generation chalcopyrite before it replaced first generation chalcopyrite (Figure 5.7; Figure 5.8). Galena is only found in this type of association and formed at chalcopyrite-bornite grain boundaries (Figure 4.19; Figure 4.25).

Chalcocite in Group B occur as small anhedral bodies that were replaced by covelline (Figure 4.13; Figure 5.9). Both covelline and chalcocite are primarily confined to the replacement of bornite. This particular type of chalcocite (confined to Group B) formed at variable depths (e.g. MT-16 and MT-53).

Unlike Group A, this group contains only one cobalt pentlandite generation and no pentlandite proper. Bornite formed reaction rims around the cobalt pentlandite (Figure 5.10), unlike the sphalerite rims in Group A. X-bornite occurs in extremely small amounts in this group (Figure 5.11). The exact same assemblage is present in MT-52, although this sample is indicative of sulphide mineralisation from a banded carbonatite.

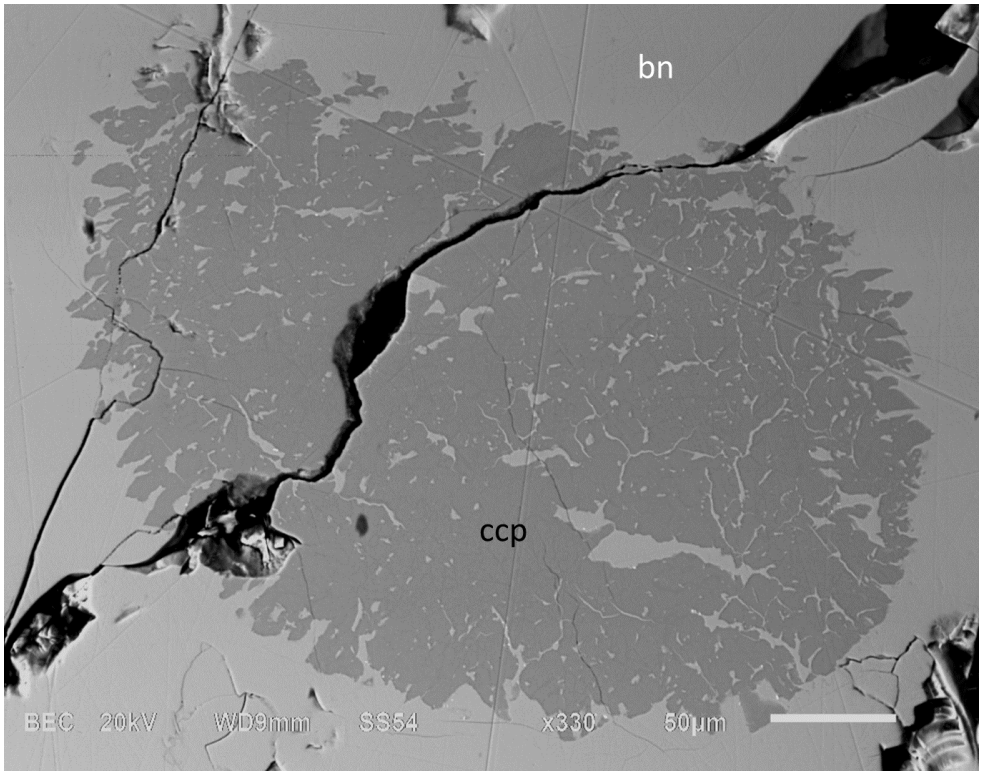

Figure 5.6: Irregularly shaped chalcopyrite grain completely enclosed and replaced by bornite. BSE image, sample MT-19.

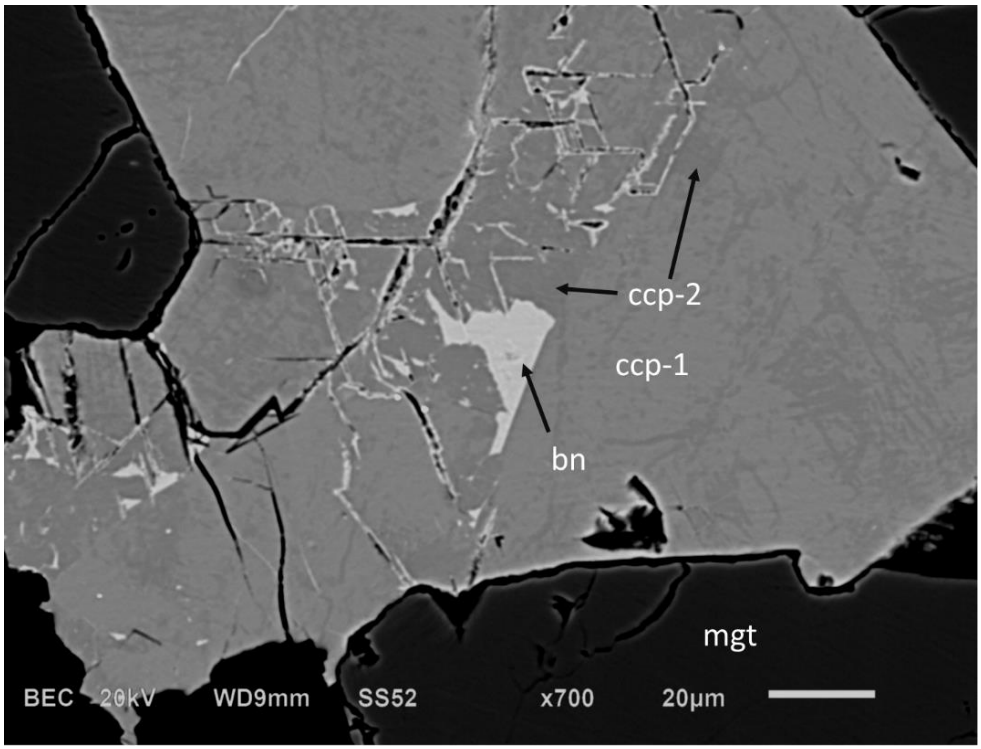

Figure 5.7: First generation chalcopyrite (ccp-1) and second generation chalcopyrite (ccp-2) replaced by bornite. Second generation chalcopyrite replaced before first generation chalcopyrite. BSE image, sample MT-49.

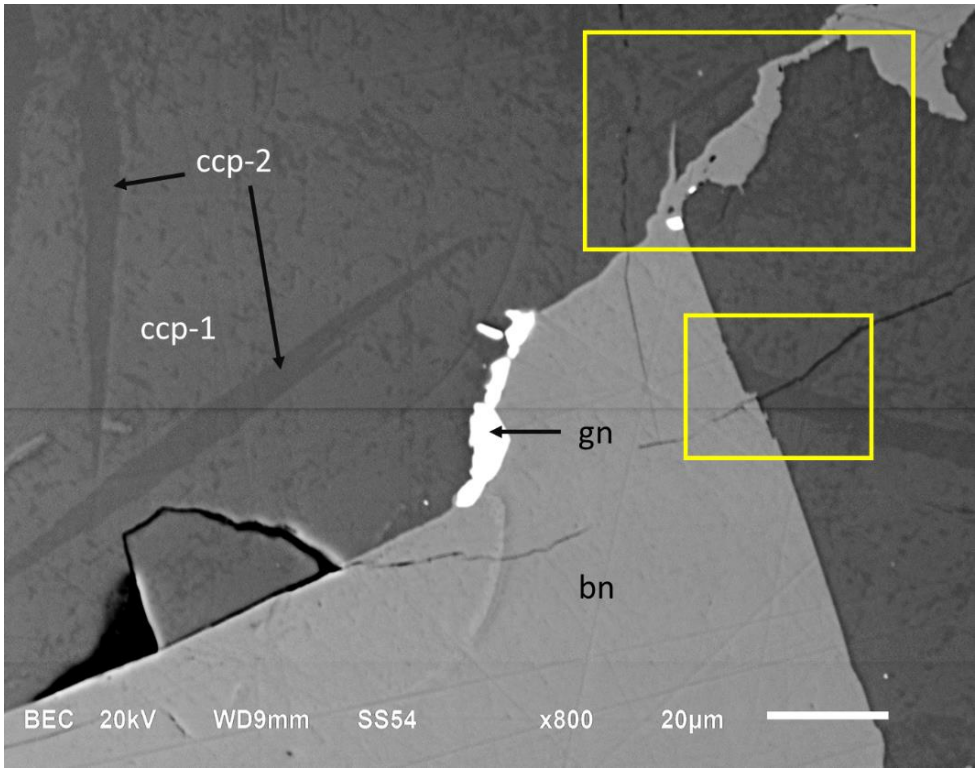

Figure 5.8: First generation chalcopyrite, second generation chalcopyrite, and bornite replaced by galena. Notice the progression of second generation replacement by bornite (yellow rectangles). BSE image, sample MT-19.

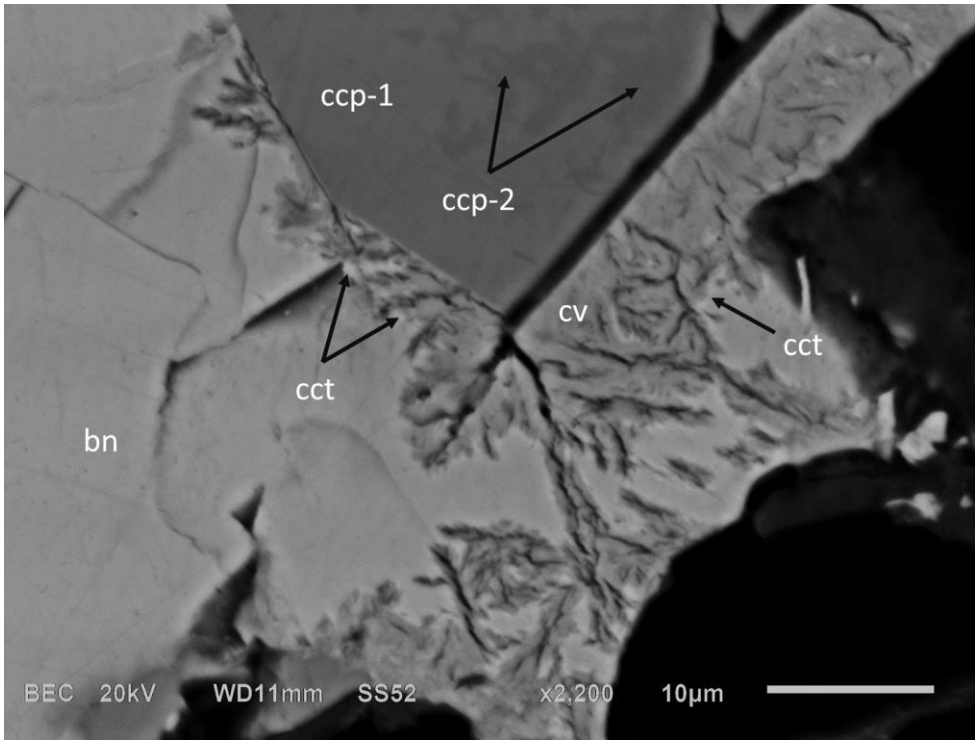

Figure 5.9: Bornite replaced by chalcocite and covelline. Chalcocite replaced by covelline. BSE image, sample MT-16.

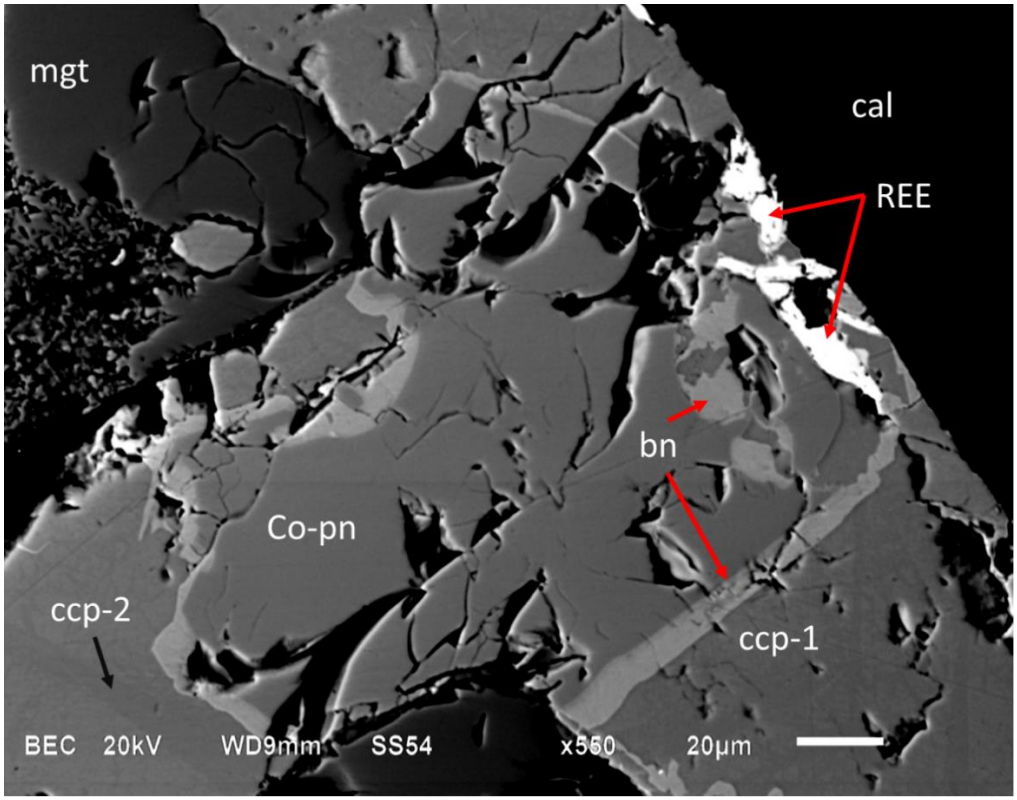

Figure 5.10: Cobalt pentlandite and chalcopyrite replaced by bornite rims. Chalcopyrite, cobalt pentlandite, and bornite replaced by magnetite. BSE image, sample MT-19.

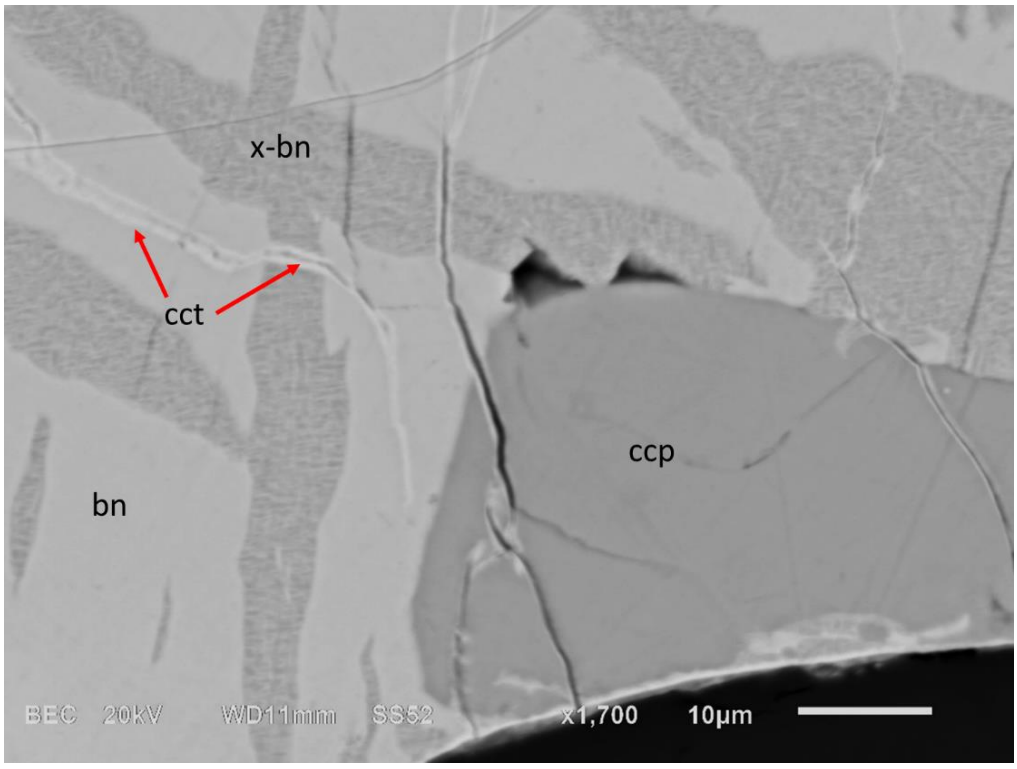

Figure 5.11: Chalcopyrite replaced by bornite. X-bornite exsolved from bornite. Chalcopyrite, bornite, and x-bornite replaced by chalcocite. BSE image, sample MT-52.

5.1.3. Bornite-x-bornite-chalcocite-cobalt pentlandite group (Group C).

Group C is characterised by the presence of large quantities of x-bornite that exsolved from bornite and large chalcocite veins that replaced the bornite and x-bornite (Figure 4.22; Figure 5.12). Only this particular type of chalcocite contains shandite (Figure 4.22; Figure 4.23; Figure 4.24). Group C chalcocite is only present at shallower depths (e.g. MT-11, MT-13, and MT-15) compared to the depths at which the smaller anhedral chalcocite grains of Group B can occur. Furthermore, the chalcocite of Group C shows no signs of covelline replacement, unlike the chalcocite from Group B. X-bornite is also very rare in Group B but very common in Group C.

Large euhedral to subhedral sphalerite grains (Figure 5.13) are common in this assemblage and not as rare as in Group A. However, this group lacks anhedral sphalerite grains that are common in Group A. Cobalt pentlandite is also associated with this group, seeing that it is found in both MT-11 and 15. Unlike the cobalt pentlandite in Group A (first generation) and Group B, the cobalt pentlandite in Group C replaced all the other sulphide phases, instead of being the replaced phase (Figure 5.14). The Co content of these cobalt pentlandites are closer to cobaltian pentlandite proper compared to that from any other group (Figure 5.15).

The best representative samples for this group are MT-11 and MT-15. These samples reveal that bornite and large chalcocite veins actually seldom occur in contact with one another. There always seems to be a more or less constant boundary/range between the chalcocite and bornite, with x-bornite found in between (Figure 4.22; Figure 5.16). For example, a smaller chalcocite vein (branch) curved away from the larger chalcocite body. This curvature was mimicked by adjacent bornite grains that were being replaced by x-bornite. This indicates that chalcocite provided a “newer” boundary from which x-bornite replacement progressed from. This also explains why the larger x-bornite islands, enclosed by later formed chalcocite, have no adjacent bornite enclosed as well. X-bornite replacement probably replaced all of the bornite as x-bornite formation progressed inward from the chalcocite-bornite boundaries.

A spectacular example of two differing ages of bornite grains in very close proximity is presented by MT-13 (Figure 5.17). The sample shows a symplectic intergrowth between chalcocite and bornite, although the chalcocite present within this particular group is known to have primarily replaced bornite instead of forming intergrowths with it. Careful observation indicated that the bornite-chalcocite intergrowth formed a border along older

bornite grains at the outer reaches of the image where the older bornite grains were being replaced by the same chalcocite formation phase. This can be interpreted as bornite formation at the outer areas, but a sulphide forming liquid that was still present in the central area. Replacement of bornite by chalcocite already occurred at the outer bornite grains, while the central bornite forming sulphide liquid was still decreasing in temperature. The intergrowth formed as chalcocite formation was introduced inward at the exact same time of younger bornite formation, thus forming the intergrowth. This can be interpreted as an overlap in the paragenetic positions of the two sulphide minerals.

It is apparent that the majority of sulphide replacement in Group C initiated at sulphide-non-sulphide grain boundaries. None of the minerals present in this group show any formational association towards a major fracturing event, unlike Group A. This group also shows no association towards chalcopyrite, unlike Group A and Group B. This makes it difficult to compare the paragenetic positions of this group with minerals that actually show some sort of association with chalcopyrite.

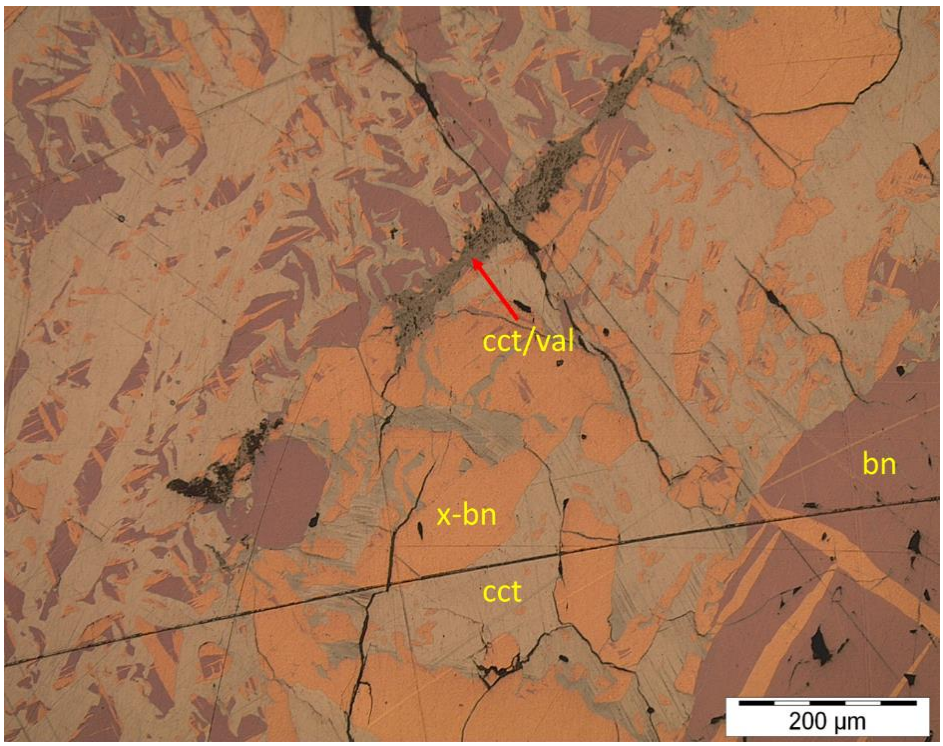

Figure 5.12: X-bornite exsolution intergrowths within bornite. Bornite replaced further by x-bornite. X-bornite and bornite replaced by chalcocite. Chalcocite replaced by valleriite. RL image, sample MT-13.

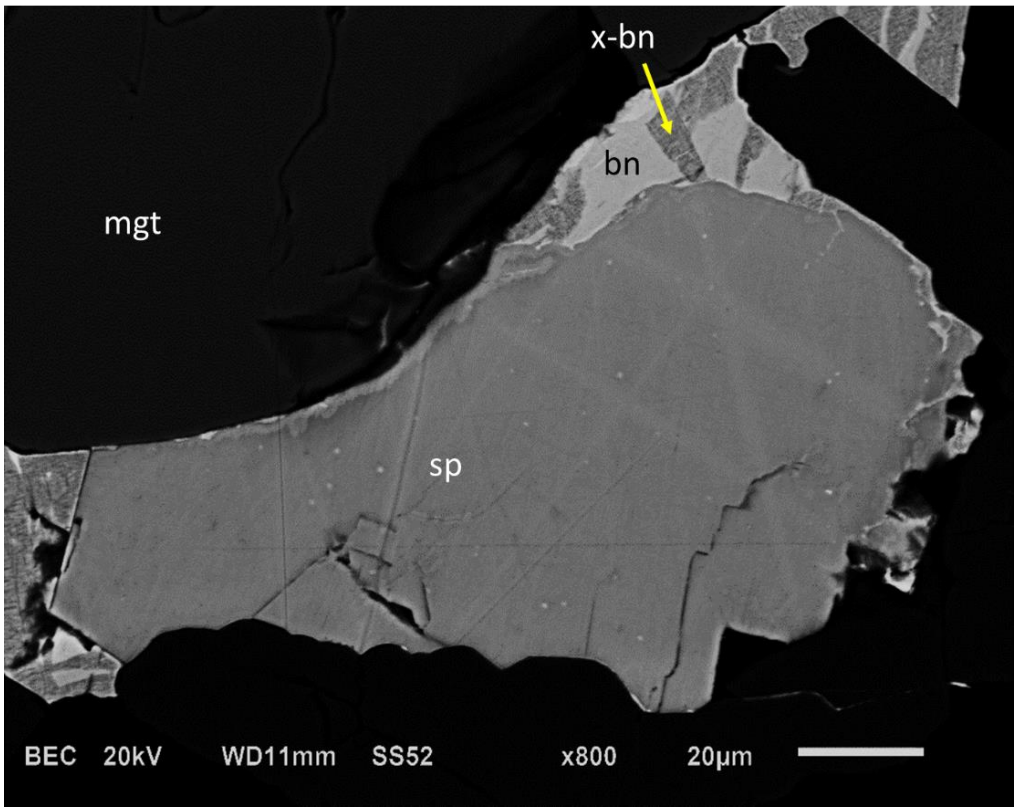

Figure 5.13: Bornite and x-bornite replaced by euhedral to subhedral sphalerite. Sphalerite, bornite, and x-bornite replaced by third generation magnetite. BSE image, sample MT-11.

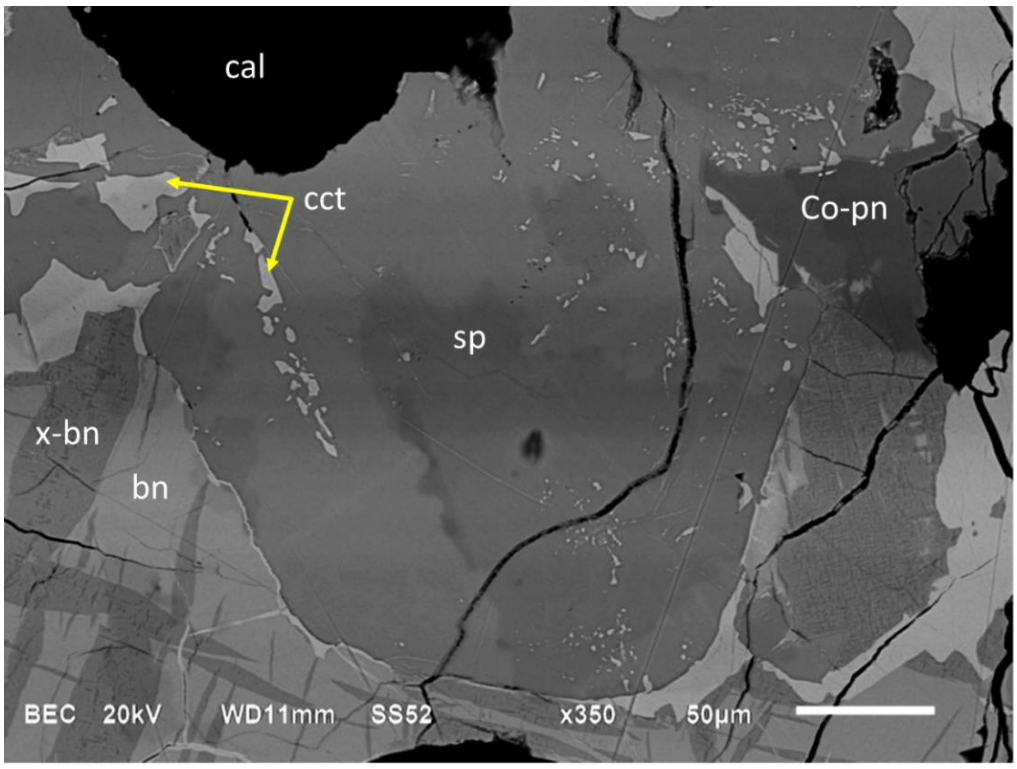

Figure 5.14: Bornite, x-bornite, and chalcocite replaced by sphalerite. X-bornite, chalcocite, and sphalerite replaced by cobalt pentlandite. BSE image, sample MT-15.

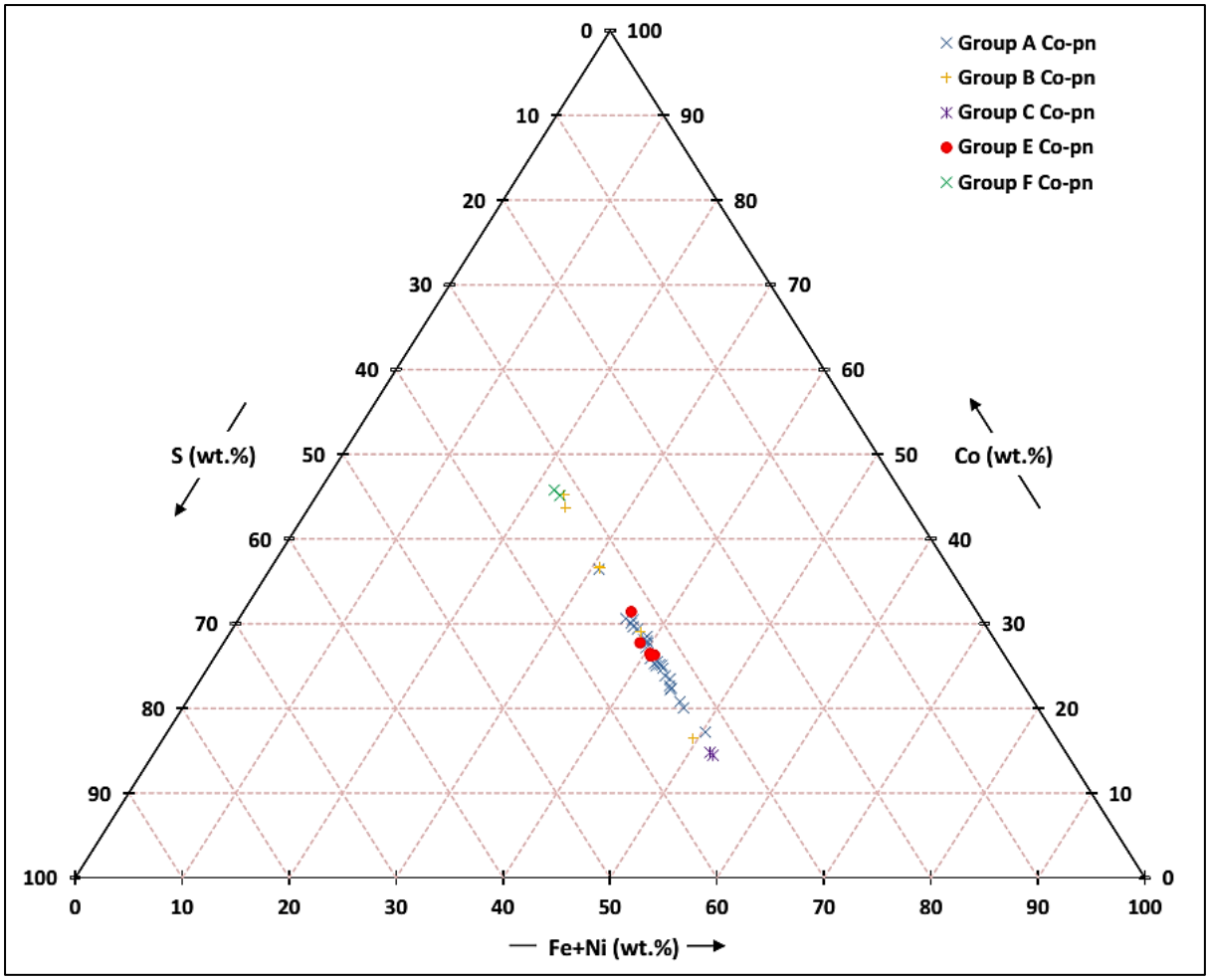

Figure 5.15: Compositions of Groups A, B, C, E and F cobalt pentlandite from transgressive carbonatite.

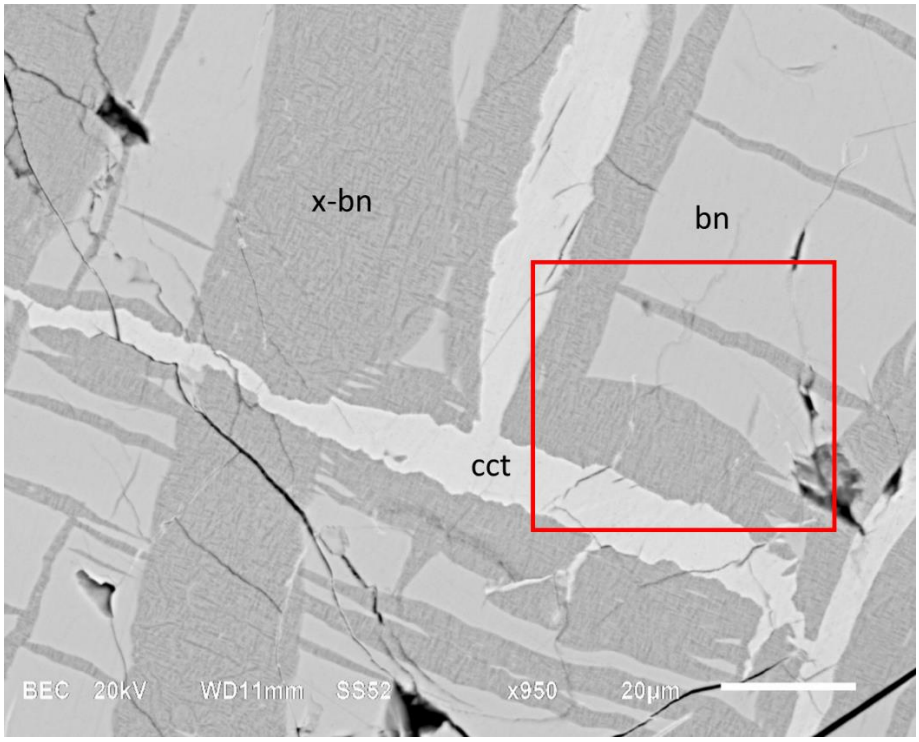

Figure 5.16: Bornite and chalcocite replaced by x-bornite from chalcocite boundary (red rectangle). Notice that the bornite appears concave inwards due to the replacement process. BSE image, sample MT-11.

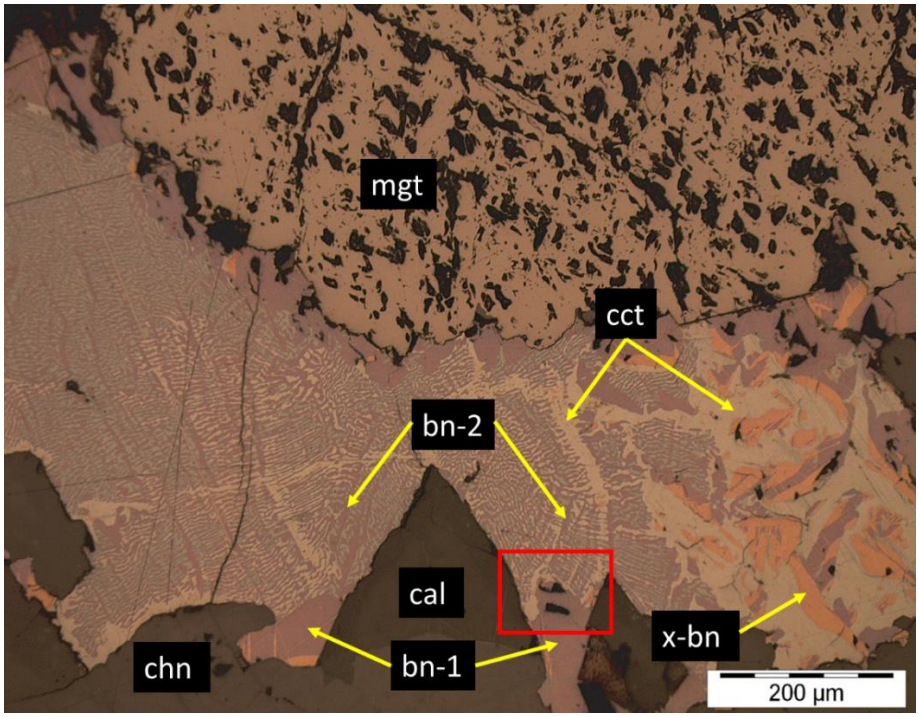

Figure 5.17: Bornite (bn-1) rimmed by chalcocite (red rectangle). Symplectic intergrowth between chalcocite and bornite (bn-2). Calcite, chondrodite, and second generation magnetite replaced by sulphides. RL image, sample MT-13.

5.1.4. Chalcopyrite-bornite-flames-and-laths group (Group D).

Group D is mainly characterised by the presence of bornite laths and flames (Figure 4.6; Figure 4.7; Figure 4.16; Figure 4.21) that formed from chalcopyrite. Unlike Group B, the bornite in Group D did not cause mass replacement of chalcopyrite and did not form from exsolved chalcopyrite, seeing that exsolved chalcopyrite is not present within this sulphide mineral assemblage. Also, the bornite in this group is a late stage phase, unlike the bornite in Group C. Heazlewoodite is only present within Group D (Figure 4.21; Figure 5.18; Figure 5.19).

Just like group A, this group also contains larger euhedral sphalerite grains with chalcopyrite inclusions. However, the sphalerite from this group shows a strong replacement association with bornite (Figure 5.20). Also, Group C lacks smaller anhedral sphalerite grains.

The sphalerite grains in Group A (first generation with respect to this particular group) and Group D probably represent the same generation, because the grains from both groups contain chalcopyrite inclusions, are euhedral to subhedral in shape, and form the same textural association with the enclosing chalcopyrite fabric. Even though the sphalerite grains from Group C are also euhedral to subhedral in shape and are geochemically similar to that of Group A and Group D (Figure 4.36), it probably represents a different generation, seeing that these grains do not contain any chalcopyrite inclusions and form part of an entirely different sulphide mineral assemblage.

MT-44 is the best representative sample for this group. The sample is indicative of numerous associations between sphalerite (with chalcopyrite inclusions present in the majority of the grains) and bornite, and it also shows that millerite can be associated with this group (Figure 5.20; Figure 5.21). The bornite mainly exists in the form of flames. These bornite flames may be connected to bornite laths and to larger irregularly shaped bornite bodies that formed at fractured zones.

The millerite that is present within MT-44 is completely confined to bornite replacement at fractured zones. It primarily replaced larger irregularly shaped bornite bodies and bornite flames. The occurrence of millerite replacing bornite laths is rarer, but does exist.

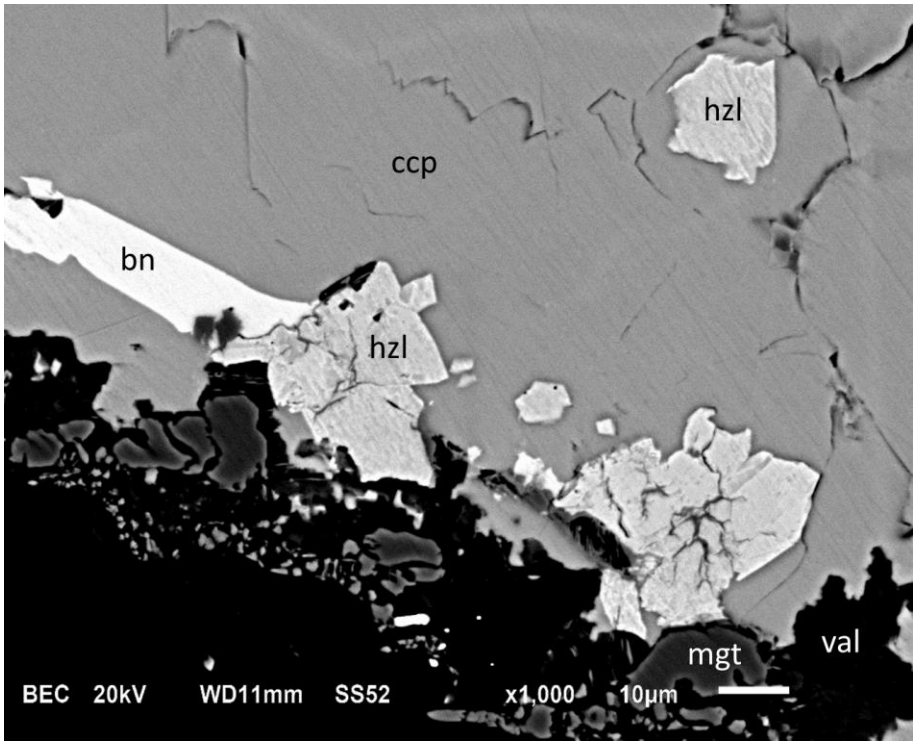

Figure 5.18: Euhedral to subhedral heazlewoodite grains filled with magnetite veinlets. Chalcopyrite replaced by heazlewoodite, bornite, and valleriite. Heazlewoodite replaced by valleriite. BSE image, sample MT-58.

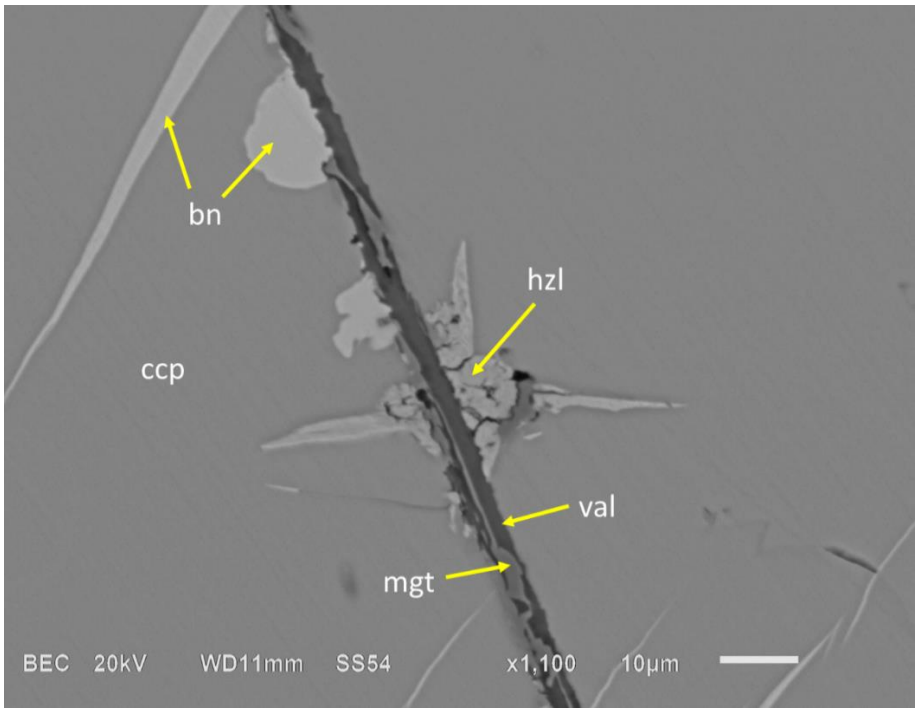

Figure 5.19: Heazlewoodite cut by third generation magnetite and replaced by valleriite. Chalcopyrite replaced by bornite, magnetite, and valleriite. Bornite replaced by valleriite. BSE image, sample MT-58.

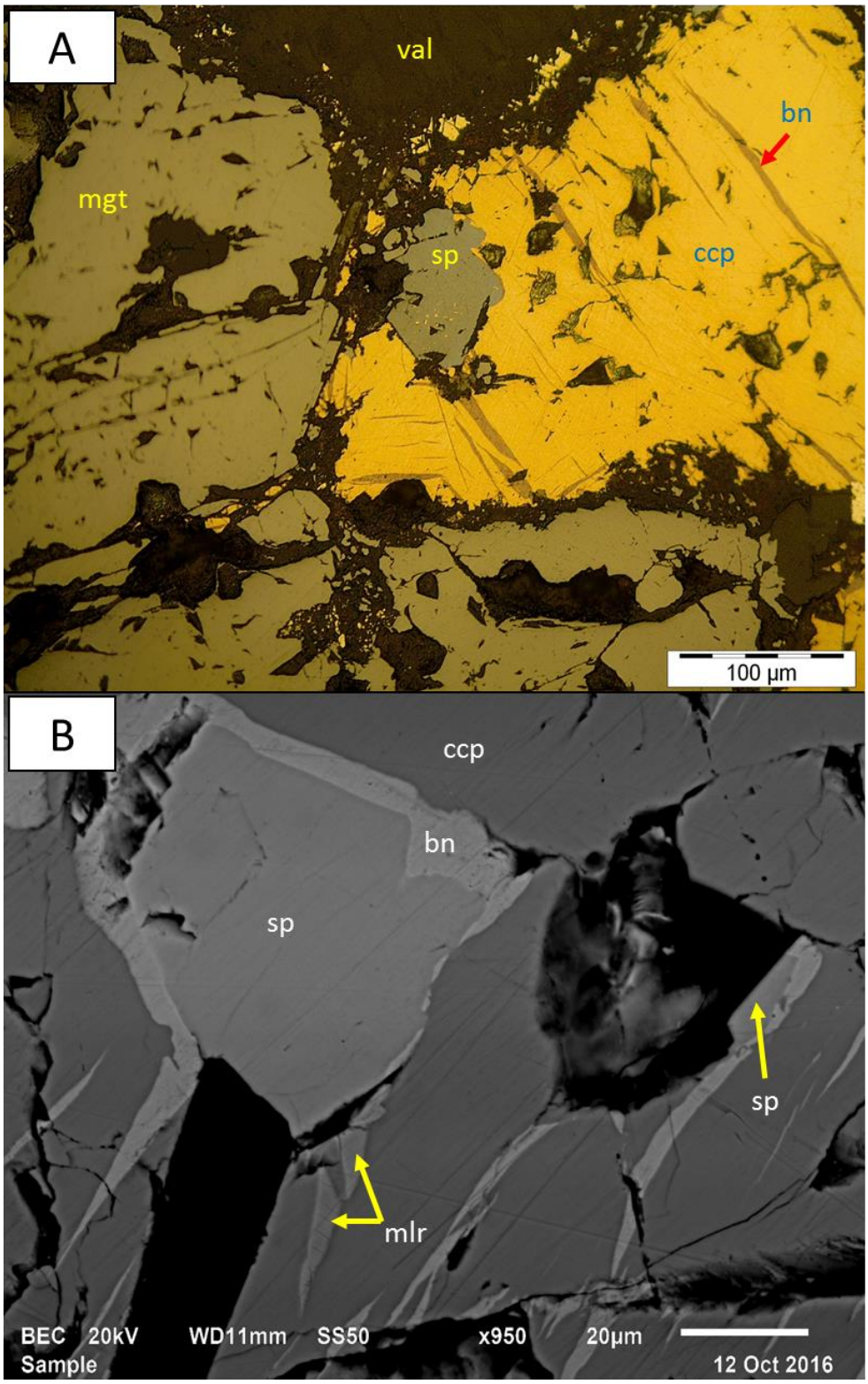

Figure 5.20: A) Euhedral to subhedral sphalerite grain (with chalcopyrite inclusions) and chalcopyrite replaced by bornite flames. Chalcopyrite, bornite, and magnetite replaced by valleriite. B) Euhedral to subhedral sphalerite grains (without chalcopyrite inclusions) and chalcopyrite replaced by bornite flames. Bornite flames replaced by millerite. RL image (A) and BSE image (B), sample MT-44.

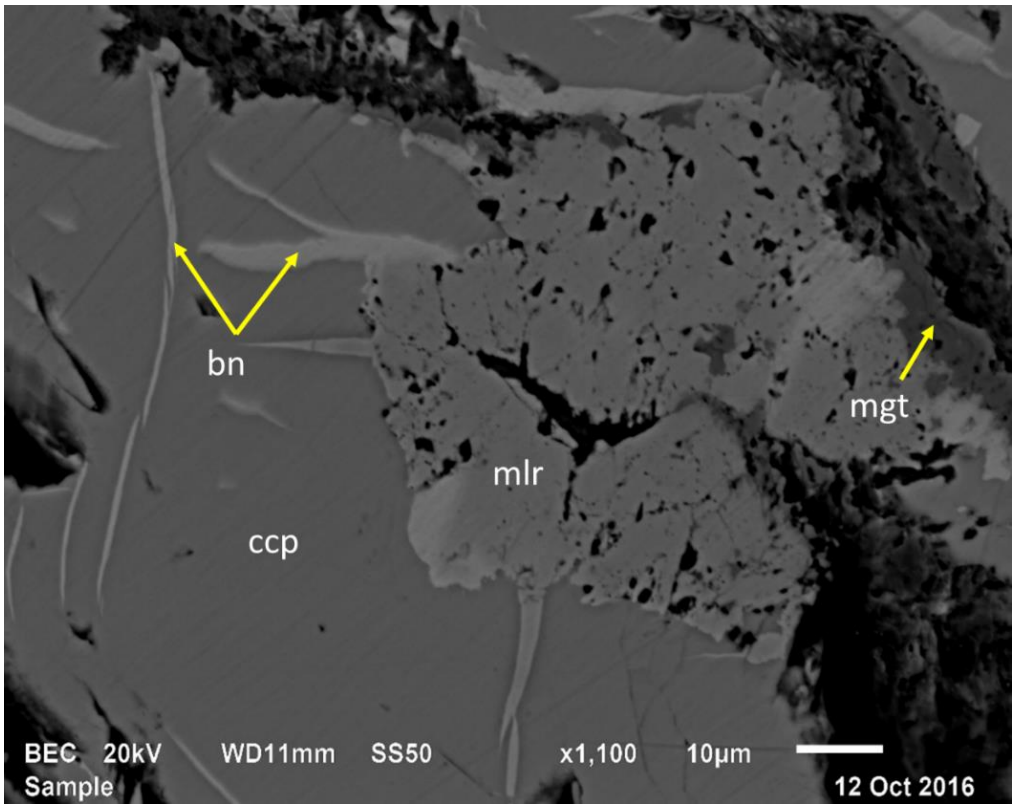

Figure 5.21: Bornite replaced by millerite. Chalcopyrite, bornite, and millerite replaced by magnetite veinlet (third generation). BSE image, sample MT-44.

5.1.5. Bornite-chalcocite-cobalt pentlandite group (Group E).

Group E is characterised by the occurrence of multiple symplectic intergrowths of chalcocite and bornite (Figure 4.14) within a sample and the strong association that exists between these intergrowths and cobalt pentlandite (Figure 5.22, A). Cobalt pentlandite replaced both bornite and chalcocite solely from sulphide-non-sulphide grain boundaries.

Group E lacks sphalerite and x-bornite, which is present within Group C. The bornite in this group is also absent from the chalcocite-covelline association portrayed by Group B. Chalcopyrite, in this group, is found in extremely small quantities as isolated blebs that are enclosed by non-sulphide minerals, thus making it difficult to compare its replacement association with the bornite-chalcocite-cobalt pentlandite assemblage.

No evidence was found which would suggest that chalcocite formation continued after bornite formation (as presented by Group C), or vice versa, even after the intergrowths formed. Group E is primarily represented by MT-55. The exact same assemblage can be found in MT-2 (Fig. 5.22, B), although this sample is indicative of sulphide mineralisation from a banded carbonatite sample.

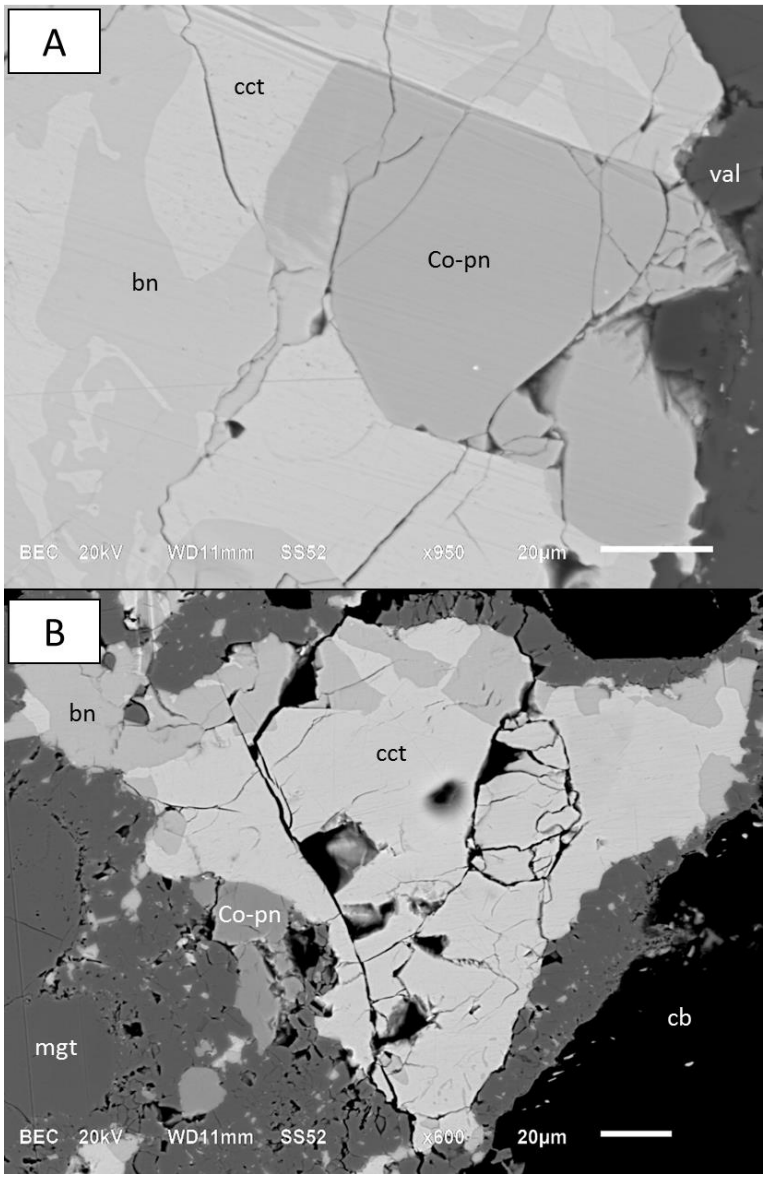

Figure 5.22: A) Symplectic intergrowth of bornite and chalcocite replaced by cobalt pentlandite. Bornite, chalcocite, and cobalt pentlandite replaced by valleriite. BSE image, sample MT-55 (TCB). B) Symplectic intergrowth of bornite and chalcocite replaced by cobalt pentlandite. Bornite, chalcocite, and cobalt pentlandite replaced by magnetite. BSE image, MT-2 (BCB).

5.1.6. Chalcopyrite-millerite group (Group F).

Group F is characterised by the existence of large quantities of chalcopyrite. The chalcopyrite in this group was replaced only by millerite at fractured zones (Figure 5.23; Figure 5.24). The millerite in this group shows no association towards any other sulphide mineral, unlike the millerite in Group D, which is completely confined to the replacement of bornite (Figure 5.21). A separate group for this assemblage is generated, seeing that this association that exist only between chalcopyrite and millerite is found in more than two samples (e.g. MT-20, MT-48, and MT-60), and because millerite occurs more in this assemblage than that found in MT-44 (Group D). Also, the millerite in this group is mostly subhedral to anhedral (Figure 5.24), while the millerite in group D is completely anhedral.

Cobalt pentlandite only occurs in one sample of this group (MT-20) and also just in small amounts. The majority of the Co content of Group B and Group F cobalt pentlandites are higher compared to that of any other group (Figure 5.15). The cobalt pentlandite grains in Group A (first generation with respect to this particular group), Group B, and Group F probably represents the same generation, seeing that these grains form the same textural association with the enclosing chalcopyrite fabric and show evidence of being the first formed sulphide minerals in each of these groups. However, the cobalt pentlandite grains in Group C probably represents a different generation, seeing that those grains from part of an entirely different sulphide mineral assemblage and formed after the other sulphide minerals within that assemblage.

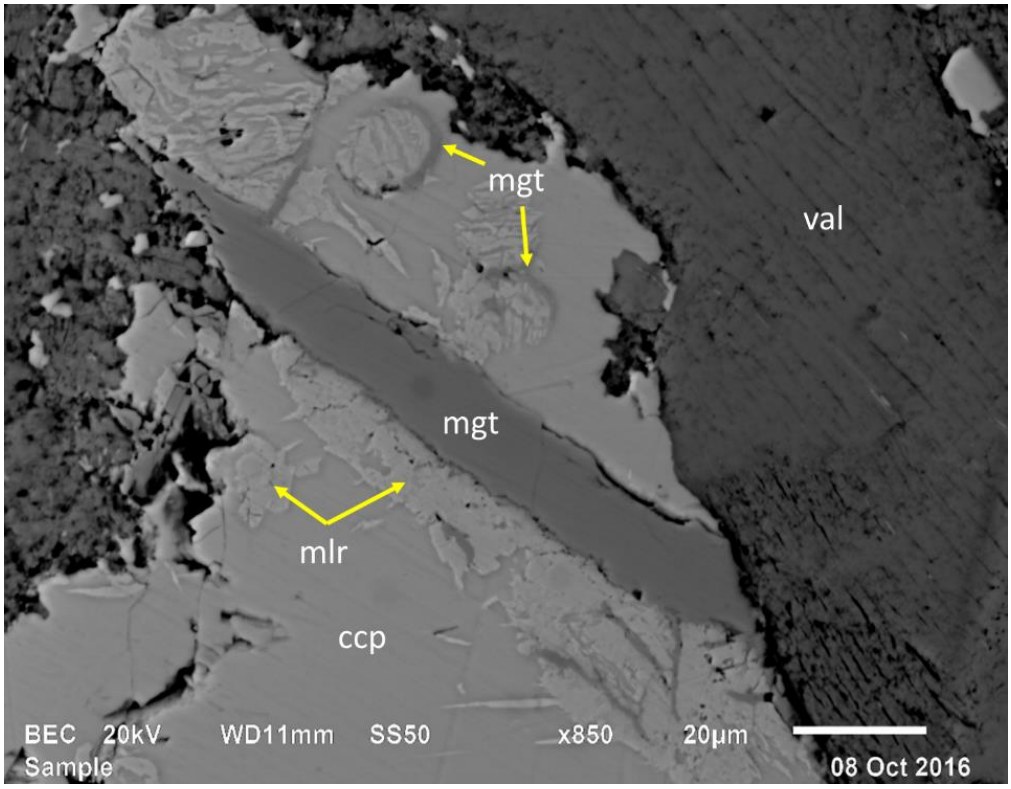

Figure 5.23: Chalcopyrite replaced by millerite, third generation magnetite, and valleriite. Millerite replaced by third generation magnetite and valleriite. Third generation magnetite replaced by valleriite. BSE image, sample MT-20.

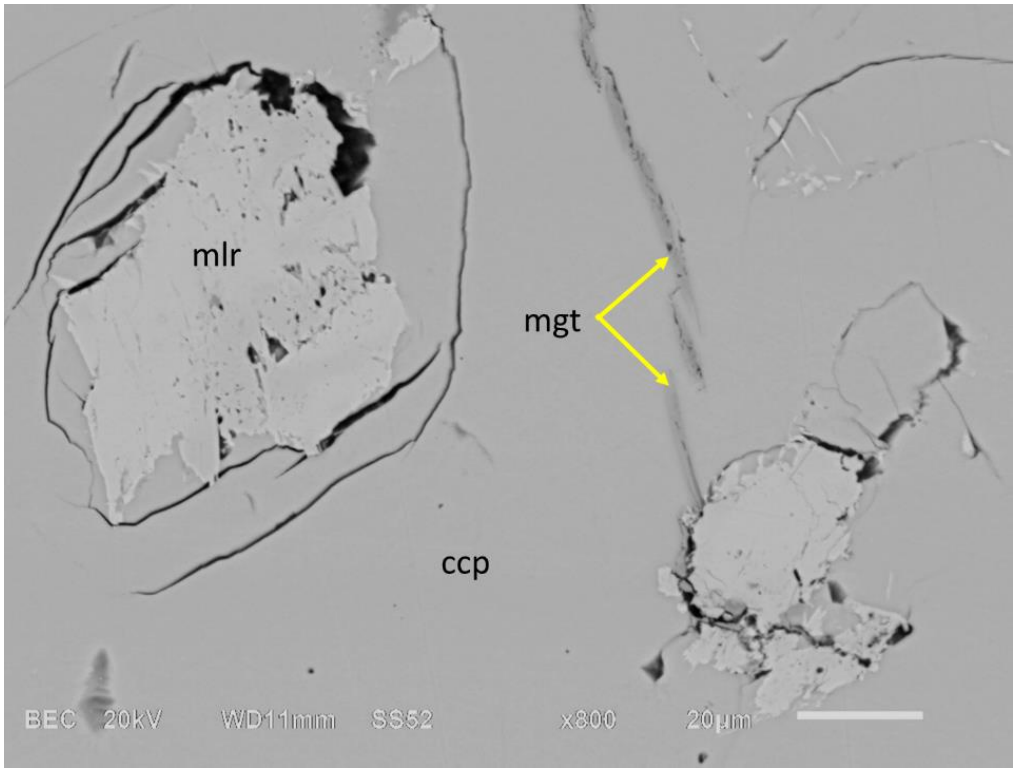

Figure 5.24: Chalcopyrite replaced by subhedral millerite grains. Millerite and chalcopyrite replaced by third generation magnetite. BSE image, sample MT-60.

5.2. Paragenetic sequences of different sulphide mineral assemblages in transgressive carbonatite.

It is now clear that certain sulphide minerals do not exist within the same assemblages. For example, the same chalcopyrite fabric that exsolved cubanite will not contain exsolved x-bornite, or an assemblage that contains bornite does not contain pyrrhotite. Therefore, the paragenetic sequences of each assemblage (group) must be illustrated separately instead of amalgamated as illustrated by Aldous (1980). The textural associations needed to create an amalgamated paragenetic sequence do not exist, simply because certain sulphide minerals do not exist in equilibrium, and thus it is impossible to compare their paragenetic positions. Even if anomalous assemblages do exist, it does not change the fact that the sulphide minerals would rather form part of the described assemblages instead of forming various combinations.

5.2.1. The paragenetic sequence of Group A.

Group A sulphide mineral crystallisation (Figure 5.25) commenced with the formation of cobalt pentlandite and pyrrhotite (Figure 4.9). The crystallisation of these two minerals was partly contemporaneous. However, pyrrhotite formation exceeded cobalt pentlandite formation and enclosed the latter in a subpoikilitic to poikilitic fashion. This was followed by the formation of chalcopyrite (Figure 4.1) and first generation sphalerite (Figure 4.15). The crystallisation of pyrrhotite and chalcopyrite was partly contemporaneous. However, the bulk of chalcopyrite mineralisation occurred somewhat later than pyrrhotite formation.

Subsequent exsolution of first generation cubanite laths from chalcopyrite was followed by the replacement of both minerals as well as cobalt pentlandite and pyrrhotite by second generation cubanite (Figure 4.2; Figure 4.3; Figure 4.4; Figure 4.12). The formation of second generation cobalt pentlandite occurred afterwards and replaced chalcopyrite and second generation cubanite (Figure 5.2).

The injection of a S-bearing liquid produced fractures within the sulphide mineral fabric. This was followed by the recrystallisation of pyrrhotite (Figure 4.27; Figure 4.29) and the crystallisation of second generation sphalerite (Figure 5.3; Figure 5.4) and pentlandite (Figure 4.18) from the S-bearing liquid at fractured zones. Mackinawite replaced chalcopyrite (Figure 4.32) and pentlandite (Figure 5.1) thereafter. Cu-rich veinlets were the last phase to form in this assemblage (Figure 5.3; Appendix D, Spectral Image 2).

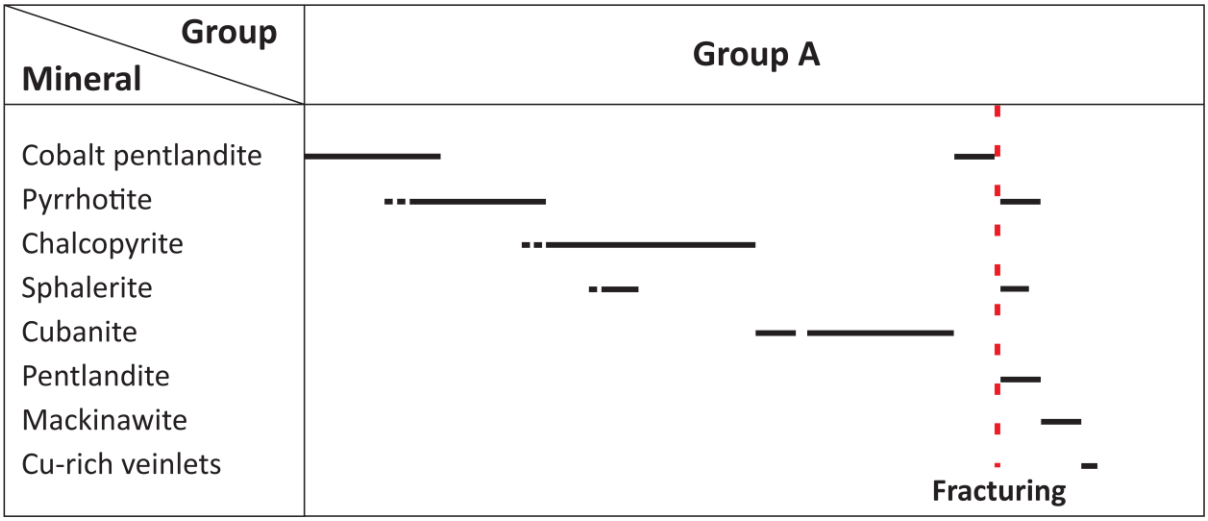

Figure 5.25: Paragenetic scheme for Group A sulphide minerals of transgressive carbonatite.

5.2.2. The paragenetic sequence of Group B.

Group B sulphide mineral crystallisation (Figure 5.26) commenced with the formation of cobalt pentlandite (Figure 5.10). Subsequent formation of first generation chalcopyrite was followed by the exsolution of second generation chalcopyrite from first generation chalcopyrite (Figure 4.25). The mass replacement of both chalcopyrite phases by bornite occurred afterwards (Figure 4.5; Figure 4.25; Figure 5.6; Figure 5.7). During the same period, galena replaced chalcopyrite and bornite at chalcopyrite-bornite boundaries as the mass replacement of the chalcopyrite fabric continued (Figure 4.19; Figure 4.20; Figure 5.8). In other words, as the replacement of chalcopyrite by bornite continued, it continued to provide new chalcopyrite-bornite boundaries from which galena could form. However, in the majority of cases, bornite causes the complete replacement of chalcopyrite, without the formation of galena.

Small amounts of x-bornite then exsolved from the larger bornite fabric (Figure 5.11). Chalcocite replaced bornite (Figure 4.13; Figure 5.9) and x-bornite subsequently (Figure 5.11). Chalcocite was replaced by covelline afterwards (Figure 4.13; Figure 5.9).

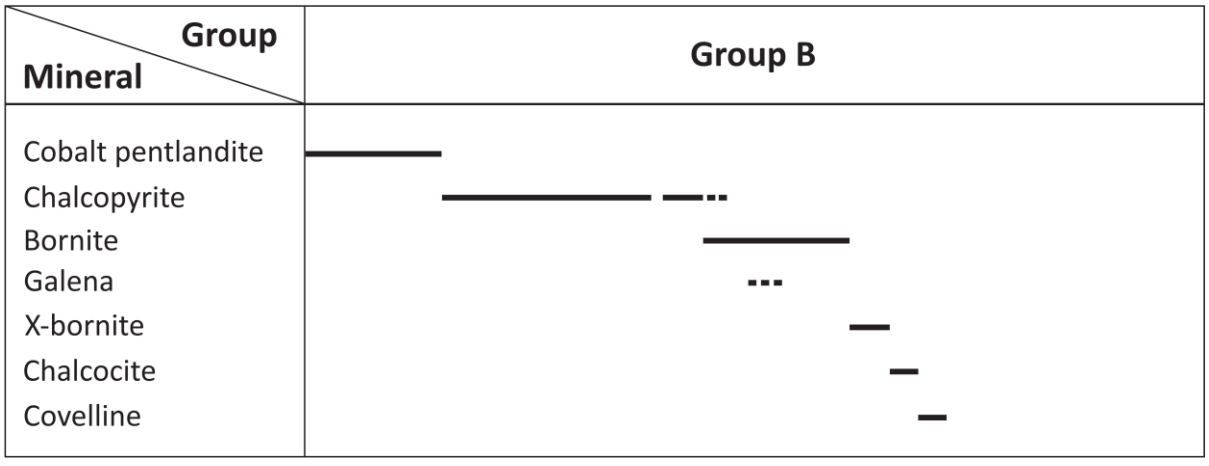

Figure 5.26: Paragenetic scheme for Group B sulphide minerals of transgressive carbonatite.

5.2.3. The paragenetic sequence of Group C.

Group C sulphide mineral crystallisation (Figure 5.27) commenced with the formation of bornite (Figure 5.12). X-bornite then exsolved from the bornite fabric. This was followed by

the replacement of both bornite and x-bornite by large chalcocite veins, and the replacement of chalcocite by shandite (Figure 4.22; Figure 4.23; Figure 4.24). X-bornite formation still continued at bornite-chalcocite boundaries thereafter (Figure 5.16) and is the reason for the rare occurrence of bornite-chalcocite boundaries. Subsequent replacement of bornite, x-bornite, and chalcocite by sphalerite was followed by the replacement of x-bornite, chalcocite, and sphalerite by cobalt pentlandite (Figure 5.14).

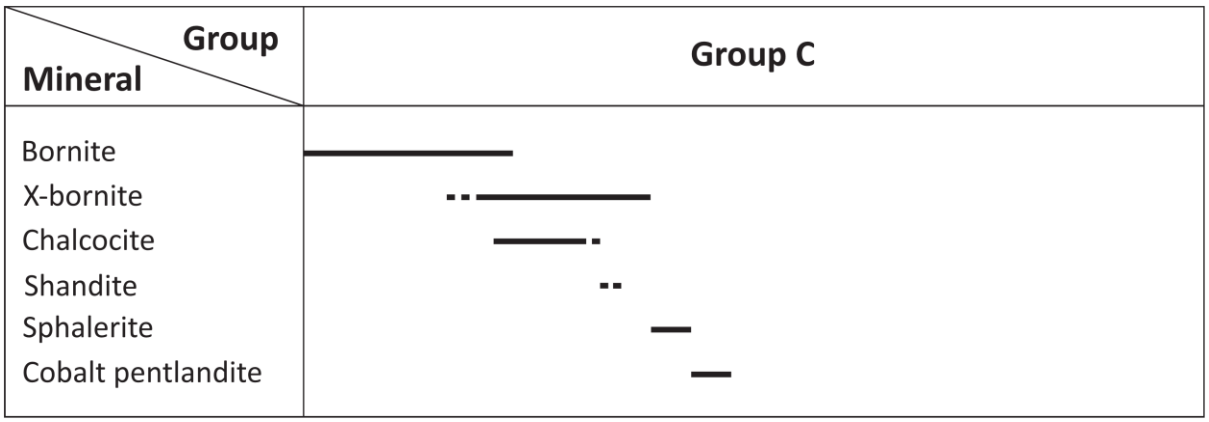

Figure 5.27: Paragenetic scheme for Group C sulphide minerals of transgressive carbonatite.

5.2.4. The paragenetic sequence of Group D.

Group D sulphide mineralisation (Figure 5.28) commenced with the crystallisation of chalcopyrite, and sphalerite with chalcopyrite inclusions (Figure 5.20). This was followed by the replacement of chalcopyrite by heazlewoodite (Figure 5.18). The injection of a S-bearing liquid produced fractures within the sulphide mineral fabric thereafter (Figure 5.18; Figure 5.19). Subsequent crystallisation of bornite from the S-bearing liquid at fractured zones was followed by the replacement of bornite by millerite (Figure 4.16; Figure 5.21).

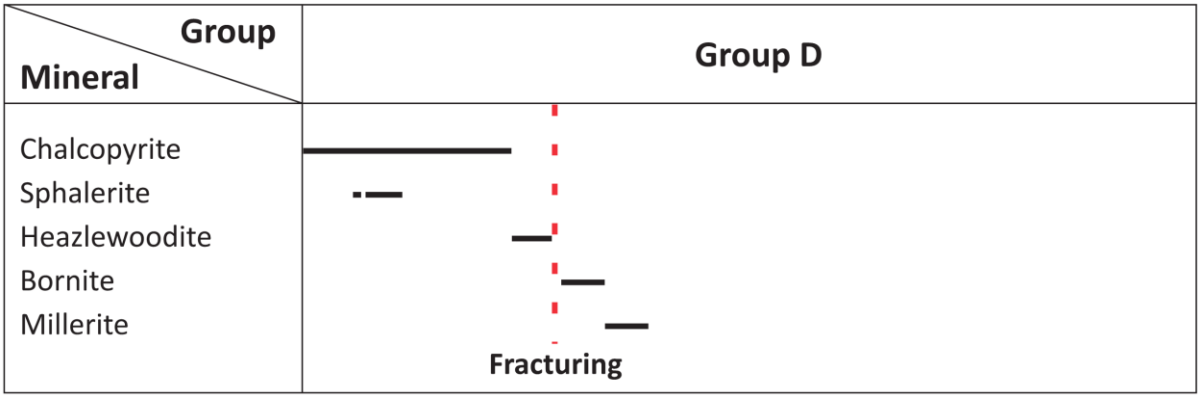

Figure 5.28: Paragenetic scheme for Group D sulphide minerals of transgressive carbonatite.

5.2.5. The paragenetic sequence of Group E.

Group E sulphide mineralisation (Figure 5.29) commenced with the simultaneous formation of bornite and chalcocite. Cobalt pentlandite replaced bornite and chalcocite afterwards (Figure 5.22, A).

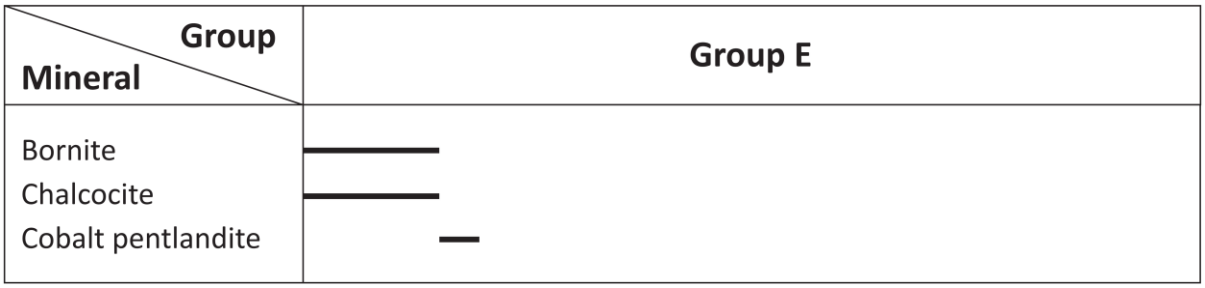

Figure 5.29: Paragenetic scheme for Group E sulphide minerals of transgressive carbonatite.

5.2.6. The paragenetic sequence of Group F.

Group F sulphide mineralisation (Figure 5.30) commenced with the crystallisation of cobalt pentlandite. Chalcopyrite replaced cobalt pentlandite afterwards. The injection a S-bearing liquid produced fractures within the sulphide mineral fabric thereafter. The formation of millerite from the S-bearing liquid, at fractured zones caused the replacement of chalcopyrite (Figure 5.23; Figure 5.24).

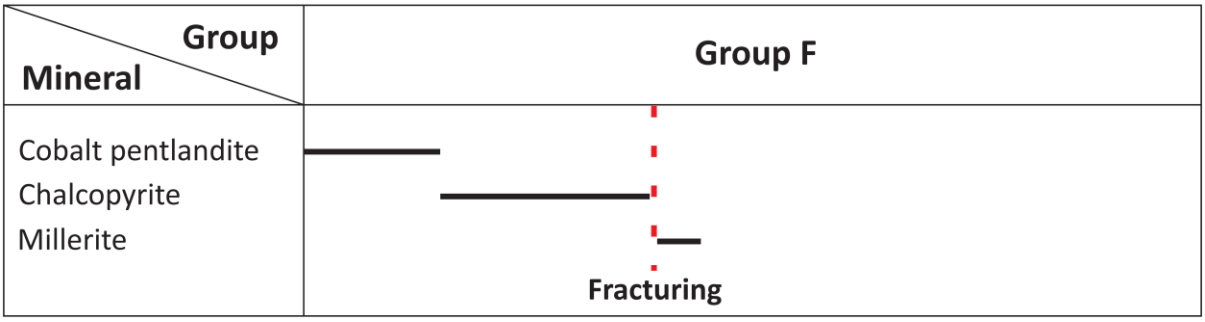

Figure 5.30: Paragenetic scheme for Group F sulphide minerals of transgressive carbonatite.

5.3. The paragenetic sequence of sulphide mineralisation within phoscorite.

Sulphide mineralisation within phoscorite (Figure 5.31) commenced with the crystallisation of cobalt pentlandite (Figure 4.40; Figure 4.43). This was followed by the simultaneous crystallisation of bornite and chalcocite, which either formed symplectic intergrowths (Figure 4.40), or individual fabrics (Figure 4.41; Figure 4.42). The subsequent replacement of bornite and cobalt pentlandite by chalcopyrite (Figure 4.44; Figure 4.45) was followed by the formation of millerite (Figure 4.45). Valleriitisation occurred afterwards (Fig. 4.44).

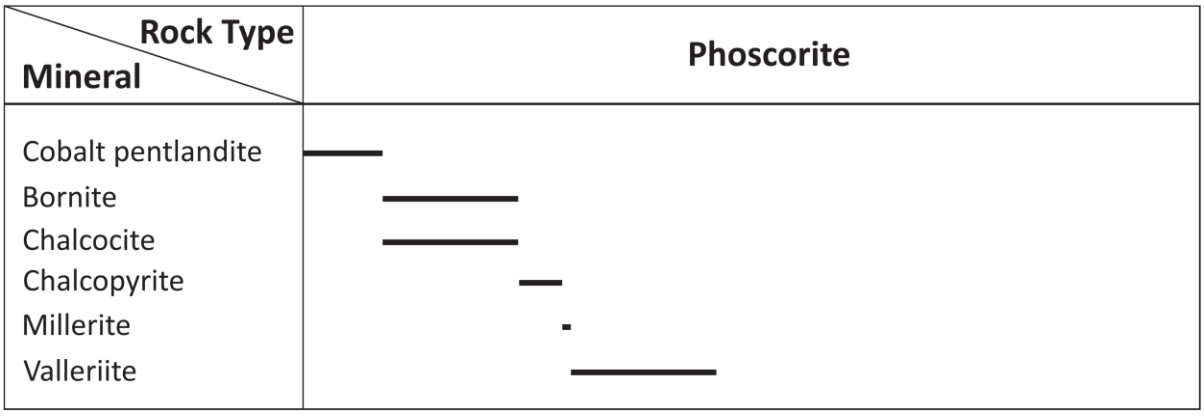

Figure 5.31: Paragenetic scheme for phoscorite of the Loolekop pipe.

5.4. The relationship between banded- and transgressive carbonatite sulphide mineralisation.

Two contradictory hypotheses that describe the emplacement stage(s) of sulphide mineralisation within banded- and transgressive carbonatite were originally presented by Lombaard (1964) and Heinrich (1970). According to Lombaard (1964), the first stage of sulphide mineralisation occurred after the formation of banded carbonatite, but before transgressive carbonatite emplacement, while the second stage occurred after the emplacement of transgressive carbonatite.

Heinrich (1970) argued that sulphide mineralisation occurred after the formation of banded and transgressive carbonatite, during a single stage. The majority of authors, e.g. Hanekom *et al.* (1965) and Mariano (1989), side with the hypothesis proposed by Lombaard (1964), seeing that they described the sulphide mineralisation events as proposed by Lombaard (1964), but not that of Heinrich (1970). No in-depth research has been done to prove which one of these statements are actually correct.

However, this study has shown that certain sulphide mineral assemblages that are present within transgressive carbonatite are also present within banded carbonatite, e.g. Group B (Figure 4.61, A & B) and Group E (Figure 5.22, A & B) assemblages. Thus this dissertation supports the hypothesis proposed by Heinrich (1970) to a certain extent, seeing that a single stage of sulphide mineralisation may very well be the cause of the exact same sulphide mineral assemblages that are present within both carbonatite types. It is proposed in this dissertation that a second stage of sulphide mineralisation occurred afterwards and is confined to magnetite-filled fractured zones that are present within the sulphide mineral fabric of transgressive carbonatite. This is followed by the process of valleriitisation, which represents the third stage of sulphide mineralisation.

5.5. The nature of the S-rich liquid(s) that is responsible for sulphide mineralisation in transgressive carbonatite.

A scenario in which the first sulphide mineralisation event within transgressive carbonatite affected both rock types gives some information about the origin of the sulphide forming

liquid. Firstly, it eliminates the process of autometasomatism proposed by Aldous (1980) as a possibility, because autometasomatism is a localised event and will not explain the disseminated occurrence of the same sulphide mineral assemblages that are present within two carbonatite types of differing ages. In other words, if autometasomatism did occur during the formation of transgressive carbonatite (after banded carbonatite formation), it would not have been able to affect banded carbonatite, seeing that the process would have been confined to the formation of transgressive carbonatite.

It is a possibility that autometasomatism could have occurred during the formation of banded carbonatite and again during the formation of transgressive carbonatite. Thus two stages of autometasomatism. However, this hypothesis still does not explain why a process that took part in different periods and conditions would have been able to generate the exact same sulphide mineral assemblages that are present within two differing carbonatites.

Take the sulphide mineralisation within phoscorite as an example. The differing textural associations and paragenetic scheme for phoscorite (Figure 5.31) can easily be assigned to a separate sulphide mineralisation event when comparing its sulphide mineral assemblages to that of the carbonatites (Figure 5.25; Figure 5.26; Figure 5.27; Figure 5.28; Figure 5.29; Figure 5.30). The same cannot be said when comparing banded and transgressive carbonatite sulphide mineralisation.

Also, a factor which plays a major role in autometasomatism is the partitioning of elemental components into the first formed minerals (e.g. olivine, apatite, magnetite, etc.), which thereafter effects the content of the local residual liquid from which other minerals can form from. Thus, if the sulphide minerals did form during autometasomatism from a residual fluid, after the formation of the first formed minerals, then it would have resulted in more random sulphide mineral combinations seeing that the sulphide minerals would have formed from residual fluids with greatly differing elemental components. However, the study indicates a handful of sulphide mineral assemblages which repeated themselves as observed from samples with different first formed mineral combinations and modal percentages. Thus it would have been highly unlikely for patterns to emerge from the sulphide mineral assemblages. These patterns are indicative of sulphide mineral assemblages which show evidence of elemental component independence from the intruded first formed minerals.

This means that the first sulphide mineralisation event/stage within transgressive carbonatite was either caused by the injection of a S-rich melt or S-rich hydrothermal fluid, which effected both carbonatite types, but probably not phoscorite. However, the reason why certain authors do not believe in a hydrothermal origin for sulphide mineralisation is due to the fact that hydrothermal activity causes the formation of well-defined veins and the alteration of the intruded fabric. The transgressive carbonatites do not contain these features (Aldous, 1980; Aldous, 1986).

This study also shows no clear signs of alteration of the intruded fabric that can be linked to the emplacement of the primary sulphide minerals (e.g. cobalt pentlandite, pyrrhotite, bornite-chalcocite intergrowths, and chalcopyrite), during the first sulphide mineralisation event. No sulphide-induced alteration rims or signs of discolouration of the carbonatite fabric exist where it is bordered by primary sulphide minerals (Figure 4.73; Figure 4.74), despite the great abundance of sulphide mineralisation and the differing formational conditions of the different sulphide mineral assemblages. In addition, the sulphide veins are in fact not well-defined (Figure 4.60; Figure 4.61, A & B). So the evidence from this study is also strongly against a hydrothermal origin. Thus the author of this dissertation agree with Aldous (1980), but disagree with Hanekom (1965) concerning this particular topic. This dissertation proposes that the primary sulphide minerals of the first sulphide mineralisation event formed from a S-rich melt.

Even though this might be true concerning the first sulphide mineralisation event (that formed the primary sulphide minerals) within transgressive carbonatite, it is not necessarily the case for the second sulphide mineralisation event (that formed the secondary sulphide minerals) and the process of valleriitisation. The S-bearing fluid that caused fracturing (Figure 5.25, Figure 5.28, and Figure 5.30) and formed the secondary sulphide minerals (e.g. millerite, pentlandite, mackinawite, and bornite flames and bornite laths) did in fact cause the alteration of chalcopyrite. Also, these sulphide minerals are located adjacent to well-defined magnetite veinlets.

Thus this dissertation proposes that the injection of a late stage (post-magmatic) inherent hydrothermal fluid at the magmatic-hydrothermal transition caused: 1) the formation of fractures (thus hydrothermally-induced) primarily within the first stage sulphide fabrics; 2) the chemical remobilisation of components from first stage sulphide minerals (e.g. from

cobalt pentlandite); 3) the formation of second stage sulphide minerals from the remobilised components (e.g. the formation of pentlandite from remobilised cobalt pentlandite elemental components), and; 4) the formation of magnetite veinlets.

When observing the process of valleriitisation (representing the third sulphide mineralisation event), it does in fact cause discolouration of the carbonatite fabric and also the alteration of all the minerals within transgressive carbonatite (Figure 4.48; Figure 4.49). The same is true for the process of serpentinisation (Figure 4.88; Figure 4.100). As claimed by Mücke (2017), valleriite is a product of secondary hydrothermal conditions (ranging from mesothermal to low katathermal). This means that at least the secondary sulphides and valleriite formation are hydrothermal in origin, and that the Cu-rich veinlets probably formed from a residual hydrothermal solution afterwards. Also, if hydrothermal fluids were responsible for the recrystallisation of carbonate minerals (Figure 4.51), as proposed by Giebel *et al.* (2017), then it may very well have been responsible for the recrystallisation of pyrrhotite as well (Figure 4.27; Figure 4.29).

When comparing the size of the well-defined magnetite veinlets, as well as the size of the well-defined baryte veinlets, to that of the large irregularly-shaped sulphide veins, it is not so hard to assign the formation of first stage sulphide minerals to be the product of magmatic activity. There is clearly a difference in shape and size of these minerals which might be indicative of different formational processes. This strengthens the hypothesis that the primary sulphide minerals are not hydrothermal in origin but probably magmatic in origin.

However, the most compelling evidence of a magmatic origin for the first sulphide mineralisation event is presented by Figure 4.10 and Figure 4.11. The sulphide mineral associations in these figures strongly resemble an interstitial texture. Also, the cobalt pentlandite-pyrrhotite association presented by Figure 4.1 may very well be indicative of remelting via a chalcopyrite-forming melt. According to Wager *et al.* (1960), remelting is a common process which affects magmatically formed minerals.

Areas in which cobalt pentlandite and pyrrhotite occur, and the possible remelting of these two sulphide minerals, would probably represent the central region of the intruded S-rich melt, where temperatures were at their highest. Both Hanekom (1965) and Aldous (1980) agree that cobalt pentandite and pyrrhotite formed at the highest temperatures with respect

to sulphide mineral crystallisation in transgressive carbonatite. This means that the different sulphide mineral assemblages ultimately represents zonation, with pyrrhotite and cobalt pentlandite being more abundant in Group A (which represents the central region of the sulphide-melt intrusion), but less abundant or completely absent in the groups characterised by low temperature sulphide mineral crystallisation (which represents the outer region of the sulphide-melt intrusion). Appendix B, Table B.1 indicates that samples which represent the Group A assemblage also contains the highest average sulphide mineral modal percentages. This strengthens the theory that Group A represents the central region of the intruded S-rich melt, seeing that primary sulphide mineral crystallisation would have been higher in these regions.

A magmatic origin for the first sulphide mineralisation event can also explain the mass replacement of chalcopyrite by bornite (Figure 4.61 (A & B), representing Group B). Kavecsanszki (2012) explains that when a sulphide magma is accompanied by reducing volatiles (such as H_2S) and is introduced into a magnetite-phyric carbonatite magma, an oxidation reaction may occur which will result in the reaction between magnetite (generated from a carbonatite liquid) and the sulphide liquid. This will result in sulphide mineral reaction rims to form at magnetite-sulphide boundaries. Thus it may be interpreted that the S-rich melt was introduced into magnetite-rich regions, and a reaction occurred between the magnetite and the S-rich melt. This caused the alteration of chalcopyrite, which continued over a certain time period.

5.6. The integrated paragenetic scheme of transgressive carbonatite.

Magmatic crystallisation (stage 1; Figure 5.32) commenced with the crystallisation of baddeleyite and uranothorianite (Figure 4.79). This was followed by the crystallisation of first generation apatite, which enclosed baddeleyite and uranothorianite in a poikilitic fashion (Figure 4.76; Figure 4.80). Olivine poikilitically enclosed baddeleyite (Figure 4.91) and first generation apatite afterwards (Figure 4.84; Figure 4.85; Figure 4.87).

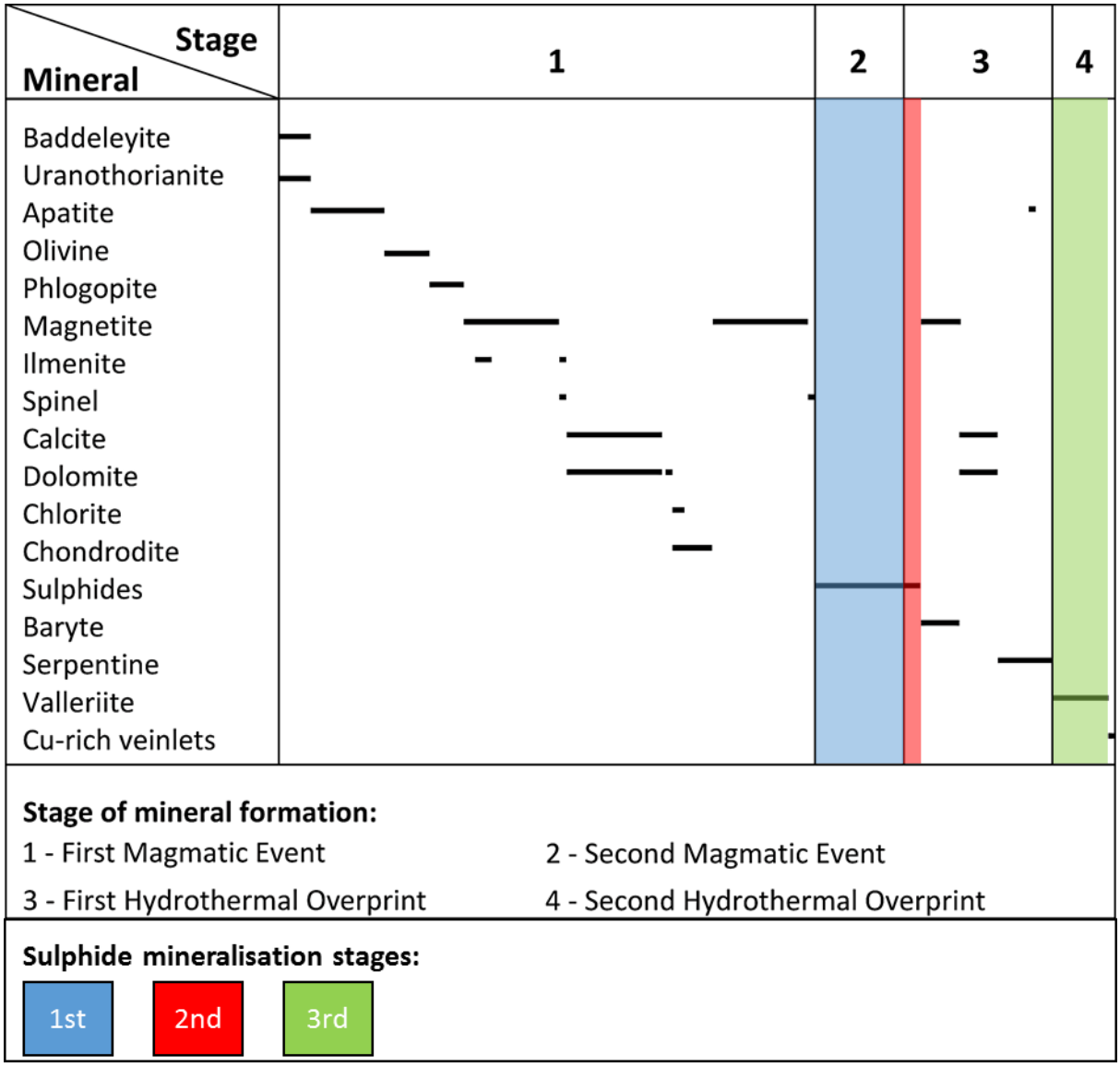

Figure 5.32: Paragenetic scheme for transgressive carbonatite of the Loolekop pipe. Scenario A.

This is the crystallisation sequence of baddeleyite, uranothorianite, apatite, and olivine as observed from visual evidence from this particular research project. However, the crystallisation sequence of these four minerals are different from the paragenetic scheme of Giebel *et al.* (2017). The paragenetic scheme of Giebel *et al.* (2017) illustrates that olivine formed first, followed by baddeleyite and uranothorianite, and apatite thereafter. It is thus concluded that the visual evidence of this study shows the existence of ovelaps for the paragenetic positions of olivine, baddeleyite, uranothorianite, and apatite in the paragenetic scheme of Giebel *et al.* (2017) (Figure 5.33).

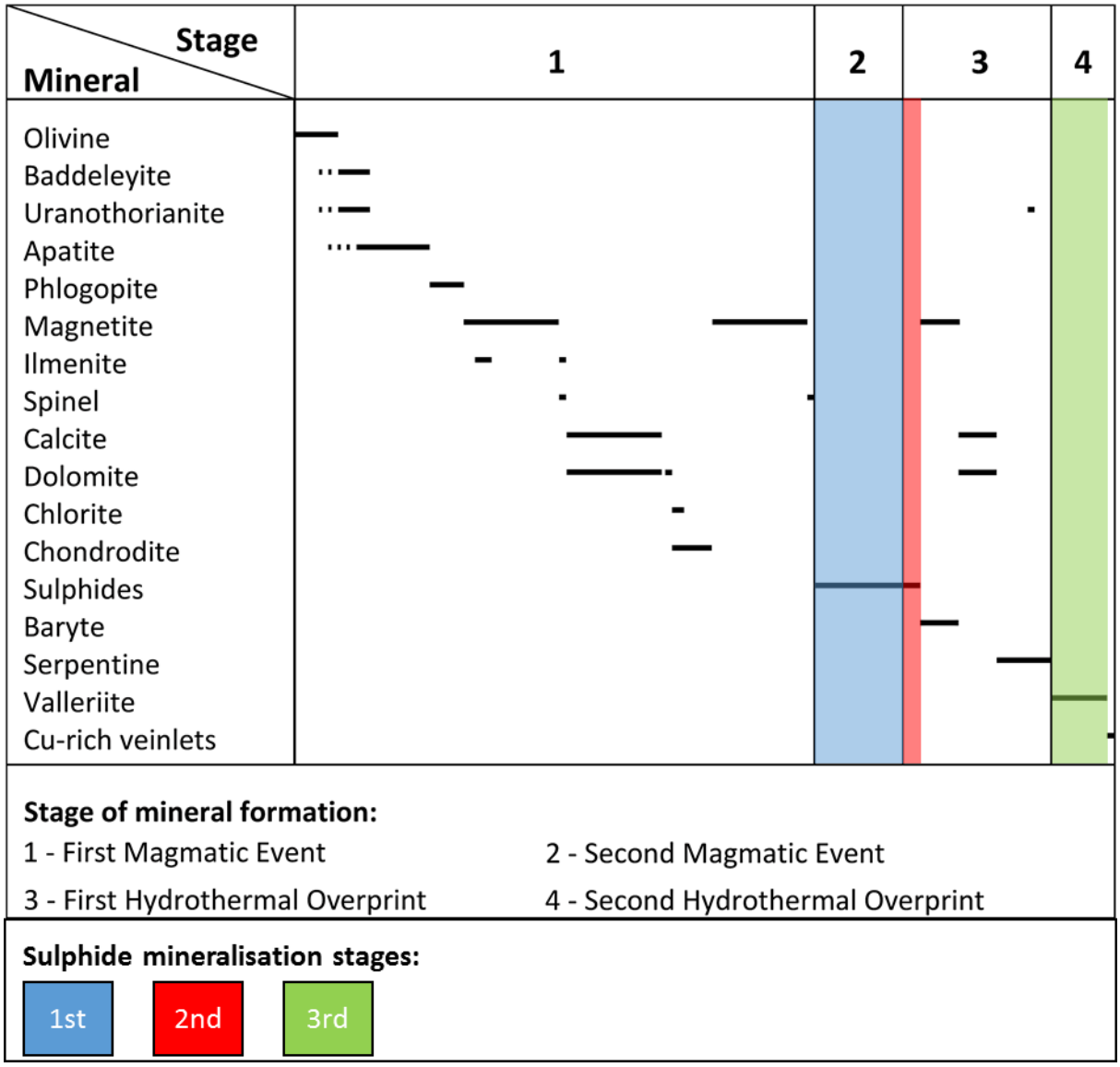

Figure 5.33: Paragenetic scheme for transgressive carbonatite of the Loolekop pipe. Scenario B.

The formation of these minerals was followed by the crystallisation of magmatic phlogopite (Figure 4.107), which replaced olivine and enclosed apatite primarily in a poikilitic fashion (Figure 4.106). Later crystallisation of first generation magnetite resulted in the replacement of above listed minerals (Figure 4.107). First generation ilmenite existed contemporaneously with first generation magnetite (Figure 4.65; Figure 4.66; Figure 4.107). Magnetite exsolved spinel (Figure 4.72) and second generation ilmenite (Figure 4.67) thereafter.

Straining then produced cracks and micro fractures in first generation magnetite, which made the subsequent replacement of magnetite and ilmenite by magmatically formed calcite and dolomite easier (Figure 4.69; Figure 4.70). These carbonate minerals crystallised simultaneously. However, calcite exsolved further dolomite during later cooling (Figure 4.50).

The replacement of primarily olivine (but the carbonate minerals and phlogopite as well) by chondrodite (Figure 4.96), and the chloritisation of olivine (Figure 4.103; Figure 4.107) occurred afterwards. Later crystallisation of second generation magnetite (Figure 4.95; Figure 4.103) was followed by the injection of a sulphide-rich melt (stage 2), which crystallised first stage sulphide minerals that are primarily rich in Cu and Fe (Figure 4.61, A). This concludes the magmatic stages.

Hydrothermal crystallisation (stage 3) commenced by the formation of second stage sulphide minerals (Figure 4.16; Figure 4.18), the formation of third generation magnetite (Figure 5.21; Figure 5.23) and baryte veinlets (Figure 4.109), the recrystallisation of carbonate minerals (Figure 4.51; Figure 4.109), and the formation of acicular apatite needles (Figure 4.88) during serpentinisation (Figure 4.110). Subsequent valleriitisation, which represents the third sulphide mineralisation stage (stage 4; Figure 4.99; Figure 4.102), and the formation of Cu-rich veinlets (Figure 5.3) concludes the hydrothermal stages.

The textural evidence obtained during this research project indicates that both magmatic and hydrothermal processes were operationsal during the evolution of transgressive carbonatite. Guilbert and Park (1986) suggested that as crystallisation abates, crystal fractionation and hydrothermal activity may overlap. This overlap is probably represented by the process of chloritisation (Figure 5.32). It may be interpreted that the fluids which caused the chloritisation process were generated locally and most likely exsolved from interstitial liquid. However, chondrodite formation is still representative of the magmatic process. Guilbert and Park (1986) also explains that olivine may react postdepositionally with melt to form a rim of bronzite. This study suggests that olivine reacted postdepositionally with the melt to form a rim of chondrodite.

6. CONCLUSIONS

6.1. The main mineralogical associations in transgressive carbonatite.

The minerals that showed the strongest associations towards one another (excluding exsolved phases) are:

a) Cobalt pentlandite and pyrrhotite.
b) Pentlandite and mackinawite.
c) Bornite and chalcocite.
d) Ilmenite and magnetite.
e) Olivine and serpentine.
f) Acicular apatite needles and serpentine.

6.2. The main sulphide mineralisation fabrics in transgressive carbonatite.

Depending on the conditions of formation, the S-rich liquid formed the following main fabrics:

a) A chalcopyrite fabric that exsolved either cubanite, bornite, or chalcopyrite.
b) A bornite fabric that exsolved x-bornite.
c) Symplectic intergrowths between chalcocite and bornite.

6.3. The extension of most recent paragenetic schemes.

6.3.1. The paragenetic schemes of this study supports that of Aldous' (1980) by indicating that:

a) Pentlandite group sulphides and pyrrhotite were the first sulphide minerals to form.
b) Second generation bornite, second generation chalcocite, millerite, and valleriite were some of the last sulphide minerals to form.
c) At least two generations of bornite exist.
d) At least two generation of chalcocite exist.

6.3.2. The paragenetic schemes of this study extends that of Aldous' (1980):

a) By providing detailed paragenetic schemes for each sulphide mineral assemblage.

b) By providing a paragenetic scheme for the non-sulphide minerals.
c) By categorising the sulphide minerals via different formational processes.
d) By specifying that cobalt pentlandite (not pentlandite proper) was one of the first sulphide minerals to form.
e) By providing the paragenetic positions of x-bornite, pentlandite proper, mackinawite, and Cu-rich veinlets.
f) By the discovery and indication of the paragenetic positions of shandite and heazlewoodite.
g) By indicating that at least two generations of cobalt pentlandite exist.
h) By indicating that at least two generations of pyrrhotite exist.
i) By indicating that at least two generations of cubanite exist.
j) By indicating that at least two generations of sphalerite exist.

6.3.3. The integrated paragenetic scheme of this study supports that of Giebel's *et al.* (2017) by indicating that:

a) At least four separate stages of mineral formation occurred during transgressive carbonatite formation.
b) Earlier stages of mineral crystallisation are characterised by the formation of olivine, baddeleyite, uranothorianite, apatite, phlogopite, magnetite, ilmenite, spinel, calcite, dolomite, chlorite, and chondrodite.
c) Overlaps exist for the paragenetic positions of olivine, baddeleyite, uranothorianite, and apatite.
d) A separate stage of sulphide formation occurred after the first stage.
e) Later stages of mineral crystallisation are characterised by the formation of recrystallised carbonates, baryte, magnetite, serpentine, and valleriite.
f) At least three generations of magnetite exist.
g) At least two generations of calcite and dolomite exist.

6.3.4. The integrated paragenetic scheme of this study extends that of Giebel's *et al.* (2017):

a) By providing paragenetic schemes for sulphide mineral crystallisation.

b) By indicating that second generation magnetite formed after, and not during chondrodite formation.
c) By suggesting that there is no overlap in the paragenetic position of baryte and recrystallised carbonates, and that the recrystallised carbonates formed after baryte.
d) By suggesting that there is no overlap in the paragenetic position of baryte and serpentine, and that serpentinisation occurred after baryte crystallisation.
e) By indicating that serpentinisation occurred after carbonate mineral recrystallisation, not during carbonate mineral recrystallisation.
f) By indicating the position of an apatite generation that is associated with the serpentinisation process.
g) By indicating that valleriitisation occurred after, and not during serpentinisation.
h) That Cu-rich veinlets are the last phase to form in transgressive carbonatite, not valleriite.

The paragenetic schemes of Aldous (1980) and Giebel *et al.* (2017) are extended by the addition of a paragenetic scheme for sulphide mineralisation in phoscorite.

Studying the major and minor elemental contents of the different generations of certain sulphide minerals emphasised their differences in chemistry, even though trace elemental contents where not studied.

6.4. The categorisation of transgressive carbonatite sulphide minerals into different formational processes.

The Palabora Carbonatite Complex is an example of a magmatic-hydrothermal transitional system. The formation of transgressive carbonatite minerals primarily took place in four stages. Sulphide mineralisation of this rock type took place in three sub-stages and produced different recurring sulphide mineral assemblages. The author believes that the different sulphide mineral assemblages formed at approximately the same time period but under different formational conditions.

The fabrics summarised in 6.2 constitutes first stage sulphide minerals. The first sulphide mineralisation event affected both carbonatite types of the Palabora Carbonatite Complex.

Pentlandite, mackinawite, millerite, second generation sphalerite (with respect to Group A), and bornite from Group D constitutes second stage sulphide minerals. The second sulphide mineralisation event only affected transgressive carbonatites. Valleriite constitutes the third stage of sulphide mineralisation. Valleriitisation affected both carbonatite types. First stage sulphide minerals formed due to magmatic activity, while second and third stage sulphide minerals formed due to hydrothermal activity (post-magmatic).

REFERENCES

Aldous, R.T.H. (1980) *Ore genesis in copper bearing carbonatites: A geochemical fluid inclusion and mineralogical study*, pp.58, 77, 86, 92, 93 and 98. Ph.D. dissertation, Imperial College of Science and Technology (University of London), London.

Aldous, T.H. (1986) *Copper-Rich Fluid Inclusions in Pyroxenes from the Guide Copper Mine, a Satellite Intrusion of the Palabora Igneous Complex, South Africa*. Economic Geology, 81, 143-155.

Anthony, J.W. (1990) *Handbook of Mineralogy (vol.1): Elements, sulphides, sulfosalts*. Mineral Data Publishing, Tucson, Arizona.

Anthony, J.W. (1995) *Handbook of Mineralogy (vol.2): Silica, Silicates*. Mineral Data Publishing, the University of California.

Bernard-Griffiths, J., Peucat, J.J., Fourcade, S., Kienast, J.R. and Ouzegane, K. (1988) *Origin and evolution of 2 Ga old carbonatite complex (Ihouhaouene, Ahaggar, Algeria): Nd and Sr isotopic evidence*. Contribution to Mineralogy and Petrology, 100(3), 339-348.

Bideaux, R.A., Bladh, K.W., Nichols, M.C, and Anthony, J.W. (2000) *Handbook of Mineralogy (vol.4): Arsenates, Phosphates, Vanadates*. Mineral Data Publisher, ISBN 10: 0962209732.

Bouabdellah, M., Hoernle, K., Kchit, A., Duggen, S., Hauff, F., Klügel, A., Lowry, D and Beaudoin, G. (2010) *Petrogenesis of the Eocene Tamazert Continental Carbonatites (Central High Atlas, Morocco): Implications for a Common Source for the Tamazert and Canary Cape Verde Island Carbonatites*. Journal of Petrology, 51(8), 1655-1686.

Brassinnes, S., Balaganskaya, E. and Demaiffe, D. (2005) *Magmatic evolution of the differentiated ultramafic, alkaline and carbonatite intrusion of Vuoriyarvi (Kola Peninsula, Russia). A LA-ICP-MS study of apatite*. Lithos, 85, 76-92.

Cooper, A.F., Paterson, L.A. and Reid, D.L. (1995) *Lithium in carbonatites – consequence of an enriched mantle source?* Mineralogical Magazine, 59(3), 401-408.

Dawson, J.B., and Hinton, R.W. (2003) *Trace-element content and partitioning in calcite, dolomite and apatite in carbonatite, Phalaborwa, South Africa*. Mineralogical Magazine, 67(5), 921-930.

Dawson, J.B., Steele, I.M., Smith, J.V. and Rivers, M.L. (1996) *Minor and trace element chemistry of carbonates, apatites and magnetites in some African carbonatites*. Mineralogical Magazine, 60(400), 415-425.

Eriksson, S.C. (1984) *Age of carbonatite and phoscorite magmatism of the Phalaborwa Complex (South Africa)*. Isotope Geoscience, 2, 291-299.

Eriksson, S.C., Fourie, P.J. and De Jager, D.H. (1985) *A cumulate origin for the minerals in clinopyroxenites of the Phalaborwa Complex*. Transactions of the Geological Society of South Africa, 88, 207-214.

Frank, D. and Edmond, L. (2001) *Feasibility for Identifying Mineralogical and Geochemical Tracers for Vermiculite Ore Deposits*. EPA 910-R-01-002, p. 7.

Fontana, J. (2006) Phoscorite-Carbonatite Pipe Complexes: A promising new platinum group element target in Brazil. *Platinum Metals Review*, 50(3), 130-138.

Forster, I.F. (1958) Paragenetical Ore Mineralogy of the Loolekop-Phalaborwa Carbonatite Complex, Eastern Transvaal. *Transactions of the Geological Society of South Africa*, 61, 359-365.

Giebel R.J., Gauert C.D.K., Marks, M.A.W., Costin, G., and Markl, G. (2017) Multi-stage formation of REE minerals in the Palabora Carbonatite Complex, South Africa. *American Mineralogist*, 102(6), 1218-1233.

Giesekke, E.W. and Harris P.J. (1994) *The role of polyoxyethylene alkyl ethers in apatite flotation at Foskor, Phalaborwa (South Africa)*. Minerals Engineering, 7(11), 1345-1361.

Gittins, J. and Harmer, R.E. (1997) *What is ferrocarbonatite? A revised classification*. Journal of African Earth Sciences, 25(1), 159-168.

Google Earth 7.3. (2018) *Phalaborwa 23°56'34.76"S, 31°8'27.85"E, elevation 437 m.* 3D map, viewed, 15 May 2018. < https://www.google.com/earth/>

Groves, D.I., Bierlein, F.P., Meinert, L.D. and Hitzman, M.W. (2010) *Iron Oxide Copper-Gold (IOCG) Deposit through Earth History: Implications for Origin, Lithospheric Setting, and Distinction from Other Epigenetic Iron Oxide Deposits*. Economic Geology, 105(3), 641-654.

Gupta, C.K., and Krishnamurthy, N. (2005) *Extractive Metallurgy of Rare Earths*, pp. 64, 74, 121. CRC Press, Boca Raton.

Guilbert, M. and Park, C.F. (1986) *The geology of ore deposits,* p. 309, 312 and 354. W.H. Freeman and Company, New York.

Hanekom, H.J., Van Staden, C.M.V.H., Smit, P.J., and Pike, D.R. (1965) *The Geology of the Palabora Igneous Complex*, p. 69, 70 and 71. South African Geological Survey, Pretoria.

Harmer, R.E. and Gittins, J. (1997) *The origin of dolomitic carbonatites: field and experimental constraints*. Journal of African Earth Sciences, 25(1), 5-28.

Harris, D.C. and Nickel, E.H. (1972) *Pentlandite compositions and associations in some mineral deposits*. Canadian Mineralogist, 11(4), 861-878.

Heinrich, E.W. (1970) *The Palabora Carbonatitic Complex – A Unique Copper Deposit*. The Canadian Mineralogist, 10(3), 585-598.

Hornig-Kjarsgaardh, I. (1998) *Rare Earth Elements in Sövitic Carbonatites and their Mineral Phases*. Journal of Petrology, 39(11-12), 2105-2121.

Howie, R.A. (1998*) Handbook of Mineralogy (vol.3): Halides, Hydroxides, Oxides*. In the Mineralogical Magazine, 62(3), 432-433.

Jago, B.C. and Gittins, J. (1991) *The role of fluorine in carbonatite magma evolution*. Letters to Nature, 349, 56-58.

Jones, P.J., Genge, M., and Carmody, L. (2013) Carbonate Melts and Carbonatites. In R.M. Hazen, A.P. Jones and J.A. Baross, Eds., *Carbon in Earth*, p. 289-322. Reviews in Mineralogy & Geochemistry, Mineralogical Society of America, Chantilly, Virginia.

Kavecsanszki, D., Moore, K.R., Rollinson, G.K., Wall, F., and Lusty, P.A.J. (2012) Magma mingling between sulphide-rich and carbonatite magmas to form multi-commodity metal deposit: reconstruction using QEMSCAN analysis. In E. Jonsson, Eds., *Conference Proceedings*. 12th Biennial SGA Meeting: Mineral deposit research for a high tech world, 3, p. 1024 – 1027. Uppsala, Sweden.

Kuschke, O.H. and Tonking M.J.H. (1971) *Geology and Mining operations at Palabora Mining Company Limited, Phalaborwa, N-E Transvaal*. Journal of the South African Institute of Mining and Metallurgy, 72(1), 12-23.

Korobeinikov, A.N., Mitrofanov, F.P., Gehör, S., Laajoki, K., Pavlov, V.P. and Mamontov, V.P. (1998) *Geology and Copper Sulphide Mineralisation of the Salmagorskii Ring Igneous Complex, Kola Peninsula, NW Russia*. Journal of Petrology, 39(11-12), 2033-2041.

Le Bas, M.J. (1981) *Carbonatite magmas*. Mineralogical Magazine, 44, 133-140.

Le Bas, M.J. (2008) *Fenites associated with carbonatites*. The Canadian Mineralogist, 46, 915-932.

Lee, M.J., Lee, J.I. and Kim, Y. (2003) *Occurrence and Petrogenesis of Phoscorite-Carbonatite Complexes in the Kola Alkaline Province, Arctic*. Ocean and Polar Research, 25(1), 119-128.

Lee, W.J., Fanelli, M.F., Cava, N. and Wyllie, P.J. (2000) *Calciocarbonatite and magnesiocarbonatite rocks and magmas represented in the system CaO-MgO-CO_2-H_2O at 0.2 GPa*. Mineralogy and Petrology, 68(4), 225-256.

Lombaard, A.F., Ward-Able, N.M. and Bruce, R.W. (1964) The exploration and main geological features of the copper deposit in carbonatite at Loolekop, Palabora Complex. In S.H. Haughton, Eds., *The Geology of Some Ore Deposits in Southern Africa*, 2, p. 315-337. Geological Society of South Africa, Johannesburg.

Mariano, A.N. (1989) Nature of economic mineralisation in carbonatites and related rocks. In K. Bell, Ed., Carbonatites: Genesis and evolution, p. 149-176. Unwin Hyman, London.

Mitchell, R.H. (2005) *Carbonatites and Carbonatites and Carbonatites*. The Canadian Mineralogist, 43(6), 2049-2068.

Mücke, A. (2017) *Review on Mackinawite and Valleriite: Fromulae, Localities, Associations and Intergrowths of the Minerals, Mode of Formation and Optical Features in Reflected Light*. Journal of Earth Science & Climatic Change, 8(11), 1-18. doi:10.4172/2157-7617.1000419

Muiambo, H.F., Focke, W.W., Atanasova, M., Van Der Westhuizen, I. and Tiedt, L.R. (2010) *Thermal properties of sodium-exchanged palabora vermiculite*. Applied Clay Science, 50(1), 51-57.

Palabora Mining Company Limited Mine Geological and Mineralogical Staff (1976) *The Geology and the Economic Deposits of Copper, Iron, and Vermiculite in the Palabora Igneous Complex: A Brief Review*. Economic Geology, 71(1), 177-192.

Palabora Mining Company (2017) Pala Connector. PMC Newsletter, October, November & December 2017 Edition, 1-36.

Pell, J. (1994) *Carbonatites, nepheline syenites, kimberlites and related rocks in British Columbia*. Ministry of Energy, Mines and Petroluem, Bulletin, ISSN 0226-7497; 88, p. 1.

PMC staff, (2018) Personal communication, 3D illustrations of the open pit mine, Palabora Mining Company (PMC).

Reischmann, T. (1995) *Precise U/Pb age determination with baddeleyite (ZrO_2), a case study from the Phalaborwa Igneous Complex, South Africa*. South African Journal of Geology, 98(1), 1-4.

Reischmann, T., Brügmann, G.E., Jochum, K.P. and Todt, W.A. (1995) *Trace element and isotopic composition of baddeleyite*. Mineralogy and Petrology, 53(1), 155-164.

Richardson, D.G., and Birkett, T.C. (1996) Carbonatite-associated deposits. In O.R. Eckstrand, W.D. Sinclair and R.I. Thorpe, Eds., *Geology of Canadian Mineral Deposit Types*, p. 541-558. Geological Survey of Canada, Geology of Canada, Ottawa, Canada (also Geological Society of America, The Geology of North America, v. P-1).

Sawkins, F.J. (1990) *Metal Deposits in Relation to Plate Tectonics*, 2nd edn, pp. 258 and 261. Springer-Verlag, Berlin.

Schot, E.H., Ottemann, J. and Omenetto, P. (1972) *Some new observations on mackinawite and valleriite*. Rendiconti della Società Italiana di Mineralogia e Petrologia, 28, 241-295.

Shankar, R., Vijayagopal, B. and Kumar, A. (2014) *Precise Pb-Pb baddeleyite ages of 1765 Ma for a Singhbhum 'newer dolerite' dyke swarm*. Current Science, 106(9), 1306-1310.

Sharygin, V.V., Zhitova, L.M., and Nigmatulina, E.N. (2011) *Fairchildite $K_2Ca(CO_3)_2$ in phoscorite from Phalaborwa, South Africa: the first occurrence in alkaline carbonatite complexes*. Russian Geology and Geophysics, 52, 208-219.

Suwa, K., Oana, S., Wada, H. and Osaki, S. (1975) *Isotope geochemistry and petrology of African carbonatites*. Physics and Chemistry of the Earth, 9, 735-745.

Vail, J.R. (1989) *Ring complexes and related rocks in Africa*. Journal of African Earth Sciences, 8(1), 19-40.

Verplanck, P.L., Van Gosen, B.S., Seal, R.R. and McCafferty, A.E. (2014) A deposit model for carbonatite and peralkaline intrusion-related rare earth element deposits: U.S. Geological Survey Scientific Investigations Report 2010-5070-J, 58, http://dx.doi.org/10.3133/sir20105070J

Verwoerd, W.J. (1986) *Mineral deposits associated with carbonatites and alkaline rocks*. Mineral Deposits of Southern Africa, 1 & 2, 2173-2191.

Verwoerd, W.J. (1993) *Update on carbonatites of South Africa and Namibia*. South African Journal of Geology, 96(3), 75-95.

Verwoerd, W.J., and Du Toit, M.C. (2006) The Phalaborwa and Schiel Complexes. In M.R. Johnson, C.R. Anhaeusser and R.J. Thomas, Eds., *The Geology of South Africa*, p. 291-299. Council for Geoscience, Pretoria.

Vielreicher, N.M., Groves, D.I. and Vielreicher, R.M. (2000) The Phalaborwa (Palabora) Deposit and its Potential connection to Iron-Oxide Copper-Gold Deposits of Olympic Dam Type. In T.M. Porter, Eds., *Hydrothermal Iron Oxide Copper-Gold & Related Deposits: A Global Perspective*, 1, p. 321-329. PGC Publishing, Adelaide.

Wager, L.R, Brown, G.M. and Wadsworth, W.J. (1960) *Types of Igneous Cumulates*. Journal of Petrology, 1(1), 73-85.

Wilson, M.G.C. (1998) Copper. In M.G.C. Wilson and C.R. Anhaeusser, Eds., The mineral resources of South Africa, p. 209-217. Council for Geoscience, Pretoria.

Woolley, A.R. (1989) The spatial and temporal distribution of carbonatites. In K. Bell, Ed., *Carbonatites: Genesis and evolution*, p. 15-34. Unwin Hyman, London.

Woolley, A.R. and Kempe, D.R.C. (1989) Carbonatites: Nomenclature, average chemical compositions, and element distribution. In K. Bell, Ed., *Carbonatites: Genesis and evolution*, p. 1-13. Unwin Hyman, London.

Woolley, A.R. and Kjarsgaard, B.A. (2008) *Paragenetic types of carbonatite as indicated by the diversity and relative abundances of associated silicate rocks: Evidence from a global database*. The Canadian Mineralogist, 46(4), 741-752.

Wu, F.-Y., Yang, Y.-H., Xie., L.-W., Yang, J.-H., and Xu, P. (2006) *Hf isotopic compositions of the standard zircons and baddeleyites used in U-Pb geochronology*. Chemical Geology, 234 (1-2), 105-126.

Wu, F.-Y., Yang, Y.-H., Li, Q.-L., Mitchell, R.H., Dawson, J.B., Brandl, G. and Yuhara, M. (2011) *In situ determination of U-Pb ages and Sr-Nd-Hf isotopic constraints on the petrogenesis of the Phalaborwa carbonatite Complex, South Africa*. Lithos, 127(1-2), 309-322.

Yuhara, M., Kohno, M., Kagami, H., Hiroi, Y. and Tsuchiya, N. (2003) *Geochemistry of syenite of the Phalaborwa Carbonatite Complex, South Africa*. Polar Geoscience, 16, 176-195.

Yuhara, M., Hirahara, Y., Nishi, N. and Kagami, H. (2005) *Rb-Sr, Sm-Nd ages of the Phalaborwa Carbonatite Complex, South Africa*. Polar Geoscience, 18, 101-113.

APPENDIX A

DRILL CORE DATA.

Table A.1: Additional drill core data indicating the dip of the drill hole and the elevation of the samples (TCB = Transgressive carbonatites; BCB = Banded carbonatites; FOS = Phoscorite; Dol = Dolerite).

Nr.	Sample code	Core_ID	Dip (degrees)	Sample Elevation (m)	Depth (m)		Rock type
					From	To	
1	MT	MET01_UFS01	41.26	-864.31	7.86	8.02	FOS / TCB (transition)
2	MT	MET01_UFS02	41.26	-866.34	10.96	11.10	BCB
3	MT	MET01_UFS03	41.26	-869.84	16.23	16.43	TCB
4	MT	MET01_UFS04	41.26	-871.86	19.30	19.49	FOS / TCB (transition)
5	MT	MET01_UFS05	41.26	-876.21	25.88	26.10	TCB
6	MT	MET01_UFS06	41.26	-881.62	34.12	34.27	TCB
7	MT	MET01_UFS07	41.26	-884.76	38.90	39.00	TCB
8	MT	MET01_UFS08	41.26	-886.69	41.83	41.93	TCB
9	MT	MET01_UFS09	41.26	-890.86	48.15	48.27	TCB
10	MT	MET01_UFS10	41.26	-894.67	53.93	54.04	TCB
11	MT	MET01_UFS11	41.26	-898.93	60.37	60.52	TCB
12	MT	MET01_UFS12	41.26	-901.46	64.23	64.34	FOS / BCB (transition)
13	MT	MET01_UFS13	41.26	-907.46	73.28	73.46	TCB
14	MT	MET01_UFS14	41.26	-910.61	78.09	78.22	TCB
15	MT	MET01_UFS15	41.26	-917.46	88.47	88.60	TCB
16	MT	MET01_UFS16	41.26	-921.75	94.98	95.10	TCB
17	MT	MET01_UFS17	41.26	-924.18	98.64	98.81	BCB
18	MT	MET01_UFS18	41.26	-928.73	105.59	105.68	TCB
19	MT	MET01_UFS19	41.26	-934.32	114.08	114.13	TCB
20	MT	MET01_UFS20	41.26	-934.48	114.31	114.38	TCB
21	MT	MET01_UFS21	41.26	-940.40	123.25	123.39	TCB
22	MT	MET01_UFS22	41.26	-945.54	131.05	131.18	TCB
23	MT	MET01_UFS23	41.26	-947.47	133.96	134.12	TCB

Table A.1: (continued) additional drill hole data indicating the dip of the drill hole and the elevation of the samples (TCB = Transgressive carbonatites; BCB = Banded carbonatites; FOS = Phoscorite; Dol = Dolerite).

Nr.	Sample code	Core_ID	Dip (degrees)	Sample Elevation (m)	Depth (m)		Rock type
					From	To	
24	MT	MET01_UFS24	41.26	-951.14	139.56	139.65	TCB
25	MT	MET01_UFS25	41.26	-952.93	142.26	142.40	FOS
26	MT	MET01_UFS26	41.26	-957.75	149.57	149.71	TCB
27	MT	MET01_UFS27	41.26	-958.53	150.75	150.88	TCB
28	MT	MET01_UFS28	41.26	-961.92	155.91	156.00	TCB
29	MT	MET01_UFS29	41.26	-967.53	164.40	164.52	TCB
30	MT	MET01_UFS30	41.26	-970.93	169.54	169.70	TCB
31	MT	MET01_UFS31	41.26	-975.86	177.06	177.14	TCB
32	MT	MET01_UFS32	41.26	-981.06	184.94	185.03	TCB
33	MT	MET01_UFS33	41.26	-981.77	186.00	186.10	TCB
34	MT	MET01_UFS34	41.26	-985.63	191.87	191.95	TCB
35	MT	MET01_UFS35	41.26	-989.29	197.40	197.52	TCB
36	MT	MET01_UFS36	41.26	-993.04	203.08	203.22	TCB
37	MT	MET01_UFS37	41.26	-996.93	209.00	209.10	TCB
38	MT	MET01_UFS38	41.26	-1004.10	219.85	219.97	TCB
39	MT	MET01_UFS39	41.26	-1007.02	224.30	224.40	TCB
40	MT	MET01_UFS40	41.26	-1011.53	231.14	231.24	TCB
41	MT	MET01_UFS41	41.26	-1016.79	239.10	239.23	DOL
42	MT	MET01_UFS42	41.26	-1024.37	250.58	250.72	DOL
43	MT	MET01_UFS43	41.26	-1033.46	264.37	264.50	DOL
44	MT	MET01_UFS44	41.26	-1039.62	273.74	273.83	TCB
45	MT	MET01_UFS45	41.26	-1042.78	278.53	278.60	TCB

Table A.1: (continued) additional drill hole data indicating the dip of the drill hole and the elevation of the samples (TCB = Transgressive carbonatites; BCB = Banded carbonatites; FOS = Phoscorite; Dol = Dolerite).

Nr.	Sample code	Core_ID	Dip (degrees)	Sample Elevation (m)	Depth (m)		Rock type
					From	To	
46	MT	MET01_UFS46	41.26	-1046.65	284.34	284.52	TCB
47	MT	MET01_UFS47	41.26	-1051.26	291.36	291.50	TCB
48	MT	MET01_UFS48	41.26	-1055.52	297.82	297.94	TCB
49	MT	MET01_UFS49	41.26	-1058.78	302.77	302.89	TCB
50	MT	MET01_UFS50	41.26	-1069.94	319.69	319.81	BCB
51	MT	MET01_UFS51	41.26	-1077.86	331.72	331.81	TCB
52	MT	MET01_UFS52	41.26	-1082.73	339.10	339.21	TCB
53	MT	MET01_UFS53	41.26	-1085.35	343.07	343.18	TCB
54	MT	MET01_UFS54	41.26	-1098.59	363.12	363.27	DOL
55	MT	MET01_UFS55	41.26	-1113.72	386.10	386.18	TCB
56	MT	MET01_UFS56	41.26	-1118.00	392.59	392.66	FOS
57	MT	MET01_UFS57	41.26	-1118.86	393.90	393.96	TCB
58	MT	MET01_UFS58	41.26	-1126.05	404.80	404.88	TCB
59	MT	MET01_UFS59	41.26	-1128.51	408.52	408.60	TCB
60	MT	MET01_UFS60	41.26	-1133.52	416.13	416.20	TCB
61	MT	MET01_UFS61	41.26	-1137.03	421.44	421.53	DOL
62	MT	MET01_UFS62	41.26	-1138.96	424.34	424.49	TCB
63	MT	MET01_UFS63	41.26	-1146.80	436.25	436.36	TCB
64	MT	MET01_UFS64	41.26	-1152.07	444.23	444.35	TCB
65	MT	MET01_UFS65	41.26	-1156.53	450.98	451.13	FOS
66	MT	MET01_UFS66	41.26	-1156.93	451.61	451.71	TCB
67	MT	MET01_UFS67	41.26	-1161.66	458.78	458.88	TCB
68	MT	MET01_UFS68	41.26	-1162.75	460.43	460.53	TCB

Table A.1: (continued) additional drill hole data indicating the dip of the drill hole and the elevation of the samples (TCB = Transgressive carbonatites; BCB = Banded carbonatites; FOS = Phoscorite; Dol = Dolerite).

Nr.	Sample code	Core_ID	Dip (degrees)	Sample Elevation (m)	Depth (m)		Rock type
					From	To	
69	MT	MET01_UFS69	41.26	-1167.89	468.23	468.33	TCB
70	MT	MET01_UFS70	41.26	-1172.07	474.57	474.67	TCB
71	MT	MET01_UFS71	41.26	-1178.19	483.87	483.94	TCB
72	MT	MET01_UFS72	41.26	-1181.82	489.36	489.46	TCB
73	MT	MET01_UFS73	41.26	-1184.99	494.15	494.26	TCB

APPENDIX B

ESTIMATED SULPHIDE MINERAL MODAL COMPOSITIONS FOR SELECTED THIN SECTIONS.

Table B.1: Estimated Sulphide Mineral Modal Compositions for Selected Thin Sections.

Sample	Rock Type	Ccp	Bn	Cub	Po	Co-pn	Pn	Cct	Mk	Sp	Mlr	X-bn	Cv	Val	Gn	Hzl	Sh	Total
MT-2	BCB	<1% (5th)	<1% (2nd)	-	-	<1% (3rd)	-	<1% (1st)	-	-	-	-	-	<1% (4th)	-	-	-	<1%
MT-3	TCB	<1% (3rd)	-	40%	<1% (2nd)	<1% (4th)	-	-	<1% (6th)	-	-	-	-	<1% (5th)	-	-	-	41%
MT-5	TCB	4%	-	7%	6%	<1% (4th)	-	-	<1% (5th)	<1% (7th)	-	-	-	<1% (6th)	-	-	-	18%
MT-7	TCB	12%	-	14%	<1% (4th)	1%	-	-	<1% (5th)	<1% (6th)	-	-	-	<1% (7th)	-	-	-	28%
MT-8	TCB	<1% (1st)	-	-	-	-	-	-	-	-	-	-	-	<1% (2nd)	-	-	-	1%
MT-11	TCB	-	<1% (2nd)	-	-	<1% (5th)	-	<1% (3rd)	-	<1% (4th)	-	1%	-	-	-	-	-	2%
MT-13	TCB	-	1%	-	-	-	-	<1% (2nd)	-	-	-	<1% (3rd)	-	-	-	-	-	2%
MT-14	TCB	22%	-	-	-	<1% (5th)	-	-	<1% (4th)	<1% (3rd)	-	-	-	<1% (2nd)	-	-	-	23%
MT-15	TCB	-	4%	-	-	<1% (5th)	-	3%	-	<1% (4th)	-	18%	-	-	-	-	<1% (6th)	25%
MT-16	TCB	2%	<1% (2nd)	-	-	-	-	<1% (3rd)	-	-	-	<1% (5th)	<1% (4th)	-	-	-	-	3%
MT-19	TCB	10%	50%	-	-	<1% (3rd)	-	-	-	-	-	-	-	-	<1% (4th)	-	-	61%
MT-20	TCB	13%	-	-	-	<1% (3rd)	-	-	-	-	<1% (4th)	-	-	1%	-	-	-	14%
MT-23	TCB	53%	-	1%	-	<1% (5th)	<1% (6th)	-	<1% (7th)	<1% (3rd)	-	-	-	<1% (4th)	-	-	-	55%

Table B.1: (continued) Estimated Sulphide Mineral Modal Compositions for Selected Thin Sections.

Sample	Rock Type	Ccp	Bn	Cub	Po	Co-pn	Pn	Cct	Mk	Sp	Mlr	X-bn	Cv	Val	Gn	Hzl	Sh	Total
MT-26	TCB	48%	-	1%	<1% (5th)	<1% (3rd)	<1% (5th)	-	<1% (7th)	<1% (8th)	-	-	-	<1% (6th)	-	-	-	50%
MT-27	TCB	<1% (2nd)	-	-	-	-	-	-	-	-	-	-	-	<1% (1st)	-	-	-	1%
MT-28	TCB	<1% (2nd)	-	-	-	-	-	-	-	-	-	-	-	<1% (1st)	-	-	-	1%
MT-32	TCB	-	-	-	-	-	-	-	-	-	-	-	-	<1% (1st)	-	-	-	<1%
MT-35	TCB	4%	-	5%	2%	<1% (5th)	-	-	<1% (6th)	<1% (7th)	-	-	-	<1% (4th)	-	-	-	11%
MT-38	TCB	5%	-	9%	<1% (5th)	<1% (4th)	<1% (8th)	-	<1% (6th)	<1% (7th)	-	-	-	<1% (3rd)	-	-	-	14%
MT-40	TCB	<1% (1st)	<1% (2nd)	-	-	-	-	<1% (3rd)	-	-	-	-	-	<1% (4th)	-	-	-	1%
MT-44	TCB	20%	<1% (3rd)	-	-	-	-	<1% (6th)	-	<1% (4th)	<1% (5th)	-	-	2%	-	-	-	22%
MT-48	TCB	6%	-	-	-	-	-	-	-	-	<1% (3rd)	-	-	<1% (2nd)	-	-	-	15%
MT-49	TCB	10%	<1% (1st)	-	-	<1% (2nd)	-	-	-	<1% (3rd)	-	-	-	-	-	-	-	11%
MT-52	BCB	<1% (1st)	<1% (2nd)	-	<1% (4th)	<1% (8th)	-	<1% (6th)	-	-	-	<1% (3rd)	<1% (5th)	<1% (7th)	<1% (8th)	-	-	2%
MT-53	TCB	<1% (4th)	<1% (1st)	-	-	-	-	<1% (2nd)	-	-	-	<1% (6th)	<1% (5th)	<1% (3rd)	-	-	-	1%
MT-55	TCB	<1% (5th)	<1% (3rd)	-	-	<1% (4th)	-	<1% (2nd)	-	-	-	-	-	4%	-	-	-	5%

Table B.1: (continued) Estimated Sulphide Mineral Modal Compositions for Selected Thin Sections.

Sample	Rock Type	Ccp	Bn	Cub	Po	Co-pn	Pn	Cct	Mk	Sp	Mlr	X-bn	Cv	Val	Gn	Hzl	Sh	Total
MT-56	FOS	<1% (4th)	<1% (2nd)	-	-	-	-	<1% (3rd)	-	-	<1% (6th)	-	<1% (5th)	2%	-	-	-	3%
MT-58	TCB	5%	<1% (3rd)	-	-	<1% (2nd)	-	<1% (8th)	-	<1% (7th)	-	<1% (6th)	-	<1% (4th)	-	<1% (5th)	-	7%
MT-60	TCB	2%	<1% (6th)	<1% (5th)	<1% (3rd)	<1% (1st)	-	-	-	-	<1% (4th)	-	-	<1% (2nd)	-	-	-	3%
MT-65	FOS	-	-	-	-	<1% (3rd)	-	<1% (1st)	-	-	-	-	-	<1% (2nd)	-	-	-	<1%
MT-71	TCB	<1% (1st)	<1% (3rd)	-	-	-	-	<1% (4th)	-	-	-	<1% (2nd)	-	<1% (5th)	-	-	-	1%
Rank		1st	3rd	2nd	6th	5th	12th	8th	9th **(5.75)**	10th **(5.25)**	11th	7th	13th	4th	14th	15th	16th	

APPENDIX C

DATA FROM SEM-EDS ANALYSES.

Within the SEM location column of the table, the number in front of the point refers to the marked location of interest. The number after the point indicates the grain on which the point analyses was performed. For example, if two locations of two different point analyses sets are represented by the same number in front of the point, but a different number after the point, then a point analyses was conducted on two different grains located in the same approximate area (e.g. 10.1. and 10.2). If the numbers before the point differ, then point analyses were conducted on two different locations on the thin section (e.g. 9.2 and 10.3). If two locations are represented by the same numbers before and after the point, then point analyses were conducted twice on the same grain (e.g. 10.1 and 10.1).

Each individual row/set of weight percentages represents the point analysis that is closest to the average weight percentage of 15 point analyses that were obtained at an acquisition time of 50 seconds per point. Primarily, these 15 points are more or less equally distributed within a 2 µm to 4 µm radius on the analysed grain. Instead of running point analyses on numerous thin sections, the analysis is more association specific. Thus numerous point analyses are done per thin section.

Table C.1: SEM-EDS Analyses of Galena, Covelline, Heazlewoodite and Shandite.

Mineral				**Weight percentages**		
Galena	**Sample**	**Rock Type**	**SEM Location**	**Pb**	**S**	
	MT-19	TCB	1.1 (replacing chalcopyrite and bornite)	86.06	13.94	
	MT-19	TCB	5.1 (replacing bornite, chalcopyrite and calcite)	86.94	13.06	
	MT-19	TCB	5.2 (replacing bornite, chalcopyrite and calcite)	86.76	13.24	
Covelline	**Sample**	**Rock Type**	**SEM Location**	**Cu**	**Fe**	**S**
	MT-16	TCB	7.1 (replacing chalcocite)	66.23	2.25	31.50
	MT-16	TCB	7.2 (replacing chalcocite)	66.03	1.77	32.20
Heazlewoodite	**Sample**	**Rock Type**	**SEM Location**	**Ni**	**Fe**	**S**
	MT-58	TCB	1.1 (replacing chalcopyrite)	71.04	1.68	27.28
	MT-58	TCB	1.2 (replacing chalcopyrite)	70.99	2.10	26.91
	MT-58	TCB	4.1 (replacing chalcopyrite)	71.78	1.99	26.23
Shandite	**Sample**	**Rock Type**	**SEM Location**	**Pb**	**Ni**	**S**
	MT-15	TCB	15.1 (associated with large chalcocite veins)	67.23	23.63	9.15
	MT-15	TCB	15.2 (associated with large chalcocite veins)	67.85	23.73	8.42
	MT-15	TCB	15.3 (associated with large chalcocite veins)	67.51	23.87	8.62
Mackinawite	**Sample**	**Rock Type**	**SEM Location**	**Fe**	**Ni**	**S**
	MT-5	TCB	8.1 (replacing chalcopyrite)	59.03	4.13	36.84
	MT-23	TCB	4.1 (replacing chalcopyrite)	58.94	4.18	36.88
	MT-38	TCB	10.1 (replacing pentlandite)	57.36	5.27	37.37
	MT-38	TCB	10.2 (replacing pentlandite)	57.80	4.87	37.33

Table C.2: SEM-EDS Analyses of Sphalerite.

Sphalerite			Weight percentages		
Sample	**Rock Type**	**SEM Location**	**Zn**	**Fe**	**S**
MT-5	TCB	1.1 (very small anhedral grain; replacing chalcopyrite)	57.78	8.56	33.66
		1.2 (replacing chalcopyrite)	57.71	8.97	33.33
		1.2 (replacing chalcopyrite)	57.61	8.93	33.46
MT-11	TCB	8.1 (larger subhedral to euhedral grain; replacing bornite and x-bornite)	63.31	4.76	31.93
MT-14	TCB	6.1 (smaller anhedral grains; replacing chalcopyrite)	58.26	8.02	33.73
MT-15	TCB	17.1 (larger subhedral to euhdral grain; replacing bornite, x-bornite and chalcocite)	66.34	1.71	31.94
MT-23	TCB	6.1 (with chalcopyrite inclusions; replacing chalcopyrite)	62.41	5.40	32.20
MT-38	TCB	5.1 (larger anhedral grain replacing cubanite; cubanite-cobalt pentlandite boundary)	57.88	9.45	32.67
		5.1 (larger anhedral grain replacing cubanite; cubanite-cobalt pentlandite boundary)	58.01	9.15	32.84
		5.2 (smaller anhedral grain replacing cubanite)	55.15	11.78	33.06
		5.2 (smaller anhedral grain replacing cubanite)	55.80	11.21	32.98
		5.3 (smaller anhedral grain replacing cubanite)	55.82	11.34	32.84
MT-44	TCB	3.1 (larger subhedral to euhedral grain enclosed by bornite flames; no inclusions)	65.46	2.10	32.43
		3.1 (larger subhedral to euhedral grain enclosed by bornite flames; no inclusions)	65.10	2.39	32.52
		3.2 (a bit smaller subhedral to euhedral grain enclosed by bornite flames; no inclusions)	63.08	3.50	33.43
		3.2 (a bit smaller subhedral grain enclosed by bornite flames; no inclusions)	61.83	4.09	34.08
		4.1 (larger euhedral grain enclosed by bornite flames; no inclusions)	65.36	2.05	32.60
MT-58	TCB	1.1 (medium sised subhedral grain; replacing chalcopyrite)	66.13	1.91	31.96

Table C.3: SEM-EDS Analyses of X-bornite.

X-bornite			Weight percentages		
Sample	**Rock Type**	**SEM Location**	**Cu**	**Fe**	**S**
MT-11	TCB	5.1	46.35	22.88	30.78
		5.2	46.45	22.64	30.91
		6.1	46.99	22.29	30.71
MT-13	TCB	7.1	46.25	22.94	30.81
		7.2	46.19	22.81	31.00
		7.3	46.22	22.46	31.32
		9.1	46.52	22.43	31.05
MT-15	TCB	15.1	49.58	21.36	29.06
		17.1	49.76	21.08	29.16
MT-52	BCB	2.1	46.59	22.39	31.02
		2.1	46.28	22.66	31.07
MT-58	TCB	5.1 (big lath)	48.84	21.36	29.80
		5.1 (big lath)	47.93	21.99	30.08
MT-71	TCB	10.1 (big flame)	46.07	22.70	31.23
		10.1 (big flame)	46.36	22.71	30.93

Table C.4: SEM-EDS Analyses of Pentlandite.

Pentlandite			Weight percentages			
Sample	**Rock Type**	**SEM Location**	**Co**	**Fe**	**Ni**	**S**
MT-23	TCB	2.1 (being replaced by mackinawite; replacing chalcopyrite)	0	35.66	31.40	32.94
		2.1 (being replaced by mackinawite; replacing chalcopyrite)	0	34.62	32.57	32.81
		9.1 (being replaced by mackinawite; replacing chalcopyrite)	0	32.88	34.05	33.07
MT-26	TCB	3.1 (replacing chalcopyrite)	3.59	31.48	33.00	31.93
		6.1 (replacing cubanite)	5.18	30.93	31.61	32.28
MT-38	TCB	6.1 (replacing chalcopyrite)	0	36.28	29.53	34.19
		6.1 (being replaced by mackinawite; replacing chalcopyrite)	0	36.66	28.45	34.89
		10.1 (being replaced by mackinawite; replacing chalcopyrite)	0	36.14	29.02	34.84
		10.1 (being replaced by mackinawite; replacing chalcopyrite)	0	36.04	28.96	35.00

Table C.5: SEM-EDS Analyses of Chalcopyrite.

Chalcopyrite			Weight percentages		
Sample	**Rock Type**	**SEM Location**	**Cu**	**Fe**	**S**
MT-5	TCB	1.1	32.28	32.60	35.12
		1.2	32.56	32.27	35.17
		7.1	32.21	31.95	35.84
		8.1	32.67	31.59	35.75
MT-7	TCB	1.1	33.10	31.82	35.08
		1.1	33.15	31.79	35.05
		4.1	32.75	31.68	35.58
		4.1	32.92	31.34	35.74
		4.1	33.10	31.41	35.49
		4.2	32.80	32.01	35.20
		6.1	33.03	31.86	35.11
		14.1	33.28	31.53	35.19
MT-14	TCB	6.1	33.20	33.16	33.64
MT-16	TCB	7.1 (darker using SEM)	33.46	31.83	34.72
		7.2 (darker using SEM)	33.87	30.92	35.21
		7.3 (lighter using SEM)	36.10	30.37	33.53
		7.4 (lighter using SEM)	36.10	30.18	33.72
		7.5 (darker using SEM)	33.73	31.38	34.89
		7.5 (lighter using SEM)	35.69	30.69	33.62
MT-19	TCB	1.1 (lighter using SEM)	37.26	29.94	32.80
		2.1 (lighter using SEM)	35.98	30.78	33.24
MT-20	TCB	1.1	33.69	31.32	34.99
		1.1	33.04	31.76	35.20
		4.1	33.14	31.58	35.28

Table C.5: (continued) SEM-EDS Analyses of Chalcopyrite.

Chalcopyrite			Weight percentages		
Sample	**Rock Type**	**SEM Location**	**Cu**	**Fe**	**S**
MT-23	TCB	1.1	32.41	31.81	35.78
MT-35	TCB	1.1	33.30	32.28	34.42
MT-38	TCB	1.1	33.74	31.33	34.93
		1.2	33.62	31.18	35.20
		1.3	33.15	31.88	35.47
		1.4 (lathed; enclosed by cubanite)	32.50	32.34	35.16
		6.1	33.67	31.20	35.13
		10.1	32.64	32.16	35.20
MT-40	TCB	1.1	34.06	31.30	34.64
MT-44	TCB	3.1	33.32	31.43	35.25
		9.1	33.62	30.87	35.35
		9.2	33.51	31.33	35.17
MT-48	TCB	1.1	33.17	31.65	35.18
		1.2	33.15	31.40	35.45
		7.1	33.22	31.67	35.11
MT-49	TCB	1.1 (darker using SEM)	33.27	31.61	35.12
		1.1 (darker using SEM)	33.21	31.67	35.13
		2.1 (lighter using SEM)	36.34	30.36	33.30
		4.1 (lighter using SEM)	36.04	30.28	33.68
MT-52	BCB	2.1 (Ni-blebs)	32.91	32.07	35.02
		2.1 (Ni-blebs)	33.12	31.97	34.92
		2.1 (Ni-blebs)	33.23	31.89	34.88

Table C.5: (continued) SEM-EDS Analyses of Chalcopyrite.

Chalcopyrite			Weight percentages		
Sample	**Rock Type**	**SEM Location**	**Cu**	**Fe**	**S**
MT-56	FOS	5.1 (flames; replacing bornite)	33.52	31.52	34.96
MT-58	TCB	1.1	33.61	31.62	34.76
		5.1 (mass replacement by bornite)	36.74	30.40	32.87
MT-60	TCB	4.1 (at cobalt pentlandite-bornite association)	33.48	31.32	35.20
MT-71	TCB	10.1 (replacing x-bornite)	32.30	32.79	34.91
		10.2 (replacing x-bornite)	32.79	32.21	35.00

Table C.6: SEM-EDS Analyses of Pyrrhotite.

Pyrrhotite			Weight percentages	
Sample	**Rock Type**	**SEM Location**	**Fe**	**S**
MT-3	TCB	15.1 (lighter using SEM)	63.83	36.17
		15.1 (lighter using SEM)	63.79	36.21
		15.2 (darker using SEM)	61.75	38.25
		15.2 (darker using SEM)	61.74	38.26
MT-5	TCB	1.1	63.55	36.45
		1.1	63.58	36.42
		1.2 (enclosed by cobalt pentlandite)	63.41	36.59
		7.1	63.08	36.92
MT-7	TCB	1.1 (associated with cobalt pentlandite)	63.22	36.78
		1.2 (enclosed by cobalt pentlandite)	63.48	36.52
		1.2	63.08	36.92
		13.1 (associated with larger cobalt pentlandite grain)	63.74	36.26
		13.1 (associated with larger cobalt pentlandite grain)	63.81	36.19
		20.1 (replaced by cubanite)	63.28	36.72
		20.2 (replaced by cubanite)	63.53	36.47
MT-26	TCB	1.1	63.97	36.03
MT-35	TCB	1.1	62.47	37.53
		2.1 (streaks)	62.40	37.60
		2.1 (streaks)	62.47	37.53
		2.1 (streaks)	62.63	37.37
		2.2 (streaks)	62.49	37.51

Table C.6: (continued) SEM-EDS Analyses of Pyrrhotite.

Pyrrhotite			Weight percentages	
Sample	**Rock Type**	**SEM Location**	**Fe**	**S**
MT-38	TCB	1.1 (replaced by cubanite)	63.28	36.72
		1.1 (replaced by cubanite)	63.22	36.78
		1.2 (replaced by cubanite)	63.22	36.78
		1.3 (replaced by cubanite)	63.52	36.48
		1.4 (replaced by cubanite)	63.72	36.28
		10.1 (very small; replaced by cubanite; adjacent to cobalt pentlandite)	63.48	36.52
		10.1 (very small; replaced by cubanite; adjacent to cobalt pentlandite)	63.38	36.62
MT-52	BCB	4.1 (pyrrhotite replacing chalcopyrite; lighter using SEM)	63.84	36.16
		4.1 (pyrrhotite replacing chalcopyrite; lighter using SEM)	64.07	35.93
MT-58	TCB	1.1 (lighter using SEM)	63.88	36.12
		1.1 (darker using SEM)	61.81	38.19
		3.1 (lighter using SEM)	63.86	36.14
		3.1 (darker using SEM)	61.81	38.19

Table C.7: SEM-EDS Analyses of Cubanite.

Cubanite			Weight percentages		
Sample	**Rock Type**	**SEM Location**	**Cu**	**Fe**	**S**
MT-5	TCB	1.1 (lath)	22.30	41.92	35.77
		1.2	22.06	42.37	35.57
		1.3 (smaller lath; about 15 micro meters in width)	22.48	42.02	35.49
		1.4 (larger lath)	21.92	42.42	35.66
MT-7	TCB	1.1 (larger lath)	22.26	42.17	35.56
		1.1 (larger lath)	21.99	42.37	35.64
		1.2 (smaller lath)	22.14	42.15	35.71
		1.2 (smaller lath)	22.23	41.91	35.85
		1.3 (even smaller lath)	22.26	41.86	35.88
		1.3 (even smaller lath)	22.05	42.07	35.88
		4.1 (not lathed)	21.59	42.45	35.96
		4.1 (not lathed)	21.94	42.43	35.63
		14.1 (not lathed)	22.30	42.10	35.60
		20.1 (not lathed; replacing cobalt pentlandite and pyrrhotite)	22.11	42.44	35.35
		20.1 (not lathed; replacing cobalt pentlandite and pyrrhotite)	22.11	42.40	35.50
MT-23	TCB	3.1 (lathed)	22.14	42.21	35.65
MT-26	TCB	4.1 (lathed)	22.45	42.51	35.04
MT-35	TCB	1.1 (lathed)	22.09	43.00	34.91
		4.1 (smaller lath)	22.40	42.37	35.23
		4.2 (larger lath)	22.26	42.74	35.01

Table C.7: (continued) SEM-EDS Analyses of Cubanite.

Cubanite			Weight percentages		
Sample	**Rock Type**	**SEM Location**	**Cu**	**Fe**	**S**
MT-38	TCB	1.1 (not lathed)	21.77	42.03	36.19
		1.1 (not lathed)	21.85	42.50	35.65
		1.2 (not lathed)	22.33	42.17	35.50
		5.1 (not lathed)	21.87	42.32	35.81
		5.2 (not lathed)	22.08	42.06	35.87
		10.1 (not lathed)	21.97	42.30	35.73

Table C.8: SEM-EDS Analyses of Bornite.

Bornite			Weight percentages		
Sample	**Rock Type**	**SEM Location**	**Cu**	**Fe**	**S**
MT-2	BCB	1.1 (bornite-chalcocite symplectic intergrowth)	61.80	12.92	25.28
		1.1 (bornite-chalcocite symplectic intergrowth)	62.97	11.80	25.23
MT-11	TCB	5.1 (replaced by large chalcocite veins)	62.69	11.60	25.72
		6.1 (replaced by large chalcocite veins)	62.78	11.48	25.74
		6.2 (replaced by large chalcocite veins)	62.38	11.65	25.97
MT-13	TCB	7.1 (bulk mineralisation; replaced by large chalcocite veins)	62.94	11.40	25.66
		9.1 (bulk mineralisation)	62.66	11.68	25.66
MT-15	TCB	15.1 (bulk mineralisation)	63.19	11.63	25.18
MT-16	TCB	7.1 (replacing chalcopyrite)	63.15	11.56	25.28
		7.1 (replacing chalcopyrite)	63.27	11.53	25.20
		7.2 (replacing chalcopyrite)	62.70	11.72	25.59
MT-19	TCB	1.1 (replacing chalcopyrite)	63.83	11.37	24.80
MT-40	TCB	1.1 (flames)	62.40	12.48	25.48
		1.1 (flames)	62.37	11.79	25.84
		1.2 (flames)	62.45	12.26	25.30
		5.1 (large amount; intergrown with chalcocite; not symplectic)	63.37	11.16	25.47
MT-44	TCB	3.1 (smaller bornite flames)	61.30	12.26	25.88
		3.2 (larger bornite mass close to edge)	61.60	12.36	26.04
		3.5 (bornite enclosing sphalerite)	60.90	13.11	25.99
		5.1 (intergrown with chalcocite)	62.73	10.98	26.29
MT-49	TCB	2.1 relict chalcopyrite	62.60	11.82	25.58
		2.1 relict chalcopyrite	62.45	12.36	25.19

Table C.8: (continued) SEM-EDS Analyses of Bornite.

Bornite			**Weight percentages**		
Sample	**Rock Type**	**SEM Location**	**Cu**	**Fe**	**S**
MT-52	BCB	2.1 relict chalcopyrite	62.88	11.70	25.41
		2.2	62.83	11.72	25.45
MT-55	TCB	22.1 (bornite-chalcocite symplectic)	63.13	11.50	25.38
MT-56	FOS	5.1	62.70	11.64	25.67
		5.2	62.68	11.98	25.34
		5.3 (chalcocite-bornite intergrowth)	62.86	11.43	25.72
		5.3 (chalcocite-bornite intergrowth)	62.88	11.38	25.74
		5.3 (chalcocite-bornite intergrowth)	62.87	11.19	25.94
MT-58	TCB	1.1 (lathed/distorted band)	61.63	12.98	25.39
		5.1 (mass replacing chalcopyrite)	63.42	11.42	25.16
MT-60	TCB	4.1 (at cobalt pentlandite association; lath)	61.89	12.38	25.73
MT-71	TCB	10.1 (replaced by x-bornite)	62.65	11.76	25.59
		10.2 (replaced by x-bornite)	62.79	11.69	25.52

Table C.9: SEM-EDS Analyses of Cobalt pentlandite.

Cobalt pentlandite			Compound percentages			
Sample	**Rock Type**	**SEM Location**	**Co**	**Fe**	**Ni**	**S**
MT-2	BCB	1.1 (replacing myrmekitic intergrowth)	26.22	23.87	16.83	33.08
		1.1 (replacing myrmekitic intergrowth)	26.50	23.92	16.57	33.02
		1.2 (replacing myrmekitic intergrowth)	26.33	24.53	16.44	32.70
MT-3	TCB	15.1	24.74	24.51	18.05	32.70
		15.1	25.11	24.32	17.96	32.62
MT-5	TCB	1.1 (large euhedral grain)	27.21	25.05	14.72	33.03
		1.1	25.88	25.87	14.95	33.30
		1.2 (flame-like; closer to stem where attached to pyrrhotite)	23.85	24.79	18.44	32.92
MT-7	TCB	1.1	29.64	24.84	12.48	33.03
		1.1	30.08	24.44	12.51	32.97
		1.1	30.46	24.60	12.32	32.62
		14.1 (one of the larger sised grains)	27.98	26.53	12.91	32.59
		14.1 (one of the larger sised grains)	27.74	26.63	13.02	32.61
		20.1 (smaller; replaced by cubanite)	30.62	22.23	13.94	33.21
		20.2 (a bit larger; replaced by cubanite)	36.44	20.08	10.67	32.82
MT-11	TCB	6.1 (replacing x-bornite and chalcocite)	14.81	29.05	22.90	33.25
MT-15	TCB	17.1 (replacing bornite, x-bornite, chalcocite and sphalerite)	14.48	28.27	24.11	33.14
MT-19	TCB	2.1	45.20	9.40	13.73	31.66
MT-20	TCB	4.1 (subhedral to euhedral grain)	45.13	9.68	13.07	32.13
		4.1 (subhedral to euhedral grain)	45.77	8.99	12.91	32.33
MT-23	TCB	1.1	29.38	19.35	18.53	32.74
MT-26	TCB	2.1	23.50	22.08	21.77	32.65
		3.1	28.50	20.39	18.83	32.29
MT-35	TCB	1.1	17.20	25.35	24.95	32.47

Table C.9: (continued) SEM-EDS Analyses of Cobalt Pentlandite.

Cobalt pentlandite			Weight percentages			
Sample	**Rock Type**	**SEM Location**	**Co**	**Fe**	**Ni**	**S**
MT-38	TCB	1.1 (small; replaced by cubanite)	28.14	20.99	18.11	32.76
		1.1 (small; replaced by cubanite)	27.70	21.31	18.18	32.81
		1.2 (small; replaced by cubanite)	22.66	23.50	20.72	33.13
		1.2 (small; replaced by cubanite)	22.38	24.48	20.06	33.08
		1.3 (small; replaced by cubanite)	22.21	24.34	20.18	33.27
		5.1 (relatively big)	25.31	22.61	18.89	33.19
		5.1 (relatively big)	25.51	22.52	19.16	32.81
		5.2 (relatively big)	25.05	22.45	19.32	33.18
		5.2 (relatively big)	25.18	22.43	19.62	32.77
		10.1 (very small; replaced by cubanite)	20.79	25.43	20.71	33.08
		10.1 (very small; replaced by cubanite)	20.07	25.66	21.18	33.08
MT-49	TCB	1.1 (relatively big)	36.66	12.97	17.73	32.67
		1.2 (relatively big)	36.57	13.01	17.71	32.71
		4.1 (unknown original size; medium, rimmed and replaced by bornite)	43.69	9.78	14.21	32.32
MT-52	BCB	9.1 (replacing bornite and x-bornite)	16.46	25.99	23.55	34.00
MT-55	TCB	22.1 (replacing symplectic intergrowth; medium sised))	27.76	15.13	23.78	33.33
		23.1 (slightly larger than in 22.1)	31.41	11.78	24.49	32.32
MT-56	FOS	5.1. (replaced by chalcopyrite)	33.33	11.74	22.28	32.65
MT-58	TCB	1.1 (big grains)	29.00	15.55	22.79	32.66
MT-60	TCB	4.1 (at bornite laths association)	21.44	19.91	26.06	32.58
		4.2 (at bornite laths association)	21.41	20.49	25.25	32.85
		4.3 (at bornite laths association)	16.93	22.11	28.47	32.49
MT-65	FOS	1.1 (replaced by chalcocite)	15.01	24.17	27.56	33.26

Table C.10: SEM-EDS Analysis of Chalcocite.

Chalcocite			Weight percentages		
Sample	**Rock Type**	**SEM Location**	**Cu**	**Fe**	**S**
MT-2	BCB	1.1 (symplectic)	78.52	0.83	20.64
		1.1 (symplectic)	78.08	1.11	20.81
		5.1 (symplectic)	78.87	0.62	20.51
MT-11	TCB	5.1 (large replacement veins)	78.48	0.92	20.60
		5.1 (large replacement veins)	78.89	0.55	20.55
		5.1 (large replacement veins)	78.69	0.59	20.72
		6.1 (large replacement veins)	78.86	0.58	20.56
MT-13	TCB	7.1 (large replacement veins)	79.15	0	20.85
		7.1 (large replacement veins)	79.38	0	20.62
		7.2 (large replacement veins)	79.27	0	20.73
		9.1 (large replacement veins)	79.01	0.33	20.66
		9.2 (large replacement veins)	79.01	0	20.99
		9.3 (large replacement veins)	79.10	0	20.90
MT-15	TCB	15.1 (large replacement veins)	80.03	0	19.97
		15.2 (large replacement veins)	80.02	0	19.98
		18.1	80.04	0	19.96
MT-40	TCB	5.1 (large amount; intergrown with bornite; not symplectic)	79.18	0	20.62
		5.1 (large amount; intergrown with bornite; not symplectic)	79.03	0	20.97
MT-44	TCB	5.1 (intergrown with bornite)	77.04	0.54	22.42
MT-55	TCB	22.1 (symplectic)	79.28	0	20.72
		23.1 (symplectic, large mass)	79.35	0	20.65

Table C.10: (continued) SEM-EDS Analyses of Chalcocite.

Chalcocite			Weight percentages		
Sample	**Rock Type**	**SEM Location**	**Cu**	**Fe**	**S**
MT-56	FOS	5.1 (chalcocite-bornite intergrowth)	78.81	0	21.19
		5.1 (chalcocite-bornite intergrowth)	78.86	0	21.14
MT-65	FOS	1.1 (replacing cobalt pentlandite; large mass)	80.01	0	19.99
		3.1 (large mass)	79.70	0	20.30

APPENDIX D

SPECTRAL IMAGES.

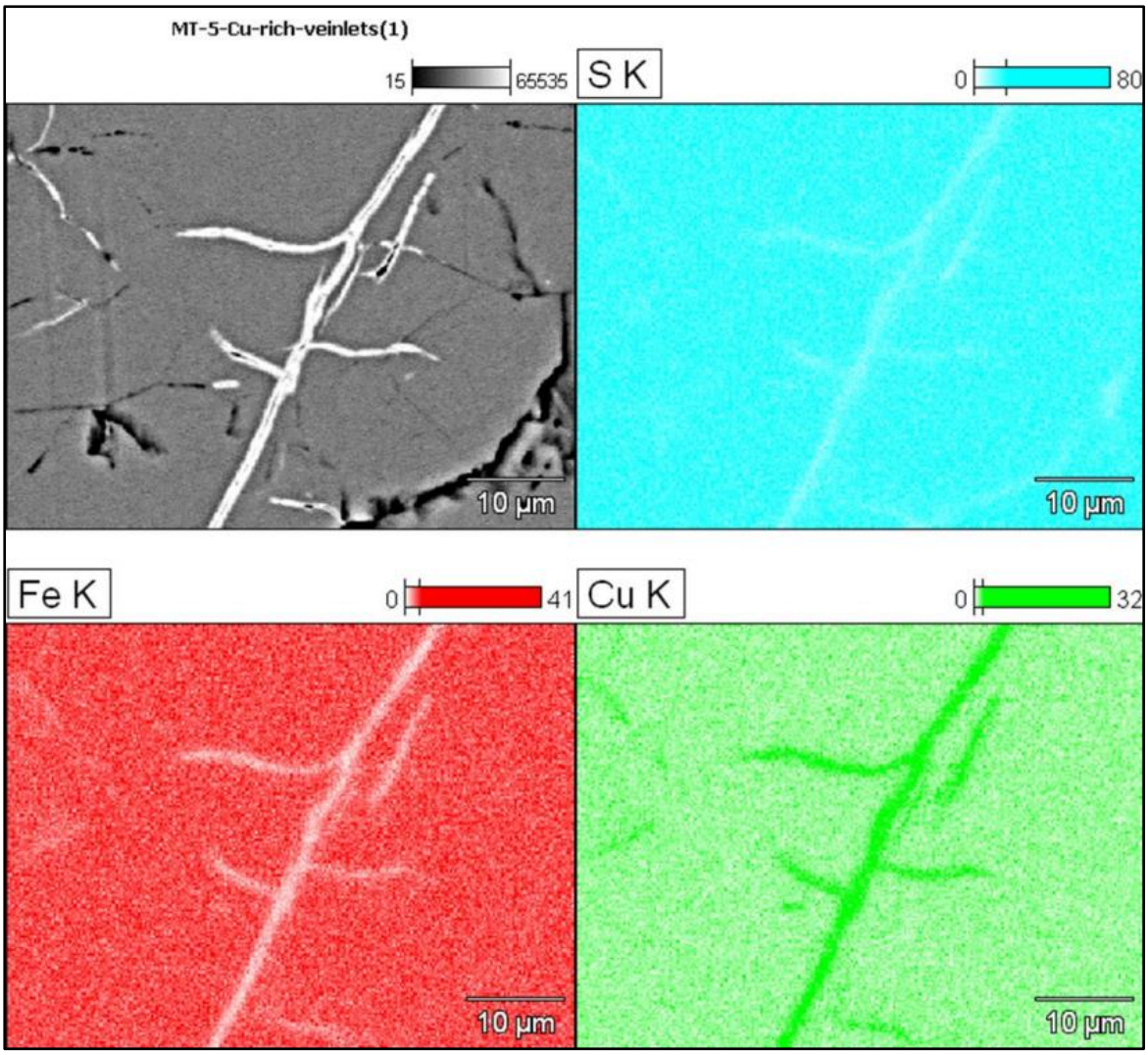

Spectral Image 1: Partitioning of S, Fe, and Cu between Cu-rich phase (white) and cubanite (grey). Sample MT-5.

Data Type:	Counts
Image Resolution:	512 by 384
Image Pixel Size:	0.11 µm
Map Resolution:	256 by 192
Map Pixel Size:	0.23 µm
Acc. Voltage:	20.0 kV
Magnification:	2200

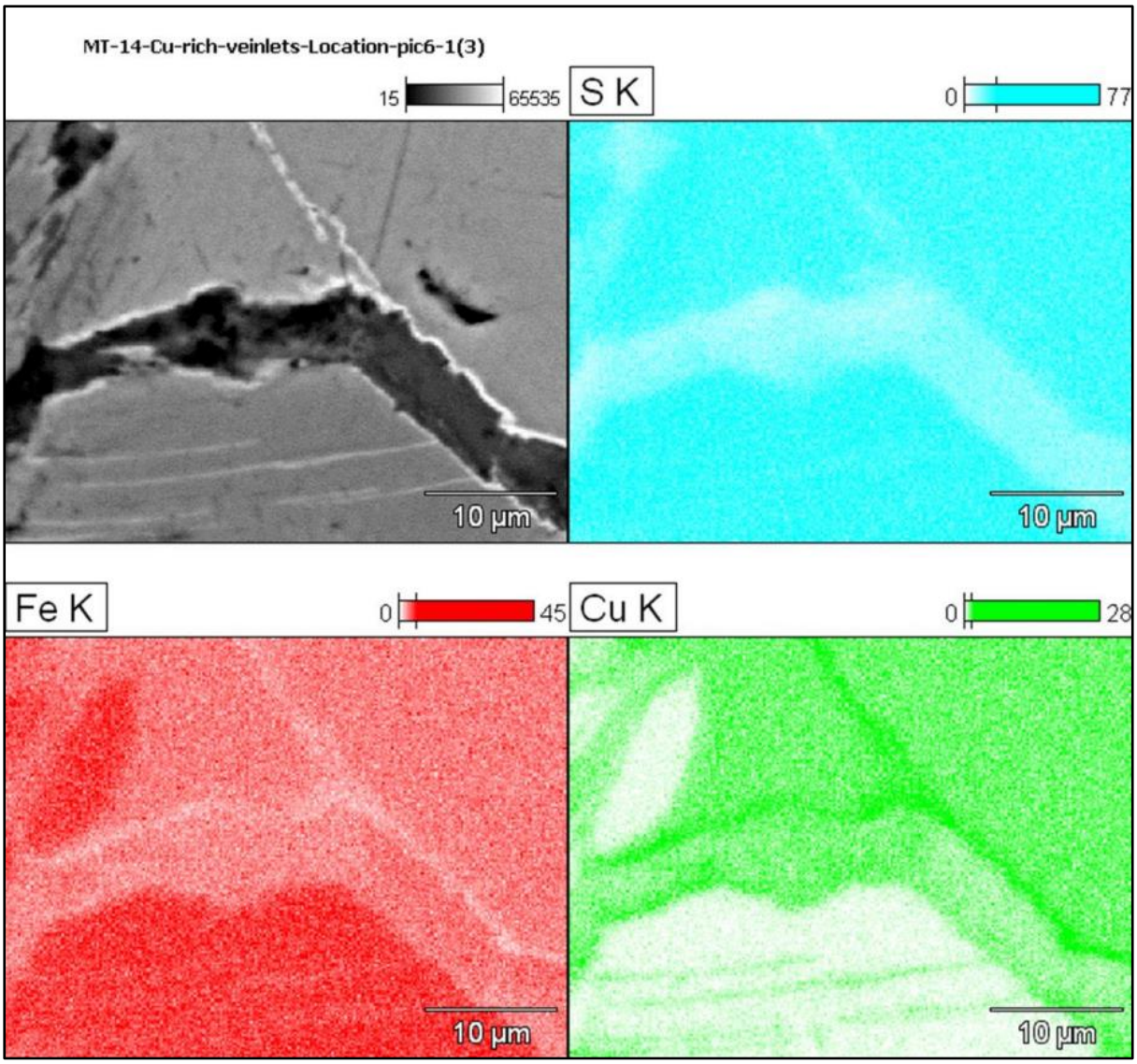

Spectral Image 2: Partitioning of S, Fe, and Cu between Cu-rich veinlets (white), chalcopyrite (light-grey, upper region), mackinawite (grey, lower region), and valleriite (dark-grey, central region). Sample MT-14.

Data Type:	Counts
Image Resolution:	512 by 384
Image Pixel Size:	0.08 µm
Map Resolution:	256 by 192
Map Pixel Size:	0.17 µm
Acc. Voltage:	20.0 kV
Magnification:	3000

APPENDIX E

ESTIMATED MODAL COMPOSITIONS OF THE PRIMARY MINERALS AND COMMON ACCESSORY MINERALS FOR SELECTED THIN SECTIONS.

Table E.1: Estimated Modal Compositions of the Primary Minerals and Common Accessory Minerals for Selected Thin Sections.

Sample	Rock Type	Cb	Ol	Chn	Srp	Ap	Phl	Mgt	Sulph	Bdl	Ilm	Other
MT-2	BCB	52	15	0	15	9	0	7	<1	<1	1	0
MT-3	TCB	54	1	2	0	1	<1	<1	41	<1	0	<1
MT-5	TCB	74	3	0	0	4	0	<1	18	<1	0	0
MT-7	TCB	60	0	2	0	9	<1	<1	28	<1	0	0
MT-8	TCB	37	0	5	0	5	5	45	1	2	0	0
MT-11	TCB	65	12	<1	0	8	<1	12	2	<1	<1	<1
MT-13	TCB	74	<1	<1	0	3	<1	20	2	0	0	<1
MT-14	TCB	37	0	0	0	0	40	<1	23	0	0	0
MT-15	TCB	43	0	0	0	3	4	25	25	0	0	0
MT-16	TCB	76	<1	0	0	5	4	12	3	0	0	0
MT-19	TCB	17	0	0	3	8	<1	10	61	<1	<1	0
MT-20	TCB	27	0	0	0	6	<1	52	14	<1	0	0
MT-22	TCB	73	0	0	10	8	<1	8	<1	0	<1	<1
MT-23	TCB	37	0	6	<1	<1	<1	1	55	0	0	0
MT-26	TCB	48	<1	0	<1	1	<1	<1	50	<1	0	<1
MT-27	TCB	22	<1	0	30	2	0	45	1	0	0	0
MT-28	TCB	62	2	0	4	12	<1	18	1	<1	0	0
MT-32	TCB	74	<1	0	1	4	0	20	<1	<1	0	0
MT-35	TCB	74	<1	0	0	4	<1	10	11	0	0	0
MT-38	TCB	55	0	0	<1	8	<1	22	14	<1	0	<1
MT-40	TCB	57	0	<1	1	<1	<1	40	1	0	0	<1
MT-44	TCB	59	0	0	3	<1	<1	15	22	<1	0	0
MT-48	TCB	70	0	2	1	5	1	6	15	<1	0	0

Table E.1: (continued) Estimated Modal Compositions of the Primary Minerals and Common Accessory Minerals for Selected Thin Sections.

Sample	Rock Type	Cb	Ol	Chn	Srp	Ap	Phl	Mgt	Sulph	Bdl	Ilm	Other
MT-49	TCB	61	0	0	0	8	<1	20	11	0	0	0
MT-52	BCB	90	0	<1	0	2	<1	5	2	0	0	0
MT-53	TCB	86	1	<1	4	4	<1	3	1	<1	0	0
MT-55	TCB	34	0	0	15	20	<1	25	5	<1	0	0
MT-56	FOS	19	0	0	6	8	<1	63	3	<1	0	0
MT-58	TCB	32	0	<1	0	<1	0	60	7	<1	0	0
MT-60	TCB	91	0	<1	0	5	<1	<1	3	0	0	0
MT-65	FOS	28	0	25	0	22	<1	24	<1	0	0	<1
MT-67	TCB	63	0	5	2	4	0	25	<1	0	<1	0
MT-71	TCB	63	0	0	0	5	1	30	1	0	0	0

APPENDIX F

TRANSGRESSIVE CARBONATITE SULPHIDE MINERAL ASSOCIATIONS.

Table F.1: Transgressive Carbonatite Sulphide Mineral Associations.

Sample	Rock Type	Main Group	With	Without
MT-2	BCB	Bornite-chalcocite-cobalt pentlandite.	Bornite-chalcocite symplectic intergrowth. Replacement of bornite and chalcocite by cobalt pentlandite	N/A
MT-3	TCB	Cobalt pentlandite-pyrrhotite-chalcopyrite-cubanite-mackinawite.	Cobalt pentlandite and pyrrhotite residual islands replaced by cubanite (relict ccp). Chalcopyrite. Cubanite replacing cubanite laths. Mackinawite replacing chalcopyrite.	Pentlandite. Sphalerite. Cu-rich veinlets.
MT-5	TCB	Cobalt pentlandite-pyrrhotite-chalcopyrite-cubanite-mackinawite.	Second generation cobalt pentlandite replacing cubanite (relict ccp). Normal cobalt pentlandite. Pyrrhotite. Chalcopyrite. Cubanite (laths and relict ccp). Smaller anhedral (mostly) to subhedral sphalerite grains replacing chalcopyrite. Mackinawite replacing chalcopyrite. Cu-rich veinlets at chalcopyrite-cubanite association.	Pentlandite. Larger subhedral to euhedral sphalerite grains.

Table F.1: (continued) Transgressive Carbonatite Sulphide Mineral Associations.

Sample	Rock Type	Main Group	With	Without
MT-7	TCB	Cobalt pentlandite-pyrrhotite-chalcopyrite-cubanite.	Second generation cobalt pentlandite (hexagonal) replacing cubanite (relict ccp). Cobalt pentlandite and pyrrhotite residual streaks in cubanite (relict ccp). Chalcopyrite. Cubanite laths as well. Mackinawite replacing cobalt pentlandite and chalcopyrite. Smaller anhedral (mostly) to subhedral sphalerite grains replacing chalcopyrite and cubanite (laths and relict ccp). Cu-rich veinlets at chalcopyrite cubanite association.	Pentlandite. Larger subhedral to euhedral sphalerite grains.
MT-8	TCB	N/A	Chalcopyrite. Valleriite.	N/A
MT-11	TCB	Bornite-x-bornite-chalcocite-cobalt pentlandite.	Large amounts of bornite replaced by x-bornite. Large veins of chalcocite replacing bornite-x-bornite association. Cobalt pentlandite (Co-poorer) replacing x-bornite and large chalcocite veins. Large euhedral, star-shaped sphalerite grains.	Symplectic intergrowth between bornite and chalcocite. Pb-Ni sulphide phase. Ag-phase.

Table F.1: (continued) Transgressive Carbonatite Sulphide Mineral Associations.

Sample	Rock Type	Main Group	With	Without
MT-13	TCB	Bornite-x-bornite-chalcocite-cobalt pentlandite.	Large amounts of bornite replaced by x-bornite. Large veins of chalcocite replacing bornite-x-bornite association. Symplectic intergrowth between bornite and chalcocite.	Cobalt pentlandite. Sphalerite. Pb-Ni sulphide phase. Ag-phase.
MT-14	TCB	Cobalt pentlandite-pyrrhotite-chalcopyrite-cubanite.	Cobalt pentlandite. Chalcopyrite. Smaller subhedral to anhedral (mostly) sphalerite grains replacing chalcopyrite. Cu-rich veinlets at chalcopyrite-mackinawite association.	Pentlandite. Pyrrhotite. Cubanite. Larger subhedral to euhedral sphalerite grains.
MT-15	TCB	Bornite-x-bornite-chalcocite-cobalt pentlandite.	Large amounts of bornite replaced by x-bornite. Large veins of chalcocite replacing bornite-x-bornite association. Cobalt pentlandite (co-poorer) replacing bornite, x-bornite, chalcocite, and sphalerite. Large subhedral, star-shaped sphalerite grains. Pb-Ni sulphide phase. Ag-phase.	Symplectic intergrowth between bornite and chalcocite.

Table F.1: (continued) Transgressive Carbonatite Sulphide Mineral Associations.

Sample	Rock Type	Main Group	With	Without
MT-16	TCB	Cobalt pentlandite-chalcopyrite-chalcopyrite-bornite.	Less-Cu-chalcopyrite exsolution flames replacing chalcopyrite. Mass replacement of subhedral to euhedral chalcopyrite grains by bornite (relict ccp). Extremely minor amounts of x-bornite replacing bornite at bornite-chalcopyrite boundary. Small anhedral chalcocite grains and veinlets replacing bornite (confined to bornite). Covelline replacing chalcocite.	Galena. Cobalt pentlandite. Sphalerite. Ni inclusions in chalcopyrite.
MT-19	TCB	Cobalt pentlandite-chalcopyrite-chalcopyrite-bornite.	Less-Cu-chalcopyrite exsolution flames replacing chalcopyrite. Mass replacement of subhedral to euhedral chalcopyrite grains by bornite (relict ccp). Bornite rims around cobalt pentlandite. Galena.	X-bornite. Chalcocite. Covelline. Sphalerite. Ni inclusions in chalcopyrite.
MT-20	TCB	Chalcopyrite-Millerite.	Millerite replacing chalcopyrite mainly along magnetite veinlets. Subhedral cobalt pentlandite grains.	N/A

Table F.1: (continued) Transgressive Carbonatite Sulphide Mineral Associations.

Sample	Rock Type	Main Group	With	Without
MT-23	TCB	Cobalt pentlandite-pyrrhotite-chalcopyrite-cubanite.	Pentlandite flames replacing chalcopyrite. Mackinawite replacing pentlandite flames. Cobalt pentlandite. Chalcopyrite. Cubanite (large laths). Sphalerite (larger subhedral to euhedral (mostly) grains with chalcopyrite inclusions replacing chalcopyrite. Smaller anhedral to subhedral (mostly) grains replacing cubanite and chalcopyrite and also rimming cobalt pentlandite.	Pyrrhotite. Cu-rich veinlets.
MT-26	TCB	Cobalt pentlandite-pyrrhotite-chalcopyrite-cubanite.	Pentlandite flames replacing chalcopyrite and cubanite. Mackinawite replacing pentlandite flames and chalcopyrite. Cobalt pentlandite. Pyrrhotite. Chalcopyrrite. Cubanite (large laths). Extremely small amounts of smaller anhedral to subhedral sphalerite replacing cubanite laths.	Larger subhedral to euhedral sphalerite grains. Cu-rich veinlets.
MT-27	TCB	N/A	Chalcopyrite. Valleriite.	N/A
MT-28	TCB	N/A	Chalcopyrite. Valleriite.	N/A

Table F.1: (continued) Transgressive Carbonatite Sulphide Mineral Associations.

Sample	Rock Type	Main Group	With	Without
MT-32	TCB	N/A	Valleriite.	N/A
MT-35	TCB	Cobalt pentlandite-pyrrhotite-chalcopyrite-cubanite.	Cobalt pentlandite. Cubanite (relict and laths). Residual cobalt pentlandite islands and pyrrhotite streaks replaced by cubanite. Chalcopyrite. Smaller anhedral to suhedral sphalerite grains replacing cubanite (relict ccp). Mackinawite replacing chalcopyrite.	Pentlandite. Larger subhedral to euhedral sphalerite grains. Cu-rich veinlets.
MT-38	TCB	Cobalt pentlandite-pyrrhotite-chalcopyrite-cubanite.	Pentlandite replacing chalcopyrite. Mackinawite replacing pentlandite. Co-poorer cobalt pentlandite. Cobalt pentlandite and pyrrhotite residual streaks replaced by cubanite (relict ccp). Chalcopyrite. Smaller anhedral (mostly) to subhedral sphalerite grains replacing cubanite (relict ccp) (mostly) and chalcopyrite.	Cubanite laths. Larger subhedral to euhedral sphalerite grains. Cu-rich veinlets.

Table F.1: (continued) Transgressive Carbonatite Sulphide Mineral Associations.

Sample	Rock Type	Main Group	With	Without
MT-40	TCB	Mainly chalcopyrite-bornite-flames-and-laths (transitional; bornite-chalcocite-cobalt pentlandite group lower; no cobalt pentlandite).	Bornite flames replacing chalcopyrite. Chalcocite and bornite symplectic intergrowth (transitional).	Large subhedral to euhedral sphalerite grains. Millerite. Cobalt pentlandite. Heazlewoodite.
MT-44	TCB	Mainly chalcopyrite-bornite-flames-and-laths (transitional; bornite-chalcocite-cobalt pentlandite group lower; no cobalt pentlandite, but millerite replacing association).	Bornite flames, laths and bodies replacing chalcopyrite. Millerite replacing bornite flames and bodies. Large subhedral to euhedral (mostly) sphalerite grains with chalcopyrite inclusions replacing bornite. Cobalt pentlandite (one grain). Chalcocite and bornite symplectic intergrowths (transitional).	Heazlewoodite.

Table F.1: (continued) Transgressive Carbonatite Sulphide Mineral Associations.

Sample	Rock Type	Main Group	With	Without
MT-48	TCB	Chalcopyrite-Millerite.	Millerite replacing chalcopyrite mainly along magnetite veinlets.	Cobalt pentlandite.
MT-49	TCB	Cobalt pentlandite-chalcopyrite-chalcopyrite-bornite.	Less-Cu-chalcopyrite exsolution flames replacing chalcopyrite. Mass replacement of subhedral to euhedral chalcopyrite grains by bornite (relict ccp). Bornite rims around cobalt pentlandite. Subhedral grains of sphalerite (2 grains) replacing chalcopyrite.	Galena. Chalcocite. Covelline. Ni inclusions in chalcopyrite.
MT-52	BCB	Mainly cobalt pentlandite-chalcopyrite-chalcopyrite-bornite (transitional; bornite-x-bornite-chalcocite-cobalt pentlandite (Co-poorer), very small amount).	Less-Cu-chalcopyrite exsolution flames replacing chalcopyrite. Mass replacement of subhedral chalcopyrite grains by bornite (relict ccp). Larger amounts of x-bornite replacing bornite (confined to bornite). Small anhedral chalcocite grains replacing bornite (confined to bornite). Small chalcocite flame replacing bornite and x-bornite. Covelline replacing chalcocite. Cobalt pentlandite replacing bornite and x-bornite. Ni-blebs in chalcopyrite.	Cobalt pentlandite. Sphalerite.

Table F.1: (continued) Transgressive Carbonatite Sulphide Mineral Associations.

Sample	Rock Type	Main Group	With	Without
MT-53	TCB	Cobalt pentlandite-chalcopyrite-chalcopyrite-bornite.	Mass replacement of chalcopyrite by bornite (relict ccp). Extremely minor amounts of x-bornite replacing bornite at bornite-chalcopyrite boundary. Smaller anhedral chalcocite grains replacing bornite (confined to bornite). Larger subhedral chalcocite grains replacing bornite. Covelline replacing chalcocite (confined to smaller anhedral grains).	Galena. Cobalt pentlandite. Sphalerite. Less-Cu-chalcopyrite exsolution flames replacing chalcopyrite. Ni inclusions in chalcopyrite.
MT-55	TCB	Bornite-chalcocite-cobalt pentlandite.	Bornite-chalcocite symplectic intergrowth. Replacement of bornite and chalcocite by cobalt pentlandite.	N/A
MT-56	FOS	N/A	N/A	N/A

Table F.1: (continued) Transgressive Carbonatite Sulphide Mineral Associations.

Sample	Rock Type	Main Group	With	Without
MT-58	TCB	Mainly chalcopyrite-bornite-flames-and-laths (transitional; cobalt pentlandite-chalcopyrite-chalcopyrite-bornite).	Subhedral to euhedral (mostly) heazlewoodite grains replacing chalcopyrite, and bornite flames and laths. Medium-sised subhedral (mostly) sphalerite grains replacing chalcopyrite at chalcopyrite-cobalt pentlandite boundary. X-bornite replacing bornite flames. Chalcocite veins replacing x-bornite, bornite and chalcopyrite.	Millerite.
MT-60	TCB	Mainly chalcopyrite-millerite (transitional; cobalt pentlandite-pyrrhotite-chalcopyrite group (lower)).	Millerite replacing chalcopyrite. No association with any other sulphide. Cobalt pentlandite-Bornite laths/flames-chalcopyrite association mass. Pyrrhotite-cobalt pentlandite-cubanite (laths)-chalcopyrite association-mass.	Cobalt pentlandite.

Table F.1: (continued) Transgressive Carbonatite Sulphide Mineral Associations.

Sample	Rock Type	Main Group	With	Without
MT-65	FOS	N/A	N/A	N/A
MT-71	TCB	Transition; Bornite-x-bornite-chalcocite-Co-rich-pentlandite, and Cobalt pentlandite-chalcopyrite-chalcopyrite-bornite.	Ni-blebs in chalcopyrite. X-bornite replacing bornite. Chalcopyrite replacing bornite-x-bornite association. Chalcopyrite replacing x-bornite. Chalcocite vein replacing bornite-x-bornite association. Valleriite replacing chalcocite vein.	N/A